Universitat Autònoma de Barcelona

From preconcentration to rapid detection of exosomes as biomarkers in clinical diagnosis

Silio Lima de Moura

Universitat Autònoma de Barcelona

From preconcentration to rapid detection of exosomes as biomarkers in clinical diagnosis

Silio Lima de Moura

Ph.D. Thesis

Ph.D. program in Chemistry

Supervisors: **Maria Isabel Pividori**
Mercè Martí Ripoll

Department of Chemistry

Faculty of Science

2020

Doctoral thesis dissertation submitted to be considered for the Ph.D. degree,

Universitat Autònoma de Barcelona

From preconcentration to rapid detection of exosomes as biomarkers in clinical diagnosis

by Silio Lima de Moura

Director's approval

_____

Dr. María Isabel Pividori Gurgo
Department of Chemistry
Universitat Autònoma de Barcelona

_____

Dr. Mercè Martí Ripoll
Department of Cell Biology, Physiology and Immunology
Universitat Autònoma de Barcelona

Barcelona, July 2020

Dedicated to my parents, Bartolomeu Moura and Luzineide Moura.

“for their endless love, support and encouragement”

∞ + 1

Contents

Chapter overview

This dissertation explores the role of exosomes as biomarkers of different clinical conditions, including breast cancer. Furthermore, different approaches for the sensitive and selective preconcentration and detection of the exosomes are studied and compared with the conventional laboratory methodologies.

The study of exosomes as novel biomarkers of cancer is addressed since the extracellular vesicles play an important role in cell-to-cell communication. Among them, nanovesicles, as bilipid membrane of the endosomal system, the so-called exosomes, can be considered as biomarkers of differentiation, signaling or regulation status of the cellular machinery. Exosomes express membrane-bound proteins and contain nucleic acids, such as deoxyribonucleic acid (DNA), messenger ribonucleic acid (mRNA) and microRNA (miRNA). Therefore, exosomes are currently considered promising biomarkers in liquid biopsy for early clinical diagnosis. In order to achieve this, in this doctoral thesis, the exosomes are produced from breast cancer cell lines, separated, preconcentrated and characterized using different techniques, including nanoparticle tracking analysis, transmission electron and confocal microscopy and flow cytometry. The main objective of these preliminary studies is to track the expression profile of the exosomes comparatively to the cell lines which produce them. The applicability of exosomes as biomarkers in cancer patients is finally assessed. Forthcoming chapters are summarized in the next paragraphs.

Chapter 1 is an introductory overview of extracellular vesicles, including the exosomes. This chapter is especially focused on exosomes and their history, biogenesis, function, and their role as an early biomarker for cancer. Furthermore, the traditional and emerging methods for the detection, quantification and the physical and (bio)chemical characterization are briefly described. Special focus is paid on the advances in the detection of exosomes, as well as on electrochemical biosensing as an emerging technology for the rapid detection of exosomes.

In Chapter 2, the aims of this dissertation are presented, including a w description of the specific objectives of each of the chapters.

As previously stated, the exosomes are considered promising candidates as biomarkers to improve the current clinical diagnostic methods and to develop rapid tests. One of the main drawbacks is that they must be detected at low concentration in very complex samples. Accordingly, conventional procedures for exosome detection usually require relatively large sample volumes and involve preliminary purification and :entration steps by ultracentrifugation. Therefore, chapter 3 addresses one of the

bottlenecks that should be considered to simplify the analytical procedure in the detection of exosomes: the study and development of novel solid-phase separation methods in order to avoid ultracentrifugation. This chapter studies the role of specific isolation of exosomes on particle-based magnetic enrichment, which can be easily coupled with emerging technologies for the rapid detection of exosomes. A rational study of the surface proteins in exosomes, which can be recognized by magnetic particles, is presented. Different commercial antibodies against selected receptors were immobilized on tosyl-activated magnetic particles, including the general tetraspanins CD9, CD63 and CD81, and cancer-related receptors (CD24, CD44, CD54, CD326 and CD340). The effect of the serum matrix on the immunomagnetic separation was then carefully evaluated by spiking the exosomes in depleted human serum. The interferences of free receptors present in the serum, including the tetraspanins CD9 and CD63, can prevent or interfere the immunomagnetic separation based on these receptors. Interestingly, the immunomagnetic separation of the exosomes based on CD81 is not affected by the serum (even if it is undiluted). Based on this study, the exosomes were preconcentrated by immunomagnetic separation on antiCD81-modified magnetic particles in order to achieve further optical or electrochemical readout.

Chapter 4 describes the study of exosomes as emerging biomarkers for the detection of cancer. This chapter firstly addresses the production, separation and characterization of exosomes from three different breast cancer cell lines (MCF7, MDA-MB-231 and SKBR3). This study was initially performed by classical methods, including isolation by ultracentrifugation, and characterization by Transmission Electron Microscopy (TEM), Nanoparticle Tracking Analysis (NTA), confocal microscopy and surface protein screening by Flow Cytometry. A rational comparative study of the biomarker profiling of the cells and their derived exosomes is discussed. To achieve that, several molecular biomarkers, including the general tetraspanins CD9, CD63 and CD81, and the specific cancer-related receptors (CD24, CD44, CD54, CD326 and CD340) are comparatively studied in the cells and their derived exosomes. After a careful selection of the biomarkers, a multiplexed magneto-actuated immunoassay for the detection of epithelial-cell derived exosomes is proposed as an alternative to ultracentrifugation and flow cytometry, preventing the interference of serum matrix. In this approach, the exosomes are separated and preconcentrated on magnetic particles by immunomagnetic separation (IMS), and labeled with a second antibody conjugated with an enzyme for the optical readout performed with a standard microplate reader. This immunoassay is able to detect 10^5 exosomes μL^{-1} directly in human serum without any treatment, such as ultracentrifugation. Moreover, an increased amount in the serum of exosomes expressing epithelial cells molecular patterns is proposed as a biomarker for

breast cancer patients. This approach is a highly suitable alternative method to flow cytometry, providing a sensitive method but by using instrumentation widely available in resource-constrained laboratories and requiring low-maintenance, as is the case of a microplate reader operated by filters.

Chapter 5 describes a novel method for the detection of exosomes combining IMS with electrochemical immunosensor. Different formats for the characterization and quantification of exosomes derived from three breast cancer cell lines (MCF7, MDA-MB-231 and SKBR3) are discussed in terms of analytical performance, including specificity, sensitivity and matrix effect. Among the different formats, the electrochemical immunosensor is able to reach a limit of detection of 10^5 exosomes μL^{-1} directly in human serum, when performing the IMS with antiCD81 modified magnetic particles and the labeling based on CD24 and CD340 as a cancer-related biomarker, avoiding the interference from free receptors in the serum matrix. Furthermore, the electrochemical immunosensor shows reliable results for the differentiation of healthy donors and breast cancer patients based on specific epithelial biomarkers. This approach is a highly suitable alternative method for the detection of exosomes in scarce resource settings.

In Chapter 6, two different methods for the detection of the intrinsic enzyme activity of alkaline phosphatase (ALP) expressed on the exosomes is presented, based on colorimetric and electrochemical readout in which no further labelling step is required. The ALP activity was firstly demonstrated on exosomes derived from human fetal osteoblastic (hFOB) cell line. Further studies are shown in serum-derived exosomes from breast cancer patients. Interestedly, an increased ALP activity is observed in exosomes from cancer patients. In this case, the approach combined the specific capture of exosomes by epithelial cancer-related biomarker, and further detection based on the intrinsic ALP activity. The presence of ALP in osteoblastic-derived exosomes and breast cancer patients was detected and quantified by monitoring the rate of hydrolysis of p-nitrophenyl phosphate (pNPP) substrate in p-nitrophenol (pNP), as well as the use of ALP activity signal for the total count of exosomes. In addition, the electrochemical biosensor was able to discriminate healthy and breast cancer patients based on specific epithelial cancer-related biomarkers. Moreover, it is important to highlight that the electrochemical assay is more sensitive than the gold standard colorimetric assay. The electrochemical readout was performed on boron-doped microcrystalline diamond (BDD) by square wave voltammetry (SWV).

In the Chapter 7, a draft of the final remarks and the future perspectives of this Ph.D. thesis, including some potential approaches for the improvement in exosomes detection for applications in communicable and non-communicable diseases, are

considered. Finally, in Chapter 8, the main science communication during the Ph.D. thesis period is presented.

List of symbols and abbreviations

i	Current
F	Faraday constant
g	Gravity force
f	Frequency
µA	MicroAmper
mV	MiliVolt
eV	Electron-Volt
E	Potential
E_{sw}	Pulse potential amplitude
E_{sp}	Step potential
V	Volt
λ	Wavelength
ALP	Alkaline phosphatase
antiCD	Anti-Cluster of differentiation
BCA	Bicinchoninic acid
BDD	Boron-doped diamond
BIO	Biotin
BQ	Benzoquinone
BSA	Bovine serum albumin
BW	Bulk wave
CD	Cluster of differentiation
cDNA	Complementary DNA
Cryo-TEM	Cryogenic transmission electron microscopy
CTC	Circulating tumor cell
CV	Cyclic voltammetry or cyclic voltammograms
Cy5	Far-red-fluorescent dye; excitation 647 nm, emission 665 nm
DG-UCF	Density gradient ultracentrifugation
DNA	Deoxyribonucleic acid
dNTPs	2'-deoxyribonucleoside-5'-triphosphates
dsDNA	Double-stranded DNA
EGFR	Epidermal growth factor receptor
ELISA	Enzyme-linked immunosorbent assay
EpCAM	Epithelial cell adhesion molecule
EVs	Extracellular vesicles
Fab	Antigen binding fragment of an antibody
FACS	Fluorescence-activated cell sorting
FRET	Fluorescence resonance energy transfer
FSC	Forward scattered light
GNPs	Gold nanoparticle probes
GOX	Glucose oxidase
HPLC	High-performance liquid chromatography
HQ	Hydroquinone
HRP	Horseradish Peroxidase
HSA	Human serum albumin
IEF	Isoelectric focusing
ILVs	Intraluminal vesicles
IMS	Immunomagnetic separation
LC	Liquid chromatography
LOD	Limit of detection
MAA	Methacrylic acid
m-GEC	Magneto-actuated graphite-epoxy composite
MHC	Major histocompatibility complex
MIPs	Molecularly imprinted polymers
miR	MicroRNA
M-MLV	Moloney murine leukemia virus
MPs	Magnetic particles
mRNA	Messenger RNA
MS	Mass spectroscopy
MVBs	Multivesicular bodies
MVEs	Multivesicular endosomes
MVs	Microvesicles
nPES	Nanoplasmonic-enhanced scattering
NTA	Nanoparticle tracking analysis
OXPHOS	Oxidative phosphorylation
pAP	para-Aminophenol
PBS	Phosphate-buffered saline

PCM	Polarizable continuum model
PCR	Polymerase chain reaction
PEGs	Polyethylene glycols
pNP	para-Nitrophenol
pNPP	para-Nitrophenyl phosphate
QCM	Quartz crystal microbalance
qPCR	Quantitative polymerase chain reaction
Rev	Reverse primer
RNA	Ribonucleic acid
rRNA	Ribosomal RNA
RT	Reverse transcription
SAW	Surface acoustic wave
SCF	Self-consistent-field
SEC	Size-exclusion chromatography
SEM	Scanning electron microscopy
SPR	Surface plasmon resonance
SSC	Side scattered light
SWV	Square wave voltammetry
TMB	3,3',5,5'-tetramethylbiphenyl-4,4'-diamine
tRNA	Transfer RNA
UCF	Ultracentrifugation
VFC	Vesicle flow cytometry

.

CHAPTER 1

Introduction

1.1. The biomarkers in clinical diagnosis

The term *biomarker* is shorthand for a biological marker, which may be related to a normal or abnormal process, a condition or disease. A definition of a biomarker is provided by the World Health Organization (WHO), as follows:

> "*A biomarker is any substance, structure or process that can be measured in the body or its products and influence or predict the incidence of outcome or disease*".

A biomarker can be found in biological fluids such as blood, urine, saliva or tissues. Examples may range from blood pressure, gene expression patterns, the levels of a particular protein in body fluid, or even changes in electrical activity in the brain. Biomarkers are used in research for early diagnosis, enabling more accurate, predictive, and preventive clinical care. The U.S. Food and Drug Administration (FDA) and European Medicines Agency (EMA) emphasize that the biomarkers can speed up the access of patients to safer and more effective treatments, thus reducing the time and cost of clinical trials. Biomarkers are not only useful tools in early diagnosis, but also in drug development, by indicating the drug efficiency or, eventually, toxicity (Kraus, 2018).

Many researchers focus their research on diagnostic biomarkers, which are related to the early detection of a disease or condition, as is the case of cancer.

Currently, the early diagnosis of cancer is performed, in most instances, by visualizing the tumor. This is the case of breast cancer. The American Joint Committee on Cancer estimates that a detectable 0.2 mm cancer cell cluster contains at least 200 cells (Gress et al., 2017). In this case, an early diagnosis can be misleading, because the tumor has already been in the patient for years. Therefore, an ideal and desirable early diagnosis should be performed before growing, spreading and forming new tumors to reduce the mortality rate. Advances in cancer screening require thus more sensitive and specific diagnostic biomarkers.

1.2. The exosomes

Nowadays, extracellular vesicles (EVs) become a worldwide research topic, since they are related to cell-to-cell communication and their production rate are increased in cancer cells (Mathieu et al., 2019; Théry et al., 2018). EVs can be found in both prokaryotic and eukaryotic organisms. They are under intense study because of their role in many physiological and pathological processes. Many scientific meetings are being held to

discuss the EVs' origin, structure, functions, size and other characteristics. For instance, exosomes are agreed to be smaller in diameter (typically 150 nm or smaller) than microvesicles (typically up to 1 μm).

The role of exosomes as biomarkers for early diagnosis has been receiving increasing attention. For instance, it was reported that a breast cancer cell showed an exosomes secretion rate of ~60-65 exosomes per cell per hour (Chiu et al., 2016). This high number of exosomes released by a single cell reveals the potential application of exosomes as biomarkers at early tumor stages.

1.2.1. History of exosomes

Almost four decades ago, two research groups, one in Montreal (Canada) and another in Saint Louis (USA) reported almost simultaneously that immature sheep red blood cells (RBCs) during its maturation process released transferrin receptor and small (~50 nm in diameter) membrane vesicles (Harding et al., 1983; Pan and Johnstone, 1983). A few years later, these vesicles were named as exosomes (Johnstone et al., 1987). The potential use of exosomes in many research areas was increasing during the last years. Fig. 1.1 shows a clear exponential interest in exosomes since the first publication in 1987 (Johnstone et al., 1987) who coined the term exosomes, with >4100 new publications estimated for 2020 (if continue to follow the exponential equation). This exponential interest is related to on the role of exosomes on cell-to-cell communication, immunity, tumor, therapy, intercellular shuttle-like with genetics, lipids, and protein cargo, among others (Mathieu et al., 2019; Théry et al., 2018). Detailed bibliometric analysis of exosomes can be found in the literature (Roy et al., 2018; Y. Wang et al., 2017).

Several meeting around the world were consolidated in societies, as the case of International Society for Extracellular Vesicles and The American Society for Exosomes and Microvesicles, and even a dedicated magazine, Journal of Extracellular Vesicles, due to the potential applications of exosomes. In this context, many consolidated diagnosis companies started to offer commercial kits for the detection, quantification, and characterization of exosomes.

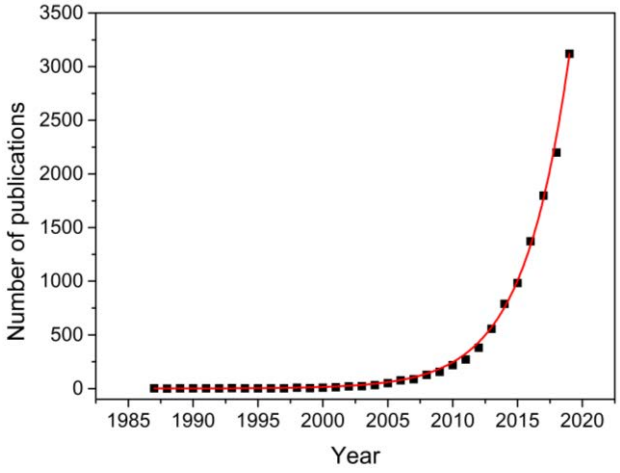

Fig. 1.1. Publications in exosome research annually since 1987 retrieved from a PubMed search of the term "exosome".

1.2.2. Nomenclature recommendation

All living cells can release (exocytosis) and uptake (endocytosis) particles, such as DNA and RNA fragments, vesicles, proteins and lipids, by complex machinery. Among all these entities, the group called extracellular vesicles (EVs) was defined by the International Society for Extracellular Vesicles (ISEV) as:

> "*Extracellular Vesicles is a generic term for particles naturally released from the cell that are delimited by a lipid bilayer and cannot replicate, i.e. do not contain a functional nucleus*" (Théry et al., 2018).

The EVs is a generic terms including all types of vesicles, such as exosomes, ectosomes, microvesicles, apoptotic and non-apoptotic vesicles, among others (Al-Nedawi et al., 2008; Théry et al., 2018). However, many studies used the generic term EVs, or their types, indiscriminately to name any type of secreted vesicles. In the past, the term exosome was used in a wrong way for all kinds of vesicles that sediment after centrifugation at ~70,000-100,000 *g* (Johnstone et al., 1987). This misconception is understandable, due to tiny differences among them in biogenesis, size and cargo. Fig. 1.2 shows a size comparison of exosomes to DNA, red and white blood cells and a circulating tumor cell (CTC).

Exosomes can be thus defined as nanovesicles ranging from 25 to 200 nm in diameter, and with biogenesis arising from multivesicular bodies (MVBs) within the endocytic pathway (Mathieu et al., 2019; Théry et al., 2018). By a mechanism not fully understood (Zhang, 2013), exosomes are filled with cytoplasmic contents of the cell. One possible path can be a fusion with the plasmatic membrane to release exosomes into the

intracellular space (Mathieu et al., 2019; Théry et al., 2018). Exosomes show density ranging from 1.13 to 1.19 g mL^{-1} in sucrose (Théry et al., 2009), although some differences in this parameter, depending on their cellular origin were reported (Raposo et al., 1996). More details on exosomes will be discussed later in this dissertation.

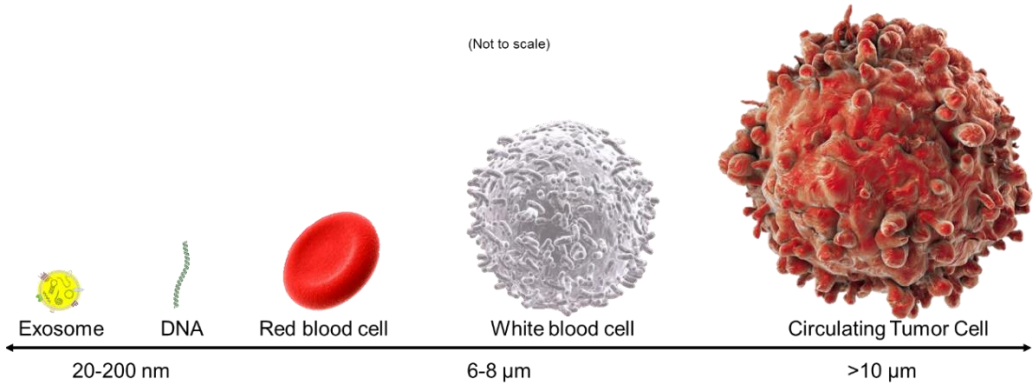

Fig. 1.2. Comparison of the size of exosomes with DNA molecule, red and white blood cell and a circulating tumor cell (CTC). Figure created using Servier Medical Art templates, which are licensed under a Creative Commons Attribution 3.0 Unported License.

Ectosomes are, instead, 100 to 500 nm in diameter. They have their biogenesis from the outward budding of the plasma membrane and may contain nucleic acids (Meldolesi, 2018; Théry et al., 2018). Ectosomes contain proteins such as integrins, tetraspanins and a few receptors at relatively low density (Meldolesi, 2018). In fact, the CD81 tetraspanin is 22-fold enriched in exosomes compared to ectosomes derived from SH-SY5Y neuroblastoma cell line, while other tetraspanins, such as TSPAN9 and TSPAN14, are exclusively identified in exosomes (Keerthikumar et al., 2015). Nonetheless, ectosomes are also described as having a density similar to the exosomes, ranging from 1.14 to 1.20 g mL^{-1} in sucrose gradient (Keerthikumar et al., 2015). Other microvesicles (MVs) are ranged from 500 to 1000 nm in diameter and, as well as the ectosomes, they also have their biogenesis from the outward budding of the plasma membrane, and a density ranging from 1.04 to 1.07 g mL^{-1} in sucrose (Théry et al., 2009).

Cells undergoing apoptosis and fragmentation also release vesicles formed by apoptotic cell membrane blebbing (Théry et al., 2018). Apoptotic vesicles are much larger (>1000 nm) and are described as having a density ranging from 1.16 to 1.28 g mL^{-1} in sucrose (Théry et al., 2009).

Recently, it was demonstrated by scanning electron microscopy (SEM), an HIV-1 membrane-enclosed structure of ~120 nm in diameter, very similar to exosomes (Dick et al., 2018). Nonetheless, HIV-1 virus membranes are also enriched in tetraspanins, such as

CD63 (Orentas and Hildreth, 2009) and CD81 (Grigorov et al., 2009), which are also the most frequently identified proteins in exosomes and considered as classical biomarkers (Chow et al., 2015; Hemler, 2013). Also, nanovesicles and HIV-1 virus have similar densities to be separated by sucrose density gradients (Gluschankof et al., 1997). Gluschankof et al., estimated a 1.15 g mL^{-1} sucrose density for the HIV-1 virus (Gluschankof et al., 1997), which may overlap with the density of the EVs (Théry et al., 2009). This is just one example of how complicated it may be to isolate and purify exosomes from other EVs. Circulating vesicles are a complex composition of exosomes, ectosomes and other MVs. It is important to highlight that the current purification methods, as discussed later, do not allow discrimination among them.

1.2.3. Other extracellular vesicles

In the last few years, different studies have revealed new types of EVs, such as the oncosomes (Al-Nedawi et al., 2008) and the spheresomes (Junquera et al., 2016). Non-apoptotic membrane blebs can be shed from cancer cells in the form of large vesicles ranging from 1 to 10 μm, called large oncosomes.

Another type of EVs released by the cells in the extracellular media is the spheresomes, with a lipid bilayer membrane ranging from 40 to 125 nm diameter (Junquera et al., 2016). Spheresomes are shedding from a spherical membrane structure (0.5 to 1.5 μm), and are not released through the fusion of MVBs or plasma membrane budding as exosomes, ectosomes or other MVs, but as a cluster wrapped by large multivesicular spheres surrounded by a limiting lipid membrane (Junquera et al., 2016).

The study of the biogenesis, membrane composition and internal content of EVs is highly important to establish their functions. Currently, the role of large oncosomes (Meehan et al., 2016; Minciacchi et al., 2015a, 2015b) and spheresomes (Junquera et al., 2016) is under investigation (Minciacchi et al., 2015a, 2015b).

Among the different types of EVs, this Ph.D. thesis is focused on exosomes from 20-150 nm originated from MVEs, enriched with membrane-bound tetraspanin proteins and obtained by ultracentrifugation at 100,000 *g*.

1.2.4. Biogenesis and composition

As briefly explained in the previous sections, the exosomes (Johnstone et al., 1987) are cell-derived nano-sized and spherical-shaped vesicles (Théry et al., 2002), enclosed by

a lipid bilayer, with varied diameter depending on their origin. As a difference of plasma membrane microvesicles (MVs), exosomes are derived from the endosomal secretory pathway. This interesting topic was extensively reviewed (Stuffers et al., 2009; Zhang, 2013).

The Fig. 1.3 summarizes the biogenesis of exosomes and microvesicles. Briefly, exosomes are produced from the in-budding of endosomes via endocytic invagination within the endosomal network. These endosomes at early stage fuse with endocytic vesicles (i) and incorporate their content, (ii) as well as the cytoplasmic cargo (iii), are selected by sorting mechanisms (as yet not comprehensively elucidated) into vesicles destined for recycling, degradation, or exocytosis (Zhang, 2013). Then, early endosomes turn forms in late endosomes or multivesicular bodies (MVBs) that contain intra-luminal vesicles (ILVs). The main fate of MVBs is the fusion with lysosomes (iv), but in many eukaryotic and prokaryotic cells types, MVBs fuse with the plasma membrane (v). These findings indicate that the MVBs have a dual destination, iv) the fusion with the lysosome, or v) the fusion with the plasma membrane. The lysosome fusion route is the end line of the MVBs. On the other hand, the cell membrane fusion route to release ILVs extracellularly as exosomes in the extracellular space opens many destination routes for ILVs (Zhang, 2013).

Interestingly, one of the findings of this dissertation is that eukaryotic cells in culture can release MVBs-like around 200-600 nm and non-uniform shape. However, 40-150 nm exosomes showed a well-circular shape. It was not confirmed, since it is beyond the topic of this dissertation, whether these types of MVBs-like were sprouted from plasmatic membrane, or by the storage conditions. Nonetheless, a single exosome was observed with one or more than one lipid bilayer, (Fig. 1.4 panel A and B, respectively), as well as MVBs with ILVs (exosomes) inside them (Fig. 1.4 panel C and D, respectively). These findings were obtained by cryogenic transmission electron microscopy (Cryo-TEM).

Different types of cell lines, including normal and tumor cells, release exosomes in many different biological fluids such as blood (Qi et al., 2016), plasma (Gallart-Palau et al., 2015), saliva (Sun et al., 2016), semen (Vojtech et al., 2014), serum (Hornick et al., 2015), urine (Fenner, 2016).

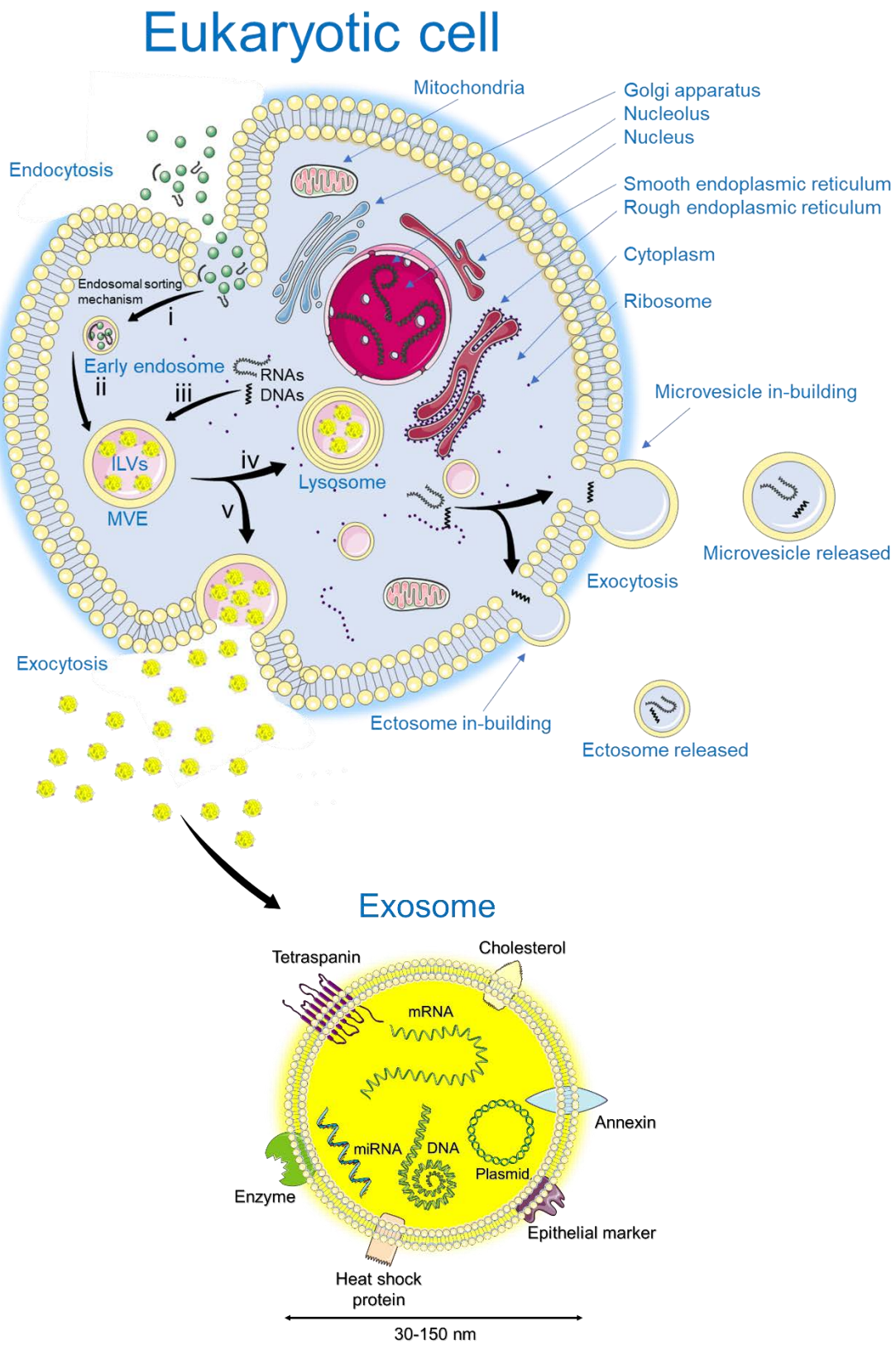

Fig. 1.3. Biogenesis and release of exosomes and microvesicles. A schematic representation of the exosomes also is represented. Figure created using Servier Medical Art templates, which are licensed under a Creative Commons Attribution 3.0 Unported License.

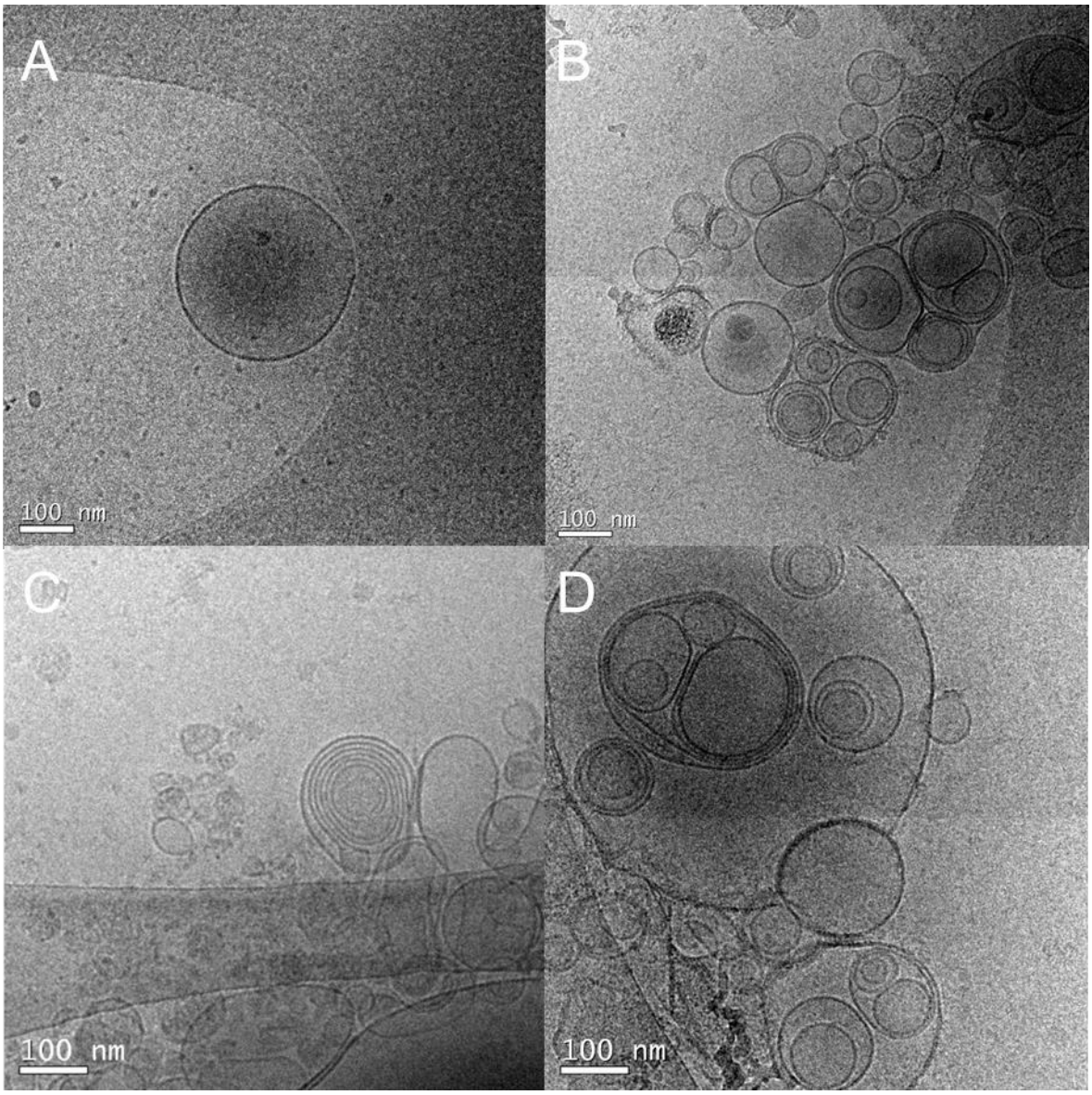

Fig. 1.4. Cryo-TEM images of the exosomes-derived from human serum. These exosomes were applied onto formvar-carbon EM grids, maintained at -182 °C with 200-kV acceleration voltage during the whole process. The images were obtained in the Service of Microscopy, Universitat Autònoma de Barcelona.

Besides the endosomal biogenesis of exosomes being different from plasma membrane MVs, exosomes are somewhat unique in their composition and highly stables in many biological fluids, as described above (Boukouris and Mathivanan, 2015), as well as their cargo (Sanz-Rubio et al., 2018). For instance, messenger RNA (mRNA) (Shao et al., 2015), microRNA (mRNA or miR) (Alexander et al., 2015), ribosomal RNA (rRNA) (Kilchert et al., 2016), transfer RNA (tRNA) (Houseley et al., 2006), deoxyribonucleic acid (DNA) (Balaj et al., 2011), lipids and proteins (Théry et al., 2002) were isolated from exosomes. A web-based compendium of exosomal cargo, ExoCarta, provides a list of 9,769 proteins, 3,408 mRNAs and 2,838 miRNAs, which several play important roles in many biological mechanisms (Mathivanan and Simpson, 2009). A schematic representation of the

exosomes is shown in Fig. 1.3. Further complete and well-detailed information on the mechanistic of biogenesis and composition of the exosomes was previously reviewed in detail (Zhang, 2013).

1.2.5. The function of exosomes

The first discovery of the biological-related function of exosomes, includes glucose and nucleoside transporter and transferrin receptor (Johnstone et al., 1987). Since then, it was reported that the exosomes contain in their membrane as well as in their cargo, a range of material from their parental cell. The interest in exosomes and their wide range of intrinsic functions and possible applications in many biological mechanisms has considerably increased. Among them, exosomes were described as an intercellular shuttle-like of cargo as mRNA (Shao et al., 2015), microRNA (Alexander et al., 2015), rRNA (Kilchert et al., 2016), tRNA (Houseley et al., 2006), DNA (Balaj et al., 2011), lipids and proteins (Théry et al., 2002). The exosomes may play a role in several normal and abnormal biological mechanisms, such as communication for tissue regeneration (Bjørge et al., 2018), transport transcription (Silla et al., 2018), blood coagulation (Kapustin et al., 2017), activation of cell surface receptors (Hong et al., 2017), carrier of immunosuppressive cargo in cellular immunotherapy (Hong et al., 2017), as well as in cancer progression and metastasis (Fu et al., 2018), to name only a few. This topic is discussed in the next section.

1.2.6. Role of exosomes in cancer

As it was previously stated, there is strong evidence indicating that exosomes operate as an intercellular shuttle-like transferring their cargo from donor to recipient cells, promoting the cell-to-cell communication (Mathieu et al., 2019). As a consequence of this activity, exosomes can affect physiological and pathological processes. It is important to mention their role in both cancer metastasis suppression (Plebanek et al., 2017) and progression (Fu et al., 2018).

The exosomes released by cancer cells contain diverse biomolecules that are transferred to others, promoting a long-range cancer proliferation and establishing a premetastatic status within the tumor microenvironment (Maia et al., 2018). It was reported that tumor-derived exosomes can activate anti-apoptotic pathways by a ligand-receptor interaction involving TGF-β1, which promotes the proliferation and survival of tumor cells, both *in vitro* and *in vivo* (Raimondo et al., 2015). Exosomes-mediated transfer of long noncoding RNA ZFAS1 promotes gastric cancer tumor growth and metastasis (Pan et al.,

2017). Tumor-derived exosomes deliver miRNA, such as miR-9, which are uptake in vivo by normal fibroblasts turn on into cancer-associated fibroblasts (Baroni et al., 2016).

Although tetraspanins themselves are commonly used as general biomarkers of exosomes, it was demonstrated that altered levels of tetraspanins in exosomes can transfer metastasis-related function to a non-tumorigenic cellular population (Brzozowski et al., 2018). Tumor-derived exosomes secreted by breast cancer cells were capable of transforming normal human mammary epithelial cells into cancer cells, by transferring cross-linking enzyme tissue transglutaminase (tTG) (Antonyak et al., 2011).

Breast cancer-derived exosomes also contain miRNAs that regulate the tumor microenvironment. For instance, exosome-mediated miR-10b secretion can be transferred among different cell lines through direct uptake, promoting cell invasion ability in breast cancer cells (Singh et al., 2014). Several other exosome-mediated miRNAs were associated with breast cancer development (Santos et al., 2018; Takahashi et al., 2015; Zhou et al., 2014).

Several studies also showed that the release of exosomes induced by hypoxia promoted cancer progression. For instance, low pH and hypoxia, potentially favored the release of exosomes and their uptake by cancer cells (Parolini et al., 2009). A similar effect was evidenced for breast cancer cell lines under severe (0.1% O_2) hypoxia, where the release of exosomes may be mediated by hypoxia-inducible factor (HIF-1α) oxygen-sensing system (King et al., 2012). Recently, it was demonstrated a higher number of exosomes secreted by prostate cancer cells under hypoxia, by promoting also tumor growth. Interestingly, hypoxic exosomes also showed a higher amount of lactic acid (Panigrahi et al., 2018).

1.2.7. Role of exosomes in early diagnosis

As it was previously discussed, due to the role of exosomes in cell-to-cell communication in cancer, they are currently under intensive study as novel biomarkers for the early diagnosis of cancer (Mathieu et al., 2019). Moreover, exosomes showed to have high stability in different biological fluids (Boukouris and Mathivanan, 2015), which make them an ideal candidates for minimally invasive liquid biopsy.

The Table 1.1 summarizes a description of the biomarkers selected in this thesis, highlighting the most prominent carcinomas in 2018 correlated with such biomarkers. For instance, higher levels of CD147/CD9 in exosomes were found in colon cancer patients than healthy controls (Yoshioka et al., 2014). Overexpression of epithelial cell adhesion

molecule (EpCAM or CD326) in exosomes was related to the severity of ovarian carcinoma compared to healthy controls (Taylor and Gercel-Taylor, 2008). EpCAM and CD24-positive exosomes were respectively 6.5-fold and a 3-fold increase in ovarian cancer patients (Zhao et al., 2016). More recently, circulating EpCAM-positive exosomes showed to be increased significantly in breast cancer patients compared to healthy controls (Fang et al., 2017). These findings demonstrated that EpCAM and CD24 tumor-derived exosomes could be useful for the diagnosis of cancer patients.

Another point that should be considered on the potential use of exosomes as biomarkers in early diagnosis is their release rate. The use of exosomes in this thesis as a promising biomarker is based on the expected improvement in the sensitivity compared to conventional biomarkers, considering that one altered cell can produce (and eventually release) a huge amount of exosomes (Davidson et al., 2018). For instance, it was reported that a single breast cancer cell can release ~60-65 exosomes per hour (Chiu et al., 2016). Similar studies from glioblastoma multiforme and medulloblastoma was estimated to ~270 and ~527 exosomes per cell per hour, respectively (Balaj et al., 2011). This high amount of exosomes released by a single cell reveals the potential application of exosomes as biomarkers for the sensitive detection at early stages of a disease, compared to conventional biomarkers. Moreover, a single exosome can also display a high number of repeated biomarkers on the membrane or as a cargo.

It is important to highlight that the number of exosomes released or uptake by a cell is dependent on the type, as well as by external factors (culture medium, supplement, stress, just to mention a few) (Davidson et al., 2018). The number of EVs in biological fluids was estimated at 1×10^1 to 3×10^7 exosomes μL^{-1} (Zhang et al., 2016). The high exosome release rate by a single cell per hour is very promising for applications of exosomes as biomarker for an ideal and minimal invasive early diagnosis by detecting the presence of tumor cell and tumor deposit in the very early stage of growth.

1.3. Exosome isolation methods

As it was previously discussed in this dissertation, the purification of exosomes is a challenging task, not only due to the low concentration of exosomes, but also due to the complexity of the nanovesicles as well as the presence of soluble biomarkers in the complex matrixes. The next sections describe the different methods for exosome isolation and preconcentration. Among them, differential and density gradient centrifugation, size exclusion chromatography, filtration and polymer-based precipitation are the most popular isolation methods for exosomes.

Table 1.1. Description of the biomarkers selected in this work.

Biomarker	Length/Mass*	Description*	Function*	Most prominent carcinomas in 2018**	Reference
CD9	141-228 aa / 15.9-25.4 kDa	Cell-surface proteins member of the transmembrane 4 superfamily, also known as the tetraspanin family. Tetraspanins are extensively and variably glycosylated.	Involved in cell adhesion, migration and motility and also platelet activation and aggregation.	Breast Prostate Lung Colorectum Stomach Liver	(Rappa et al., 2015) (Zvereff et al., 2007) (Kohmo et al., 2010) (Kim et al., 2016) (Yoshioka et al., 2014) (Murayama et al., 2015) (Zheng et al., 2005)
CD63	133-238 aa / 14.3-25.6 kDa			Breast Prostate Lung Colorectum Stomach Liver	(Tominaga et al., 2014) (Gong et al., 2013) (Kwon et al., 2007) (Wang et al., 2015) (Miki et al., 2018) (Cho et al., 2017)
CD81	51-274 aa / 5.6-29.8 kDa			Breast Prostate Lung Colorectum Stomach Liver	(Zhang et al., 2018) (Logozzi et al., 2017) (Guilmain et al., 2011) (Chiba et al., 2012a) (Yoo et al., 2013) (Bruening et al., 2018)
CD24	37-129 aa / 4.1-13 kDa	Cell-surface small protein that is heavily and distinctly glycosylated. It is a sialoglycoprotein expressed in B-cell development and B-cell neoplasia and a large variety of malignant tumors.	Involved in the regulation of cell binding capacity, proliferation, maturation and tumor metastasis.	Breast Prostate Lung Colorectum Stomach Liver Ovarian	(Fang et al., 2010) (Y. Zhang et al., 2017) (Kristiansen et al., 2003) (Ke et al., 2012) (Wang et al., 2014) (Lee et al., 2011) (Zhao et al., 2016)

Table 1.1. *Cont.*

CD44	78-742 aa / 8.8-81.5 kDa	Cell-surface transmembrane glycoprotein which is a receptor for hyaluronic acid (HA) and other ligands, such as osteopontin, collagens, and matrix metalloproteinases (MMPs). It is also frequently called HCAM (homing cell adhesion molecule)	Involved in in cell activation, proliferation, differentiation, recirculation and homing, hematopoiesis and tumor metastasis.	Breast Prostate Lung Colorectum Stomach Liver	(Louderbough and Schroeder, 2011) (Iczkowski, 2010) (Hu et al., 2018) (Shiozawa et al., 2014) (Heo et al., 2015) (Dhar et al., 2018)
CD54	180-532 aa / 19.4-57.8 kDa	Cell-surface transmembrane glycoprotein of the immunoglobulin superfamily. Typically expressed on endothelial cells and also found in epithelial cells and cells of the immune system. Frequently called ICAM-1 (intercellular adhesion molecule 1).	Involved in leukocyte endothelial transmigration, cell signaling, adhesion, polarity, cell-cell interaction, tissue stability and tumor metastasis.	Breast Prostate Lung Colorectum Stomach Liver	(Guo et al., 2014) (Li et al., 2017) (Gerbitz et al., 2005) (Fang et al., 2016) (Yashiro et al., 2005) (J. Wang et al., 2013)
CD326	199-342 aa / 21-37.9 kDa	Cell-surface transmembrane glycoprotein which mediates cell adhesion in epithelia. Plays a role in tumorigenesis and metastasis of carcinomas. It is also frequently called EpCAM (epithelial cell adhesion molecule).	Involved in cell signaling, migration, proliferation, differentiation and tumor metastasis.	Breast Prostate Lung Colorectum Stomach Liver Ovarian	(Vang et al., 2017) (Fang et al., 2017) (Beretov et al., 2018) (Hasegawa et al., 2017) (Nicolazzo et al., 2017) (Dai et al., 2017) (Matsumoto et al., 2017) (Taylor and Gercel-Taylor, 2008)
CD340	102-1255 aa / 11.5-137.9 kDa	Cell-surface transmembrane glycoprotein that is a receptor for members of the epidermal growth factor (EGF) family. Plays a role in tumorigenesis and metastasis of carcinomas. Frequently called HER2 (human epidermal growth factor receptor 2).	Involved in the binding with ligand-bound epidermal growth factor (EGF) receptor family members, enhancing kinase-mediated activation of downstream signaling pathways and tumor metastasis.	Breast Prostate Lung Stomach Liver	(Levva et al., 2017) (Day et al., 2017) (Bethune et al., 2010) (Galizia et al., 2007) (Komposch and Sibilia, 2015)

*****Data were taken from The Human Protein Atlas; https://www.proteinatlas.org/
******Most prominent carcinomas in 2018 were taken from Global Cancer Observatory: https://gco.iarc.fr/
Table from Moura et al., 2020a.

On the other hand, solid-phase methods are currently under development for their integration in point-of-need, rapid tests, such as microfluidic and biosensing platforms.

Each of these isolation methods has its own advantages and disadvantages or limitations. A brief review of traditional and emerging methods for the isolation from biological samples is provided below.

1.3.1. Traditional methods for isolation of exosomes

1.3.1.1. Differential centrifugation

Differential centrifugation remains one of the most popular techniques and is still considered the gold-standard method for exosome isolation (Fig. 1.5). This technique was the first one described to isolate exosomes from reticulocyte tissue culture medium (Johnstone et al., 1987) and it was further optimized (Théry et al., 2006) by increasing *g* values to up to 100,000 *g*. The main objective of centrifugation is to eliminate dead cells and debris (Fig. 1.5, panel A). It is important to highlight that the exosomes from biological fluids (blood plasma, serum or saliva) usually require higher-speed and longer time compared to exosomes obtained from cell culture supernatants (Théry et al., 2006).

Differential centrifugation has the advantages of being a well-establish methodology, moderately time-consuming with little or no sample pretreatments and cost-saving (compared with density-gradient centrifugation). Moreover, it usually provides larger yields. The major drawbacks of differential ultracentrifugation are the use of costly, benchtop equipment, requiring maintenance and laboratory facilities. Moreover, ultracentrifugation can produce mechanical damage and low purity of isolated exosomes with the coexistence of other non-exosome vesicles and protein aggregates. These issues can be minimized by combining ultracentrifugation with a previous filtration step (with 0.22 μm filter diameter). In this instance, the purity of the isolated exosomes increased, but the yields may be adversely affected.

1.3.1.2. Density gradient centrifugation

Density gradient ultracentrifugation (Witwer et al., 2013) typically improves the particle separation efficiency, by isolating exosomes from non-vesicular particles, such as proteins and protein/RNA aggregates (Fig. 1.5, panel B).

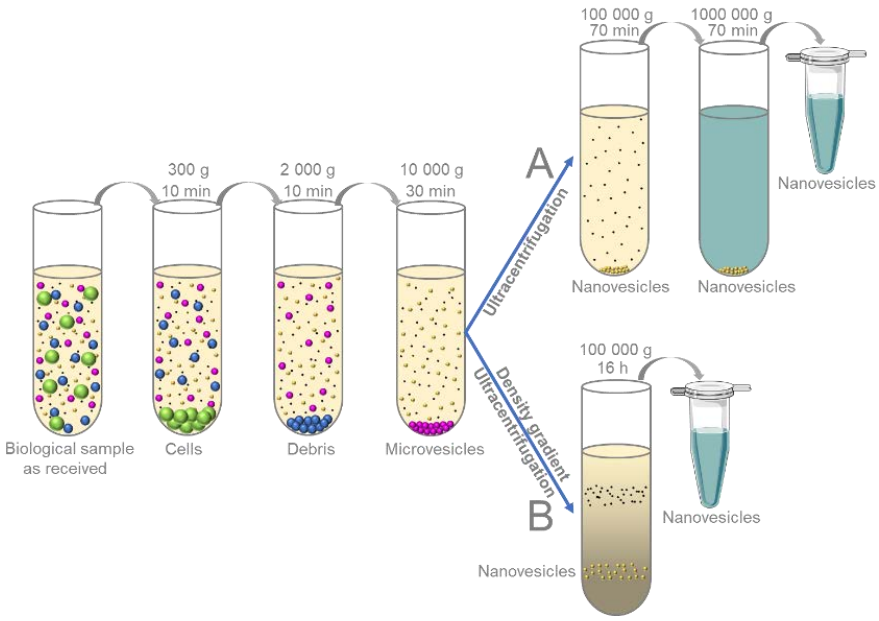

Fig. 1.5. Differential centrifugation consists of consecutive steps, including low-speed centrifugation to remove cells and apoptotic debris (300 *g* and 2,000 *g*), higher speed spin to eliminate larger vesicles (10,000 *g*) and finally, high-speed centrifugation to precipitate exosomes (100,000 *g*) (panel A). Finally, the isolated exosomes are once again re-suspended and stored at -80 ºC for further analysis. Panel B shows the density gradient ultracentrifugation from 10,000 *g* centrifuged sample with a sucrose density gradient. The isolated exosomes can be obtained in fractions. Figure created using Servier Medical Art templates, which are licensed under a Creative Commons Attribution 3.0 Unported License.

Density gradient ultracentrifugation enables the separation of subcellular components, such as mitochondria, peroxisomes, and endosomes (Araùjo et al., 2008; Graham, 2001). Nonetheless, is one of the most efficient methods for isolating exosomes in high viscosity samples, as saliva (Iwai et al., 2016). OptiPrep™ (Abbott Laboratories, Chicago, Illinois, USA) is a density gradient medium commercially available kit for the isolation and purification of a wide range of particles, including exosomes (Van Deun et al., 2014). OptiPrep™ is a non-ionic iodixanol-based medium with a density of 1.320 g mL^{-1}.

Density gradient ultracentrifugation method provides exosomes of higher purity and yields while maintaining their structure. The centrifugation time is a critical parameter, because particles with similar densities may contaminate other exosomal fractions.

1.3.1.3. Size-exclusion chromatography

Size-exclusion chromatography is used to separate particles based on their size. The particles move through the filtration column at different rates accordingly to their size (Taylor and Shah, 2015). Size-exclusion chromatography is widely implemented to isolate exosomes from blood plasma (Taylor et al., 2002) and urine (Lozano-Ramos et al., 2015). Although the size-exclusion chromatography method is used for obtaining purified

exosomes at short isolation time, damage may occur (Witwer et al., 2013). Sepharose-based columns offer good cost-benefit to obtain purity exosomes (Gámez-Valero et al., 2016; Lozano-Ramos et al., 2015). Commercial kits are available, such as Exopure™ (BioVision, Milpitas, CA, USA), PURE-EVs Columns (HansaBioMed, Tallinn, Estonia), qEV Exosome Isolation (Izon Science, Christchurch, Canterbury, New Zealand).

1.3.1.4. Filtration

Micro- or ultrafiltration membranes can also be used for the isolation of exosomes, being an alternative to ultracentrifugation. It is based on pore size or molecular weight (MW) filtration membrane, that allows particles with specific sizes or MW to pass through the porous membrane, while the particles with higher sizes and MW remain trapped in the filtration membrane. As an example, ultrafiltration based molecular-weight membrane was used to isolate urinary exosomes (Rood et al., 2010) and from a bronchial epithelial cell culture supernatant (Benedikter et al., 2017).

An advantage of filtration is that it is less time-consuming and simpler than ultracentrifugation. However, as air pressure is used to facilitate the pass of the particles through the membrane, the clogging of the membrane pores due to newly formed aggregates can cause the loss and damage of exosomes (Taylor and Shah, 2015). Also, the membranes are expensive, and it is not possible to reuse them.

Although large and rigid particles are separated, large (100 nm), but flexible particles are able to pass through the filter. Therefore, to increase the purity of the exosomes, ultrafiltration is commonly used in combination with size exclusion chromatography (Benedikter et al., 2017; Rood et al., 2010). Some commercial membranes are available in different pore sizes (800-100 nm pore diameters), such as ExoMirTM (Bioo Scientific Corporation, Austin, TX, USA), Durapore® Membrane Filter (Merck Chemicals & Life Science S.A, Darmstadt, Hessen, Germany), Vivaspin® (Sartorius Lab Instruments GmbH & Co. KG, Goettingen, Lower Saxony, Germany) and exoEasyTM (Qiagen, Hilden, North Rhine-Westphalia, Germany).

1.3.1.5. Polymer-based precipitation

This methodology relies on precipitation using polymers, such as polyethylene glycols (PEGs) (Lewis and Metcalf, 1988). The principle of Polymer-based precipitationis to use a reagent that binds to water molecules and thereby forcing the less-soluble

components, such as EVs, to sediment out of the solution, allowing them to be collected by a short, relatively low-speed centrifugation or filtration.

The polymer-based precipitation features for exosomes isolation were reported by many researchers (Deregibus et al., 2016; Niu et al., 2017; Rider et al., 2016). Polymer-based precipitation demonstrates to be efficient, preserving biological activities of exosomes from the endometrial cell line (Niu et al., 2017), as well as from healthy human serum and saliva (Deregibus et al., 2016). Some commercial kits based on this principle are ExoQuick™ (System Biosciences, Mountain View, CA, USA), Exo-spin™ (Cell Guidance Systems, Babraham, Cambridge, UK), ExoPrep (HansaBioMed, Tallinn, Estonia), Exosome Purification Kit (Norgen Biotek, Thorold, Ontario, Canada), miRCURY Exosome Isolation Kit (Exiqon, Vedbaek, Denmark) and Total Exosome Isolation Reagent (Life Technologies Corporation, Carlsbad, CA, USA). These polymer-based precipitation kits are effective for extracts exosomes of 40-180 nm in diameter, excluding macrovesicles. As the main drawbacks of this tecnhique, contaminants non-vesicular components such as lipoproteins, albumin, apolipoprotein E and Tamm–Horsfall protein, can be coextracted with the exosomes, which impair their subsequent analysis (Lobb et al., 2015; Van Deun et al., 2014). Finally, these kits are expensive.

1.3.2. Novel methods for isolation of exosomes

1.3.2.1. Solid-phase separation based on paramagnetic particles

The immunomagnetic separation (IMS), as in the case of other biological targets, uses biomarker-coated magnetic particles that can specifically bind to a target. Our group has recently reviewed current advances on magnetic separation for biomarker detection of global infectious diseases (Carinelli et al., 2015) and foodborne pathogens (Brandão et al., 2015), showing that this technology is widely incorporated for researchers worldwide in classical methods, in biomolecular tools and emerging technologies, including biosensors and microfluidic devices.

Furthermore, magnetic particles (MPs) are used as a powerful and versatile preconcentration tool in a variety of analytical and biotechnology applications (Reddy et al., 2012). MPs are usually coated with antibodies against the exosome-receptor molecules. Once the exosomes are captured, a magnetic field is then applied to separate the exosomes-coated MPs from the biological sample for further analysis without the interference of the matrix. For instance, commercial Dynabeads® M-450 tosyl activated (Life Technologies Corporation, Carlsbad, CA, USA) superparamagnetic particles (MPs, 4.5 μm in diameter) has a core of iron oxide salt encapsulated by a polystyrene polymer, which

has a polyurethane external layer with the p-toluenesulfonate group (Xu et al., 2012). It is a good leaving group, which allows an S_N2 reaction to occur in the presence of a nucleophile (Cahiez et al., 2012; Hoogenboom et al., 2010). A nucleophilic reaction by an antibody, protein, peptide, or glycoprotein removes and replaces the sulfonyl ester groups from the polyurethane layer.

Fig. 1.6 shows an example of covalent immobilization approaches of antibodies on tosylactivated magnetic particles (panel A), followed by immunomagnetic separation of the exosomes (panel B). The covalent immobilization (Fig. 1.6, panel A) is based on a S_N2 reaction, involving a nucleophilic reaction by the amine moieties mainly from lysine residues of the proteins, removing and replacing the sulfonyl ester groups from the polyurethane layer. The IMS (Fig. 1.6, panel B) is based on the immunoaffinity of the antibody immobilized on MPs towards the specific receptor present on the exosomal surface. Other types of magnetic particles are widely available in companies such as System Biosciences, Pierce, Miltenyi Biotec, HansaBioMed, Aethlon Medical, New England Peptide, etc.

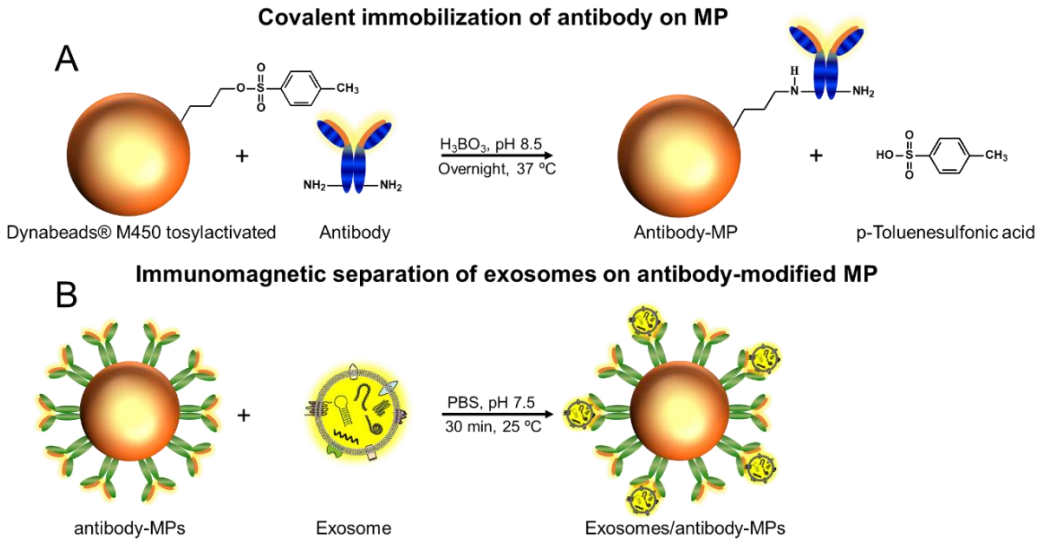

Fig. 1.6. Immobilization approaches of exosomes on Dynabeads® M-450 tosyl activated (MPs). (A) Covalent immobilization of specific antibodies on MPs, or (B) IMS on antibody-modified MPs. Figure created using Servier Medical Art templates, which are licensed under a Creative Commons Attribution 3.0 Unported License.

Venceremin peptide (Ghosh et al., 2014), heparin (Balaj et al., 2015), annexin A5 (Shih et al., 2016), tetraspanins (Doldán et al., 2016) and aptamers (Dong et al., 2018), were successfully used for the IMS of exosomes. CD9, CD63 and CD81 tetraspanins molecules as the most frequently identified proteins in exosomes and are considered classical biomarkers for exosomes. As a consequence, these general tetraspanins are commonly used for the isolation of exosomes using IMS (Chow et al., 2015; Hemler, 2013; Moura et al., 2020b, 2020a, 2020c).

The main advantage of the IMS is the ability to isolate exosomes by a specific immunological reaction, separating an exosome subpopulation expressing a biomarker. Moreover, IMS is a very gentle method that ensures integrity and purity. Also, it is easy to carry out by one-step incubation with the sample to form exosome-magnetic particle complexes and does not require benchtop instrumentation. Another advantage is the low cost per assay, comparing with other methods, such as size-exclusion chromatography, polymer-based precipitation and filtration. The particle-based magnetic enrichment simplifies exosomes isolation and can be easily coupled with emerging technologies as is the case of microfluidic chips or biosensors. However, a main drawback of IMS is the lack of classification based on the size. We also demonstrated the interferences of free receptors present in the serum, including the tetraspanins CD9 and CD63, which can prevent or interfere with the immunomagnetic separation based on these receptors. Interestingly, the immunomagnetic separation of the exosomes based on CD81 is not afected by the serum (even if it is undiluted) (Moura et al., 2020a).

Table 1.2 summarized the commercial antibodies which were successfully immobilized on tosylactivated MP for further IMS of the exosomes.

Table 1.2. Summary of the antibodies covalently immobilized on Dynabeads® M450 Tosylactivated, nº 14013, 4.5 µm diameter for the immunomagnetic isolation of exosomes (adapted with permission from Moura et al., 2020a)

Antibody	Target	Clonality	Conjugate	Host	Reference	Commercial source
antiCD24	CD24	monoclonal	no	mouse	ab76514	Abcam
antiCD54	CD54	monoclonal	no	mouse	ab2213	Abcam
antiCD326(*)	CD326	monoclonal	no	mouse	ab7504	Abcam
antiCD340	CD340	monoclonal	no	mouse	Ab30	Abcam
antiCD9	CD9	monoclonal	no	mouse	10626D	Thermo Fisher
antiCD63	CD63	monoclonal	no	mouse	10628D	Thermo Fisher
antiCD81	CD81	monoclonal	no	mouse	10630D	Thermo Fisher
antiCD44	CD81	monoclonal	no	mouse	BMS113	eBioscience
antiCD81	CD81	polyclonal	no	rabbit	HPA007234	Sigma-Aldrich

Note (*) No isolation of exosomes were obtained for CD326 (Epcam during IMS, since upon immobilization on the MP, no binding of exosomes was observed, perhaps due to a bad orientation during covalent immobilization). However, this antibody was useful for indirect labelling (as primary antibody) in flow cytometry, ELISA and electrochemical immunosensor.

1.3.2.2. On-chip isolation of exosomes

Microfluidic is currently being used for the development of handheld point-of-need isolation of exosomes. Some examples are described in this section.

A microfluidic device based on a porous silicon nanowire-on-micropillar structure (Z. Wang et al., 2013) demonstrated to selectively trap lipid vesicles within interstitial sites between the nanowires during filtration of biofluids.

Acoustic-based microfluidic platform (Lee et al., 2015) demonstrated efficiency to isolate exosomes from human ovarian carcinoma cell culture supernatant and packed red blood cell (pRBC) units. Recently, the acoustofluidic platform was able to isolate exosomes directly from undiluted blood samples with high purity and yield (Wu et al., 2017).

IBM Thomas J. Watson Research Center has developed a deterministic lateral displacement pillar arrays (Wunsch et al., 2016) which separates and concentrates exosomes derived from human urine as small as 20 nm in continuous flow. The device applies the principle of deterministic lateral displacement (Huang et al., 2004) across each pillar arrays contained on a single chip.

Microfluidic viscoelastic flows (C. Liu et al., 2017) separate exosomes from cell culture media and serum in a continuous and size-dependent manner by using a polymer as the additive in a media to control the viscoelastic forces exerted on exosomes. The principle is based on the addition of a polymer (poly-(oxyethylene)), making the fluid highly viscoelastic and, consequently, generate elastic support forces on the suspended nanoparticles in a Poiseuille flow to control their positions. Then, large and small nanoparticles migrate to microchannels at different rates of migration.

Alternating current electrokinetic device (Ibsen et al., 2017) isolated glioblastoma exosomes from undiluted human plasma samples. The principle is based on alternating current (AC) electric field, creating a dielectrophoretic separation force. The difference in the dielectric constant properties of the nanoparticles and surrounding fluid determines the dielectrophoretic forces, which responds sensitively to an external electric field (Ramos et al., 1998). When an external electric field is applied, nanoparticles into fluid medium are reorienting themselves at different speeds, which pull the nanoparticles into the dielectrophoretic high-field regions of the alternating current electrokinetic device.

Exosome Total Isolation Chip (ExoTIC) (F. Liu et al., 2017) is another microfluidic device that uses the filtration approach by a nanoporous membrane (polycarbonate and polyethersulfone filters) in which exosomes in the 30-200 nm size range are obtained.

Although microfluidic devices hold several advantages over traditional methods in terms of analytical simplification, the cost of production and the expensive fabrication processes, as well as the requirement, in most cases, of bench-top equipment for the readout, still constitutes a bottleneck and may put them out of range for end users.

1.4. Exosome characterization

In addition to their potential role as biomarker (Saeedi et al., 2019), the exosomes are designed to bring molecular cargo from one cell to another (Murphy et al., 2019). The exosomes could thus be loaded with a therapeutic cargo, enabling highly targeted delivery of drugs to specific types of cells, and sparing all the other kinds of cells from damage (Kojima et al., 2018).

Unfortunately, realizing the potential of these vesicles will require technical improvement, since the exosomes are exceptionally challenging to characterization with current technologies. Exosomes have size that makes them out of the sensitivity range to most cell-oriented sorting or analysis platforms, as is the case of the classical flow cytometers.

The most common methods for targeting exosomes to date typically involve, after purification as discussed in § 1.3, the specific characterization of their cargo. Identification of membrane vesicles as exosomes also requires morphological analysis (Théry et al., 2006). Given their small size, exosomes can only be visualized with an electron microscope. Nanoparticle tracking analysis (NTA) is usually used to count the exosomes, followed by downstream processes for specific detection, including LC-MS/MS and Western Blot for proteins and qPCR for genetic material. The whole procedure is time consuming, requiring thus skilled personnel as well as laboratory facilities and benchtop instrumentation. To summarize, current methodologies have limitations in isolating, detecting and characterizing exosomes with high specificity, sensitivity and simplicity. All these methods will be discussed in the following sections.

1.4.1. Scanning electron microscopy

Scanning electron microscopy (SEM) is widely used to study EVs (Shao et al., 2012), providing information about their size and morphology. SEM is based on a focused beam of electrons that scan the sample, which interacts with the atoms in the sample to provide three-dimensional surface topography information. However, conventional SEM is

performed under a high vacuum and it requires complex and extensive sample processing, including dehydration, fixation, and metallization of the sample. Fig. 1.7 shows conventional SEM images of exosomes derived from human serum, which typically have a distorted, cup-shaped morphology (Shao et al., 2012). However, SEM was used with the previous cryofixation of the sample, which reduces exosome damage (Enderle et al., 2015). Recently, low-voltage SEM was demonstrated to be a promising method for studying EVs since it does not require a layer of conductive coating (Kondratov et al., 2017).

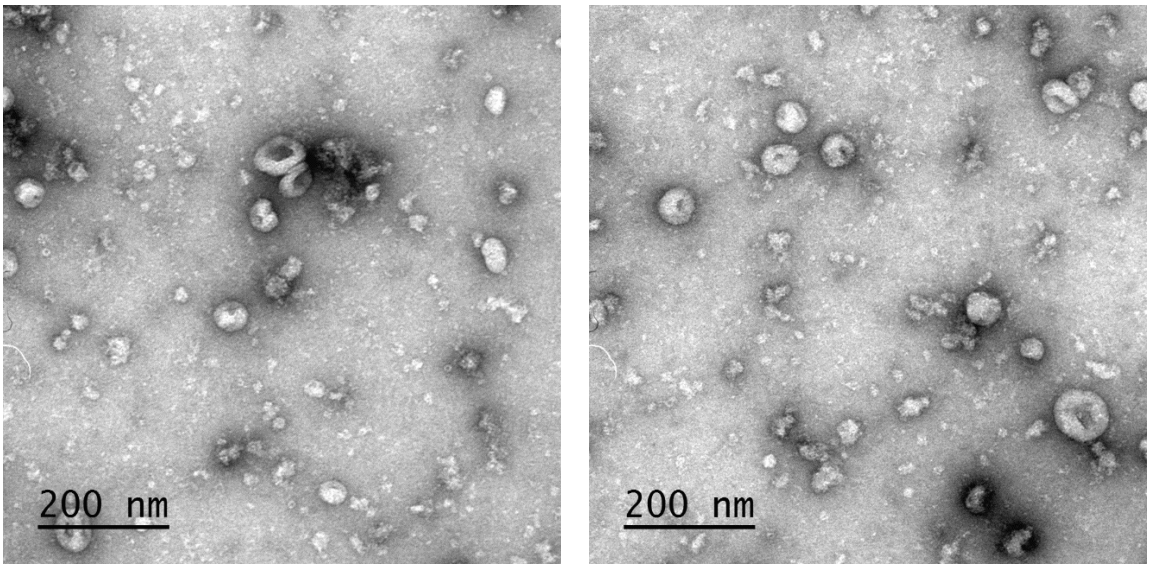

Fig. 1.7. SEM images of the exosomes-derived from human serum. These exosomes were immobilized onto formvar-carbon EM grids, then sputter-coated with a thin layer of gold-palladium alloy, maintained at 4 °C with 10-kV acceleration voltage during the whole process. The images were obtained in the Service of Microscopy, Universitat Autònoma de Barcelona.

1.4.2. Transmission electron microscopy

Transmission electron microscopy (TEM) is probably the most common type of electron microscopy for exosomes imaging (Choi and Mun, 2017), providing information on size and morphology. TEM is based on the illumination of electron beams through a sample, and the electrons can either be transmitted or diffracted by the sample. The transmitted electrons provide brightfield images, while scattered electrons are collected to generate dark-field images, revealing the structure with higher contrast. Conventional TEM involves the same sample preparation than in conventional SEM, including the preparation under high vacuum, with complex and extensive processing, including dehydration, fixation, and metallization of the sample. The TEM images usually revealed a distorted, cup-shaped morphology of the exosomes at low resolution (Lobb et al., 2015).

To overcome this drawback, TEM in a cryogenic environment (Cryo-TEM) was developed. With Cryo-TEM, biological samples are analyzed at very low temperatures (e.g., −180 °C). Also, in Cryo-TEM imaging, the sample preparation is much easier, since it is

directly applied to a copper grid which is vitrified, allowing thus the imaging of the sample near in its native state. Fig. 1.8 shows high-resolution Cryo-TEM images of exosomes derived from human serum, which reveal their nearly-native structure with cup-shaped morphology (Choi and Mun, 2017).

Cryo-TEM is considered a key methodology in contributing to the elucidation of the structure of biomolecules in their native state. Jacques Dubochet, Joachim Frank, and Richard Henderson were awarded the Nobel Prize in Chemistry in 2017 "*for developing cryo-electron microscopy for the high-resolution structure determination of biomolecules in solution*".

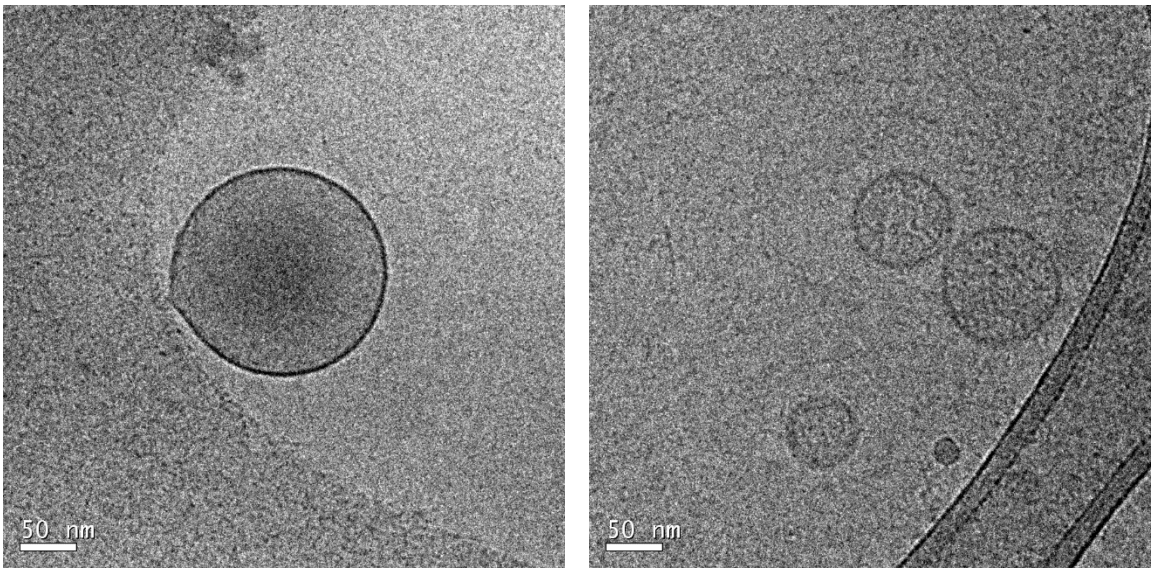

Fig. 1.8. Cryo-TEM images of the exosomes-derived from human serum. These exosomes were applied onto formvar-carbon EM grids, maintained at -182 °C with 200-kV acceleration voltage during the whole process. The images were obtained in the Service of Microscopy, Universitat Autònoma de Barcelona.

1.4.3. Atomic force microscopy

Atomic force microscopy (AFM) is another high-resolution imaging technique for EV characterization (Sharma et al., 2010). AFM uses a probe, often made of silicon or silicon nitride, to scan the surface of a sample, producing changes in the probe position and generating topographic images of the sample. Similar to Cryo-TEM, AFM requires minimal sample preparation. The sample is adsorbed onto a mica holder and gently dried for subsequent scanning with a probe. The mica holder can also be coated with antibodies, providing images from specific EVs (Yuana et al., 2010).

1.4.4. Dynamic light scattering

Dynamic light scattering is an emerging technique for tracking a single EV (Sitar et al., 2015). Dynamic light scattering is based on temporal fluctuations when a particle in solution is struck by monochromatic light. The light scattering occurs due to Brownian motion. Through the Stokes-Einstein equation (Chu, 1970), the temporal fluctuation rate of the light scattering can be converted to the diffusivity of the particle to determine its hydrodynamic diameter. Since each photon is scattered by one particle, DLS is very sensitive to small amounts of aggregates, since larger particles scatter exponentially more light than smaller particles ((Hoo et al., 2008). Furthermore, DLS cannot provide the concentration of particles

1.4.5. Tunable resistive pulse sensing

Tunable resistive pulse sensing is another emerging technique for tracking a single EV (Akers et al., 2016). Tunable resistive pulse sensing is based on the Coulter principle at the nanoscale. It detects variations in electrical impedance in the ionic current, generated by the transport of EVs through a size-tunable nanopore in a non-conductive polyurethane membrane (Roberts et al., 2010). The concentration and size distribution of EVs can be calculated by referring to the observed pulse height and rate to pulses induced by reference particles of known volume and concentration. However, even when using a non-conductive polyurethane membrane, biological materials can interact with the walls of the pore (Roberts et al., 2010). Furthemore, the contribution of EV aggregates or other non-lipid particles to the EV count can be misleading (Akers et al., 2016).

1.4.6. Flow cytometry

Conventional flow cytometry is a laser-based technology used to characterize EVs that are greater than 300 nm in diameter (Van Der Pol et al., 2010). It is based on a laser beam that illuminates the EVs passing through a channel in a hydrodynamically-focused fluid stream, and the forward scattered light (FSC) and side scattered light (SSC) are measured. The FSC light is used to detect the size, while the SSC is related to the granularity and complexity of the particle in the light path (Brown and Wittwer, 2000). Directly analyzing the nanometer size of the exosomes by flow cytometry is a major challenge. In fact, the technique usually uses an ~5 µm fluidic stream and ~10 µm laser beam heights, resulting in an illuminated cylinder volume ($V = \pi r^2 h$) of ~200 µm^3.

Considering a 100 nm exosome, the estimated volume ($V = \frac{4}{3}\pi r^3$) should be 5.2 × 10^{-4} μm^3, meaning that for detection it is necessary to have hundreds of 100-nm exosomes forming an exosome cluster in the fluidic stream. In this case, the fluorescence data from many exosomes will merge into a single fluorescence event, resulting in inadequate data acquisition. To overcome this limitation, exosomes are immobilized on large beads and then reacted with specific antibodies labeled with a fluorophore (Lozano-Ramos et al., 2015; Suárez et al., 2017). Fig. 1.9 shows flow cytometry histograms, in which the exosomes were immobilized on large magnetic bead surfaces (4.5 µm diameter). The relative fluorescence is on the allophycocyanin-axis (APC-axis) and the number of events (beads or exosome-bead count) is on the count-axis. The population of the negative control (beads only) and the positive relative pattern (exosome-beads) are shown in the blue and red regions, respectively. When the laser beam passes through the beads in a negative sample (in which no exosomes were immobilized), no fluorescence is produced, since the labeled antibody cannot bind the magnetic particles (Fig. 1.9, panel A). On the contrary, in the positive samples the fluorophore-labelled antibody which specifically reacts with the exosome immobilized on the beads will produce FSC light (Fig. 1.9, panel B). Although this approach does not provide the size distribution of the exosomes, it is widely used as an alternative to flow cytometry to provide information about the exosome membrane receptors (Lozano-Ramos et al., 2015; Moura et al., 2020b, 2020a; Suárez et al., 2017).

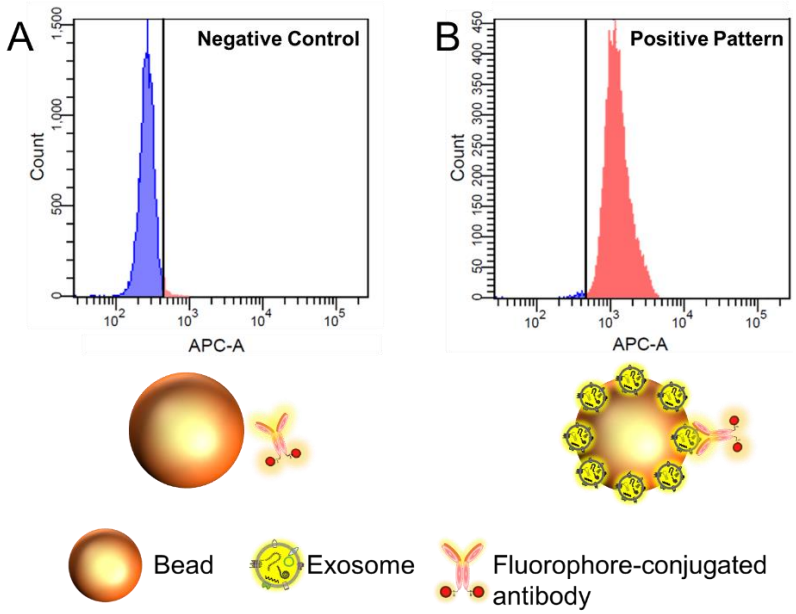

Fig. 1.9. Flow cytometry based on bead-assisted for the exosomes-derived from human serum. Population negative control (beads only) and positive relative patterns (exosomes-beads) are shows in the stained-blue and -red regions, respectively. Figure created using Servier Medical Art templates, which are licensed under a Creative Commons Attribution 3.0 Unported License.

Recently, high-resolution flow cytometry, termed vesicle flow cytometry (VFC), was developed for the characterization of EVs smaller than 300 nm in diameter (Akers et al., 2016; Stoner et al., 2016). In contrast to cFC (light scatter), fluorescence-based flow cytometry is performed at customized angles and involves the use of a specific fluorescent antibody or fluorescence membrane probe to trigger the detection of a particular subset of EVs. In VFC, the fluorescence intensity is standardized as the molecule of an equivalent soluble fluorophore (MESF), determined by comparing the fluorescence intensity signal from a bead standard to the signal from a solution of the same fluorophore (Schwartz et al., 2002). Although the use of VFC technology has opened the possibility of sorting small particles (<100 nm) and since the approximation of MESF values has been applied for fluorescent standardization in EV analysis (Stoner et al., 2016), the discrimination of vesicles from vesicle/protein aggregates does not allow for efficient sorting of these vesicles (Akers et al., 2016), and the use of MESF must be validated.

1.4.7. Nanoparticle tracking analysis

Nanoparticle tracking analysis (NTA) is the most widely used technique, currently considered as a gold standard for measuring the concentration and size distribution of EVs (Gardiner et al., 2013). NTA as dynamic light scattering, is a method for visualizing and analyzing particles in solution, relating the rate of Brownian motion to the particle size. NTA uses a hydraulic pump to inject the particles into a chamber, providing analysis in real-time, recording videos of the scattered light of each particle tracked, which enables better statistical calculation of particle size distribution by the Stokes-Einstein equation. Since the volume of the chamber is known, the particle concentration can be calculated. Fig. 1.10 shows the NTA of exosomes derived from human serum, and a screenshot of the chamber with the exosomes is also presented (inset of Fig. 1.10). The peak-to-peak resolution for different exosomes subpopulations can be easily discriminated, and each one can be quantified by Gaussian fitting. The light points in the screenshot are due to scattered light produced by exosomes. The NTA method is considered more accurate for polydispersed suspensions than dynamic light scattering (Filipe et al., 2010; Hoo et al., 2008). NTA-integrated fluorescence mode is also capable of analyzing a subpopulation of labeled EVs, providing specificity. However, proper dilution of the sample is necessary into the chamber, which can be problematic in term of sensibility if the sample concentration is limited. Furthermore, camera-level and detection-threshold variables were found to be a critical aspect affecting the limit of detection of the NTA-based quantification of EVs (Maas et al., 2015). Another limitation is the particle concentration range at which accurate quantification

data can be obtained, ranging from 10^7 to 10^9 particles mL^{-1} (Dragovic et al., 2011; Filipe et al., 2010; Maas et al., 2015). Since the number of EVs in biological fluids ranges from 1×10^1 to 3×10^7 exosomes μL^{-1} (Zhang et al., 2016), NTA may not be feasible in detecting and quantifying EVs in biological fluids in some applications. Concerning the NTA-integrated fluorescence mode, unless the expression of the studied marker is high, the measures will be unsuccessful, resulting in poor data acquisition (Szatanek et al., 2017). This occurs because particles move in and out of focus and the antibody fluorochromes are susceptible to photobleaching (Szatanek et al., 2017).

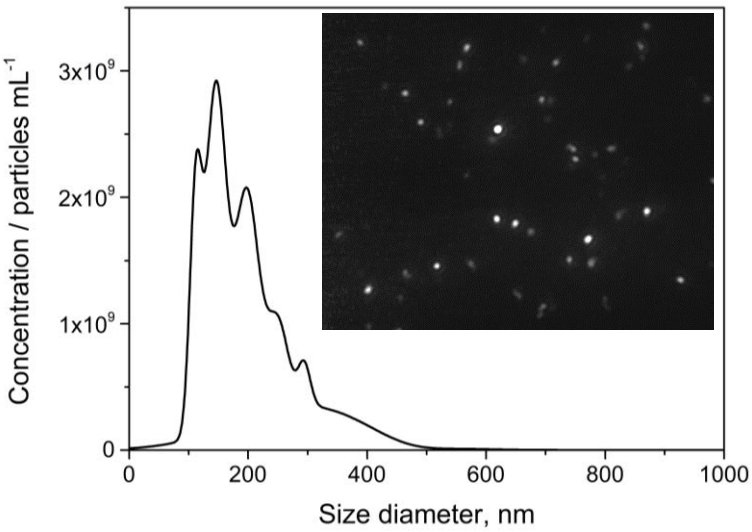

Fig. 1.10. NTA of the exosomes-derived from human serum. The purified exosomes were diluted in sterile-filtered 10 mmol L^{-1} PBS buffer (pH 7.5). Nanosight NTA Software analyzed raw data videos by triplicate during 60 s with 50 frames per second and the temperature of the laser unit set at 24.8 °C. The corresponding screenshot of the chamber with exosomes is also shown in the inset. The images were obtained in the Service of Microscopy, Institut de Ciència de Materials de Barcelona.

1.5. Chemical and biochemical characterization of exosomes

1.5.1. The protein cargo

The membrane proteins of the exosomes not only provide information on exosome biogenesis, but they are also widely used in many different applications, as is the case of the specific exosome isolation, previously discussed in § 1.3.2. Since exosomes in different biological fluids present a high degree of heterogeneity, the International Society for Extracellular Vesicles recommends a carefully characterization of exosome proteins (Lötvall et al., 2014). The exosome proteins are divided into four different categories: transmembrane, cytosolic, intracellular, and extracellular proteins.

A web-based compendium of exosomal cargo, ExoCarta, provides a list of 9,769 proteins (April 2020), and several play important roles in many biological mechanisms (Mathivanan and Simpson, 2009).

The intravesicular proteins present in EVs are shared with those of the cytoplasm of the releasing cell, such as heat-shock proteins (HSPs), gene (TSG), annexins, and the cytoskeleton (Graner et al., 2009). Exosomes derived from murine brain tumors demonstrated that 50% of the protein content was derived from the intracellular environment (Graner et al., 2009).

On the other hand, transmembrane proteins present in EVs are also shared with those of the plasma membrane of the releasing cell, especially from the superfamily of proteins with four transmembrane domains, named tetraspanins (van Niel et al., 2011). Tetraspanins are highly glycosylated and are involved in cell adhesion, migration, and motility, platelet activation and aggregation (Andreu and Yáñez-Mó, 2014). Tetraspanins are highly expressed in exosomes, regardless of their origin. Among them, CD9, CD63, and CD81 are the most frequently identified proteins in exosomes and they are considered classical biomarkers for exosomes (Chow et al., 2015). Accordingly, tetraspanins are widely used in EV enrichment and detection in different materials and devices (Im et al., 2014; Oliveira-Rodríguez et al., 2016; Xia et al., 2017; Yadav et al., 2017; Zhao et al., 2016), just to mention a few examples. Another transmembrane protein found in exosomes is the exosomal major histocompatibility complex (MHC), which is involved in antigen-specific activation of T-cells and modulation of the immune response. This protein was also used in EV enrichment and detection (Admyre et al., 2003; Van Niel et al., 2001).

Cancer-related transmembrane proteins are also used in EV enrichment and detection, such as the epithelial cell adhesion molecule (EpCAM or CD326) (Fang et al., 2017), epidermal growth factor receptors (EGFR or CD340) (H. Zhang et al., 2017), and CD24 (Zhao et al., 2016), as detailed discussed in § 1.2.7 (Table 1.1).

1.5.2. Methods for protein analysis and characterization

The total exosome protein quantification can be performed by a colorimetric reaction based on general protein reagents, as is the case of Bradford (Coomassie Blue reagent) or BCA (bicinchoninic acid reagent). The BCA protein assay is the most popular method for colorimetric detection and quantitation of total protein. BCA Protein Assays have a unique advantage over the Coomassie dye–based assays (Bradford), since they are compatible

with samples that contain up to 5% surfactants (detergents), and are affected much less by protein compositional differences, providing greater protein-to-protein uniformity.

The identification and characterization of different proteins in exosomes based on their MW is usually performed by sodium dodecyl sulfate-polyacrylamide gel electrophoresis (SDS-PAGE) (Gao et al., 2019; Santucci et al., 2019). Further specific identification of the separated proteins by using specific antibodies (western blot) is also commonly used (Yang et al., 2015). Electrophoresis is also coupled with microfluidic devices to simultaneously isolate exosomes and preconcentrate them (Marczak et al., 2018). Isoelectric focusing (IEF) is widely used for the separation of exosome proteins and further characterization based on their charge (isoelectric point) (Anderson et al., 2016; Yang et al., 2015). Then, the proteins can be first separated using isoelectric focusing and then by SDS-PAGE (Burkova et al., 2019). Liquid chromatography (LC) is widely used for the separation and further characterization of exosome proteins based on the MW, charge, hydrophobicity or specific binding interactions (Anderson et al., 2016; Yang et al., 2015). For instance, it was reported the characterization of urinary exosome proteins from microvesicles based on liquid chromatography (Singhto et al., 2019). Mass spectroscopy (MS) is based on the measurement of the mass-to-charge ratio of charged particles. MS is widely used for the separation (MS/MS) and detection of exosome proteins (Anderson et al., 2016; Yang et al., 2015).

The enzyme-linked immunosorbent assay (ELISA) is the most common immunoassay for protein quantification. For the special case of the exosomes as antigens, the following different formats can be used: direct, indirect, and sandwich (with either direct and indirect labelling), as depicted in Fig. 1.11. In detail: (i) direct assay, when the antigen (exosome) is directly attached on a solid phase, and detected with a primary enzyme-labeled antibody which binds to the antigen; (ii) indirect assay, when the antigen is also attached on the solid phase, but in this instance a primary non-labeled antibody binds the antigen, followed by an incubation with a secondary-labelled antibody (an anti-antibody), (iii) sandwich assay (two-epitopes assay) when the antibody is attached on the solid support, and the antigen is sandwiched between the capturing and the labelling antibody. Either a direct or indirect labelling can be used in a sandwich format. In all cases for ELISA, the label is an enzyme. Accordingly, the addition of a chromogenic substrate for the enzyme is required in order to achieve the visible color change, indicating the presence of antigen. The conversion of substrate to a product may be measured continuously, in a kinetic assay, in which the rate of conversion increases with increasing free antigen concentration. More often, a fixed-time approach is used; after a given incubation time, the reaction is stopped by the addition of strong acid or base that denatures the enzyme. Product quantification

then yields a calibration curve in which product concentration increases with increasing free antigen concentration.

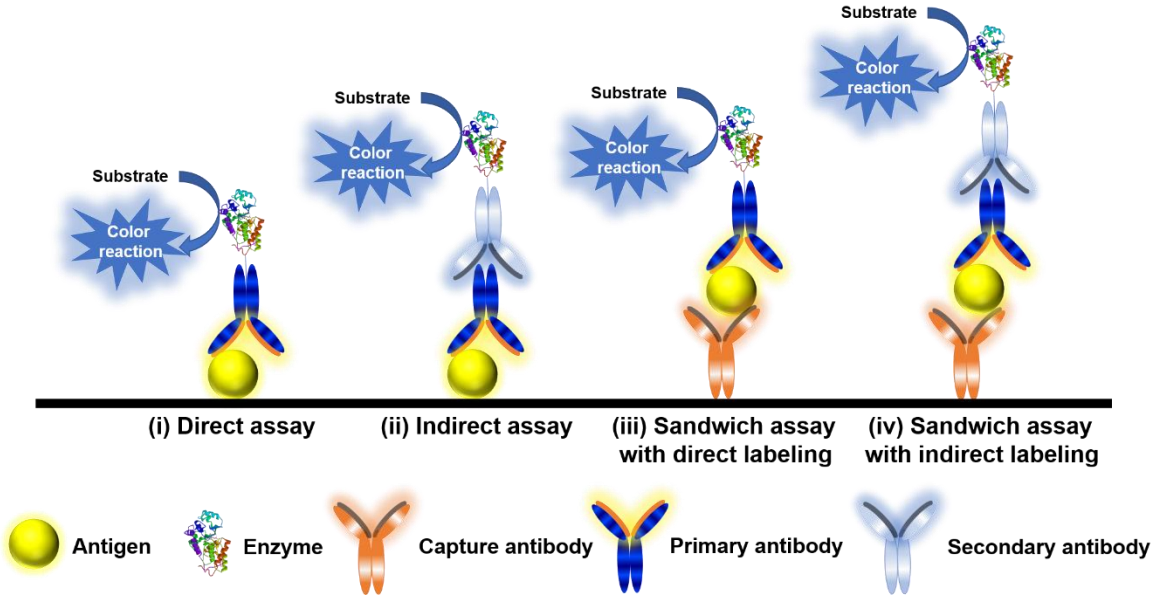

Fig. 1.11. Schematic representation of the different ELISAs formats: (i) Direct assay; (ii) Indirect assay; (iii) Sandwich assay with (iii) direct and (iv) indirect labelling. Figure created using Servier Medical Art templates, which are licensed under a Creative Commons Attribution 3.0 Unported License.

ELISA in its direct format is faster, as it is only necessary to apply one antibody. In the indirect format, the sensitivity increases, as each primary antibody has several epitopes to which the secondary antibody can bind, which amplifies the signal. In the sandwich format, the specificity can be increased since two different epitopes of the antigen can be targeted with two antibodies. These different formats have been recently reported for the multiplex detection and characterization of breast cancer exosomes by magneto-actuated immunoassay using as a solid support magnetic particles (Moura et al., 2020b, 2020a).

1.5.3. The nucleic acids cargo

The exosomes are also carriers of transcriptomes, such as protein-coding mRNA as well as non-coding RNA, such as microRNA (miRNA), long non-coding RNA, (lnc-RNA), ribosomal RNA (rRNA), transfer RNA (tRNA), and other ncRNAs. A web-based compendium of exosomal cargo, ExoCarta, provides a list of 3,408 mRNAs and 2,838 miRNAs (April 2020). This cargo plays important roles in many biological mechanisms (Mathivanan and Simpson, 2009). Another recently created web-based repository of different exosome RNA molecules is the exoRBase, showing also RNA expression profiles,

spanning normal individuals and diseased patients (Li et al., 2018). Other useful databases are miRBase database, which provides a list of 2,654 mature miRNA and miRbase.

As it was previously explained, the release of exosome is a normal biological process. However, an increase releasing rate, as well as a differential cargo expression, can be related, for instance, with some pathological conditions as cancer progression and metastasis. Exosome-mediated transfer of mRNA and miRNA molecules is involved in the genetic exchange between cells (Valadi et al., 2007). Currently, this topic is under intense investigation, with many efforts focused on nucleic acid enrichment, identification, and quantification in exosomes using high-throughput technologies.

mRNA encompasses a large family of single-stranded RNA molecules, which encodes the amino acid sequence of a protein, as well as the gene expression (Ravasi et al., 2006). mRNA length usually ranges from ~400 to ~12,000 nucleotides, with the average size of the transcripts at 2,100 (Ravasi et al., 2006). The type and proportion of exosome-derived RNA can be substantially different from its release cells (Batagov and Kurochkin, 2013; Skog et al., 2008; Wei et al., 2017; Xiao et al., 2012).

Recently, a systematic characterization of exosome-derived RNA from the plasma of 50 healthy individuals and 142 cancer patients (colon, prostate, and pancreatic carcinomas) was performed (Yuan et al., 2016). The most noticeable mRNA molecules included C15orf52, ST8SIA1, and MTRNR2L5.

Among the mRNA molecules, glyceraldehyde-3-phosphate dehydrogenase (GAPDH) (Jella et al., 2016; Jenjaroenpun et al., 2013; Yang et al., 2014) and β-actin genes (Jiang et al., 2015) were found in the exosomes, and they are used as two major internal control for mRNA normalization (housekeeping genes). Moreover, GAPDH is a key glycolytic enzyme, and it is responsible for the dysregulation of glycolysis in cancer (Krasnov et al., 2013). It was demonstrated that many cancer cells exhibit increased aerobic glycolysis, generating ATP and metabolic intermediates for cancer cell proliferation (Fernandez-de-Cossio-Diaz and Vazquez, 2017; Jiang, 2017). For instance, GAPDH gene expression was found to be overexpressed in human lung (Tokunaga et al., 1987), prostate (Rondinelli et al., 1997), renal (Vilà et al., 2004), breast (Révillion et al., 2000), pancreatic (Mikuriya et al., 2007), and colorectal carcinomas (Tang et al., 2012) when compared to the normal tissues.

Several studies have suggested the use of exosomal mRNA molecules as biomarkers. For instance, mRNA signatures of tumor-derived exosomes have shown promise for potential circulating diagnostic biomarkers in glioblastoma (Skog et al., 2008),

as well prostate (Nilsson et al., 2009), lung (Fujita et al., 2014), ovarian (Yokoi et al., 2017), and breast cancer (Tsai et al., 2018).

MicroRNA (miRNA or miR) is a short family of non-coding RNA molecules that regulate gene expression. This action is post-transcriptionally produced by binding to target mRNA molecules to inhibit translation and/or to promote mRNA degradation (Batagov and Kurochkin, 2013; He and Hannon, 2004). miRNA is ~19 to ~25 nt in length, cleaved from ~70 nucleotide hairpin pre-miRNA precursors (He and Hannon, 2004). Exosome-derived miRNA can have up-regulation and/or down-regulation biological pathways.

Similar to the mRNA mentioned above, miRNA profiles from exosomes were systematically characterized from the plasma of 50 healthy individuals and 142 cancer patients (Yuan et al., 2016). The study demonstrated that miRNA molecules are the most abundant RNA type, and the most noticeable miRNA is miR-99a-5p. miR-125a-5p and miR-1343-3p are the two most commonly down-regulated miRNA molecules in association with all cancer types tested (colon, prostate, and pancreatic carcinomas).

Tumor-derived exosomal miRNA molecules undoubtedly present their potential clinical applicability as novel biomarkers for cancer diagnosis. Tumor-derived exosomal miRNA molecules for adenocarcinoma diagnosis have demonstrated a sensitivity of 80.65% and a specificity of 91.67% (Jin et al., 2017). Many other non-coding RNA types have been identified in exosomes (Li et al., 2018; Yuan et al., 2016). For instance, transfer RNA (tRNA, ~76–90 nt), ribosomal RNA [rRNA, 18S (1.9 kilobases, kb) and 28S (5.0 kb)], circular RNA (circRNA, “unexpected size pattern”), small nuclear RNA (snRNA, 150 nt), small nucleolar RNA (snoRNA, ~20–24 nt), as well as long non-coding RNA (lncRNA, <200 nt) (Azmi, 2018; Li et al., 2018; Yuan et al., 2016) have been identified. In addition to exosomal RNA types, several studies provided evidence that exosomes carry double-stranded DNA (dsDNA) (Balaj et al., 2011; Kahlert et al., 2014). dsDNA fragments can range from 100 base pairs (bp) to 2.5 kbp (Thakur et al., 2014). Wang et al. (Wang et al., 2018) demonstrated that tumor-derived exosomal dsDNA shares the same mutations in its susceptibility genes as those of the parent tumor cells, and it is highly consistent with the paired tumor genome.

1.5.4. Methods for nucleic acid analysis and characterization

The main obstacle in the detection of exosomal RNA/DNA is the relatively low abundance per exosome, with all studies above using high-throughput technologies, such as real-time quantitative polymerase chain reaction (qRT-PCR). This technique will be described in the following sections.

1.5.4.1. Polymerase chain reaction

PCR is an amplification-based assay that enables the measurement of panels of both RNA and DNA. The PCR technique revolutionized the molecular biology, as a rapid, *in vitro* DNA amplification process that can synthetize up to a billion copies of a given nucleic acid target. The creator of PCR, Kary B Mullis, was awarded the Nobel Prize in Chemistry in 1993 "for his invention of the polymerase chain reaction (PCR) method".

PCR amplification uses the thermostable DNA polymerase (Taq polymerase), which is an enzyme that synthesizes DNA molecules from deoxyribonucleotides, the building blocks of DNA, in a 5'→3' direction from a single-stranded template. In summary, PCR amplification is based on Taq polymerase and two specific oligonucleotides (the primer sequences) flanking a specific DNA region. In addition to Taq polymerase and primers, the PCR mixture contains the cofactor magnesium ion (Mg^{2+}), the four 2'-deoxyribonucleoside-5'-triphosphates (dNTPs), and the buffer (Metzker and Caskey, 2009). Fig. 1.12 shows a schematic PCR cyclic process based on 1) double-strand separation of DNA by heat denaturation, 2) specific hybridization or annealing of short oligonucleotide primers to single-stranded DNA, 3) and synthesis elongation by DNA polymerase (Mullis and Faloona, 1987; Saiki et al., 1985). Each cycle doubles the region marked by the primer sequences, which exponentially (2^{cycles}) generate up to a billion copies of the target within just a few hours (Fig. 1.12).

The parameters in PCR (specially number of cycles, annealing temperature) are important parameters for high-quality PCR results. The optimal number of cycles is dependent on the starting DNA template concentration, and it typically ranges from 25 to 35 cycles. Increasing the number of cycles will significantly increase the amount of nonspecific PCR products (such as primer dimers). PCR can reliably amplify target sizes up to 3-4 kb. The sample can be applied directly in PCR, but impurities from crude extracts may inhibit Taq DNA polymerase. This issue can be minimized by diluting the sample (Metzker and Caskey, 2009), since PCR needs only few hundred template copies to start. It is recommended that PCR primers should be between 18 and 25 nucleotides in length, having roughly equal numbers of the four nucleotides, and showing guanine (G) + cytosine (C) composition of 50–60% (Metzker and Caskey, 2009). However, G and C -rich regions tend to form secondary structures, such as hairpin loops, resulting in a difficult separation in the denaturation step and impairing/blocking the synthesis of the new strands by DNA polymerase (Metzker and Caskey, 2009). Adjustments towards a higher annealing temperature and shorter annealing time can prevent nonspecific binding of GC-rich primers. The use of reagents such as dimethyl sulfoxide (DMSO), glycerol, and betaine can prevent

secondary structures of G and C-rich sequences, facilitating the double-strand separation (Metzker and Caskey, 2009). Nonetheless, like all enzymes, DNA polymerases are also prone to error, leading to mutations in the generated PCR fragments (Zhou et al., 1991). A deep description of the PCR technique is provided elsewhere (Metzker and Caskey, 2009; Mullis and Faloona, 1987; Saiki et al., 1985). After the amplification, in conventional end-point PCR the product (the amplicon) is usually analyzed by gel electrophoresis at the end of the process, in order to confirm that only one band of the specific MW is obtained, as expected in a positive sample.

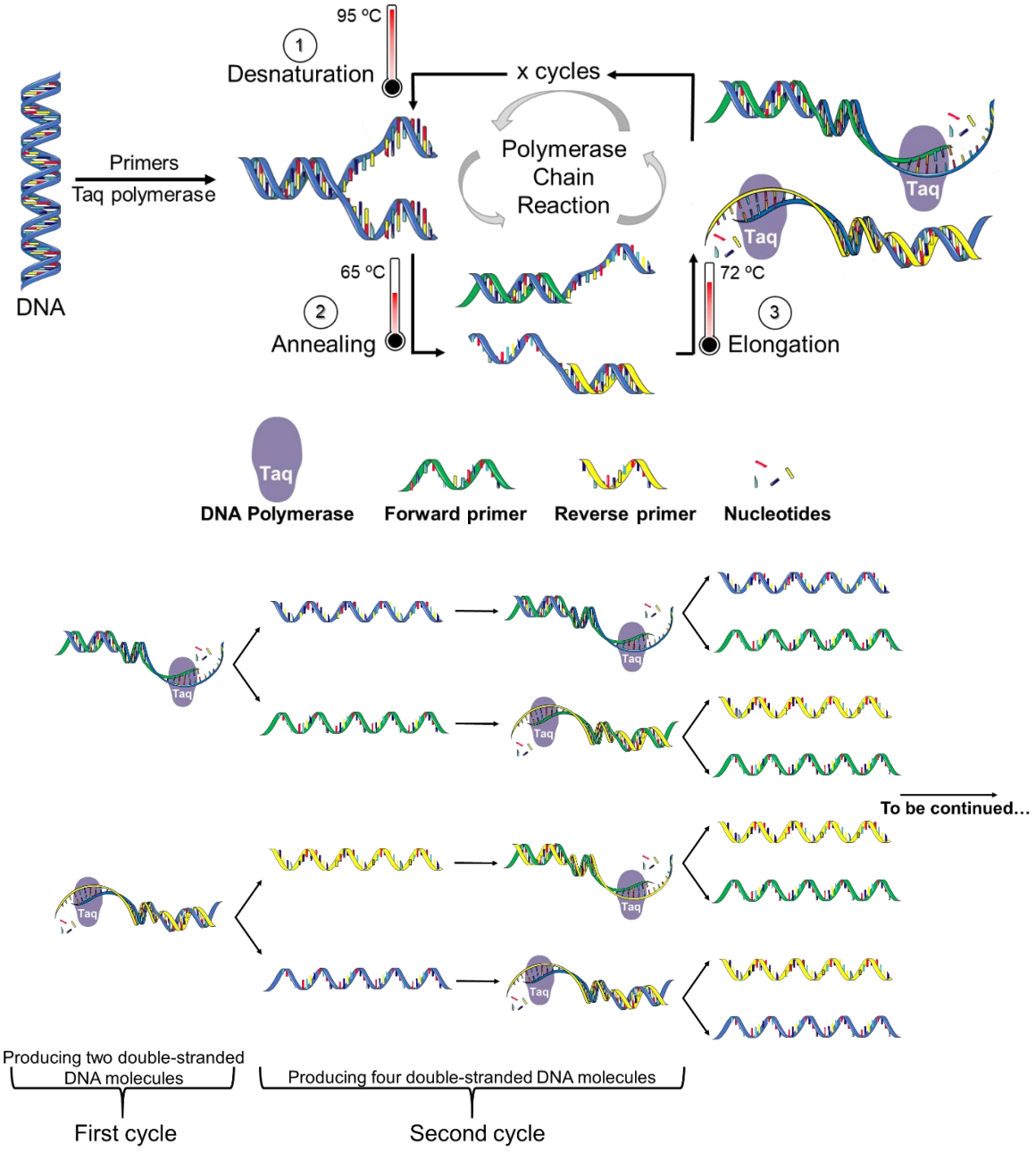

Fig. 1.12. The PCR amplification cycles. Figure created using Servier Medical Art templates, which are licensed under a Creative Commons Attribution 3.0 Unported License.

1.5.4.2. Real-time polymerase chain reaction

A variant of conventional PCR is the real-time polymerase chain reaction, also known as quantitative polymerase chain reaction (qPCR). In qPCR, the amplification of the template is monitored cycle to cycle (Metzker and Caskey, 2009). In contrast to conventional PCR, qPCR is based on fluorescent labeling, and the fluorescence signal is collected as PCR progress, cycle to cycle (Metzker and Caskey, 2009). In the simpler version, a dsDNA binding dye (traditionally SYBR green) is used for measuring the fluorescence after each elongation step. The main drawback of this technique is the presence of interferences such as dimers of primers, which provides high backgrounds, (Metzker and Caskey, 2009). To overcome this limitation, different strategies using specific DNA probes (incorporating fluorophores and quenchers) were developed, but all of them are based on the principle of fluorescence resonance energy transfer (FRET). In the case of the hydrolysis proves, the FRET prevents the emission of the fluorophore via the quencher while the probe is intact (Metzker and Caskey, 2009). However, during the PCR reaction, the probe is hydrolyzed during primer extension and amplification, and cleavage of the probe separates the fluorophore from the quencher, resulting in amplification-dependent fluorescence. Probe-based qPCR is more specific than dye-based qPCR. Some commercial qPCR kits include the SABiosceinces PCR array, TaqMan OpenArray, TaqMan Gene Expression Assays, TaqMan TLDA microfluidic cards by Applied Biosystems, miScript miRNA PCR Array by Qiagen, and miRCURY LNA qPCR by Exiqon.

1.5.4.3. Reverse transcription polymerase chain reaction

When the template of PCR is RNA, reverse transcription is required to undergo a PCR. In RT-PCR, the RNA template thus is first converted into a complementary DNA (cDNA) using a reverse transcriptase. The cDNA is then used as a template for exponential amplification using PCR. The retrotranscription and the PCR can be done in separated or combined steps. However, the retrotranscription should be done as soon as possible since the transcripts are non-stable (Metzker and Caskey, 2009).

The genomic profile of the exosome, including mRNA, miRNA, lncRNA, and tRNA, appears to be a potential biomarker source for classifying tumor types (Yuan et al., 2016), and can be achieve by qRT-PCR. Strong evidences suggested that exosomal RNA molecules are promising cancer biomarker candidates, playing an important role in human health and disease (Sun et al., 2017; Zhao et al., 2017) (Eichelser et al., 2014) (Zhao et al., 2017) (Hannafon et al., 2016) (J. Wang et al., 2017). Nonetheless, new evidence suggests

that a large proportion of human blood plasma cell-free DNA is localized in exosomes (Fernando et al., 2017).

1.5.5. Progress in the detection of exosomes

As it was discussed in the previous sections, the exosomes are promising biomarkers for a more sensitive, non-invasive, early detection of non-communicable diseases. Besides non-communicable diseases, exosomes can also reveal priceless information of latent infection diseases (Lyu et al., 2019).

To summarize, the most common methods for targeting exosomes to date typically involve purification followed by the specific characterization of their cargo (Théry et al., 2006) . The isolation of the exosomes is best performed with differential ultracentrifugation. Purification can also be done with precipitation, size-exclusion chromatography, or ultrafiltration (Lyu et al., 2019). Identification of membrane vesicles as exosomes also requires morphological analysis (Théry et al., 2006). Given their small size, exosomes can only be visualized with an electron microscope. Nanoparticle tracking analysis (NTA) is usually used to count the exosomes, followed by downstream processes for specific detection, including LC-MS/MS and Western Blot for proteins and qRT-PCR for genetic material. Unfortunately, current methodologies have limitations in isolating, detecting and characterizing exosomes with high specificity, sensitivity and simplicity.

One of the greatest challenges in EV-based diagnostics is the complexity of the biological sample in which EVs are found, such as plasma, serum, urine, CSF, among others. Due to the worldwide interest in exosomes, several studies have focused their efforts on the detection and quantification of exosomes directly in the matrix sample or with minimal sample treatment.

Table 1.3 shows a comparison of the different platforms for the detection of exosomes, highlighting the limit of detection (LOD) of exosomes in complex samples. Most platforms are based on immunomagnetic separation (IMS) of exosomes using antibody-modified solid supports coupled to microfluidic devices. CD9, CD63, and CD81 tetraspanin molecules are the most frequently identified proteins in exosomes and they are considered classical biomarkers of exosomes (Chow et al., 2015; Hemler, 2013), then used to exosome isolation using IMS. Other platforms are exosomes label-free, such as electrochemical (Kilic et al., 2018) and cantilever arrays (Etayash et al., 2016). These platforms have demonstrated their strong potential for detection and quantification of exosomes, and some of them can detect exosomes in whole-serum samples, such as the electrochemical-based

(Yadav et al., 2017), electrohydrodynamic (Vaidyanathan et al., 2014), and SPR-based (Sina et al., 2016) approaches. According to Table 1.3, there are platforms capable of detecting the impressive number of only 77 (Kilic et al., 2018), 200 (Etayash et al., 2016), or 1000 (Zhang et al., 2019) exosomes per milliliters in clean buffers or diluted plasma. However, none of them were able to detect exosomes in whole-serum below 2,000,000 exosomes per milliliter. Although these methods have demonstrated high sensitivities, their approaches involved complex electrode pretreatment and labeling procedures, and, in some instances, high cost of the instrumentations and maintenance. Other analytical platforms require highly complex manufacturing components, such as the nanomechanical cantilever (W. Wang et al., 2018). Based on the above facts, the implementation of cancer early diagnosis programs remains economically unviable and reflects in the planning and implementing cancer control programs in low – and middle- income countries. Therefore, novel, simple, and low-cost platforms are necessary for the screening of exosome biomarkers that can be used in resource-limited settings, where sophisticated instrumentations are not available due to laboratory requirements, maintenance, and the cost of the assay.

1.5.6. Progress in the detection of nucleic acid in exosomes

Exosome tumor-derived RNA/DNA has demonstrated great potential in clinical applications, since their concentrations are found to be substantially elevated compared to their release cells. In fact, many mRNA, miRNA, and DNA molecules are highly enriched or even exclusively present in tumor-derived exosomes, which suggests the existence of a dedicated mechanism for selective targeting of the nucleic acids in the exosomes (Kalluri and LeBleu, 2016; Li et al., 2015; Skog et al., 2008; Valadi et al., 2007; L. Wang et al., 2018). However, the exosome nucleic acid transfer is cell-type-dependent, and the mechanism and role of this phenomenon remains largely unknown (Kalluri and LeBleu, 2016; L. Wang et al., 2018). The low abundance of RNA/DNA molecules per exosome is relatively challenging, with all studies using high-throughput technologies, such as qRT-PCR.

Table 1.3. Comparison of different platforms for the detection of exosomes based on protein receptors.

Detection platform	Biomarker	Targeted disease	Real sample evaluated*	LOD (Exosomes μL^{-1})	Reference
Electrochemical antiCD81-modified electrode	CD81	Breast cancer	NO	0.077	(Kilic et al., 2018)
Cantilever arrays	CD24, CD63, CD340 and GPC1	Breast cancer	50% of human serum	0.2	(Etayash et al., 2016)
3D-nanopatterned microfluidic fluorescence-based device	CD24, CD326 and FRα	Ovarian cancer	10% of human plasma	10	(Zhang et al., 2019)
Microfluidic graphene oxide-based interface	CD9, CD81 and CD326	Ovarian cancer	10% of human plasma	50	(Zhang et al., 2016)
Rolling circle amplification with fluorescence detection	CD63 and nucleolin	Leukemia	50% of fetal bovine serum	100	(Lin Huang et al., 2018)
Microfluidic fluorescence-based detection	CD9, CA-125, CD24 and CD326	Ovarian cancer	NO	750	(Zhao et al., 2016)
Electrochemical antiCD63-modified electrode	CD63	Liver cancer	10% of fetal bovine serum	1000	(Zhou et al., 2016)
Surface-enhanced Raman scattering	CD63 and CD340	Lung cancer	NO	1200	(Zong et al., 2016)
Microfluidic SPR-based assay	CD9, CD63 and CD340	Breast cancer	non-diluted human serum	2070	(Sina et al., 2016)
Microfluidic electrohydrodynamic assay	CD9 and CD340	Breast cancer	non-diluted human serum	2760	(Vaidyanathan et al., 2014)
Microfluidic SPR-based nanoholes arrays	CD24 and CD326	Ovarian cancer	Ascites fluid	~3000 exosomas	(Im et al., 2014)
Microfluidic fluorescence-based detection	CD81 and GluR2	Brain injury	non-diluted mouse serum	1.0×10^4	(Ko et al., 2016)
Microfluidic DLS-based detection	T7 phage	Viral infection	non-diluted mouse plasma	1.0×10^5	(Fraikin et al., 2011)
Electrochemical antiCD9-modified electrode Differential Pulse Voltammetry	CD9 and CD340	Breast cancer	non-diluted human serum	4.7×10^5	(Yadav et al., 2017)
Colorimetric single-walled carbon nanotubes	CD63	Breast cancer	NO	5.2×10^5	(Xia et al., 2017)
Microfluidic μNMR-based detection	CD44, CD47, CD55 and CD235a	Blood quality	Packed red blood cells	2.0×10^6	(Rho et al., 2013)
Conventional ELISA	CD9, CD63 and MICA	Melanoma cancer	NO	1.0×10^7	(López-Cobo et al., 2018)
Nanoparticle tracking analysis (NTA)	-	-	NO	1.0×10^7	(Filipe et al., 2010)
Lateral flow colorimetric assay	CD9, CD63 and CD81	Melanoma cancer	NO	8.5×10^6	(Oliveira-Rodríguez et al., 2016)

.

Table 1.4. Comparison of different approaches for the detection of exosomes based on RNAs/DNAs cargo in multiple cancers.

Targeted disease	Source	Enrichment method	RNAs/DNAs cargo	Reference
Breast cancer	Cell culture	Ultracentrifugation	cirRNA (XPO1, EZH2, FOXK2, CAMSAP1, MET, CDYL)	(Li et al., 2015)
			miR-105 and miR-181a	(Zhou et al., 2014)
	Serum	ExoQuick kit	miR-101, miR-372 and miR-373	(Eichelser et al., 2014)
Colon cancer	Serum	Ultracentrifugation	mRNA (BRAF and KRAS)	(Hao et al., 2017)
	Cell culture		miR-128-3p	(Liu et al., 2019)
			mRNA (ACTB, GAPDH, RPL13A, HMBS, B2M, and TBP)	(Chiba et al., 2012b)
			miR-21, miR-34a, miR-143, miR-192, miR-215 and miR-221	
Glioblastoma	Serum	Ultracentrifugation	mRNA (EGFRvIII)	(Skog et al., 2008)
			mRNA (HOTAIR)	(Tan et al., 2018)
Lung cancer	Plasma	antiCD326-modified MP	let-7f, miR-20b, miR-30e-3p, miR-223 and miR-301	(Silva et al., 2011)
		Ultracentrifugation	DNA (EGFR)	(Thakur et al., 2014)
		Size-exclusion chromatography and antiCD326-modified MP	miR-17-3p, miR-21, miR-106a, miR-146, miR155, miR-191, miR-192, miR-203, miR-205, miR-210, miR-212, and miR-214	(Rabinowits et al., 2009)
	Cell culture	ExoQuick kit	mRNA (GAPDH)	(Munson et al., 2018)
Melanoma cancer	Plasma	Ultracentrifugation	DNA (BRAF)	(Thakur et al., 2014)
Ovarian cancer	Urine	Ultracentrifugation	miR-30a-5p	(Zhou et al., 2015)
	Serum	Exosome Isolation Reagent	mirR-21	(Cappellesso et al., 2014)
		Magnetic-activated cell sorting based on CD326	miR-21, miR-141, miR-200a, miR-200c, miR-200b, miR-203, miR-205 and miR-214	(Taylor and Gercel-Taylor, 2008)
Pancreatic cancer	Serum	Ultracentrifugation	miR-1246, miR-4644, miR-3976 and miR-4306	(Madhavan et al., 2015)
		ExoQuick kit	miR-191, miR-21 and miR-451a	(Goto et al., 2018)
	Plasma	antiCD326-modified MP	mRNA (ARG1, CK18, CD63, Erbb3, KRAS, GAPDH, H3F3A, ODC1)	(Ko et al., 2017)
Prostate cancer	Serum	ExoQuick kit	miR-1290 and miR-375	(Huang et al., 2015)
	Serum; Urine	ExoMir kit	miR-141 and miR-375; miR-107 and miR-574-3p	(Bryant et al., 2012)

.

Chevillet et al. (2014) suggested a stoichiometric model for exosome RNA content, which is described in Fig. 1.13. In summary, the following four alternative models were proposed, as depicted in Fig. 1.13: i) high-occupancy/high-miRNA concentration, ii) high-occupancy/low-miRNA concentration, iii) low-occupancy/low-miRNA concentration, and iv) low-occupancy/high-miRNA concentration. The experimental results refuted the models for both the (i) high-occupancy/high-miRNA concentration and the (ii) high-occupancy/low-miRNA concentration. However, the results were consistent with (iii) the low-occupancy/low-miRNA concentration model, in which a small fraction of the exosomes carry a low concentration of miRNA, or (iv) the low-occupancy/high-miRNA concentration model, in which there are rare exosomes in the population that carry many copies of a given RNA. These models can explain the skew in the final value for the stoichiometry of the RNA molecules per exosome.

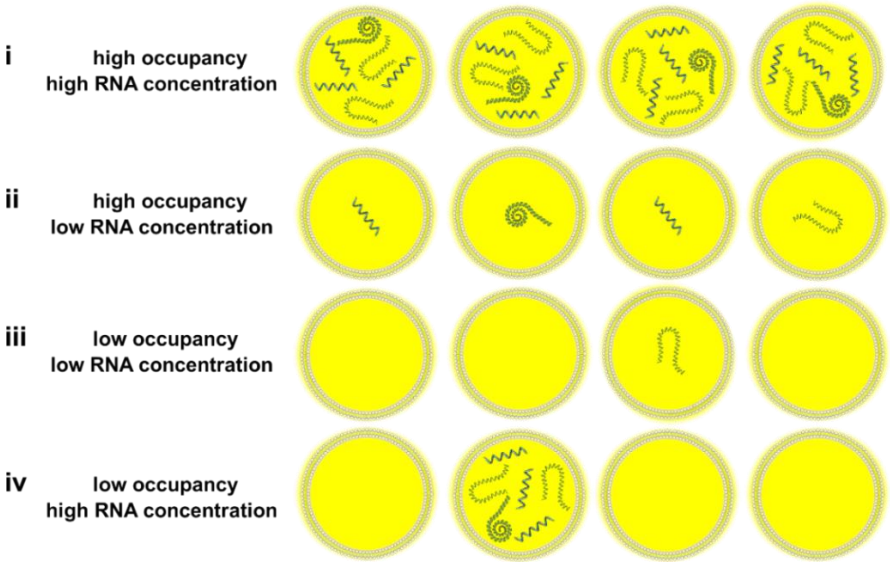

Fig. 1.13. Stoichiometric models for exosome RNA content. Figure adapted from stoichiometric models of Chevillet et al., 2014 and created using Servier Medical Art templates, which are licensed under a Creative Commons Attribution 3.0 Unported License.

Table 1.4 summarizes the application of nucleic acid in exosomes for multiple cancer. Several studies have mainly focused on exosomal mRNA, miRNA, and DNA.

Regarding the exosome enrichment methods, many studies have used ultracentrifugation as the standard isolation method (Table 1.4) for further RNA amplification by qRT-PCR. On the other hand, immunomagnetic separation based on a specific epithelial biomarker (CD326 epithelial biomarker, known as EpCAM) has been also used as a more rapid, feasible, and specific method since only epithelial cancer exosomes are isolated by immunomagnetic isolation, increasing the specificity of diagnosis (Table 1.4). EpCAM-

modified magnetic particles have been used to capture exosomes derived from ovarian (Taylor and Gercel-Taylor, 2008), lung (Rabinowits et al., 2009), glioblastoma (Silva et al., 2011), and pancreatic (Ko et al., 2017) carcinomas. EpCAM is a transmembrane glycoprotein, found to be overexpressed in many epithelial tissues, cells, and cancer exosomes (Li Huang et al., 2018).

The nucleic acid-containing exosomes have been demonstrated to not only have a role in cell-to-cell communication, but to have potential applications as reliable biomarkers in diagnosis.

1.6. Technological challenge in the detection of exosomes by rapid diagnostic test

The accurate identification and quantification of exosomes in low resource settings remains a major stumbling block due to the lack, of rapid, cost-effective platforms that can be handled for unskilled personnel to manage such a challenging biomarker in clinical samples. In this direction, the FDA defines the characteristics that a diagnostic test should ideally have low complexity for a test includes the final-user interpretation and level of training required, the number of manual manipulations and intervention steps, and the instrumentation requirements (LaBarre et al., 2011). In general, as complexity for a diagnostic test increases, the analytical performance and the quality of the analytical information remarkably improve. Unfortunately, the total assay time and the need for complex bench-top instrumentation which requires costly maintenance also increase (Lee and Allain, 2004). The preeminent formats under development as rapid diagnostic tests (RDTs) for exosomes are lateral-flow, microfluidic devices and biosensors. The lateral-flow assay (LFA) introduced in 1988 by Unipath Limited, is the most common commercially available point of care diagnostic format. Although there are many commercially available examples including the pregnancy test, the LODs of the test for exosomes applications should be improved for clinical uses (Oliveira-Rodríguez et al., 2016). Regarding microfluidic devices, although many breakthroughs have been made (Chiriacò et al., 2018). The cost of production and the requirement, in most cases, of bench-top equipment for the readout, still constitutes a bottleneck and may put them out of range for end users. Finally, and despite the massive use of glucose biosensors with electrochemical transduction, examples of other applications including diagnosis of diseases are currently very limited in the market. Many improvements should be done to achieve analytical simplification. The next sections will be focused on biosensing devices as an alternative method for the detection of exosomes.

1.6.1. Biosensor

Enormous interest in biosensors started in 1962 when Clark and Lyons published the first version of the glucose biosensors (Clark and Lyons, 1962). The International Union of Pure and Applied Chemistry (IUPAC) has defined a biosensor as the following:

> "Biosensor is a device that uses specific biochemical reactions mediated by isolated enzymes, immuno systems, tissues, organelles or whole cells to detect chemical compounds usually by electrical, thermal or optical signals".

A biosensor is an analytical device that converts a biological response into a signal. Fig. 1.14 schematically shows the main components of a biosensor. Basically, it consists of (i) a bioreceptor or biorecognition element that recognizes the target analyte; (ii) a transducer that converts the recognition event into a measurable signal; (iii) an amplifier that transforms the small input signal from the transducer into a large output signal; (iv) a signal processor, which, using a Savitzky-Golay filter, Fourier transform, and integration, converts the output signal into a working output signal, and (v) a detector, in which the working output signal is then recorded, analyzed with software and stored and displayed. There are several bioreceptor types, including tissues, microorganisms, organelles, cells, and the most common nowadays, enzymes, antibodies, nucleic acids, or biomimetic receptor. The transduction may be optical, electrochemical, thermometric, piezoelectric, magnetic, micromechanical, or combinations of one or more of these techniques.

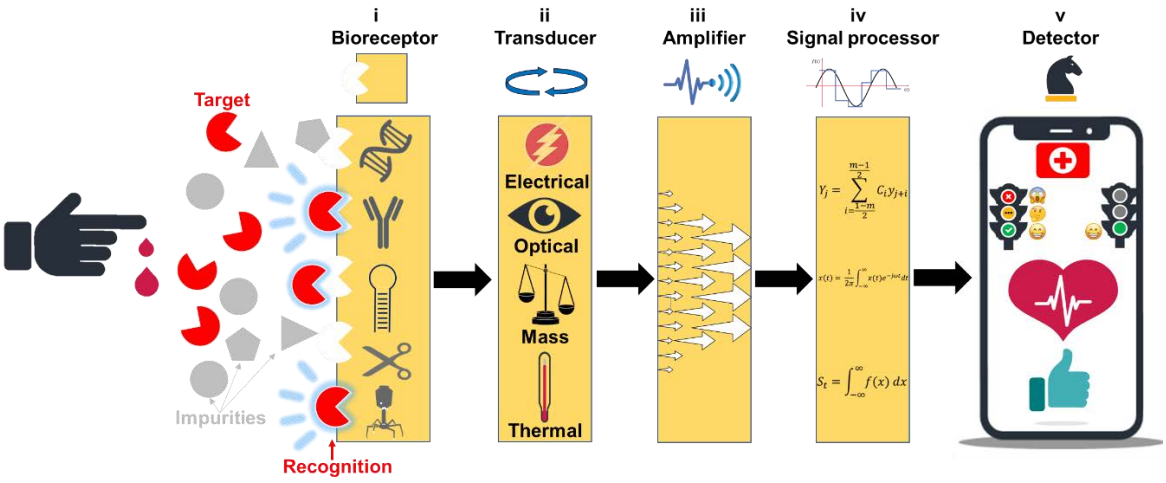

Fig. 1.14. Schematic diagram of the components of a biosensor. Figure created using Servier Medical Art templates, which are licensed under a Creative Commons Attribution 3.0 Unported License.

1.6.2. Classifications of biosensor

The assembly, lifespan, specificity, reproducibility, and portability of a biosensor is governed mainly by the choice of bioreceptor and/or transducer. Biosensors are usually classified according to these two categories, as display in Fig. 1.15. Below, we will briefly discuss each of the subcategories within the bioreceptor and transducer categories, with examples related to EVs and other molecules.

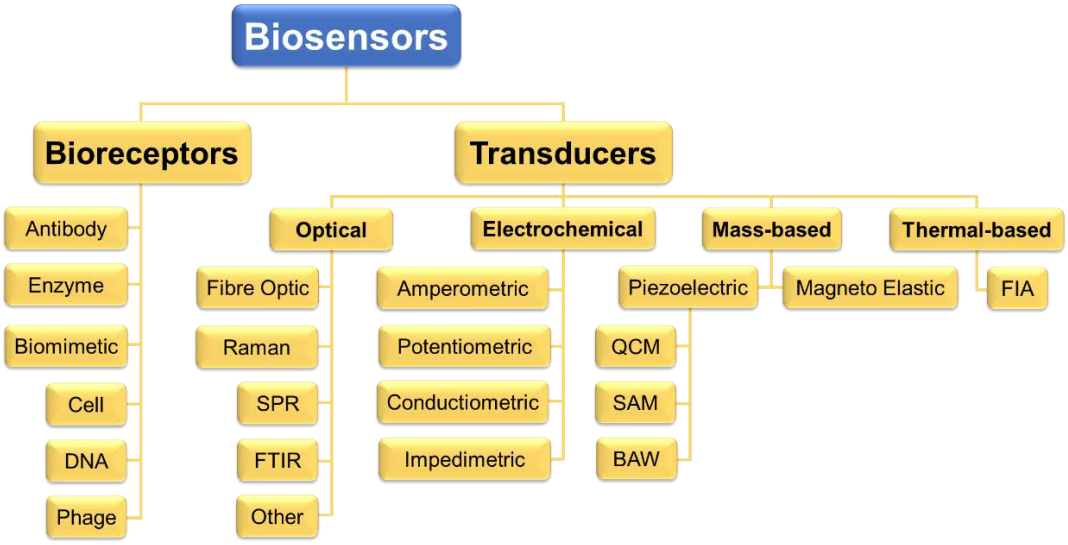

Fig. 1.15. Schematic diagram of the classifications of a biosensor. Figure adapted from Velusamy et al., 2010.

1.6.3. Bioreceptors

The classification of a biosensor can be made on the basis of the class of bioreceptor. The next section will discuss the two more popular bioreceptors, since they will be discussed in this doctoral thesis (Chapters 5 and 6).

1.6.3.1. Antibodies

Antibodies are the most common bioreceptors used in biosensors. There are different types of antibodies according to their production and specificity: polyclonal, monoclonal and recombinant. The way in which an antibody interacts with an antigen is due to affinity, and based on weak, but multiple, physical forces (Vo-Dinh and Cullum, 2000). Antibodies are generally immobilized on a substrate, which can be further integrated in the transducer or, instead, directly immobilized on the transducer surface. For instance, it was reported a SPR biosensor based on biotinylated antibody-functionalized titanium nitrite (BAF-TiN), where the exosomes were immunocaptured by CD63 and EGFRvIII proteins of

the exosomes derived from the U251 glioma cell line (Qiu et al., 2019). It was demonstrated an electrochemical biosensor based on a gold electrode functionalized with the antiCD81 antibody for the immunocapture of exosomes derived from the MFC7 breast cancer cell line (Kilic et al., 2018).

In this Ph.D. thesis, an electrochemical immunosensor based on antibody-modified magnetic platforms was developed for the detection and determination of cancer-related exosomes from breast cancer patients (see Chapter 5).

1.6.3.2. Enzymes

Enzymes were the first recognition elements applied as bioreceptors in biosensors. Clark and Lyons used glucose oxidase (GOX) entrapped at a Clark oxygen electrode using a dialysis membrane (Clark and Lyons, 1962). Enzymatic biosensors are based on the selective reaction of enzymes by a specific substrate. To the best of our knowledge, there are no studies on biosensors measuring enzyme activity on exosomes. Although studies have demonstrated the presence of the alkaline phosphatase (ALP) enzyme in osteoblastic derived exosomes (Sanchez et al., 2020), to the best of our knowledge, there are no available studies on the use of biosensors for the quantification of ALP enzyme activity in exosomes.

In this Ph.D. thesis, an electrochemical sensor combining immunomagnetic separation was developed for the detection and determination of the intrinsic catalytic activity of the ALP enzyme directly on osteoblastic-derived exosomes and cancer-related exosomes from breast cancer patients (see Chapter 6).

1.6.4. Transducers

Biosensors can also be classified according to the method of signal transduction. Although there are various types of transducers constantly being developed, optical, electrochemical, mass-based, and thermal-based transducers are the most commonly applied in biosensors. Each of these main classes contains many different subclasses. Below is an overview of some examples based on electrochemical readout, since is the transducing strategy used in this doctoral thesis.

1.6.4.1. Amperometric biosensors

Electrochemical transducers are based on electrical changes that occur when a target analyte binds to receptors immobilized on the transducer surface. Electrochemical sensing approaches provide rapid assays and affordable readout systems. Miniaturized electrochemical sensors have been used to routinely detect toxic gases and chemicals, as well as biomolecules (as is the case of the popular glucometer). They can prove highly sensitive information when combined with certain enzyme reporters for signal amplification. Among the different types of electrochemical biosensors, amperometric transducers measure the changes in the current at the working electrode due to direct oxidation of the products of a biochemical reaction.

The electron transfer in an electrochemical biosensor sometimes requires a mediator due to the irreversible redox behavior of the biological component as a result of slow heterogeneous electron transfer at the electrode surface (Fultz and Durst, 1982). Mediators are electron-transferring agents that participate in the redox reaction with the biological component, providing a rapid electron transfer. Mediators are low molecular weight redox couples that shuttle electrons from the redox center of the biological component to the electrode surface (Chaubey and Malhotra, 2002; Fultz and Durst, 1982).

The horseradish peroxidase (HRP) enzyme is one of the most commonly used enzymes for the construction of biosensors. It contains heme as a prosthetic group, which is the protein active site, along with heme-iron Fe(III). It can catalyze the oxidation of a wide variety of substrates by hydrogen peroxide (H_2O_2), and the reduced form of HRP can be chemically re-oxidized by H_2O_2. However, the direct electron transfer between HRP and an electrode is difficult because the active sites of HRP are deeply buried in a thick protein shell and because the large distance between the active sites and the electrode surface slow down the electron transfer. Electron transfer via a mediator, however, is more effective for establishing an electrical connection between the redox centers and the electrode (Chaubey and Malhotra, 2002). In the presence of a mediator such as hydroquinone (HQ), the reaction mechanism of the H_2O_2 biosensor based on the HRP enzyme can be summarized as follows (Chaubey and Malhotra, 2002; Fultz and Durst, 1982): the H_2O_2 in the solution is reduced by the HRP, and the reduced HRP is regenerated with the aid of the hydroquinone mediator, while the mediator itself is oxidized in the enzymatic reaction. Finally, the oxidized mediator is electrochemically reduced on the electrode surface, leading to an increase in the reduction current. The relationship between the current and the concentration of the analyte (in this case, the mediator) can be expressed by the Cottrell equation (Bard and Faulkner, 2001; Cottrell, 1903), as shown in Fig. 1.16. In the Cottrell

equation, i is the current (A), n is the number of electrons transferred, F is Faraday's constant (96,487 C mol^{-1}), A is the area of the planar electrode (cm2), c0 is the initial concentration of the analyte (mol mL^{-1}), D is the diffusion coefficient (cm2 s^{-1}), and t is the time elapsed since the potential was applied (s).

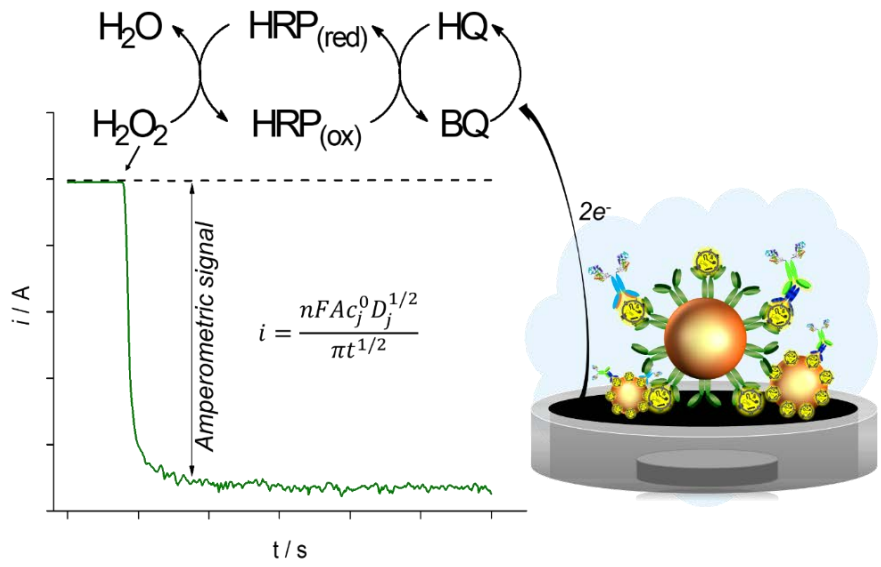

Fig. 1.16. Schematic diagram of a mediated electron transfer in an enzyme reaction sequence. Specifically, hydroquinone (HQ) as the mediator, horseradish peroxidase (HRP) as the enzyme, hydrogen peroxide (H_2O_2) as the oxidizing agent.

1.7. References

Admyre, C., Grunewald, J., Thyberg, J., et al. Exosomes with major histocompatibility complex class II and co-stimulatory molecules are present in human BAL fluid. Eur. Respir. J. 2003; 22: 578.

Akers, J. C., Ramakrishnan, V., Nolan, J. P., et al. Comparative Analysis of Technologies for Quantifying Extracellular Vesicles (EVs) in Clinical Cerebrospinal Fluids (CSF). PLoS One. 2016; 11: e0149866.

Al-Nedawi, K., Meehan, B., Micallef, J., et al. 2008. Intercellular transfer of the oncogenic receptor EGFRvIII by microvesicles derived from tumour cells. Nat. Cell Biol. 2008; 10: 619.

Alexander, M., Hu, R., Runtsch, M. C., et al. Exosome-delivered microRNAs modulate the inflammatory response to endotoxin. Nat. Commun. 2015; 6: 7321.

Anderson, J. D., Johansson, H. J., Graham, C. S., et al. Comprehensive Proteomic Analysis of Mesenchymal Stem Cell Exosomes Reveals Modulation of Angiogenesis via Nuclear Factor-KappaB Signaling. Stem Cells. 2016; 34: 601.

Andreu, Z., Yáñez-Mó, M., Tetraspanins in Extracellular Vesicle Formation and Function. Front. Immunol. 2014; 5: 442.

Antonyak, M. A., Li, B., Boroughs, L. K., et al. Cancer cell-derived microvesicles induce transformation by transferring tissue transglutaminase and fibronectin to recipient cells. Proc. Natl. Acad. Sci. U. S. A. 2011; 108: 4852.

Araùjo, M., Hube, L. A., Stasyk, T., Isolation of Endocitic Organelles by Density Gradient Centrifugation. Humana Press, 2008; 424: 317.

Azmi, A. S., Nuclear export mechanisms of circular RNAs: size does matter. Non-coding RNA Investig. 2018; 2: 52.

Balaj, L., Atai, N. A., Chen, W., et al. Heparin affinity purification of extracellular vesicles. Sci. Rep. 2015; 5: 10266.

Balaj, L., Lessard, R., Dai, L., et al. Tumour microvesicles contain retrotransposon elements and amplified oncogene sequences. Nat. Commun. 2011; 2: 180.

Bard, A. J., Faulkner, L.R., Electrochemical methods, 2nd ed. Willey, New York, 2011.

Baroni, S., Romero-Cordoba, S., Plantamura, I., et al. Exosome-mediated delivery of miR-9 induces cancer-associated fibroblast-like properties in human breast fibroblasts. Cell Death Dis. 2016; 7: e2312.

Batagov, A. O., Kurochkin, I. V. Exosomes secreted by human cells transport largely mRNA fragments that are enriched in the 3′-untranslated regions. Biol. Direct. 2013; 8: 12.

Benedikter, B. J., Bouwman, F. G., Vajen, T., et al. Ultrafiltration combined with size exclusion chromatography efficiently isolates extracellular vesicles from cell culture media for compositional and functional studies. Sci. Rep. 2017; 7: 15297.

Beretov, J., Cozzi, P., Duan, W., et al. Epithelial cell adhesion molecule (EpCAM) is involved in prostate cancer chemotherapy/radiotherapy response in vivo. BMC Cancer. 2018; 18: 1092.

Bethune, G., Bethune, D., Ridgway, N., et al. Epidermal growth factor receptor (EGFR) in lung cancer: an overview and update. J. Thorac. Dis. 2010; 2: 48.

Bjørge, I. M., Kim, S. Y., Mano, J. F., et al. Extracellular vesicles, exosomes and shedding vesicles in regenerative medicine – a new paradigm for tissue repair. Biomater. Sci. 2018; 6: 60.

Boukouris, S., Mathivanan, S. Exosomes in bodily fluids are a highly stable resource of disease biomarkers. PROTEOMICS - Clin. Appl. 2015; 9: 358.

Brandão, D., Liébana, S., Pividori, M. I. Multiplexed detection of foodborne pathogens based on magnetic particles. N. Biotechnol. 2015; 32: 511.

Brown, M., Wittwer, C. Flow cytometry: principles and clinical applications in hematology. Clin. Chem. 2000; 46: 1221.

Bruening, J., Lasswitz, L., Banse, P., et al. Hepatitis C virus enters liver cells using the CD81 receptor complex proteins calpain-5 and CBLB. PLOS Pathog. 2018; 14: e1007111.

Bryant, R. J., Pawlowski, T., Catto, J. W. F., et al. Changes in circulating microRNA levels associated with prostate cancer. Br. J. Cancer 2012; 106: 768.

Brzozowski, J. S., Bond, D. R., Jankowski, H., et al. Extracellular vesicles with altered tetraspanin CD9 and CD151 levels confer increased prostate cell motility and invasion. Sci. Rep. 2018; 8: 8822.

Burkova, E. E., Grigor'eva, A. E., Bulgakov, D. V., et al. Extra Purified Exosomes from Human Placenta Contain an Unpredictable Small Number of Different Major Proteins. Int. J. Mol. Sci. 2019; 20: 2434.

Cahiez, G., Lefèvre, N., Poizat, M., et al. A User-Friendly Procedure for the Preparation of Secondary Alkyl Chlorides. Synthesis (Stuttg). 2012; 45: 231.

Cappellesso, R., Tinazzi, A., Giurici, T., et al. Programmed cell death 4 and microRNA 21 inverse expression is maintained in cells and exosomes from ovarian serous carcinoma effusions. Cancer Cytopathol. 2014; 122; 685.

Carinelli, S., Martí, M., Alegret, S., et al. Biomarker detection of global infectious diseases based on magnetic particles. N. Biotechnol. 2015; 32: 521.

Chaubey, A., Malhotra, B.D., Mediated biosensors. Biosens. Bioelectron. 2002; 17: 441.

Chevillet, J. R., Kang, Q., Ruf, I. K., et al. Quantitative and stoichiometric analysis of the microRNA content of exosomes. Proc. Natl. Acad. Sci. U. S. A. 2014; 111: 14888.

Chiba, M., Kimura, M., Asari, S., Exosomes secreted from human colorectal cancer cell lines contain mRNAs, microRNAs and natural antisense RNAs, that can transfer into the human hepatoma HepG2 and lung cancer A549 cell lines. Oncol. Rep. 2012; 28: 1551.

Chiriacò, M., Bianco, M., Nigro, A., et al. Lab-on-Chip for Exosomes and Microvesicles Detection and Characterization. Sensors. 2018; 18: 3175.

Chiu, Y.-J., Cai, W., Shih, Y.-R. V., et al. A Single-Cell Assay for Time Lapse Studies of Exosome Secretion and Cell Behaviors. Small. 2016; 12: 3658.

Cho, Y.-E., Im, E.-J., Moon, P.-G., et al. Increased liver-specific proteins in circulating extracellular vesicles as potential biomarkers for drug- and alcohol-induced liver injury. PLoS One 2017; 12: e0172463.

Choi, H., Mun, J. Y., Structural Analysis of Exosomes Using Different Types of Electron Microscopy. Appl. Microsc. 2017; 47: 171.

Chow, A., Zhou, W., Liu, L., et al. Macrophage immunomodulation by breast cancer-derived exosomes requires Toll-like receptor 2-mediated activation of NF-κB. Sci. Rep. 2015; 4: 5750.

Chu, B. Laser Light Scattering. Annu. Rev. Phys. Chem. 1970; 21: 145.

Clark, L. C., Lyons, C. Electrode systems for continuous monitoring in cardiovascular surgery. Ann. N. Y. Acad. Sci. 1962; 102: 29.

Cottrell, F. G. Residual current in galvanic polarization regarded as a diffusion problem. Z. Phys. Chemie. 1903; 42: 385.

Dai, M., Yuan, F., Fu, C., et al. Relationship between epithelial cell adhesion molecule (EpCAM) overexpression and gastric cancer patients: A systematic review and meta-analysis. PLoS One. 2017; 12: e0175357.

Davidson, S. M., Riquelme, J. A., Zheng, Y., et al. Endothelial cells release cardioprotective exosomes that may contribute to ischaemic preconditioning. Sci. Rep. 2018; 8: 15885.

Day, K. C., Hiles, G. L., Kozminsky, M., et al. HER2 and EGFR Overexpression Support Metastatic Progression of Prostate Cancer to Bone. Cancer Res. 2017; 77: 74.

Deregibus, M. C., Figliolini, F., D'antico, S., et al. Charge-based precipitation of extracellular vesicles. Int. J. Mol. Med. 2016; 38: 1359.

Dhar, D., Antonucci, L., Nakagawa, H., et al. Liver Cancer Initiation Requires p53 Inhibition by CD44-Enhanced Growth Factor Signaling. Cancer Cell 2018; 33: 1061.e6.

Dick, R. A., Zadrozny, K. K., Xu, C., et al. Inositol phosphates are assembly co-factors for HIV-1. Nature 2018; 560: 509.

Doldán, X., Fagúndez, P., Cayota, A., et al. Electrochemical Sandwich Immunosensor for Determination of Exosomes Based on Surface Marker-Mediated Signal Amplification. Anal. Chem. 2016; 88: 10466.

Dong, H., Chen, H., Jiang, J., et al. Highly Sensitive Electrochemical Detection of Tumor Exosomes Based on Aptamer Recognition-Induced Multi-DNA Release and Cyclic Enzymatic Amplification. Anal. Chem. 2018; 90: 4507.

Dragovic, R. A., Gardiner, C., Brooks, A. S., et al. Sizing and phenotyping of cellular vesicles using Nanoparticle Tracking Analysis. Nanomedicine Nanotechnology, Biol. Med. 2011; 7: 780.

Eichelser, C., Stückrath, I., Müller, V., et al. Increased serum levels of circulating exosomal microRNA-373 in receptor-negative breast cancer patients. Oncotarget 2014; 5: 9650.

European Medicines Agency. Innovation and biomarkers in cancer drug development (IBCD) 2018. Available in: https://www.ema.europa.eu. 2020.

Enderle, D., Spiel, A., Coticchia, C. M., et al. Characterization of RNA from Exosomes and Other Extracellular Vesicles Isolated by a Novel Spin Column-Based Method. PLoS One. 2015; 10: e0136133.

Etayash, H., McGee, A. R., Kaur, K., et al. Nanomechanical sandwich assay for multiple cancer biomarkers in breast cancer cell-derived exosomes. Nanoscale 2016; 8: 15137.

Fang, C., Zhou, Z., Hu, J., et al. CD133+CD54+CD44+ circulating tumor cells as a biomarker of treatment selection and liver metastasis in patients with colorectal cancer. Oncotarget. 2016; 7: 77389.

Fang, S., Tian, H., Li, Xiancheng, et al. Clinical application of a microfluidic chip for immunocapture and quantification of circulating exosomes to assist breast cancer diagnosis and molecular classification. PLoS One. 2017; 12: e0175050.

Fang, X., Zheng, P., Tang, J., CD24: from A to Z. Cell. Mol. Immunol. 2010; 7: 100.

U.S. Food and Drug Administration. Available in: https://www.fda.gov. 2020.

Fenner, A., Biomarkers: Urinary exosome biomarkers of radiation exposure. Nat. Rev. Urol. 2016; 13: 437.

Fernandez-de-Cossio-Diaz, J., Vazquez, A., Limits of aerobic metabolism in cancer cells. Sci. Rep. 2017; 7: 13488.

Fernando, M. R., Jiang, C., Krzyzanowski, G. D., New evidence that a large proportion of human blood plasma cell-free DNA is localized in exosomes. PLoS One. 2017; 12: e0183915.

Filipe, V., Hawe, A., Jiskoot, W., Critical Evaluation of Nanoparticle Tracking Analysis (NTA) by NanoSight for the Measurement of Nanoparticles and Protein Aggregates. Pharm. Res. 2010; 27: 796.

Fraikin, J.-L., Teesalu, T., McKenney, C. M., et al. A high-throughput label-free nanoparticle analyser. Nat. Nanotechnol. 2011; 6: 308.

Fu, Q., Zhang, Q., Lou, Y., et al. Primary tumor-derived exosomes facilitate metastasis by regulating adhesion of circulating tumor cells via SMAD3 in liver cancer. Oncogene. 2018; 37: 6105.

Fujita, Y., Kuwano, K., Ochiya, T., et al. The impact of extracellular vesicle-encapsulated circulating microRNAs in lung cancer research. Biomed Res. Int. 2014; 486413.

Fultz, M. L., Durst, R. A. Mediator compounds for the electrochemical study of biological redox systems: a compilation. Anal. Chim. Acta. 1982; 140: 1.

Galizia, G., Lieto, E., Orditura, M., et al. Epidermal Growth Factor Receptor (EGFR) Expression is Associated With a Worse Prognosis in Gastric Cancer Patients Undergoing Curative Surgery. World J. Surg. 2007; 31: 1458.

Gallart-Palau, X., Serra, A., Wong, A. S. W., et al. Extracellular vesicles are rapidly purified from human plasma by protein Organic Solvent precipitation (PROSPR). Sci. Rep. 2015; 5: 14664.

Gámez-Valero, A., Monguió-Tortajada, M., Carreras-Planella, L., et al. Size-Exclusion Chromatography-based isolation minimally alters Extracellular Vesicles' characteristics compared to precipitating agents. Sci. Rep. 2016; 6: 33641.

Gao, F., Jiao, F., Xia, C., et al. A novel strategy for facile serum exosome isolation based on specific interactions between phospholipid bilayers and TiO2. Chem. Sci. 2019; 10: 1579.

Gardiner, C., Ferreira, Y. J., Dragovic, R. A., Redman, et al. Extracellular vesicle sizing and enumeration by nanoparticle tracking analysis. J. Extracell. Vesicles 2013; 2: 19671.

Gerbitz, A., Ewing, P., Olkiewicz, K., et al. A role for CD54 (intercellular adhesion molecule-1) in leukocyte recruitment to the lung during the development of experimental idiopathic pneumonia syndrome. Transplantation 2005; 79: 536.

Ghosh, A., Davey, M., Chute, I. C., et al. Rapid Isolation of Extracellular Vesicles from Cell Culture and Biological Fluids Using a Synthetic Peptide with Specific Affinity for Heat Shock Proteins. PLoS One. 2014; 9: e110443.

Gluschankof, P., Mondor, I., Gelderblom, H. R., et al. Cell Membrane Vesicles Are a Major Contaminant of Gradient-Enriched Human Immunodeficiency Virus Type-1 Preparations. Virology. 1997; 230: 125.

Gong, Y., Scott, E., Lu, R., et al. TIMP-1 Promotes Accumulation of Cancer Associated Fibroblasts and Cancer Progression. PLoS One 2013; 8: e77366.

Goto, T., Fujiya, M., Konishi, H., et al. An elevated expression of serum exosomal microRNA-191, − 21, −451a of pancreatic neoplasm is considered to be efficient diagnostic marker. BMC Cancer 2018; 18: 116.

Graham, J. M., Purification of a Crude Mitochondrial Fraction by Density-Gradient Centrifugation, in: Current Protocols in Cell Biology. John Wiley & Sons, Inc., Hoboken, NJ, USA, 2001.

Graner, M. W., Alzate, O., Dechkovskaia, A. M., et al. Proteomic and immunologic analyses of brain tumor exosomes. FASEB J. 2009; 23: 1541.

Gress, D. M., Edge, S. B., Greene, F. L., et al. Principles of Cancer Staging, in: AJCC Cancer Staging Manual. Springer International Publishing, Cham. 2017.

Grigorov, B., Attuil-Audenis, V., Perugi, F., et al. A role for CD81 on the late steps of HIV-1 replication in a chronically infected T cell line. Retrovirology. 2009; 6: 28.

Guilmain, W., Colin, S., Legrand, E., et al. CD9P-1 expression correlates with the metastatic status of lung cancer and a truncated form of CD9P-1, GS-168AT2, inhibits in vivo tumour growth. Br. J. Cancer 2011; 104: 496.

Guo, P., Huang, J., Wang, L., et al. ICAM-1 as a molecular target for triple negative breast cancer. Proc. Natl. Acad. Sci. U. S. A. 2014; 111: 14710.

Hannafon, B. N., Trigoso, Y. D., Calloway, C. L., et al. Plasma exosome microRNAs are indicative of breast cancer. Breast Cancer Res. 2016; 18: 90.

Hao, Y.-X., Li, Y.-M., Ye, M., et al. KRAS and BRAF mutations in serum exosomes from patients with colorectal cancer in a Chinese population. Oncol. Lett. 2017; 13: 3608.

Harding, C., Heuser, J., Stahl, P. Receptor-mediated endocytosis of transferrin and recycling of the transferrin receptor in rat reticulocytes. J. Cell Biol. 1983; 97: 329.

Hasegawa, K., Sato, A., Tanimura, K., et al. Fraction of MHCII and EpCAM expression characterizes distal lung epithelial cells for alveolar type 2 cell isolation. Respir. Res. 2017; 18: 150.

He, L., Hannon, G. J. MicroRNAs: small RNAs with a big role in gene regulation. Nat. Rev. Genet. 2004; 5: 522.

Hemler, M. E. Tetraspanin proteins promote multiple cancer stages. Nat. Rev. Cancer 2013; 14: 49.

Heo, D., Huh, Y.-M., Yang, J., et al. Molecular Imaging of CD44-Overexpressing Gastric Cancer in Mice Using T2 MR Imaging. J. Nanosci. Nanotechnol. 2015; 16; 196.

Hong, X., Schouest, B., Xu, H., Effects of exosome on the activation of CD4+ T cells in rhesus macaques: a potential application for HIV latency reactivation. Sci. Rep. 2017; 7: 15611.

Hoo, C. M., Starostin, N., West, P., et al. A comparison of atomic force microscopy (AFM) and dynamic light scattering (DLS) methods to characterize nanoparticle size distributions. J. Nanoparticle Res. 2008; 10: 89.

Hoogenboom, R., Fijten, M. W. M., Kickelbick, G., et al. Synthesis and crystal structures of multifunctional tosylates as basis for star-shaped poly(2-ethyl-2-oxazoline)s. Beilstein J. Org. Chem. 2010; 6: 773.

Hornick, N. I., Huan, J., Doron, B., et al. Serum Exosome MicroRNA as a Minimally-Invasive Early Biomarker of AML. Sci. Rep. 2015; 5: 11295.

Houseley, J., LaCava, J., Tollervey, D. RNA-quality control by the exosome. Nat. Rev. Mol. Cell Biol. 2006; 7: 529.

Hu, B., Ma, Y., Yang, Y., et al. CD44 promotes cell proliferation in non-small cell lung cancer. Oncol. Lett. 2018; 15: 5627.

Huang, Lin, Wang, D.-B., Singh, N., et al. A dual-signal amplification platform for sensitive fluorescence biosensing of leukemia-derived exosomes. Nanoscale. 2018; 10: 20289.

Huang, Li, Yang, Y., Yang, F., et al. Functions of EpCAM in physiological processes and diseases (Review). Int. J. Mol. Med. 2018; 42: 1771.

Huang, L. R., Cox, E. C., Austin, R. H., et al. Continuous Particle Separation Through Deterministic Lateral Displacement. Science. 2004; 304: 987.

Huang, X., Yuan, T., Liang, M., et al. Exosomal miR-1290 and miR-375 as prognostic markers in castration-resistant prostate cancer. Eur. Urol. 2015; 67: 33.

Ibsen, S. D., Wright, J., Lewis, J. M., et al. Rapid Isolation and Detection of Exosomes and Associated Biomarkers from Plasma. ACS Nano. 2017; 11: 6641.

Iczkowski, K. A., Cell adhesion molecule CD44: its functional roles in prostate cancer. Am. J. Transl. Res. 2010; 3: 1.

Im, H., Shao, H., Park, Y. II, et al. Label-free detection and molecular profiling of exosomes with a nano-plasmonic sensor. Nat. Biotechnol. 2014; 32: 490.

IUPAC. Compendium of Chemical Terminology. Research Triagle Park, NC, 2020.

Iwai, K., Minamisawa, T., Suga, K., et al. Isolation of human salivary extracellular vesicles by iodixanol density gradient ultracentrifugation and their characterizations. J. Extracell. Vesicles 2016; 5: 30829.

Jella, K. K., Yu, L., Yue, Q., et al. Exosomal GAPDH from Proximal Tubule Cells Regulate ENaC Activity. PLoS One. 2016; 11: e0165763.

Jenjaroenpun, P., Kremenska, Y., Nair, V. M., et al. Characterization of RNA in exosomes secreted by human breast cancer cell lines using next-generation sequencing. PeerJ. 2013; 1: e201.

Jiang, B., Aerobic glycolysis and high level of lactate in cancer metabolism and microenvironment. Genes Dis. 2017; 4: 25.

Jiang, H., Li, Z., Li, X., et al. Intercellular transfer of messenger RNAs in multiorgan tumorigenesis by tumor cell-derived exosomes. Mol. Med. Rep. 2015; 11: 4657.

Jin, X., Chen, Y., Chen, H., et al. Evaluation of Tumor-Derived Exosomal miRNA as Potential Diagnostic Biomarkers for Early-Stage Non–Small Cell Lung Cancer Using Next-Generation Sequencing. Clin. Cancer Res. 2017; 23: 5311.

Johnstone, R. M., Adam, M., Hammond, J. R., et al. Vesicle formation during reticulocyte maturation. Association of plasma membrane activities with released vesicles (exosomes). J. Biol. Chem. 1987; 262: 9412.

Junquera, C., Castiella, T., Muñoz, G., et al. Biogenesis of a new type of extracellular vesicles in gastrointestinal stromal tumors: ultrastructural profiles of spheresomes. Histochem. Cell Biol. 2016; 146: 557.

Kahlert, C., Melo, S. A., Protopopov, A., et al. Identification of double-stranded genomic DNA spanning all chromosomes with mutated KRAS and p53 DNA in the serum exosomes of patients with pancreatic cancer. J. Biol. Chem. 2014; 289: 3869.

Kalluri, R., LeBleu, V. S. Discovery of Double-Stranded Genomic DNA in Circulating Exosomes. Cold Spring Harb. Symp. Quant. Biol. 2016; 81: 275.

Kapustin, A. N., Schoppet, M., Schurgers, L. J., et al. Prothrombin Loading of Vascular Smooth Muscle Cell–Derived Exosomes Regulates Coagulation and Calcification. Arterioscler. Thromb. Vasc. Biol. 2017; 37: e22.

Ke, J., Wu, X., Wu, X., et al. A subpopulation of CD24+ cells in colon cancer cell lines possess stem cell characteristics. Neoplasma. 2012; 59: 282.

Keerthikumar, S., Gangoda, L., Liem, M., et al. Proteogenomic analysis reveals exosomes are more oncogenic than ectosomes. Oncotarget. 2015; 6: 15375.

Kilchert, C., Wittmann, S., Vasiljeva, L. The regulation and functions of the nuclear RNA exosome complex. Nat. Rev. Mol. Cell Biol. 2016; 17: 227.

Kilic, T., Valinhas, A. T. D. S., Wall, I., et al. Label-free detection of hypoxia-induced extracellular vesicle secretion from MCF-7 cells. Sci. Rep. 2018; 8: 9402.

Kim, K.-J., Kwon, H. J., Kim, M. C., et al. CD9 Expression in Colorectal Carcinomas and Its Prognostic Significance. J. Pathol. Transl. Med. 2016; 50: 459.

King, H. W., Michael, M. Z., Gleadle, J. M. Hypoxic enhancement of exosome release by breast cancer cells. BMC Cancer. 2012; 12: 421.

Ko, J., Bhagwat, N., Yee, S. S., et al. Combining Machine Learning and Nanofluidic Technology To Diagnose Pancreatic Cancer Using Exosomes. ACS Nano. 2017; 11: 11182.

Ko, J., Hemphill, M. A., Gabrieli, D., et al. Smartphone-enabled optofluidic exosome diagnostic for concussion recovery. Sci. Rep. 2016; 6: 31215.

Kohmo, S., Kijima, T., Otani, Y., et al. Cell Surface Tetraspanin CD9 Mediates Chemoresistance in Small Cell Lung Cancer. Cancer Res. 2010; 70: 8025.

Kojima, R., Bojar, D., Rizzi, G., et al. Designer exosomes produced by implanted cells intracerebrally deliver therapeutic cargo for Parkinson's disease treatment. Nat. Commun. 2018; 9: 1305.

Komposch, K., Sibilia, M., EGFR signaling in liver diseases. Int. J. Mol. Sci. 2015; 17: 30.

Kondratov, K. A., Petrova, T. A., Mikhailovskii, V. Y., et al. A study of extracellular vesicles isolated from blood plasma conducted by low-voltage scanning electron microscopy. Cell tissue biol. 2017; 11: 181.

Krasnov, G. S., Dmitriev, A. A., Snezhkina, A. V, et al. Deregulation of glycolysis in cancer: glyceraldehyde-3-phosphate dehydrogenase as a therapeutic target. Expert Opin. Ther. Targets 2013; 17: 681.

Kraus, V. B., Biomarkers as drug development tools: Discovery, validation, qualification and use. Nat. Rev. Rheumatol. 2018; 14: 354.

Kristiansen, G., Schlüns, K., Yongwei, Y., et al. CD24 is an independent prognostic marker of survival in nonsmall cell lung cancer patients. Br. J. Cancer. 2003; 88: 231.

Kwon, M. S., Shin, S.-H., Yim, S.-H., et al. CD63 as a biomarker for predicting the clinical outcomes in adenocarcinoma of lung. Lung Cancer. 2007; 57: 46.

LaBarre, P., Hawkins, K. R., Gerlach, J., et al. A Simple, Inexpensive Device for Nucleic Acid Amplification without Electricity—Toward Instrument-Free Molecular Diagnostics in Low-Resource Settings. PLoS One. 2011; 6: e19738.

Lee, H. H., Allain, J. P., Improving blood safety in resource-poor settings. Vox Sang. 2004; 87: 176.

Lee, K., Shao, H., Weissleder, R., et al. Acoustic Purification of Extracellular Microvesicles. ACS Nano 2015; 9: 2321.

Lee, T. K. W., Castilho, A., Cheung, V. C. H., et al. CD24(+) liver tumor-initiating cells drive self-renewal and tumor initiation through STAT3-mediated NANOG regulation. Cell Stem Cell 2011; 9: 50.

Levva, S., Kotoula, V., Kostopoulos, I., et al. Prognostic evaluation of epidermal growth factor receptor (EGFR) genotype and phenotype parameters in triple-negative breast cancers. Cancer Genomics and Proteomics 2017; 14: 181.

Lewis, G. D., Metcalf, T. G. Polyethylene glycol precipitation for recovery of pathogenic viruses, including hepatitis A virus and human rotavirus, from oyster, water, and sediment samples. Appl. Environ. Microbiol. 1988; 54: 1983.

Li, C., Liu, S., Yan, R., et al. CD54-NOTCH1 axis controls tumor initiation and cancer stem cell functions in human prostate cancer. Theranostics 2017; 7: 67.

Li, S., Li, Yuchen, Chen, B., et al. exoRBase: a database of circRNA, lncRNA and mRNA in human blood exosomes. Nucleic Acids Res. 2018; 46: D106.

Li, Y., Zheng, Q., Bao, C., et al. Circular RNA is enriched and stable in exosomes: a promising biomarker for cancer diagnosis. Cell Res. 2015; 25: 981.

Liu, C., Guo, J., Tian, F., et al. Field-Free Isolation of Exosomes from Extracellular Vesicles by Microfluidic Viscoelastic Flows. ACS Nano 2017: 11, 6968.

Liu, F., Vermesh, O., Mani, V., et al. The Exosome Total Isolation Chip. ACS Nano 2017; 11: 10712.

Liu, T., Zhang, X., Du, L., et al. Exosome-transmitted miR-128-3p increase chemosensitivity of oxaliplatin-resistant colorectal cancer. Mol. Cancer 2019; 18: 43.

Lobb, R. J., Becker, M., Wen Wen, S., et al. Optimized exosome isolation protocol for cell culture supernatant and human plasma. J. Extracell. Vesicles 2015; 4: 27031.

Logozzi, M., Angelini, D. F., Iessi, E., et al. Increased PSA expression on prostate cancer exosomes in in vitro condition and in cancer patients. Cancer Lett. 2017; 403: 318.

López-Cobo, S., Campos-Silva, C., Moyano, A., et al. Immunoassays for scarce tumour-antigens in exosomes: detection of the human NKG2D-Ligand, MICA, in tetraspanin-containing nanovesicles from melanoma. J. Nanobiotechnology. 2018; 16: 47.

Lötvall, J., Hill, A. F., Hochberg, F., et al. Minimal experimental requirements for definition of extracellular vesicles and their functions: a position statement from the International Society for Extracellular Vesicles. J. Extracell. Vesicles. 2014; 3: 26913.

Louderbough, J. M. V., Schroeder, J. A. Understanding the Dual Nature of CD44 in Breast Cancer Progression. Mol. Cancer Res. 2011; 9: 1573.

Lozano-Ramos, I., Bancu, I., Oliveira-Tercero, A., et al. Size-exclusion chromatography-based enrichment of extracellular vesicles from urine samples. J. Extracell. Vesicles 2015; 4: 27369.

Lyu, L., Zhang, X., Li, C., et al. Small RNA Profiles of Serum Exosomes Derived From Individuals With Latent and Active Tuberculosis. Front. Microbiol. 2019; 10: 1174.

Maas, S. L. N., de Vrij, J., van der Vlist, E.J., et al. Possibilities and limitations of current technologies for quantification of biological extracellular vesicles and synthetic mimics. J. Control. Release 2015; 200: 87.

Madhavan, B., Yue, S., Galli, U., et al. Combined evaluation of a panel of protein and miRNA serum-exosome biomarkers for pancreatic cancer diagnosis increases sensitivity and specificity. Int. J. Cancer 2015; 136: 2616.

Maia, J., Caja, S., Strano Moraes, M.C., et al. Exosome-Based Cell-Cell Communication in the Tumor Microenvironment. Front. Cell Dev. Biol. 2018; 6: 18.

Marczak, S., Richards, K., Ramshani, Z., et al. Simultaneous isolation and preconcentration of exosomes by ion concentration polarization. Electrophoresis. 2018; 39: 2029.

Mathieu, M., Martin-Jaular, L., Lavieu, G., et al. Specificities of secretion and uptake of exosomes and other extracellular vesicles for cell-to-cell communication. Nat. Cell Biol. 2019; 21: 9.

Mathivanan, S., Simpson, R. J. ExoCarta: A compendium of exosomal proteins and RNA. Proteomics 2009; 9: 4997.

Matsumoto, T., Takai, A., Eso, Y., et al. Proliferating EpCAM-positive ductal cells in the inflamed liver give rise to hepatocellular carcinoma. Cancer Res. 2017; 77: 6131.

Meehan, B., Rak, J., Di Vizio, D., Oncosomes - large and small: what are they, where they came from? J. Extracell. vesicles 2016; 5: 33109.

Meldolesi, J. Exosomes and Ectosomes in Intercellular Communication. Curr. Biol. 2018; 28: R435.

Metzker, M. L., Caskey, C. T. Polymerase Chain Reaction (PCR), in: Encyclopedia of Life Sciences. John Wiley & Sons, Ltd, Chichester, UK, 2009.

Miki, Y., Yashiro, M., Okuno, T., et al. Clinico-pathological significance of exosome marker CD63 expression on cancer cells and stromal cells in gastric cancer. PLoS One 2018; 13: e0202956.

Mikuriya, K., Kuramitsu, Y., Ryozawa, S., et al. Expression of glycolytic enzymes is increased in pancreatic cancerous tissues as evidenced by proteomic profiling by two-dimensional electrophoresis and liquid chromatography-mass spectrometry/mass spectrometry. Int. J. Oncol. 2007; 30: 849.

Minciacchi, V. R., Freeman, M. R., Di Vizio, D. Extracellular Vesicles in Cancer: Exosomes, Microvesicles and the Emerging Role of Large Oncosomes. Semin. Cell Dev. Biol. 2015a; 40: 41.

Minciacchi, V. R., You, S., Spinelli, C., et al. Large oncosomes contain distinct protein cargo and represent a separate functional class of tumor-derived extracellular vesicles. Oncotarget 2015b; 6: 11327.

Moura, S. L., Martì, M., Pividori, M. I., Matrix Effect in the Isolation of Breast Cancer-Derived Nanovesicles by Immunomagnetic Separation and Electrochemical Immunosensing — A Comparative Study. Sensors. 2020a; 20: 965.

Moura, S. L., Martín, C. G., Martí, M., Pividori, M. I., Multiplex detection and characterization of breast cancer exosomes by magneto-actuated immunoassay. Talanta 2020b; 211: 120657.

Moura, S. L., Martín, C. G., Martí, M., Pividori, M. I. Electrochemical immunosensing of nanovesicles as biomarkers for breast cancer. Biosens. Bioelectron. 2020c; 150: 111882.

Mullis, K. B., Faloona, F. A. Specific synthesis of DNA in vitro via a polymerase-catalyzed chain reaction. Methods Enzymol. 1987; 155: 335.

Munson, P., Lam, Y.-W., Dragon, J., et al. Exosomes from asbestos-exposed cells modulate gene expression in mesothelial cells. FASEB J. 2018; 32: 4328.

Murayama, Y., Oritani, K., Tsutsui, S. Novel CD9-targeted therapies in gastric cancer. World J. Gastroenterol. 2015; 21: 3206.

Murphy, D. E., de Jong, O. G., Brouwer, M., et al. Extracellular vesicle-based therapeutics: natural versus engineered targeting and trafficking. Exp. Mol. Med. 2019; 51: 32.

Nicolazzo, C., Raimondi, C., Francescangeli, F., et al. EpCAM-expressing circulating tumor cells in colorectal cancer. Int. J. Biol. Markers 2017; 32: e415.

Nilsson, J., Skog, J., Nordstrand, A., et al. Prostate cancer-derived urine exosomes: a novel approach to biomarkers for prostate cancer. Br. J. Cancer 2009; 100: 1603.

Niu, Z., Pang, R. T. K., Liu, W., et al. Polymer-based precipitation preserves biological activities of extracellular vesicles from an endometrial cell line. PLoS One 2017; 12: e0186534.

Oliveira-Rodríguez, M., López-Cobo, S., Reyburn, H. T., et al. Development of a rapid lateral flow immunoassay test for detection of exosomes previously enriched from cell culture medium and body fluids. J. Extracell. Vesicles 2016; 5: 31803.

Orentas, R. J., Hildreth, J. E. K. Association of Host Cell Surface Adhesion Receptors and Other Membrane Proteins with HIV and SIV. AIDS Res. Hum. Retroviruses 2009; 9: 1157.

Pan, B.-T., Johnstone, R. M. Fate of the transferrin receptor during maturation of sheep reticulocytes in vitro: Selective externalization of the receptor. Cell 1983; 33: 967.

Pan, L., Liang, W., Fu, M., et al. Exosomes-mediated transfer of long noncoding RNA ZFAS1 promotes gastric cancer progression. J. Cancer Res. Clin. Oncol. 2017; 143: 991.

Panigrahi, G. K., Praharaj, P. P., Peak, T. C., et al. Hypoxia-induced exosome secretion promotes survival of African-American and Caucasian prostate cancer cells. Sci. Rep. 2018; 8: 3853.

Parolini, I., Federici, C., Raggi, C., et al. Microenvironmental pH is a key factor for exosome traffic in tumor cells. J. Biol. Chem. 2009; 284: 34211.

Plebanek, M. P., Angeloni, N. L., Vinokour, E., et al. Pre-metastatic cancer exosomes induce immune surveillance by patrolling monocytes at the metastatic niche. Nat. Commun. 2017; 8: 1319.

Qi, H., Liu, C., Long, L., et al. Blood Exosomes Endowed with Magnetic and Targeting Properties for Cancer Therapy. ACS Nano. 2016; 10: 3323.

Qiu, G., Thakur, A., Xu, C., et al. Detection of Glioma-Derived Exosomes with the Biotinylated Antibody-Functionalized Titanium Nitride Plasmonic Biosensor. Adv. Funct. Mater. 2019; 29: 1806761.

Rabinowits, G., Gerçel-Taylor, C., Day, J. M., et al. Exosomal MicroRNA: A Diagnostic Marker for Lung Cancer. Clin. Lung Cancer. 2009; 10: 42.

Raimondo, S., Saieva, L., Corrado, C., et al. Chronic myeloid leukemia-derived exosomes promote tumor growth through an autocrine mechanism. Cell Commun. Signal. 2015; 13: 8.

Ramanathan, K., Danielsson, B. Principles and applications of thermal biosensors. Biosens. Bioelectron. 2001; 16: 417.

Ramos, A., Morgan, H., Green, N. G., Castellanos, A. Ac electrokinetics: a review of forces in microelectrode structures. J. Phys. D. Appl. Phys. 1998; 31: 2338.

Raposo, G., Nijman, H. W., Stoorvogel, W., et al. B lymphocytes secrete antigen-presenting vesicles. J. Exp. Med. 1996; 183: 1161.

Rappa, G., Green, T. M., Karbanová, J., et al. Tetraspanin CD9 determines invasiveness and tumorigenicity of human breast cancer cells. Oncotarget 2015; 6: 7970.

Ravasi, T., Suzuki, H., Pang, K. C., et al. Experimental validation of the regulated expression of large numbers of non-coding RNAs from the mouse genome. Genome Res. 2006; 16: 11.

Reddy, L. H., Arias, J. L., Nicolas, J., et al. Magnetic Nanoparticles: Design and Characterization, Toxicity and Biocompatibility, Pharmaceutical and Biomedical Applications. Chem. Rev. 2012; 112: 5818.

Révillion, F., Pawlowski, V., Hornez, L., et al. Glyceraldehyde-3-phosphate dehydrogenase gene expression in human breast cancer. Eur. J. Cancer 2000; 36: 1038.

Rho, J., Chung, J., Im, H., et al. Magnetic Nanosensor for Detection and Profiling of Erythrocyte-Derived Microvesicles. ACS Nano 2013; 7: 11227.

Rider, M. A., Hurwitz, S. N., Meckes, D. G., ExtraPEG: A Polyethylene Glycol-Based Method for Enrichment of Extracellular Vesicles. Sci. Rep. 2016; 6: 23978.

Roberts, G. S., Kozak, D., Anderson, W., et al. Tunable Nano/Micropores for Particle Detection and Discrimination: Scanning Ion Occlusion Spectroscopy. Small 2010; 6: 2653.

Rondinelli, R., Epner, D., Tricoli, J. Increased glyceraldehyde-3-phosphate dehydrogenase gene expression in late pathological stage human prostate cancer. Prostate Cancer Prostatic Dis. 1997; 1: 66.

Rood, I. M., Deegens, J. K. J., Merchant, M. L., et al. Comparison of three methods for isolation of urinary microvesicles to identify biomarkers of nephrotic syndrome. Kidney Int. 2010; 78: 810.

Roy, S., Hochberg, F. H., Jones, P. S. Extracellular vesicles: the growth as diagnostics and therapeutics; a survey. J. Extracell. Vesicles 2018; 7: 1438720.

Saeedi, S., Israel, S., Nagy, C., et al. The emerging role of exosomes in mental disorders. Transl. Psychiatry 2019; 9: 122.

Saiki, R., Scharf, S., Faloona, F., et al. Enzymatic amplification of beta-globin genomic sequences and restriction site analysis for diagnosis of sickle cell anemia. Science. 1985; 230: 1350.

Sanchez, M. A., Felice, B., Sappia, L. D., et al. Osteoblastic exosomes. A non-destructive quantitative approach of alkaline phosphatase to assess osteoconductive nanomaterials. Mater. Sci. Eng. C 2020; 110931.

Santos, J. C., Lima, N. da S., Sarian, L. O., et al. Exosome-mediated breast cancer chemoresistance via miR-155 transfer. Sci. Rep. 2018; 8: 829.

Santucci, L., Bruschi, M., Del Zotto, G., et al. Biological surface properties in extracellular vesicles and their effect on cargo proteins. Sci. Rep. 2019; 9: 13048.

Sanz-Rubio, D., Martin-Burriel, I., Gil, A., et al. Stability of Circulating Exosomal miRNAs in Healthy Subjects. Sci. Rep. 2018; 8: 10306.

Schwartz, A., Wang, L., Early, E., et al. Quantitating fluorescence intensity from fluorophore: The definition of MESF assignment. J. Res. Natl. Inst. Stand. Technol. 2002; 107: 83.

Shao, H., Chung, J., Balaj, L., et al. Protein typing of circulating microvesicles allows real-time monitoring of glioblastoma therapy. Nat. Med. 2012; 18: 1835.

Shao, H., Chung, J., Lee, K., et al. Chip-based analysis of exosomal mRNA mediating drug resistance in glioblastoma. Nat. Commun. 2015; 6: 6999.

Sharma, S., Rasool, H. I., Palanisamy, V., et al. Structural-Mechanical Characterization of Nanoparticle Exosomes in Human Saliva, Using Correlative AFM, FESEM, and Force Spectroscopy. ACS Nano 2010; 4: 1921.

Shih, C.-L., Chong, K.-Y., Hsu, S.-C., et al. Development of a magnetic bead-based method for the collection of circulating extracellular vesicles. N. Biotechnol. 2016; 33: 116.

Shiozawa, M., Guan, H.-B., Tanaka, K., et al. Prognostic significance of CD44 variant 2 upregulation in colorectal cancer. Br. J. Cancer 2014; 111: 365.

Silla, T., Karadoulama, E., Mąkosa, D., et al. The RNA Exosome Adaptor ZFC3H1 Functionally Competes with Nuclear Export Activity to Retain Target Transcripts. Cell Rep. 2018; 23: 2199.

Silva, J., García, V., Zaballos, Á., et al. Vesicle-related microRNAs in plasma of nonsmall cell lung cancer patients and correlation with survival. Eur. Respir. J. 2011; 37: 617.

Sina, A .A. I., Vaidyanathan, R., Dey, S., et al. Real time and label free profiling of clinically relevant exosomes. Sci. Rep. 2016; 6: 30460.

Singh, R., Pochampally, R., Watabe, K., et al. Exosome-mediated transfer of miR-10b promotes cell invasion in breast cancer. Mol. Cancer 2014; 13: 256.

Singhto, N., Vinaiphat, A., Thongboonkerd, V. Discrimination of urinary exosomes from microvesicles by lipidomics using thin layer liquid chromatography (TLC) coupled with MALDI-TOF mass spectrometry. Sci. Rep. 2019; 9: 13834.

Sitar, S., Kejžar, A., Pahovnik, D., et al. Size Characterization and Quantification of Exosomes by Asymmetrical-Flow Field-Flow Fractionation. Anal. Chem. 2015; 87: 9225.

Skog, J., Würdinger, T., van Rijn, S., et al. Glioblastoma microvesicles transport RNA and proteins that promote tumour growth and provide diagnostic biomarkers. Nat. Cell Biol. 2008; 10: 1470.

Stoner, S. A., Duggan, E., Condello, D., et al. High sensitivity flow cytometry of membrane vesicles. Cytom. Part A 2016; 89: 196.

Stuffers, S., Sem Wegner, C., Stenmark, H., et al. Multivesicular Endosome Biogenesis in the Absence of ESCRTs. Traffic 2009; 10: 925.

Suárez, H., Gámez-Valero, A., Reyes, R., et al. A bead-assisted flow cytometry method for the semi-quantitative analysis of Extracellular Vesicles. Sci. Rep. 2017; 7: 11271.

Sun, Y., Xia, Z., Shang, Z., et al. Facile preparation of salivary extracellular vesicles for cancer proteomics. Sci. Rep. 2016; 6: 24669.

Sun, Z., Hao, T., Tian, J. Identification of exosomes and its signature miRNAs of male and female Cynoglossus semilaevis. Sci. Rep. 2017; 7, 860.

Szatanek, R., Baj-Krzyworzeka, M., Zimoch, J., et al. The Methods of Choice for Extracellular Vesicles (EVs) Characterization. Int. J. Mol. Sci. 2017; 18: 1153.

Takahashi, R., Miyazaki, H., Ochiya, T., et al. The Roles of MicroRNAs in Breast Cancer. Cancers (Basel). 2015; 7: 598.

Tan, S. K., Pastori, C., Penas, C., et al. Serum long noncoding RNA HOTAIR as a novel diagnostic and prognostic biomarker in glioblastoma multiforme. Mol. Cancer 2018; 17: 74.

Tang, Z., Yuan, S., Hu, Y., et al. Over-expression of GAPDH in human colorectal carcinoma as a preferred target of 3-Bromopyruvate Propyl Ester. J. Bioenerg. Biomembr. 2012; 44: 117.

Taylor, D. D., Gercel-Taylor, C. MicroRNA signatures of tumor-derived exosomes as diagnostic biomarkers of ovarian cancer. Gynecol. Oncol. 2008; 110: 13.

Taylor, D. D., Lyons, K. S., Gerçel-Taylor, C. Shed membrane fragment-associated markers for endometrial and ovarian cancers. Gynecol. Oncol. 2002; 84: 443.

Taylor, D. D., Shah, S. Methods of isolating extracellular vesicles impact down-stream analyses of their cargoes. Methods 2015; 87: 3.

Thakur, B.K., Zhang, H., Becker, A., et al. Double-stranded DNA in exosomes: a novel biomarker in cancer detection. Cell Res. 2014; 24: 766.

Théry, C., Amigorena, S., Raposo, G., et al. Isolation and Characterization of Exosomes from Cell Culture Supernatants and Biological Fluids. Curr. Protoc. Cell Biol. 2006; 30: 3.22.1.

Théry, C., Ostrowski, M., Segura, E. Membrane vesicles as conveyors of immune responses. Nat. Rev. Immunol. 2009; 9: 581.

Théry, C., Witwer, K.W., Aikawa, et al. Minimal information for studies of extracellular vesicles 2018 (MISEV2018): a position statement of the International Society for Extracellular Vesicles and update of the MISEV2014 guidelines. J. Extracell. Vesicles 2018; 7: 1535750.

Théry, C., Zitvogel, L., Amigorena, S. Exosomes: composition, biogenesis and function. Nat. Rev. Immunol. 2006; 2: 569.

Tokunaga, K., Nakamura, Y., Sakata, K., et al. Enhanced expression of a glyceraldehyde-3-phosphate dehydrogenase gene in human lung cancers. Cancer Res. 1987; 47: 5616.

Tominaga, N., Hagiwara, K., Kosaka, N., et al. RPN2-mediated glycosylation of tetraspanin CD63 regulates breast cancer cell malignancy. Mol. Cancer 2014; 13: 134.

Tsai, H.-P., Huang, S.-F., Li, C.-F., et al. Differential microRNA expression in breast cancer with different onset age. PLoS One. 2018; 13: e0191195.

Vaidyanathan, R., Naghibosadat, M., Rauf, S., et al. Detecting Exosomes Specifically: A Multiplexed Device Based on Alternating Current Electrohydrodynamic Induced Nanoshearing. Anal. Chem. 2014; 86: 11125.

Valadi, H., Ekström, K., Bossios, A., et al. Exosome-mediated transfer of mRNAs and microRNAs is a novel mechanism of genetic exchange between cells. Nat. Cell Biol. 2007; 9: 654.

Van Der Pol, E., Hoekstra, A. G., Sturk, A., et al. Optical and non-optical methods for detection and characterization of microparticles and exosomes. J. Thromb. Haemost. 2010; 8: 2596.

Van Deun, J., Mestdagh, P., Sormunen, R., et al. The impact of disparate isolation methods for extracellular vesicles on downstream RNA profiling. J. Extracell. Vesicles 2014; 3: 24858.

van Niel, G., Charrin, S., Simoes, S., et al. The Tetraspanin CD63 Regulates ESCRT-Independent and -Dependent Endosomal Sorting during Melanogenesis. Dev. Cell. 2011; 21: 708.

Van Niel, G., Raposo, G., Candalh, C., et al. Intestinal epithelial cells secrete exosome–like vesicles. Gastroenterology 2001; 121: 337.

Vang, K. B., Jenkins, S. V., Zharov, V. P., et al. Triple-negative breast cancer targeting and killing by EpCAM-directed, plasmonically active nanodrug systems. npj Precis. Oncol. 2017; 1: 27.

Velusamy, V., Arshak, K., Korostynska, O., et al. An overview of foodborne pathogen detection: In the perspective of biosensors. Biotechnol. Adv. 2010; 28: 232.

Vilà, M. R., Nicolás, A., Morote, J., et al. Increased glyceraldehyde-3-phosphate dehydrogenase expression in renal cell carcinoma identified by RNA-based, arbitrarily primed polymerase chain reaction. Cancer. 2004; 89: 152.

Vo-Dinh, T., Cullum, B. Biosensors and biochips: advances in biological and medical diagnostics. Fresenius. J. Anal. Chem. 2000; 366: 540.

Vojtech, L., Woo, S., Hughes, S., et al. Exosomes in human semen carry a distinctive repertoire of small non-coding RNAs with potential regulatory functions. Nucleic Acids Res. 2014; 42: 7290.

Wang, J., Hu, J., Liu, S., et al. Expression of Intercellular Adhesion Molecule 1 by Hepatocellular Carcinoma Stem Cells and Circulating Tumor Cells. Gastroenterology 2013; 144: 1031.

Wang, J., Yan, F., Zhao, Q., et al. Circulating exosomal miR-125a-3p as a novel biomarker for early-stage colon cancer. Sci. Rep. 2017; 7: 4150.

Wang, L., Li, Y., Guan, X., et al. Exosomal double-stranded DNA as a biomarker for the diagnosis and preoperative assessment of pheochromocytoma and paraganglioma. Mol. Cancer. 2018; 17, 128.

Wang, W., Luo, J., Wang, S., Recent Progress in Isolation and Detection of Extracellular Vesicles for Cancer Diagnostics. Adv. Healthc. Mater. 2018; 7: 1800484.

Wang, X., Ding, X., Nan, L., et al. Investigation of the roles of exosomes in colorectal cancer liver metastasis. Oncol. Rep. 2015; 33: 2445.

Wang, Y.-C., Wang, J.-L., Kong, X., et al. CD24 mediates gastric carcinogenesis and promotes gastric cancer progression via STAT3 activation. Apoptosis 2014; 19: 643.

Wang, Y., Yuan, W., Kimber, M., et al. Rapid Differentiation of Host and Parasitic Exosome Vesicles Using Microfluidic Photonic Crystal Biosensor. ACS Sensors 2018; 3: 1616.

Wang, Y., Wang, Q., Wei, X., et al. Global scientific trends on exosome research during 2007-2016: a bibliometric analysis. Oncotarget 2017; 8: 48460.

Wang, Z., Wu, H., Fine, D., et al. Ciliated micropillars for the microfluidic-based isolation of nanoscale lipid vesicles. Lab Chip. 2013; 13, 2879.

Wei, Z., Batagov, A. O., Schinelli, S., et al. Coding and noncoding landscape of extracellular RNA released by human glioma stem cells. Nat. Commun. 2017; 8: 1145.

World Health Organization. Global Health Observatory. Geneva: World Health Organization. Available in: https://www.who.int. 2020.

Witwer, K. W., Buzás, E. I., Bemis, L. T., et al. Standardization of sample collection, isolation and analysis methods in extracellular vesicle research. J. Extracell. Vesicles 2013; 2: 20360.

Wu, M., Ouyang, Y., Wang, Z., et al. Isolation of exosomes from whole blood by integrating acoustics and microfluidics. Proc. Natl. Acad. Sci. 2017; 114: 10584.

Wunsch, B. H., Smith, J. T., Gifford, S. M., et al. Nanoscale lateral displacement arrays for the separation of exosomes and colloids down to 20 nm. Nat. Nanotechnol. 2016; 11: 936.

Xia, Y., Liu, M., Wang, L., et al. A visible and colorimetric aptasensor based on DNA-capped single-walled carbon nanotubes for detection of exosomes. Biosens. Bioelectron. 2017; 92: 8.

Xiao, D., Ohlendorf, J., Chen, Y., et al. Identifying mRNA, MicroRNA and Protein Profiles of Melanoma Exosomes. PLoS One. 2012; 7; e46874.

Xu, J., Mahajan, K., Xue, W., et al. Simultaneous, single particle, magnetization and size measurements of micron sized, magnetic particles. J. Magn. Magn. Mater. 2012; 324: 4189.

Yadav, S., Boriachek, K., Islam, M. N., et al. An Electrochemical Method for the Detection of Disease-Specific Exosomes. ChemElectroChem 2017; 4: 967.

Yang, J., Wei, F., Schafer, C., et al. Detection of Tumor Cell-Specific mRNA and Protein in Exosome-Like Microvesicles from Blood and Saliva. PLoS One. 2014; 9: e110641.

Yang, Y., Bucan, V., Baehre, H., et al. Acquisition of new tumor cell properties by MSC-derived exosomes. Int. J. Oncol. 2015; 47: 244.

Yashiro, M., Sunami, T., Hirakawa, K. CD54 expression is predictive for lymphatic spread in human gastric carcinoma. Dig. Dis. Sci. 2015; 50: 2224.

Yokoi, A., Yoshioka, Y., Yamamoto, Y., et al. Malignant extracellular vesicles carrying MMP1 mRNA facilitate peritoneal dissemination in ovarian cancer. Nat. Commun. 2017; 8: 14470.

Yoo, T.-H., Ryu, B.-K., Lee, M.-G., et al. CD81 is a candidate tumor suppressor gene in human gastric cancer. Cell. Oncol. 2013; 36: 141.

Yoshioka, Y., Kosaka, N., Konishi, Y., et al. Ultra-sensitive liquid biopsy of circulating extracellular vesicles using ExoScreen. Nat. Commun. 2014; 5: 3591.

Yuan, T., Huang, X., Woodcock, M., et al. Plasma extracellular RNA profiles in healthy and cancer patients. Sci. Rep. 2016; 6: 19413.

Yuana, Y., Oosterkamp, T. H., Bahatyrova, S., et al. Atomic force microscopy: A novel approach to the detection of nanosized blood microparticles. J. Thromb. Haemost. 2010; 8: 315.

Zhang, H., Deng, T., Liu, R., et al. Exosome-delivered EGFR regulates liver microenvironment to promote gastric cancer liver metastasis. Nat. Commun. 2017; 8: 15016.

Zhang, H.G. Emerging concepts of tumor exosome–mediated cell–cell communication, Emerging Concepts of Tumor Exosome-Mediated Cell-Cell Communication. Springer New York, New York, NY, 2013.

Zhang, N., Zuo, L., Zheng, H., et al. Increased Expression of CD81 in Breast Cancer Tissue is Associated with Reduced Patient Prognosis and Increased Cell Migration and Proliferation in MDA-MB-231 and MDA-MB-435S Human Breast Cancer Cell Lines In Vitro. Med. Sci. Monit. 2018; 24: 5739.

Zhang, P., He, M., Zeng, Y. Ultrasensitive microfluidic analysis of circulating exosomes using a nanostructured graphene oxide/polydopamine coating. Lab Chip. 2016; 16: 3033.

Zhang, P., Zhou, X., He, M., et al. Ultrasensitive detection of circulating exosomes with a 3D-nanopatterned microfluidic chip. Nat. Biomed. Eng. 2019; 3: 438.

Zhang, Y., Li, B., Zhang, X., et al. CD24 is a genetic modifier for risk and progression of prostate cancer. Mol. Carcinog. 2017; 56: 641.

Zhao, L., Yu, J., Wang, J., et al. Isolation and Identification of miRNAs in exosomes derived from serum of colon cancer patients. J. Cancer 2017; 8, 1145.

Zhao, Z., Yang, Y., Zeng, Y., et al. A microfluidic ExoSearch chip for multiplexed exosome detection towards blood-based ovarian cancer diagnosis. Lab Chip 2016; 16: 489.

Zheng, R., Yano, S., Zhang, H., et al. CD9 overexpression suppressed the liver metastasis and malignant ascites via inhibition of proliferation and motility of small-cell lung cancer cells in NK cell-depleted SCID mice. Oncol. Res. 2005; 15: 365.

Zhou, J., Gong, G., Tan, H., et al. Urinary microRNA-30a-5p is a potential biomarker for ovarian serous adenocarcinoma. Oncol. Rep. 2015; 33: 2915.

Zhou, Q., Rahimian, A., Son, K., et al. Development of an aptasensor for electrochemical detection of exosomes. Methods 2016; 97: 88.

Zhou, W., Fong, M. Y., Min, Y., et al. Cancer-secreted miR-105 destroys vascular endothelial barriers to promote metastasis. Cancer Cell 2014; 25: 501.

Zhou, Y., Zhang, X., Ebright, R.H. Random mutagenesis of gene-sized DNA molecules by use of PCR with Taq DNA polymerase. Nucleic Acids Res. 1991; 19: 6052.

Zong, S., Wang, L., Chen, C., et al. Facile detection of tumor-derived exosomes using magnetic nanobeads and SERS nanoprobes. Anal. Methods 2016; 8: 5001.

Zvereff, V., Wang, J.-C., Shun, K., et al. Colocalisation of CD9 and mortalin in CD9-induced mitotic catastrophe in human prostate cancer cells. Br. J. Cancer 2007; 97: 941.

CHAPTER 2

Aims of research

Early diagnosis has an important role in reducing disease burden by preventing the development of long-term complications in non-communicable diseases. Although high-quality diagnostic tests are available, these are neither affordable nor accessible to patients in scarce-resource settings, largely due to the lack of novel biomarkers for early detection. There is thus an urgent need for a rational study of emerging biomarkers for the early detection of global diseases and the improvement of the analytical performance of diagnostics platforms in order to help reducing disease burden. The aim of this doctoral thesis is to study the role of exosomes as a biomarker, and therefore to improve the specificity, sensitivity and analytical simplification of current diagnostic test, taking as a model breast cancer.

To achieve the tasks, the following specific objectives were proposed, as follows:

Chapter 3

- To obtain the isolation and purification of exosomes from culture cell supernatant and human serum.
- To characterize the exosomes, morphologically by Scanning Electron Microscopy (SEM) and Transmission Electron Microscopy (TEM) under cryogenic environment.
- To characterize the exosomes, size distribution and counting by Nanoparticle Tracking Analysis (NTA).
- To characterize the cell lines and their exosomes, through a surface protein screening by flow cytometry.
- To rational study the matrix effect in serum for the detection of exosomes.
- To characterize the surface proteins in exosomes in the presence of human serum.
- To evaluate the efficiency of the immunomagnetic separation and electrochemical sensing for the detection of exosomes in the presence of human serum.

Chapter 4

- To obtain magnetic particles modified with antibodies towards exosomes derived from MCF7, MDA-MB-231 and SKBr3 breast cancer cell lines.
- To develop a novel magneto-actuated enzyme-linked immunosorbent assay (magneto-ELISA) with optical readout, based on cancer-related exosomal proteins for the detection and quantification of exosomes.
- To characterize the exosomes, through a surface protein screening by magneto actuated immunoassay.

- To evaluate the effect of exosome-depleted human serum in the performance of immunomagnetic separation (IMS) and detection of exosomes by magneto-ELISA.
- To evaluate the expression level of cancer-related biomarkers in exosomes derived from healthy and breast cancer patients by magneto-ELISA.

Chapter 5

- To develop a novel magneto-actuated electrochemical immunosensor with amperometric readout, for the detection and quantification of exosomes based on cancer-related exosomal proteins.
- To evaluate the expression level of cancer-related biomarkers in exosomes derived from healthy and breast cancer patients by the magneto-actuated electrochemical immunosensor.
- To evaluate the performance of electrochemical immunosensing of exosomes spiked in undiluted human serum.

Chapter 6

- To characterize the exosomes derived from hFOB osteoblastic cell line, by NTA, TEM, confocal microscopy and flow cytometry.
- To estimate the kinetic parameter of the alkaline phosphatase (ALP) biomarker in exosomes derived from the hFOB osteoblastic cell line.
- To develop a novel magneto-actuated immunoassay with optical readout, based on IMS of the osteoblastic-derived exosomes by using magnetic particles modified with exosomal tetraspanin biomarkers, followed by enzymatic reaction with p-nitrophenyl phosphate substrate (pNPP), by the intrinsic activity of ALP exosomes.
- To develop a novel magneto-actuated electrochemical biosensor with amperometric readout by using a boron-doped diamond electrode (BDD), based on IMS of the osteoblastic-derived exosomes by using magnetic particles modified with exosomal tetraspanin biomarkers, followed by enzymatic reaction with p-nitrophenyl phosphate substrate (pNPP), by the intrinsic activity of ALP exosomes.
- To evaluate the expression level of alkaline phosphatase (ALP) biomarker in exosomes derived from healthy and breast cancer patients by the magneto-ELISA and magneto-actuated electrochemical sensor.

- To propose the combined detection of epithelial biomarkers and enzymatic activity for the identification of healthy and breast cancer patients.

Chapter 7

- To discuss the final remarks and the future perspectives of this Ph.D. thesis, including some potential approaches for the improvement in exosomes detection for applications in communicable and non-communicable diseases.

Chapter 8

- To show the multidisciplinary of the study in this doctoral thesis, showing the dissemination of the results generated in different areas of knowledge.

CHAPTER 3

Matrix effect in the isolation of breast cancer-derived nanovesicles by immunomagnetic separation and electrochemical immunosensing - A comparative study

Silio Lima Moura, Mercè Martì and María Isabel Pividori

Sensors **2020**, 20, 965; 1-21

DOI:10.3390/s20040965

3.1. Abstract

Exosomes are cell-derived nanovesicles released into biological fluids, which are involved in cell-to-cell communication. The analysis of the content and the surface of the exosomes allow conclusions about the cells they are originating from and the underlying condition, pathology or disease. Therefore, the exosomes are currently considered good candidates as biomarkers to improve the current methods for clinical diagnosis, including cancer. However, due to their low concentration, conventional procedures for exosome detection including biosensing usually require relatively large sample volumes and involve preliminary purification and preconcentration steps by ultracentrifugation. In this paper, the immunomagnetic separation is presented as an alternative method for the specific isolation of exosomes in serum. To achieve that, a rational study of the surface proteins in exosomes, which can be recognized by magnetic particles, is presented. The characterization was performed in exosomes obtained from cell culture supernatants of MCF7, MDA-MB-231 and SKBR3 breast cancer cell lines, including TEM and nanoparticle tracking analysis (NTA). For the specific characterization by flow cytometry and confocal microscopy, different commercial antibodies against selected receptors were used, including the general tetraspanins CD9, CD63 and CD81, and cancer-related receptors (CD24, CD44, CD54, CD326 and CD340). The effect of the serum matrix on the immunomagnetic separation was then carefully evaluated by spiking the exosomes in depleted human serum. Based on this study, the exosomes were preconcentrated by immunomagnetic separation on antiCD81-modified magnetic particles in order to achieve further magnetic actuation on the surface of the electrode for the electrochemical readout. The performance of this approach is discussed and compared with classical characterization methods.

3.2. Introduction

Breast cancer is a highly lethal malignancy and the most commonly diagnosed cancer among women (World Health Organization, WHO), with an estimated over 2 million new cases in 2018 (Bray et al., 2018). Although treatments have increased the survival rate, it is still considered a major cause of morbidity and mortality in women. Treatment efficacy is highly related to early diagnosis. There is thus a growing demand for biomarkers that can help detect diseases at an early stage, as well as for follow-up of patients and therapeutic strategies. The exosomes (Johnstone et al., 1987) have received increasingly attention in the last years as a biomarker for early cancer detection and monitoring (Halvaei et al., 2018). Exosomes are extracellular nanovesicles of 30–150 nm released by all types of cells during

fusion of the multivesicular endosomes (MVEs) with the plasmatic membrane. They carry a cargo of active molecules to proximal and distal cells of the body as a mechanism of physiological communication for maintaining the natural homeostasis or even for a pathological response (Trams et al., 1981). All types of cells use exosomes for this purpose. Importantly, one of the most remarkable features is that they are present in all the biological fluids, such as blood (Qi et al., 2016), saliva (Sun et al., 2016) and urine (Fenner, 2016), among others. Their easy accessibility is one of the most compelling reasons for developing exosomes as clinical biomarkers. Another striking characteristic is their molecular cargo, which can be useful for diagnosis and prognosis of several diseases and conditions. During the biogenesis, some components of the cell of origin remain in the exosomes. Therefore, they carry specific surface markers that indicate their cell signatures, including surface proteins such as proteins related to transport and fusion (e.g., flotillin, caveolin-1), tetraspanins (e.g., CD9, CD63, CD81), heat shock proteins (e.g., Hsp90) and lipid-related proteins, as well as micro RNA (miRNA), messenger RNA (mRNA) and DNA (Zhang and Grizzle, 2014). However, realizing the potential of these vesicles as biomarker requires technical improvement, since the exosomes are exceptionally challenging to characterization with current technologies. The most common methods for targeting exosomes to date typically involve purification (Patel et al., 2019) followed by the specific characterization of their cargo (Théry et al., 2006). The characterization firstly relies on morphological analysis (Théry et al., 2006). The nanometric size of exosomes puts them out of the sensitivity range of most cell-oriented sorting or analysis platforms, as is the case of the classical flow cytometers. Exosomes can only be visualized with an electron microscope. Nanoparticle tracking analysis (NTA) is usually used to count the exosomes, followed by downstream processes for specific detection, including LC-MS/MS, Western Blot, and RT-PCR.

Furthermore, due to their low concentration, conventional procedures for exosome characterization and detection usually require relatively large sample volumes and involve a preliminary purification and preconcentration step by ultracentrifugation, precipitation, size-exclusion chromatography or ultrafiltration, in order to prevent interferences from cells and free biomolecules in the sample. Differential centrifugation was the first technique described (Johnstone et al., 1987) and later optimized (Théry et al., 2006) by increasing *g* values (ultracentrifugation), being currently considered the gold standard for exosomes isolation. The main goal is to eliminate interferences of dead cells, cell debris and soluble protein by a physical separation. The major drawback is the lack of specificity, since it separates the whole population of exosomes, regardless their cell origin. Moreover, it can

produce mechanical damage. The whole procedure is thus time consuming, requiring skilled personnel as well as laboratory facilities and benchtop instrumentation.

Therefore, there is a growing need for novel methods to accurately characterize and specifically isolate exosomes in complex biological fluids.

Since the early reports on magnetic separation technology (Rembaum et al., 1982), magnetic particles (MPs) have been used as a powerful and versatile preconcentration tool in a variety of analytical and biotechnology applications (Reddy et al., 2012) and in emerging technologies including microfluidic devices and biosensors (Brandão et al., 2015; Carinelli et al., 2018, 2015; Lermo et al., 2008). Magnetic particles (core such as iron, nickel, neodymium or magnetite) can be easily functionalized with biomolecules (for instance antibodies) to specifically bind the exosomes and concentrate them from the complex matrix under magnetic actuation, avoiding the interference of the biofluid matrix. Exosomes are thus preconcentrated while the interfering matrix is removed at the same time, increasing the sensitivity of the detection. Recent advances demonstrated the feasibility of the integration of MPs into bioassays for the detection and quantification of exosomes. We have recently demonstrated the feasibility of particle-based magnetic enrichment for exosomes isolation avoiding the ultracentrifugation steps in undiluted human serum using a magneto-actuated enzyme-linked immunosorbent assay (magneto-ELISA), which simplifies the conventional ELISA (Moura et al., 2020b).

Furthermore, magnetic particles can be actuated on the surface of electrochemical transducers (Carinelli et al., 2018; Lermo et al., 2008). This kind of approach simplifies the analytical procedure in order to be used in resource-scarce settings by unskilled personnel, for the rapid detection of a condition, such as breast cancer, the most commonly diagnosed cancer among women (Bray et al., 2018). Most of the currently available technologies for breast cancer diagnosis are based on imaging techniques (Weissleder and Pittet, 2008). The liquid biopsies based on circulating tumor cells (CTCs) can potentially simplify the equipment requirements and operational costs (Allard, 2004; de Wit et al., 2018). However, the clinical use of liquid biopsies is limited by their rarity in the peripheral blood (Ross et al., 1993) (1 CTC in 1 × $10^{5–6}$ blood cells), hindering their detection even with benchtop equipment and requiring preconcentration from a large volume of sample (Wang et al., 2016). However, a single breast cancer cell can release up to 60–65 exosomes per hour (Chiu et al., 2016).

In this paper, we compare the analytical performance of immunomagnetic separation for the isolation of nanovesicles from breast cancer cell lines spiked in serum, and the further detection by a magneto-actuated electrochemical immunosensor. To achieve that, the culture supernatant from three breast cancer cell lines, including MCF7 (ATCC® HTB-22™),

MDA-MB-231 (ATCC® CRM-HTB-26™) and SKBr3 (ATCC® HTB-30™) were purified by ultracentrifugation and spiked in phosphate buffer and depleted human serum at a wide concentration range, in order to carefully evaluate the effect of the human serum matrix and the presence of free receptors in the immunomagnetic separation (IMS). The results suggest that the use of CD81 modified magnetic particles can be useful for the specific isolation of exosomes, and further labeling using general as well as cancer-related receptors for the electrochemical readout.

3.3. Materials and Methods

3.3.1. Instrumentation

Nanoparticle tracking analysis (NTA) was performed using the NanoSight LM10-HS system with a tuned 405 nm laser (NanoSight Ltd., Salisbury, UK). The cryogenic transmission electron microscopy (TEM) images were collected by a Jeol JEM 2011 (JEOL USA Inc, Peabody, MA, USA) transmission electron microscope at an accelerating voltage of 200 kV. The confocal images were collected on the microscope Leica, TCS SP5 (Leica Microsystems, Wetzlar, Germany). Flow cytometry was performed using BD FACSCANTO II (BD Biosciences, San Jose, CA, USA) equipment. The media fluorescence intensity (MFI) and beads count data of every sample-reading file were obtained by FlowJo analysis software. Optical measurements were performed on a TECAN Sunrise (TECAN AG, Männedorf, Switzerland) microplate reader with Magellan v4.0 software. Polystyrene microtiter plates were purchased from Nunc (Maxisorp, Roskilde, Denmark). All electrochemical experiments were performed using an AUTOLAB PGSTAT10 (Metrohm, Herisau, Switzerland) potentiostat/galvanostat electrochemical analyzer. The data were in all cases fitted using a nonlinear regression (four parameters logistic equation).

3.3.2. Chemicals and biochemicals

Magnetic particles (Dynabeads® M450 Tosylactivated, nº 14013, 4.5 μm diameter) were purchased from Thermo Fisher (Waltham, MA, USA). The antibodies are summarized in Table 3.1. The antibodies were selected towards different biomarkers that were previously reported to be expressed in the surface of exosomes, as shown in Table 1.1 (Chapter 1, § 1.2.7). The 10 mmol L^{-1} phosphate-buffered saline (PBS) buffer solution (pH 7.5) and boric acid buffer solution (pH 8.5) were prepared with ultrapure water and all other reagents were in analytical reagent grade (supplied from Sigma Aldrich, St. Louis, MO, USA). The Pierce™ TMB Substrate Kit (Ref. 34021) was purchased from Thermo Fisher. The Hoechst dye (No. 62249, Thermo Fisher) and Cy®5 fluorophore dye (anti-mouse, No. ab97037, Abcam, Cambridge, UK) used in confocal microscopy were purchased from distributors in Barcelona,

Spain. Ultrapure water (Millipore® System, resistivity 18.2 MΩ cm) was used throughout the experiments.

3.3.3. Cell culture

The breast cancer cell lines were the following: MCF7 (ATCC® HTB-22™), MDA-MB-231 (ATCC® CRM-HTB-26™) and SKBr3 (ATCC® HTB-30™). Expansion of cell population was carried out from 1,000,000 cells in a T-175 flask containing 32 mL of Dulbecco's Modified Eagle Medium (DMEM) (Ref. 31966047, Thermo Fisher), supplemented with 10% exosome-depleted fetal bovine serum (FBS) (Ref. 12007C, Sigma-Aldrich, St. Louis, MO, USA), 100 U mL^{-1} penicillin-streptomycin (Ref. 15140122, Thermo Fisher). The temperature was maintained at 37 °C in a humidified, concentrated CO2 (5%) atmosphere. Once cells reached approximately 95% confluence on the T-175 flask, the culture medium was removed and immediately centrifuged (300 *g* for 10 min, 2000 *g* for 10 min and 10000 *g* for 30 min) and stored at −80 °C until exosome isolation was achieved.

3.3.4. Exosome isolation and purification

Exosomes were purified according to Théry (Théry et al., 2006) and as schematically shown in Fig. 3.1, panel A. The supernatant from MCF7, MDA-MB-231 and SKBr3 breast cancer cell lines were subjected to differential centrifugation as follows: 1300 *g* for 5 min (removal of residual cells), 2000 *g* for 15 min and 10,000 *g* for 30 min (removal of cellular debris). Subsequently, a Beckman Coulter Optima™ L-80XP Ultracentrifuge was used at 100,000 *g* for 60 min with a 70Ti rotor to pellet exosomes. After that, the supernatant was carefully removed, and crude exosome-containing pellets were resuspended in 10 mmol L^{-1} phosphate-buffered saline (PBS) solution and pooled.

A second round of the same ultracentrifugation setting was carried out, and the resulting exosome pellet was resuspended in 500 µL (per 100 mL of supernatant) of 10 mmol L^{-1} PBS buffer solution (0.22 µm filtrated and sterile) and stored at −80 °C. All centrifugation steps were performed at a temperature of 4 °C.

3.3.5. Exosome-depleted human serum

The exosome-depleted human serum was used for several matrix effect studies. The depletion of exosomes in human serum from healthy patients was performed as described above, and is schematically shown in Fig. 3.1, panel B. This exosome-depleted human serum was spiked at a different concentration range with the exosomes obtained as above (Fig 3.1, panel A).

Table 3.1. Summary of the antibodies used in this work.

Antibody.	Target	Clonality	Conjugate	Host	Reference	Commercial Source	Use/s
antiCD24	CD24	monoclonal	no	mouse	ab76514	Abcam	1, 2, 3
antiCD54	CD54	monoclonal	no	mouse	ab2213	Abcam	1, 2, 3
antiCD326	CD326	monoclonal	no	mouse	ab7504	Abcam	1, 2, 3
antiCD340	CD340	monoclonal	no	mouse	Ab30	Abcam	1, 2, 3
antiCD9	CD9	monoclonal	no	mouse	10626D	Thermo Fisher	1, 2, 3
antiCD63	CD63	monoclonal	no	mouse	10628D	Thermo Fisher	1, 2, 3
antiCD81	CD81	monoclonal	no	mouse	10630D	Thermo Fisher	1, 2, 3
antiCD44	CD81	monoclonal	no	mouse	BMS113	eBioscience	1, 2, 3
antiCD81	CD81	polyclonal	no	rabbit	HPA007234	Sigma-Aldrich	1, 2, 3
antimouse-HRP	mouse IgG H&L	polyclonal	HRP	rabbit	ab6728	Abcam	4
antimouse-Cy5	mouse IgG H&L	polyclonal	Cy5®	rabbit	ab97037	Abcam	5
antiCD63-HRP	CD63	monoclonal	HRP	mouse	NBP2-42225H-100	BioNova	6

Uses: 1 Immunomagnetic separation when attached to tosyl-activated magnetic particles. 2 Indirect labeling in electrochemical immunosensing, as a primary antibody. 3 Indirect labeling in confocal microscopy and flow cytometry, as a primary antibody. 4 Indirect labeling in magneto-actuated enzyme-linked immunosorbent assay (magneto-ELISA) and electrochemical immunosensing, as a secondary antibody. 5 Indirect labeling in confocal microscopy and flow cytometry, as a secondary antibody. 6 Direct labeling in magneto-ELISA and electrochemical immunosensing, as a secondary antibody.

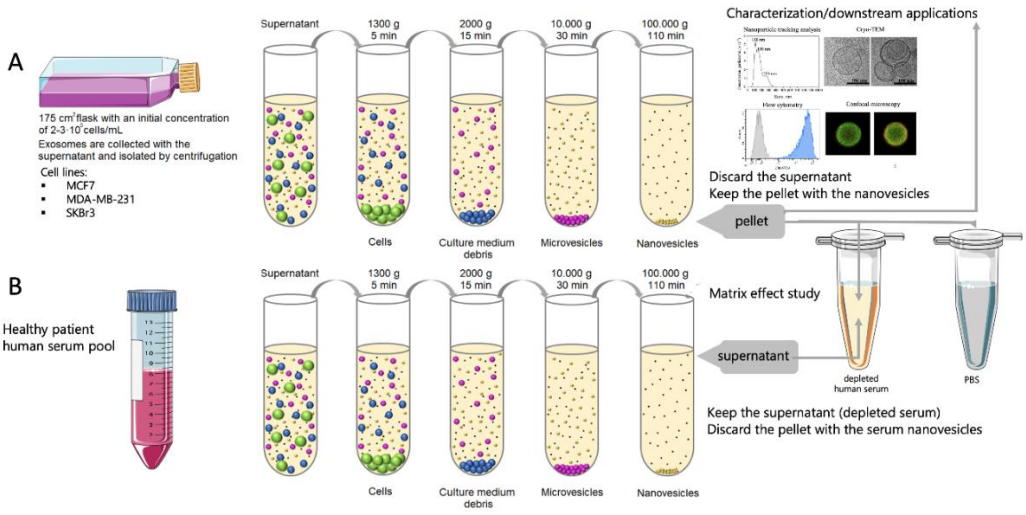

Fig. 3.1. (A) Schematic procedure for the isolation of exosomes from cell culture supernatant of breast cancer cells. (B) Schematic procedure for the obtaining of depleted human serum. The undiluted serum (as well as 10%, 25% and 50% dilutions in phosphate-buffered saline (PBS)) is then spiked with the purified exosomes, as well as PBS as a control, in order to perform the matrix effect study.

3.3.6. Covalent immobilization on magnetic particles

Dynabeads® M450 tosylactivated superparamagnetic particles (MPs, 4.5 μm in diameter) have a core of iron oxide salt encapsulated by a polystyrene polymer, which has a polyurethane external layer with the p-toluenesulfonate group (Xu et al., 2012). It is a good leaving group, which allows an S_N2 reaction to occur in the presence of a nucleophile (Hoogenboom et al., 2010). A nucleophilic reaction by an antibody, protein, peptide or glycoprotein removes and replaces the sulfonyl ester groups from the polyurethane layer.

Two different approaches were used, as depicted in Fig. 3.2. The first one involves the direct covalent immobilization of exosomes on magnetic particles (Fig. 3.2, panel A). The second approach is based on the covalent immobilization of the antibodies for a further immunomagnetic separation (IMS) of exosomes (Fig. 3.2, panel B).

Immobilization of exosomes. The immobilization of exosomes on Dynabeads® M450 tosylactivated superparamagnetic particles (MPs) (Fig. 3.2, panel A) was performed as follows: 3.5×10^{10} exosomes were added to 40 μL (1.6×10^7 MPs) tosylactivated Dynabeads® M450. The reaction kinetics were increased by adding a 0.1 mol L^{-1} pH 8.5 borate buffer, in order to ensure the nucleophilic reaction by the amine group. The incubation step was performed overnight with gentle shaking at 4 °C. After that, a 0.5 mol L^{-1} glycine solution was added to ensure the blocking of any remaining tosylactivated groups, by incubation for 2 h at 25 °C. After that, the exosome-modified magnetic particles (exosomes-MP) were resuspended in 160 μL of 10 mmol L^{-1} PBS

buffer solution in order to achieve 1 × 10^6 MPs per 10 µL. The calibration plots were performed by using 1 × 10^6 MPs per well plate and the number of exosomes ranged from 3.9 × 10^4 to 2 × 10^7 exosomes μL^{-1}.

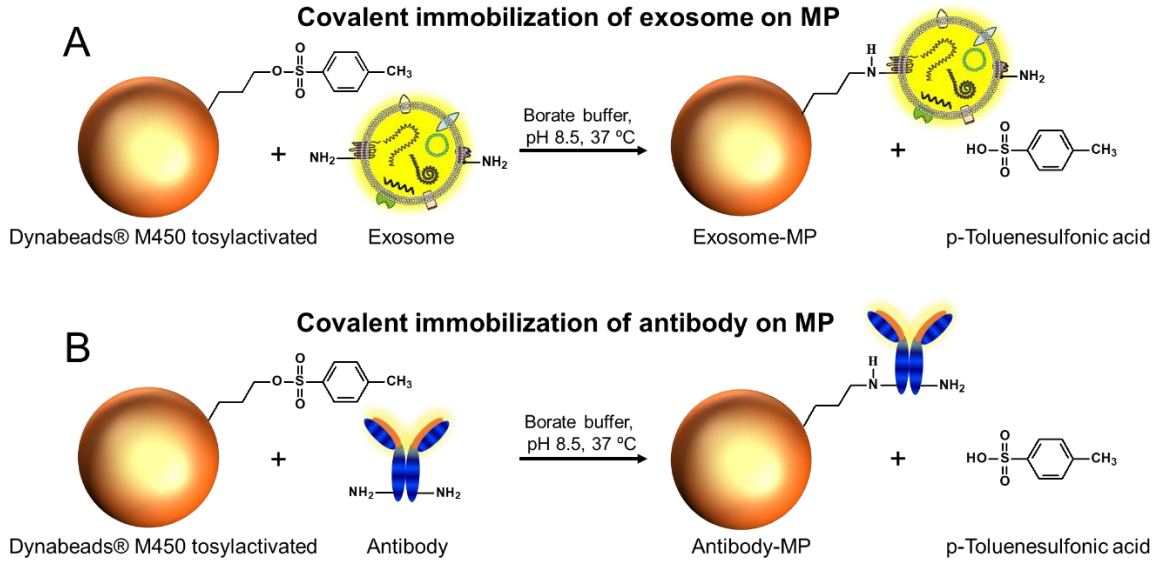

Fig. 3.2. (A) Direct covalent immobilization on Dynabeads® M450 tosylactivated. (B) Covalent immobilization of different antibodies (as depicted in Table 3.1) on Dynabeads® M450 tosylactivated.

Immobilization of antibodies. The different specific antibody (approximately 15 µg mL^{-1} antiCDX, optimized in each case as described in detail by our research group (Moura et al., 2020b) to achieve full coverage) was added to 55 µL (2.2 × 10^7 MPs) Dynabeads® M450 tosylactivated (Fig. 3.2, panel B). As above, 0.1 mol L^{-1} pH 8.5 borate buffer was added. The incubation step was performed overnight with gentle shaking at 37 °C. After that, a blocking step with 0.5 mol L^{-1} glycine solution was performed for 2 h to ensure the blocking of the any remaining tosylactivated groups. After that, the antibody-modified MPs (herein, antiCDX-MPs, where antiCDX = antiCD9, antiCD24, antiCD44, antiCD54, antiCD63, antiCD81, antiCD326 or antiCD340) were resuspended in a 220 µL (10 µL per well in order to achieve 1 × 10^6 particles per well) 10 mmol L^{-1} PBS buffer. It was not possible to immobilize CD326 satisfactorily on MPs.

3.3.7. Characterization of exosomes by nanoparticle tracking analysis

Nanoparticle tracking analysis (NTA) was used as a gold standard method to count the exosomes. This information was used for the biosensing calibration plots (Filipe et al., 2010; Q. Li et al., 2017). NTA was also used to study the size distribution of exosomes purified from cell culture supernatant. The size distribution and

concentration of exosomes were measured using the NanoSight LM10-HS system with a tuned 405 nm laser (NanoSight Ltd., Amesbury, UK). The purified exosomes were diluted in sterile-filtered PBS (50- to 100-fold). Nanosight NTA Software analyzed raw data videos by triplicate during 60 s with 50 frames per second and the temperature of the laser unit set at 24.8 °C.

3.3.8. Characterization of exosomes by transmission electron microscopy

A 10 µL aliquot of exosomes was directly laid on Formvar–carbon electron microscopy grids and frozen in ethanol. The Cryo-TEM images were collected on the on a Jeol JEM 2011 transmission electron microscope at an accelerating voltage of 200 kV. Exosomes were maintained at −182 °C during the whole process.

3.3.9. Confocal microscopy study

Confocal microscopy was used for the assessment of the molecular biomarkers expressed in the exosomes obtained by the three different cancer cell lines (MCF7, MDA-MB-231 and SKBr3). The presence of the following receptors was investigated: CD9, CD63, CD81, CD24, CD44, CD54, CD326 and CD340. As exosomes are between 30–200 nm in diameter, a size that makes them out of the sensitivity range of most cell-oriented sorting or analysis platforms, they were coupled to MPs to allow their characterization by confocal microscopy. In this study, the exosomes were attached on the surface of MPs by covalent immobilization (exosomes-MPs), as described in Fig. 3.1, panel A. In order to achieve that, 3.5×10^{10} exosomes were covalently immobilized on 1.6×10^{7} MPs overnight with gentle orbital shaking at 4 °C. The indirect labeling was performed by incubation with 100 µL (5 µg mL^{-1}) of the mouse antibodies towards the different cluster of differentiation antiCDX (CDX being either CD9, CD63, CD81, CD24, CD44, CD54, CD326 or CD340 biomarkers), for 30 min with gentle shaking at 25 °C. Subsequently, three washing steps were performed. Afterwards, 100 µL (2 µg mL^{-1}) of antimouse-Cy5 antibody (a far-red-fluorescent dye, excitation 647 nm, emission 665 nm (Bamgbelu et al., 2010)) was incubated for 30 min in darkness, with gentle shaking at 25 °C, for further readout. In all instances, the percentage of labeled entities was normalized by the highest fluorescence value for a labeled receptor. The labeled exosomes-MP were resuspended in 200 µL of PBS with 0.1% bovine serum albumin (BSA) solution. After each incubation, washing steps with PBS with 0.1% BSA solution were performed. The confocal images were then collected.

3.3.10. Flow cytometry study

The analysis of the molecular biomarkers CD9, CD24, CD44, CD54, CD63, CD81, CD326 and CD340 expressed in the exosomes derived from three different cancer cell lines (MCF7, MDA-MB-231 and SKBr3) was performed by flow cytometry. Accordingly, for the labeling of cell-derived exosomes, they were firstly immobilized on the surface of MPs by two different approaches, as described above (Fig. 3.2). In Fig. 3.2, panel A depicts the covalent immobilization of the 3.5×10^{10} exosomes on 1.6×10^{7} MPs (exosomes-MPs). The exosomes-MPs were analyzed by indirect labeling by incubation with 100 µL (5 µg mL^{-1}) of the antibodies antiCDX (mouse), (CDX being either CD9, CD24, CD44, CD54, CD63, CD81, CD326 or CD340 biomarkers), for 30 min with gentle shaking at 25 °C. After that, three washing steps with PBS pH 7.5 containing 0.5% BSA were performed. Afterwards, 100 µL (2 µg mL^{-1}) of antimouse-Cy5 antibody (a far-red-fluorescent dye, excitation 647 nm, emission 665 nm) was incubated for 30 min at 25 °C. The labeled exosomes-MPs were resuspended in PBS pH 7.5 containing 0.5% BSA. In Fig. 3.1, panel B, 1×10^{6} MPs modified with rabbit antiCD81 (antiCD81-MPs) were incubated with 4×10^{9} exosomes (1:4000 MP/exosomes ratio). Exosomes immunocaptured by antiCD81-MPs were detected using indirect labeling, as described above.

3.3.11. Matrix effect study by immunomagnetic separation and optical readout

The evaluation of the matrix effect was firstly performed by immunomagnetic separation (IMS) of MCF7-derived exosomes spiked in 0% (10 mmol L^{-1} phosphate-buffered saline (PBS) (no serum)), 10%, 25%, 50% and 100% (undiluted) exosome-depleted human serum (obtained as schematically shown in Fig. 3.1, panel B). The IMS was performed by antiCDX-MPs (CDX being either CD9, CD24, CD44, CD54, CD63, CD81, CD326 or CD340 biomarkers), followed by a direct labeling and optical readout. The procedure for the magneto-actuated immunoassay was previously described in detail by our research group (Moura et al., 2020b). To summarize, this approach involved a direct immunoassay format, and in all cases was performed in 96-well microtiter plates. The direct immunoassay format involved the following steps: (i) IMS of the exosomes with antiCDX-MPs. The antiCDX-MPs (CDX being any of CD9, CD24, CD44, CD54, CD63, CD81, CD326 or CD340 biomarkers) (containing 1×10^{6} antiCDX-MPs per well) and the exosomes (4×10^{9} exosomes per well spiked in 100 µL of any of the matrix: 0%, 10%, 25% or 50% diluted and undiluted human serum), were simultaneously incubated for 30 min with shaking at 25 °C, followed by three washing steps with PBS containing 0.5% BSA. (ii) Direct labeling. The exosomes-coated MPs were incubated with the antiCD63-HRP antibody (100 µL, 1.24 µg mL^{-1}) for 30 min with shaking at 25 °C, followed

by three washing steps with PBS containing 0.5% BSA. (iii) Optical readout. 100 µL of substrate solution (0.004% v/v H_2O_2 and 0.01% w/v TMB in citrate buffer) was then added to each well and incubated for 30 min under dark conditions. The enzymatic reaction was stopped by adding 100 µL of H_2SO_4 (2.0 mol L^{-1}). Then, exosomes-MPs were separated using a magnet plate separator, and an exosomes-MPs pellet formed on the bottom tube, followed by supernatant separation. The absorbance measurement of the supernatants was thus performed with the microplate reader at 450 nm. After each incubation or washing step, a 96-well magnet plate separator was positioned under the microtiter plate until the pellet formation on the bottom corner, followed by supernatant separation.

3.3.12. Immunomagnetic separation and electrochemical immunosensing of exosomes in human serum

Two different formats, classified accordingly to the labeling, were performed for the detection of exosomes derived in this instance from SKBr3 breast cancer cell lines, and spiked in both phosphate buffer and undiluted exosome-depleted human serum, and ranging from 0 to 2 × 10^9 exosomes, as determined by NTA. The whole procedure was performed in detail as follows:

Direct format. The magneto-actuated electrochemical immunosensing involves the following steps: (i) IMS of the exosomes with antiCD81-MPs (rabbit) (containing 1 × 10^6 antiCD81-MPs per well) and the exosomes (100 µL, ranging from 0 to 2 × 10^9 exosomes per well), were simultaneously incubated for 30 min with shaking at 25 °C, followed by three washing steps with PBS containing 0.5% BSA. (ii) Direct labeling. The modified-MPs were incubated with the antiCD63-HRP antibody (100 µL, 1.24 µg mL^{-1}) for 30 min with shaking at 25 °C, followed by three washing steps with PBS containing 0.5% BSA. (iii) Electrochemical readout, as described below.

Indirect format. The magneto-actuated electrochemical immunosensing involves the following steps: (i) IMS of the exosomes with antiCD81-MPs (rabbit) (containing 1 × 10^6 antiCD81-MPs per well) and the exosomes (100 µL, ranging from 0 to 2 × 10^9 exosomes per well), were simultaneously incubated for 30 min with shaking at 25 °C, followed by three washing steps with PBS containing 0.5% BSA. (ii) Incubation with the antiCDX mouse monoclonal antibodies (100 µL, 0.50 µg mL^{-1}) (CDX being any of the CD24 or CD340 biomarkers), which were simultaneously incubated for 30 min with shaking at 25 °C, followed by three washing steps with PBS containing 0.5% BSA. (iii) Indirect labeling. The modified-MPs were incubated with antimouse-HRP antibody (100 µL, 0.08 ng mL^{-1}) for 30 min with shaking at 25 °C, followed by three washing steps with

PBS containing 0.5% BSA. (iv) Electrochemical readout, performed as described below, after the magnetic actuation of the modified-MPs on the surface of the m-GEC electrodes.

Electrochemical measurements. All electrochemical experiments were performed using an AUTOLAB PGSTAT10 potentiostat/galvanostat electrochemical analyzer. A magneto-actuated graphite-epoxy carbon (m-GEC) as working electrode (geometric area = 0.5 cm^2), a Ag/AgCl/KCl(satd.) reference electrode, a platinum counter electrode (geometric area = 3.0 cm^2) and a standard one-compartment three-electrode cell were used in all experiments. The enzymatic electrochemical signal is based on a hydroquinone mediator. Amperometric measurements were carried out at −0.1 V vs. Ag/AgCl/KCl(satd.). All experiments were performed using a single m-GEC electrode in a 100 mmol L^{-1} phosphate-buffered saline (PBS) solution with pH 7.0 at 25 °C. A reproducible steady-current was obtained after 60 s and used for the calibration curve. An outline of this approach based on the magneto-actuated composite electrode and electrochemical readout is shown in Fig. 3.3.

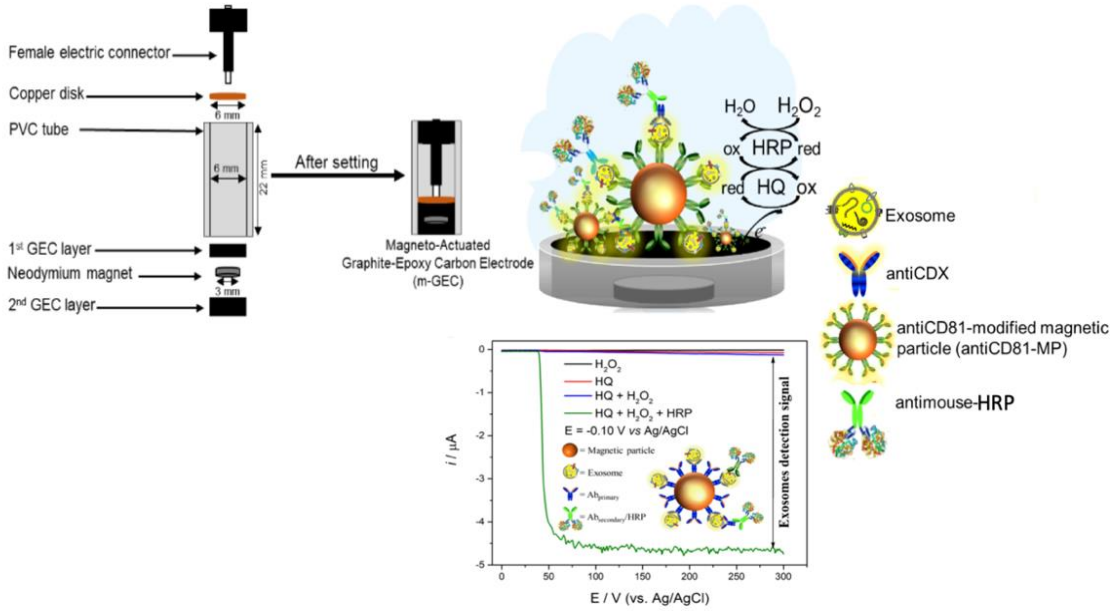

Fig. 3.3. Schematic representation of the construction of the magneto-actuated electrode based on rigid composites (m-GEC) as well as the enzymatic reaction based on hydroquinone mediator.

3.3.13. Safety considerations

All procedures involved in the manipulation of human cells were handled using Biosafety Level 2 Laboratory (BSL-2) and containment. All works were performed in a Biosafety cabinet, and all materials were decontaminated by autoclaving or disinfected before discarding in accordance with the U.S. Department of Health and Human Services guidelines for level 2 laboratory Biosafety (Chosewood and Wilson, 2009).

3.4. Results and Discussion

3.4.1. Characterization of exosomes by nanoparticle tracking analysis

An estimation of the size diameter distribution of purified exosomes derived from the MCF-7 breast cancer cell line was performed by NTA (Fig. 3.4). A size from 50 to 300 nm (considering 95.4% of a Gaussian distribution), but with dominance around 105 and 153 nm (60% and 34% of the counted particles, respectively) was obtained for the MCF-7 exosomes. However, it is important to highlight that NTA analysis is not able to distinguish isolated particles from aggregates. Similar results were obtained by NTA for the exosomes derived from the other breast cancer cell lines (MDA-MB-231 and SKBr3) (as depicted in Fig. 3.4, panels B and C, respectively).

3.4.2. Characterization of exosomes by transmission electron microscopy

Cryogenic transmission electron microscopy (TEM) provides a tool for high-resolution structural analysis for frozen biostructures, avoiding depression and even damage to the sample. Cryo-TEM micrographs on exosomes derived from breast cancer cell lines are shown in Fig. 3.5.

The image comparatively shows TEM images of exosomes derived from MCF-7 (panels A and B), MDA-MB-231 (panel C) and SKBr3 (panel D) breast cancer cell lines. The micrographs revealed the typical exosome consisting of well-shape exosome vesicles with closed circular lipid bilayers comprising packed membrane proteins with a 110 nm diameter (Fig. 3.5, panel A).

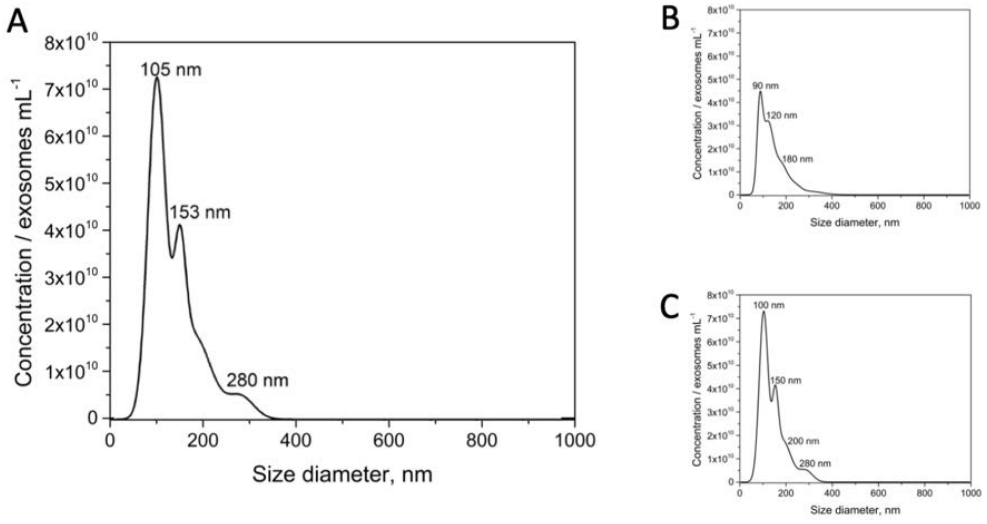

Fig. 3.4. Nanoparticle tracking analysis (NTA) on size distribution on purified exosomes derived from (A) MCF7, (B) MDA-MB-231 and (C) SKBr3 breast cancer cell lines. The purified exosomes were diluted in sterile-filtered 10 mmol L−1 PBS buffer (pH 7.5). Nanosight NTA Software analyzed raw data videos by triplicate during 60 s with 50 frames per second and the temperature of the laser unit set at 24.8 °C.

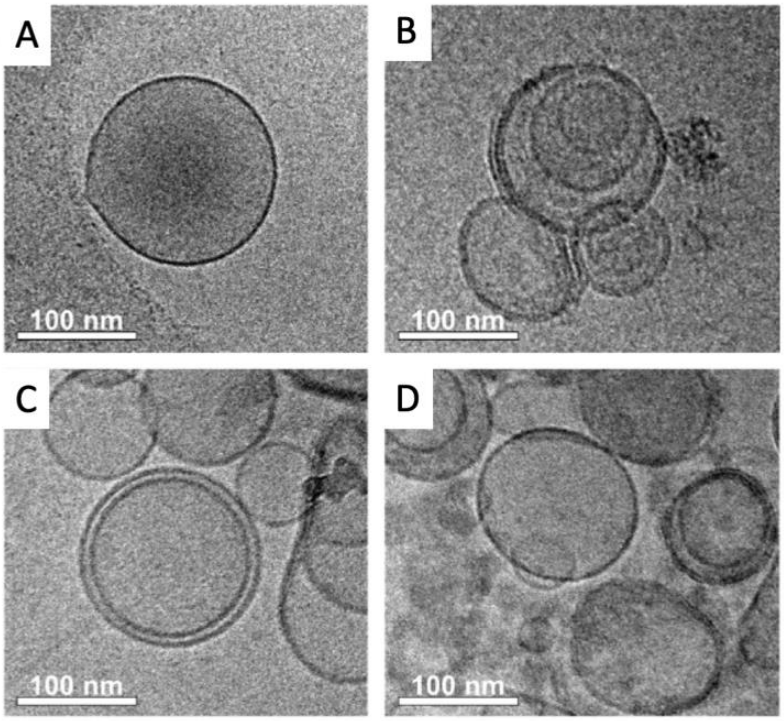

Fig. 3.5. Cryogenic transmission electron microscopy (Cryo-TEM) on purified exosomes derived from (A, B) MCF-7, (C) MDA-MB-231 and (D) SKBr3 breast cancer cell lines.

As expected, the TEM micrographs also reveal the presence of some aggregates of exosomes (Fig. 3.5, panel B), confirming that the NTA analysis cannot distinguish vesicles and vesicle aggregates. Similar results were obtained for exosomes derived from other breast cancer cell lines (MDA-MB-231 and SKBr3, Fig. 3.5, panels C and D, respectively).

3.4.3. Confocal microscopy study

Confocal microscopy was performed to comparatively study the expression patterns of different biomarkers on breast cancer cells' exosomes derived from MCF-7, MDA-MB-231 and SKBr3 cell lines. The quantitative results are summarized in Fig. 3.6.

The expression of each cell line-derived exosomes was studied after the covalent immobilization on MPs (Fig. 3.2, exosomes-MPs and Fig. 3.6, panel A for exosomes derived from MCF7, panel B for MDA-MB-231 and panel C for SKBr3 cells lines). The intense green color of the magnetic particles is due to autofluorescence around 580 nm (Agrawal et al., 2007). As expected, general tetraspanins (CD9, CD63 and CD81) (Chow et al., 2015; Hemler, 2013) were expressed in exosomes from the MCF7 breast cancer cell line (Fig. 3.6, panel A). The biomarkers related to breast cancer are weekly or not expressed. Negligible non-specific adsorption fluorescence was observed (Fig. 3.6, negative control), indicating a good blocking procedure of the remaining tosyl-activated group after covalent immobilization.

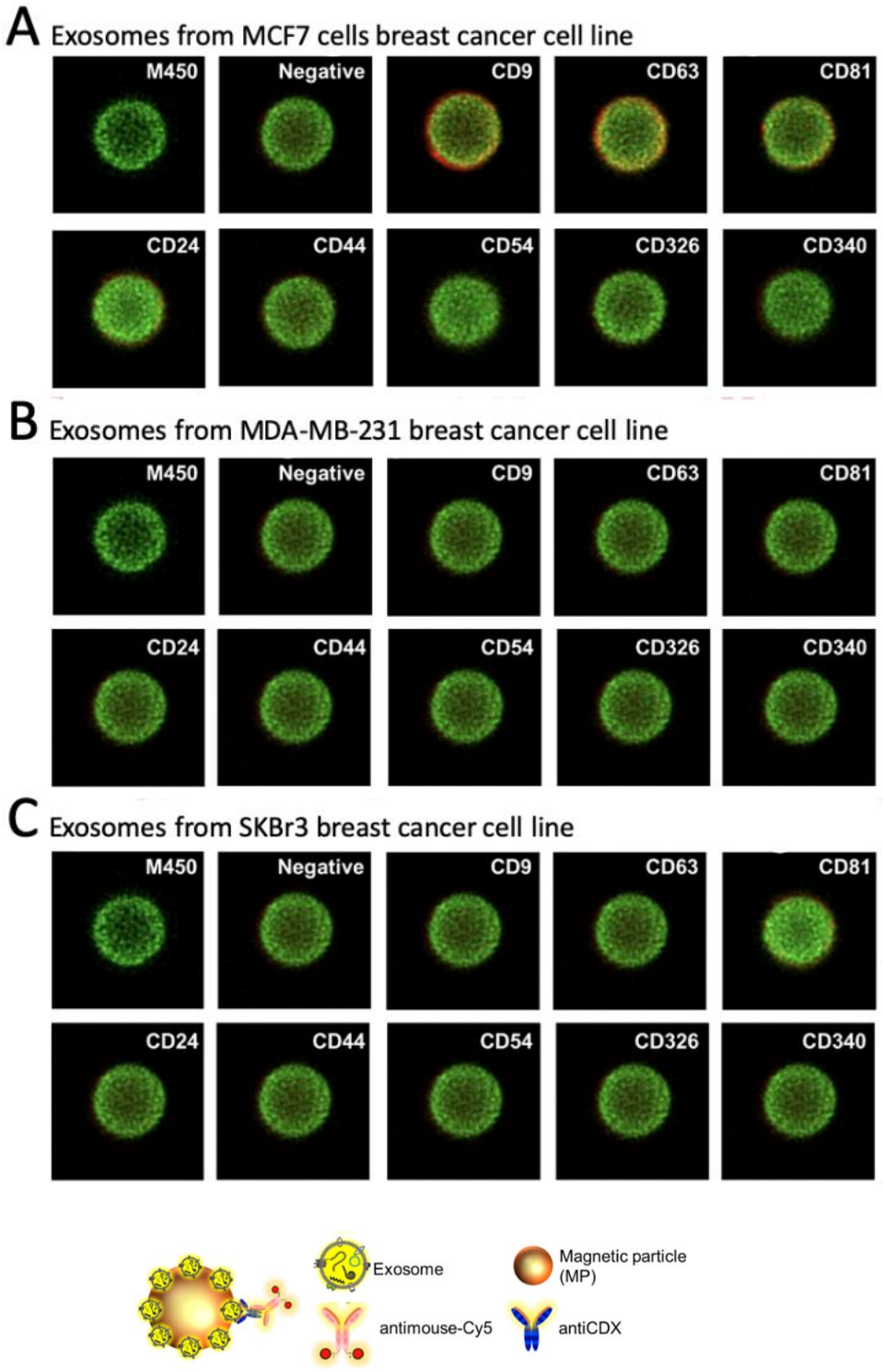

Fig. 3.6. Confocal microscopy to evaluate the relative expression of CD9, CD63, CD81, CD24, CD44, CD54, CD326 and CD340 membrane protein markers in the exosomes derived from MCF7, MDA-MB-231 and SKBr3 breast cancer cell lines. Magnetic particles appear stained in green while the membrane protein receptors, in red, represents a positive expression on the membrane of the exosomes. In all cases, the primary antibody was 5 μg mL^{-1} and 2 μg mL^{-1} of antimouse-Cy5 antibody.

On the other hand, a poorer labeling pattern was achieved for other biomarkers in MCF7 (Fig. 3.6, panel A), as well those derived from MDA-MB-231 and SKBr3 (Fig. 3.6, panels B and C). This issue can be attributed to steric hindrance of the receptor after

immobilization of the exosomes on the MPs, in agreement with the results achieved by flow cytometry as it will be further discussed. It is worth mentioning that the confocal images are the most representative and they only provide a qualitative analysis.

3.4.4. Flow cytometry study

As in the case of confocal microscopy, the main goal of this set of experiments was to assess the expression of different biomarkers (including general exosome biomarkers such as CD9, CD63 and CD81, and cancer-related biomarkers such as CD24, CD44, CD54, CD326 and CD340) on exosomes derived from the three different breast cancer cell lines (MCF7, MDA-MB-231 and SKBr3), in order to determine the good design for the electrochemical immunosensor. The results of flow cytometry are shown in Fig. 3.7, panels A and B. In the first approach, the exosomes directly immobilized on MPs were assessed towards the expression of different biomarkers selected in this study, followed by an incubation with an antimouse-Cy5 secondary antibody. Then, the labeled exosomes-MPs were acquired by the flow cytometer and further analyzed. As shown in Fig. 3.7, panel A, CD9, CD63 and CD81 were expressed on exosomes produced by MCF7 and SKBr3, but poorly expressed in the MDA-MB-231 cell line, in agreement with confocal microscopy and several other studies (Chow et al., 2015; Hemler, 2013). Besides, cancer-related biomarkers showed, in general, a poorer labeling pattern. In the second approach, the two biomarkers must be simultaneously expressed in the exosomes. One of the markers is involved in the IMS, while the other one is involved in the labeling. Accordingly, the general tetraspanin CD81 was used in this instance for the IMS by the antiCD81-MPs in order to achieve a massive capture of the exosomes, followed by further labeling by a second biomarker. As shown in Fig. 3.7, panel B, a better performance was achieved in general with this approach. Increased tetraspanin labeling on the exosomes from SKBr3 and MCF7 was respectively observed, although MDA-MB-231 also expressed low levels of these general biomarkers. Cancer-related exosomal biomarkers (for instance CD44 and CD340), which were negative when immobilized covalently on MPs, were detected by this approach. This experiment suggests that CD81 tetraspanin can be successfully used for the IMS of the exosomes. Moreover, and as expected, Fig. 3.7 shows that there is a different pattern for the expression of exosomes from different cell cancer lines.

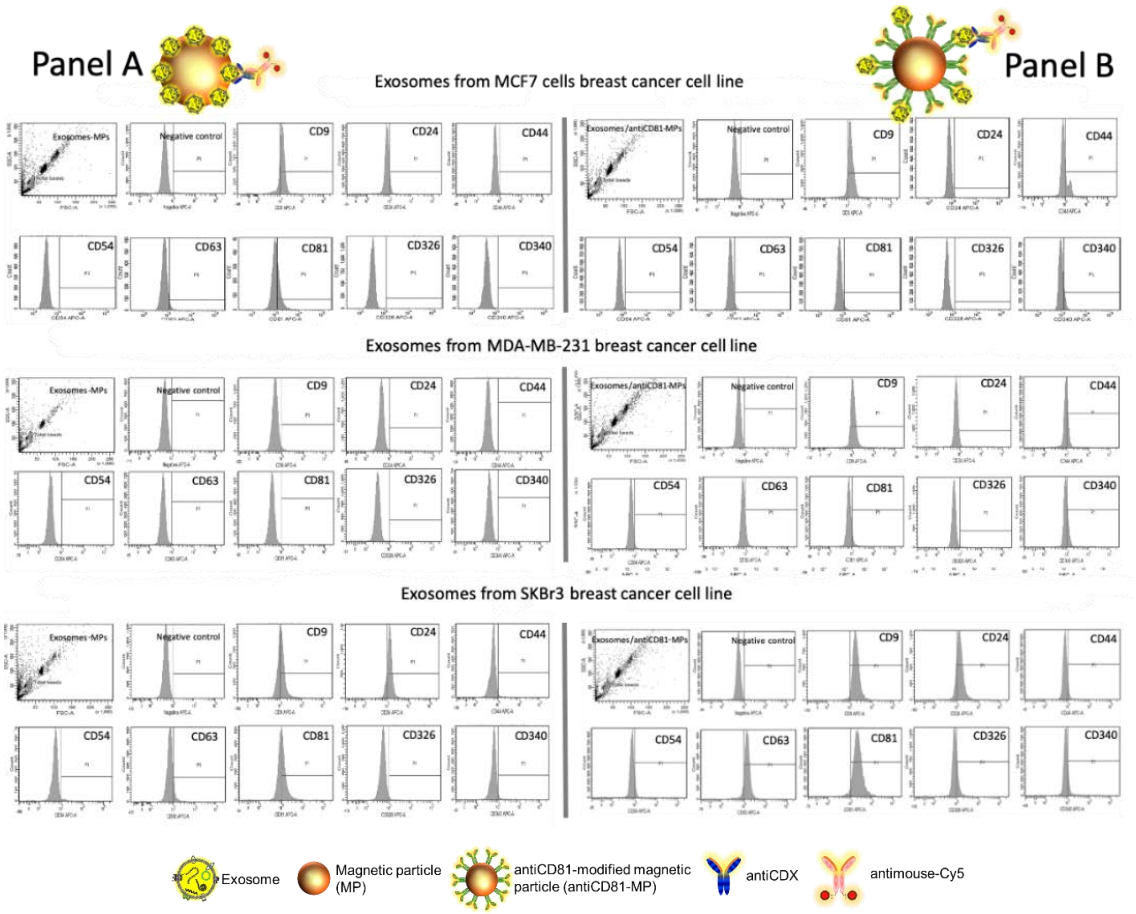

Fig. 3.7. Flow cytometry study for exosomes derived from MCF7, MDA-MB-231 and SKBr3 breast cancer cell lines attached on magnetic particles (MPs), being (Panel A) covalent immobilization of the exosomes on MPs (exosomes-MPs) and (Panel B) IMS of the exosomes on antiCD81-MPs, followed by indirect labeling with mouse antiCDX (5 μg mL^{-1}), (CDX being either CD9, CD24, CD44, CD54, CD63, CD81, CD326 or CD340 biomarkers) and antimouse-Cy5 (2 μg mL^{-1}). The concentrations of MPs and exosomes were set at 1×10^6 MPs and 4×10^9 exosomes per assay, respectively.

3.4.5. Matrix effect study by immunomagnetic separation and optical readout

The main goal of this study is to avoid the use of ultracentrifugation for the isolation of exosomes from the free proteins of the sample, and to replace it by immunomagnetic separation directly performed in undiluted human serum, in order to simplify the analytical procedure. This is a challenging task, since the free receptors (mainly proteins including tetraspanin) present in the undiluted serum can block or even prevent the separation of the exosomes by immunomagnetic separation. Accordingly, a rational study of the matrix effect of the human serum was performed, by spiking a known amount of MCF7 cancer-related exosomes (obtained as schematically shown in Fig. 3.1, panel A), in undiluted human serum depleted of exosomes (obtained as schematically shown in Fig. 3.1, panel B). The characterization of the interference of free molecules and proteins in the serum was then carefully evaluated by magneto-actuated immunoassay (optical readout), since it can be easily multiplexed. A preliminary study of the matrix effect of human serum was performed on exosomes purified by

ultracentrifugation from the MCF7 cell line (as depicted in Fig. 3.1, panel A) and spiked in 0% (PBS), 10%, 25%, 50% and 100% (undiluted) human serum. The signal was normalized by the highest absorbance value for a biomarker within each exosome immobilization approach, as shown in Fig. 3.8.

In this approach, the IMS was performed by using a specific biomarker antibody (antiCDX-MPs), followed by an optical readout using a general exosome biomarker (antiCD63-HRP antibody). This format thus requires the coexistence of two biomarkers in the same exosomes to be magneto-actuated and labeled. By comparing the pattern of signal for each of the receptors used to separate the exosomes, the better analytical performance was achieved by using the ubiquitous and highly expressed CD81 for the immunomagnetic separation with antiCD81-MPs, since no background was observed and the value was always negligible at all the matrix compositions studied. On the contrary, a high background was observed in the case of using antiCD9-MPs. This high value can be attributed to a cross reaction/interference of some component of the serum with the antibodies used in this approach. The results also show the interference of the free CD63 protein in the serum, which produces increasing backgrounds as the percentage of human serum increases in the matrix. This free CD63 receptor can thus block, and therefore prevent by competition, the binding of the exosomes to the magnetic particles. These results were confirmed by performing the same experiments in depleted human serum (no exosomes present), and the results are shown in Fig. 3.9.

Once again, it is demonstrated that some soluble proteins in the serum produce an increment in the signal, especially remarkable in the case of CD9 and CD63. Again, the CD81 commercial antibody (rabbit) is promising for the IMS of exosomes since no background is observed.

These results are also in agreement with previous studies, reporting a higher biomarker expression of CD9, CD63 and CD81 tetraspanins as well as a lower biomarker expression of CD24, CD44, CD54, CD326 and CD340 cancer-related biomarkers on breast cancer exosomes. No results were obtained for CD326 (EpCAM), since upon immobilization on the MP, no binding was observed, perhaps due to a bad orientation during covalent immobilization.

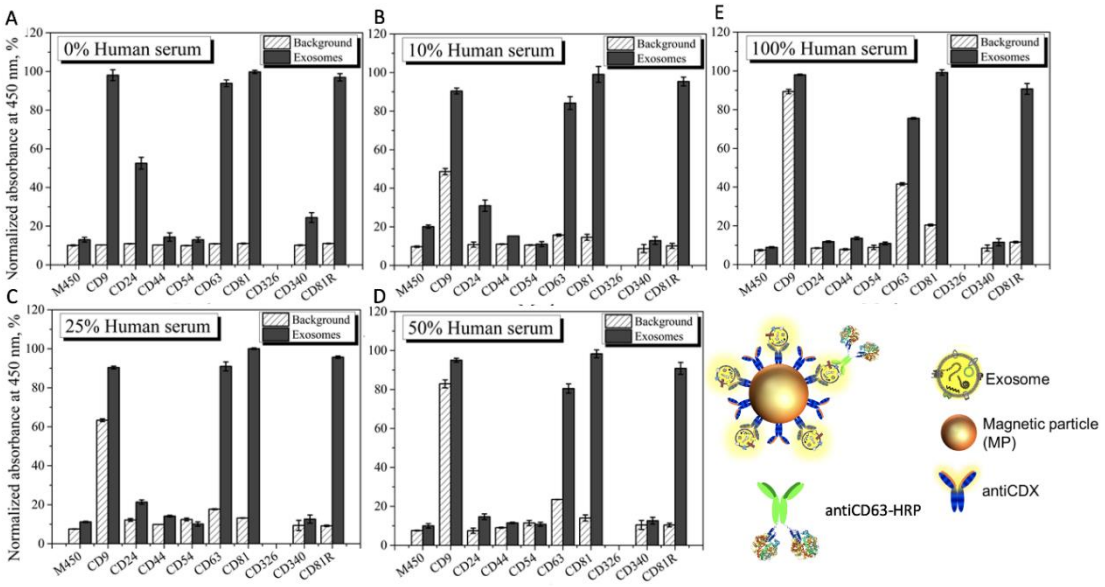

Fig. 3.8. Evaluation of the matrix effect in exosome-depleted human serum for MCF7 exosomes detection using antiCDX-MPs modified with antibodies against CD9, CD24, CD44, CD54, CD63, CD81, CD340 and CD81R (rabbit polyclonal) biomarkers for the IMS, followed by direct labeling with an antiCD63-HRP antibody (1.24 μg mL^{-1}). Detection of exosomes in (A) 0%; 10 mmol L^{-1} phosphate-buffered saline/PBS (standard for no matrix effect), (B) 10%, (C) 25%, (D) 50% and (E) 100% exosome-depleted human serum (undiluted human serum). The concentrations of MPs and exosomes were set at 1 × 10^6 MPs and 4 × 10^9 exosomes per assay, respectively. The background (as a negative control without exosomes) are also shown in all the experiments. The error bars show the standard deviation for n = 3.

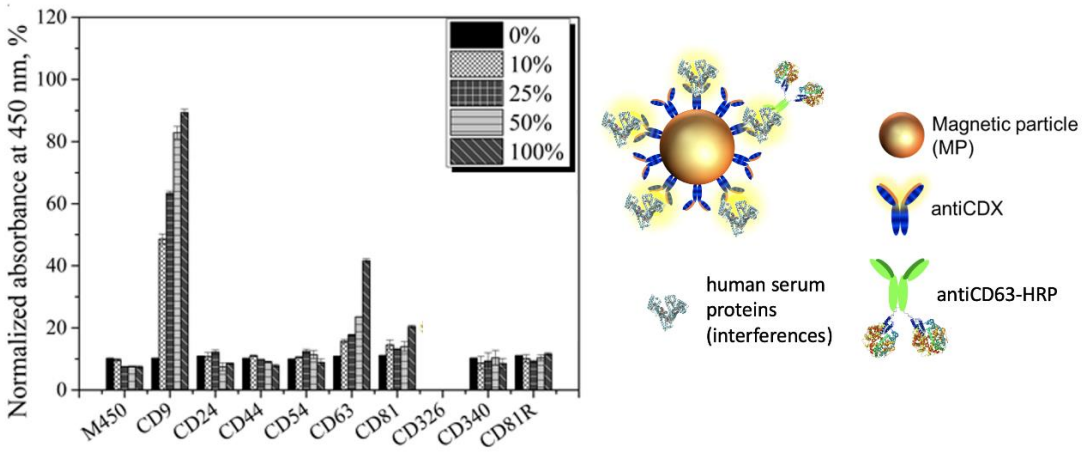

Fig. 3.9. Evaluation of the matrix effect in exosome-depleted human serum using antiCDX-MPs modified with antibodies against CD9, CD24, CD44, CD54, CD63, CD81, CD340 and CD81R (rabbit polyclonal) biomarkers for the IMS, followed by direct labeling with an antiCD63-HRP antibody (1.24 μg mL^{-1}) in depleted human serum. In this instance, no exosomes were spiked in the samples. All other conditions are as in Fig. 3.8. The error bars show the standard deviation for n = 3.

3.4.6. Immunomagnetic separation and electrochemical immunosensing of exosome in human serum

The detection of exosomes in non-diluted human serum is critical for a routine clinical diagnosis, since it can suffer from interferences of free biomarkers. In order to avoid ultracentrifugation, the evaluation of the analytical performance of the

electrochemical immunosensor coupled with IMS based on a CD81 receptor for the detection of SKBr3 exosomes spiked in depleted non-diluted human serum is shown in Fig. 3.10. The exosomes concentration ranged from 2.00×10^7 to 2.00×10^{10} exosomes mL^{-1} in order to cover the matrix effect in a wide concentration range. The exosomes concentration in healthy individuals determined by NTA in biological fluids varies notably in the literature, from 1.505 to 2.245×10^8 vesicles mL^{-1} (plasma of healthy male individuals) (Eman Abu-Seer, 2017); 9.25×10^9/2.4×10^{10}/1.8×10^{10} vesicles mL^{-1} (depending on the mode of NTA in plasma of healthy individuals) (Fernando et al., 2017); 0.7×10^8/5.3×10^8 vesicles mL^{-1} (serum)/2.3×10^8/9.9×10^8 vesicles mL^{-1} (plasma) (depending on the mode of NTA in plasma of healthy individuals) (Soares Martins et al., 2018); and 0.88×10^8 to 1.34×10^9 exosomes mL^{-1} (serum or plasma of healthy individuals) (Huang et al., 2013).

The results show the performance of the magneto-actuated electrochemical immunosensor for the detection of exosomes spiked on PBS (10 mmol L^{-1}) and on human serum (exosome-depleted), and performed by IMS on antiCD81-MPs and the detection of cancer-related biomarkers (CD24 and CD340 for Fig. 3.10, panels A and B, respectively).

The limit of detection (LOD) for each plot were estimated by fitting the raw data using a nonlinear regression (four parameters logistic equation), by processing the negative control samples (n = 10) and obtaining the mean value for each plot. The cutoff value was then determined in all cases with a one-tailed t-test at a 95% confidence level. These values were interpolated in each plot to obtain the LODs.

The LOD for the detection approach using antiCD24 was found to be 1.94×10^5 and 1.73×10^5 exosomes μL^{-1} for exosomes spiked in human serum and phosphate buffer, respectively. The LOD for the detection approach using antiCD340 was found to be 1.02×10^6 and 5.64×10^5 exosomes μL^{-1} for exosomes spiked in human serum and PBS, respectively.

Finally, the immunosensor for CD63 recognition, a LOD of 1.24×10^5 and as low as 2.34×10^4 exosomes μL^{-1} was obtained with antiCD63-HRP (Fig. 3.10, panel C) in non-diluted human serum and a phosphate buffer. Although from the results shown in Fig. 3.10, there is a matrix effect in the serum, this approach demonstrated a good performance of the electrochemical immunosensor towards cancer-related exosomes isolated by IMS in non-diluted human serum samples, without any further pretreatment (such as ultracentrifugation).

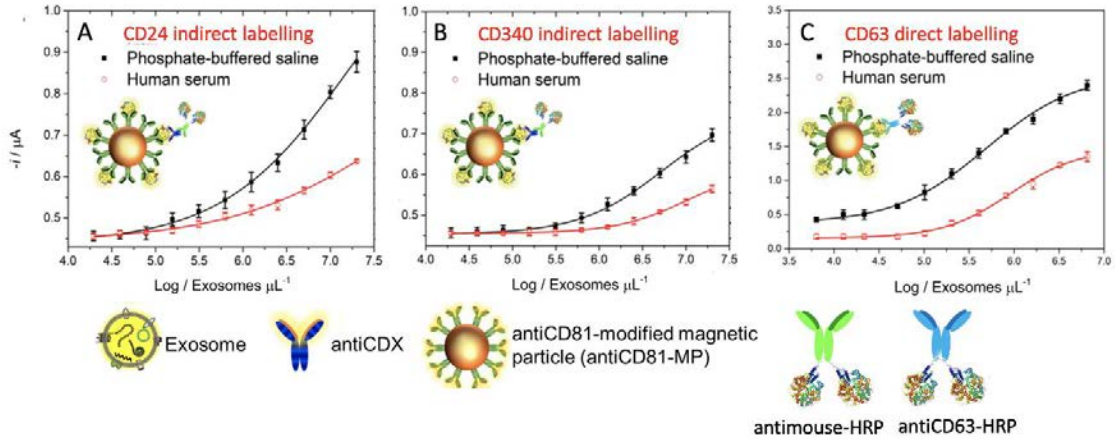

Fig. 3.10. Electrochemical immunosensor for the detection of exosomes derived from the SKBr3 breast cancer cell line spiked in exosome-depleted human serum and a phosphate buffer. IMS of the exosomes on antiCD81-MPs, followed by indirect labeling with (A) antiCD24, (B) antiCD340 and by direct labeling with (C) antiCD63-HRP antibody. In all cases, the concentration of MPs was fixed in 1 × 10^6 MPs, 0.50 μg mL^{-1} of primary antibody, 0.08 ng mL^{-1} of antimouse-HRP and 1.24 μg mL^{-1} of antiCD63-HRP antibody. Enzymatic electrochemical signals were monitored at −0.1 V vs. $Ag/AgCl_{(sat.)}$. In all cases, the replicates were obtained with three different samples measured with different m-GEC electrodes. The error bars show the standard deviation for n = 3.

3.5. Conclusions

The most important feature that should be considered to simplify the analytical procedure for the detection of exosomes at low concentration levels involves novel solid-phase separation methods to avoid ultracentrifugation. In this paper, we demonstrated that particle-based magnetic enrichment simplifies exosomes isolation and can be easily coupled with emerging technologies as is the case with electrochemical immunosensing. However, the interferences of free receptors present in the serum, including the tetraspanins CD9 and CD63, can prevent or interfere with the immunomagnetic separation based on these receptors. Interestingly, the immunomagnetic separation of the exosomes based on CD81 is not affected by the serum (even if it is undiluted), which can be easily detected by an electrochemical immunosensor using cancer related biomarkers, such as CD24 and CD340.

Moreover, the exosome electrochemical immunosensor shows an outstanding LOD as low as 10^4 exosomes μL^{-1} directly in undiluted human serum when the detection is based on CD63, this LOD being compatible with the levels of exosomes present in serum and plasma and, importantly, without any previous isolation step using ultracentrifugation. The electrochemical immunosensor, coupled with immunomagnetic separation, offers an exciting alternative, especially in resource-scarce settings that can be handled by unskilled personnel at the community care level.

3.6. References

Agrawal, A., Sathe, T., Nie, S. Single-bead immunoassays using magnetic microparticles and spectral-shifting quantum dots. J Agric Food Chem 2007; 55: 3778.

Allard, W.J. Tumor Cells Circulate in the Peripheral Blood of All Major Carcinomas but not in Healthy Subjects or Patients With Nonmalignant Diseases. Clin. Cancer Res. 2004; 10: 6897.

Bamgbelu, A., Wang, J., Leszczynski, J. TDDFT Study of the Optical Properties of Cy5 and Its Derivatives. J. Phys. Chem. A 2010; 114: 3551.

Beretov, J., Cozzi, P., Duan, W., et al. Epithelial cell adhesion molecule (EpCAM) is involved in prostate cancer chemotherapy/radiotherapy response in vivo. BMC Cancer 2018; 18: 1092.

Bethune, G., Bethune, D., Ridgway, N., et al. Epidermal growth factor receptor (EGFR) in lung cancer: an overview and update. J. Thorac. Dis. 2010; 2: 48.

Brandão, D., Liébana, S., Pividori, M. I. Multiplexed detection of foodborne pathogens based on magnetic particles. N. Biotechnol. 2015; 32: 511.

Bray, F., Ferlay, J., Soerjomataram, I., et al. Global cancer statistics 2018: GLOBOCAN estimates of incidence and mortality worldwide for 36 cancers in 185 countries. CA. Cancer J. Clin. 2018; 68: 394.

Bruening, J., Lasswitz, L., Banse, P., et al. Hepatitis C virus enters liver cells using the CD81 receptor complex proteins calpain-5 and CBLB. PLOS Pathog. 2018; 14: e1007111.

Carinelli, S., Martí, M., Alegret, S., et al. Biomarker detection of global infectious diseases based on magnetic particles. N. Biotechnol. 2015; 32: 521.

Carinelli, S., Xufré, C., Martí, M., et al. Interferon gamma transcript detection on T cells based on magnetic actuation and multiplex double-tagging electrochemical genosensing. Biosens. Bioelectron. 2018; 117: 183.

Chiba, M., Kimura, M., Asari, S. Exosomes secreted from human colorectal cancer cell lines contain mRNAs, microRNAs and natural antisense RNAs, that can transfer into the human hepatoma HepG2 and lung cancer A549 cell lines. Oncol. Rep. 2012; 28: 1551.

Chiu, Y.-J., Cai, W., Shih, Y.-R. V., et al. A Single-Cell Assay for Time Lapse Studies of Exosome Secretion and Cell Behaviors. Small 2016; 12: 3658.

Cho, Y.-E., Im, E.-J., Moon, P.-G., et al. Increased liver-specific proteins in circulating extracellular vesicles as potential biomarkers for drug- and alcohol-induced liver injury. PLoS One 2017; 12: e0172463.

Chosewood, L.C., Wilson, D. E. Biosafety in Microbiological and Biomedical Laboratories, 5th ed., in: U.S. Department of Health and Human Services. Centers for Disease Control and Prevention. 2009; 30.

Chow, A., Zhou, W., Liu, L., et al. Macrophage immunomodulation by breast cancer-derived exosomes requires Toll-like receptor 2-mediated activation of NF-κB. Sci. Rep. 2015; 4: 5750.

Dai, M., Yuan, F., Fu, C., et al. Relationship between epithelial cell adhesion molecule (EpCAM) overexpression and gastric cancer patients: A systematic review and meta-analysis. PLoS One 2017; 12: e0175357.

Day, K. C., Hiles, G. L., Kozminsky, M., et al. HER2 and EGFR Overexpression Support Metastatic Progression of Prostate Cancer to Bone. Cancer Res. 2017; 77: 74.

de Wit, S., Manicone, M., Rossi, E., et al. EpCAMhigh and EpCAMlow circulating tumor cells in metastatic prostate and breast cancer patients. Oncotarget. 2018; 9: 35705.

Dhar, D., Antonucci, L., Nakagawa, H., et al. Liver Cancer Initiation Requires p53 Inhibition by CD44-Enhanced Growth Factor Signaling. Cancer Cell 2018; 33: 1061.

Eman, A.-S. The Reliability of Plasma Exosome Concentrations in Healthy Male Individuals. J. Heal. Sci. 2017; 5: 81.

Fang, C., Zhou, Z., Hu, J., et al. CD133+CD54+CD44+ circulating tumor cells as a biomarker of treatment selection and liver metastasis in patients with colorectal cancer. Oncotarget 2016; 7: 77389.

Fang, S., Tian, H., Li, X., et al. Clinical application of a microfluidic chip for immunocapture and quantification of circulating exosomes to assist breast cancer diagnosis and molecular classification. PLoS One 2017; 12: e0175050.

Fang, X., Zheng, P., Tang, J., et al. CD24: from A to Z. Cell. Mol. Immunol. 2010; 7: 100.

Fenner, A. Biomarkers: Urinary exosome biomarkers of radiation exposure. Nat. Rev. Urol. 2016; 13: 437.

Fernando, M. R., Jiang, C., Krzyzanowski, G. D., et al. New evidence that a large proportion of human blood plasma cell-free DNA is localized in exosomes. PLoS One 2017; 12: e0183915.

Filipe, V., Hawe, A., Jiskoot, W. Critical Evaluation of Nanoparticle Tracking Analysis (NTA) by NanoSight for the Measurement of Nanoparticles and Protein Aggregates. Pharm. Res. 2010; 27: 796.

Galizia, G., Lieto, E., Orditura, M., et al. Epidermal Growth Factor Receptor (EGFR) Expression is Associated With a Worse Prognosis in Gastric Cancer Patients Undergoing Curative Surgery. World J. Surg. 2007; 31: 1458.

Gerbitz, A., Ewing, P., Olkiewicz, K., et al. A role for CD54 (intercellular adhesion molecule-1) in leukocyte recruitment to the lung during the development of experimental idiopathic pneumonia syndrome. Transplantation 2005; 79: 536.

Gong, Y., Scott, E., Lu, R., et al. TIMP-1 Promotes Accumulation of Cancer Associated Fibroblasts and Cancer Progression. PLoS One 2013; 8: e77366.

Guilmain, W., Colin, S., Legrand, E., et al. CD9P-1 expression correlates with the metastatic status of lung cancer and a truncated form of CD9P-1, GS-168AT2, inhibits in vivo tumour growth. Br. J. Cancer. 2011; 104: 496.

Guo, P., Huang, J., Wang, L., et al. ICAM-1 as a molecular target for triple negative breast cancer. Proc. Natl. Acad. Sci. U. S. A. 2014; 111: 14710.

Halvaei, S., Daryani, S., Eslami-S, Z., et al. Exosomes in Cancer Liquid Biopsy: A Focus on Breast Cancer. Mol. Ther. - Nucleic Acids 2018; 10: 131.

Hasegawa, K., Sato, A., Tanimura, K., et al. Fraction of MHCII and EpCAM expression characterizes distal lung epithelial cells for alveolar type 2 cell isolation. Respir. Res. 2017; 18: 150.

Hemler, M. E. Tetraspanin proteins promote multiple cancer stages. Nat. Rev. Cancer 2013; 14: 49.

Heo, D., Huh, Y.-M., Yang, J., et al. Molecular Imaging of CD44-Overexpressing Gastric Cancer in Mice Using T2 MR Imaging. J. Nanosci. Nanotechnol. 2015; 16: 196.

Hoogenboom, R., Fijten, M. W. M., Kickelbick, G. Synthesis and crystal structures of multifunctional tosylates as basis for star-shaped poly(2-ethyl-2-oxazoline)s. Beilstein J. Org. Chem. 2010; 6: 773.

Hu, B., Ma, Y., Yang, Y., et al. CD44 promotes cell proliferation in non-small cell lung cancer. Oncol. Lett. 2018; 15: 5627.

Huang, X., Yuan, T., Tschannen, M., et al. Characterization of human plasma-derived exosomal RNAs by deep sequencing. BMC Genomics 2013; 14: 319.

Iczkowski, K. A. Cell adhesion molecule CD44: its functional roles in prostate cancer. Am. J. Transl. Res. 2010; 3: 1.

Johnstone, R. M., Adam, M., Hammond, J. R., et al. Vesicle formation during reticulocyte maturation. Association of plasma membrane activities with released vesicles (exosomes). J. Biol. Chem. 1987; 262: 9412.

Ke, J., Wu, X., Wu, X., et al. A subpopulation of CD24+ cells in colon cancer cell lines possess stem cell characteristics. Neoplasma 2012; 59: 282.

Kim, K.-J., Kwon, H.J., Kim, M.C., et al. CD9 Expression in Colorectal Carcinomas and Its Prognostic Significance. J. Pathol. Transl. Med. 2016; 50: 459.

Kohmo, S., Kijima, T., Otani, Y., et al. Cell Surface Tetraspanin CD9 Mediates Chemoresistance in Small Cell Lung Cancer. Cancer Res. 2010; 70: 8025.

Komposch, K., Sibilia, M. EGFR signaling in liver diseases. Int. J. Mol. Sci. 2015; 17: 30.

Kristiansen, G., Schlüns, K., Yongwei, Y., et al. CD24 is an independent prognostic marker of survival in nonsmall cell lung cancer patients. Br. J. Cancer 2003; 88: 231.

Kwon, M. S., Shin, S.-H., Yim, S.-H., et al. CD63 as a biomarker for predicting the clinical outcomes in adenocarcinoma of lung. Lung Cancer 2007; 57: 46.

Lee, T. K. W., Castilho, A., Cheung, V. C. H., et al. CD24(+) liver tumor-initiating cells drive self-renewal and tumor initiation through STAT3-mediated NANOG regulation. Cell Stem Cell 2011; 9: 50.

Lermo, A., Zacco, E., Barak, J., et al. Towards Q-PCR of pathogenic bacteria with improved electrochemical double-tagged genosensing detection. Biosens. Bioelectron. 2008; 23: 1805.

Levva, S., Kotoula, V., Kostopoulos, I., et al. Prognostic evaluation of epidermal growth factor receptor (EGFR) genotype and phenotype parameters in triple-negative breast cancers. Cancer Genomics and Proteomics 2017; 14: 181.

Li, C., Liu, S., Yan, R., et al. CD54-NOTCH1 axis controls tumor initiation and cancer stem cell functions in human prostate cancer. Theranostics 2017; 7: 67.

Li, Q., Tofaris, G. K., Davis, J. J. Concentration-Normalized Electroanalytical Assaying of Exosomal Markers. Anal. Chem. 2017; 89: 3184.

Logozzi, M., Angelini, D. F., Iessi, E., et al. Increased PSA expression on prostate cancer exosomes in in vitro condition and in cancer patients. Cancer Lett. 2017; 403: 318.

Louderbough, J. M. V., Schroeder, J. A. Understanding the Dual Nature of CD44 in Breast Cancer Progression. Mol. Cancer Res. 2011; 9: 1573.

Matsumoto, T., Takai, A., Eso, Y., et al. Proliferating EpCAM-positive ductal cells in the inflamed liver give rise to hepatocellular carcinoma. Cancer Res. 2017; 77: 6131.

Miki, Y., Yashiro, M., Okuno, T., et al. Clinico-pathological significance of exosome marker CD63 expression on cancer cells and stromal cells in gastric cancer. PLoS One 2018; 13: e0202956.

Moura, S. L., Martì, M., Pividori, M. I. Matrix Effect in the Isolation of Breast Cancer-Derived Nanovesicles by Immunomagnetic Separation and Electrochemical Immunosensing — A Comparative Study. Sensors 2020a; 20: 965.

Moura, S. L., Martín, C. G., Martí, M., Pividori, M. I. Multiplex detection and characterization of breast cancer exosomes by magneto-actuated immunoassay. Talanta 2020b; 211: 120657.

Murayama, Y., Oritani, K., Tsutsui, S. Novel CD9-targeted therapies in gastric cancer. World J. Gastroenterol. 2015; 21: 3206.

Nicolazzo, C., Raimondi, C., Francescangeli, F., et al. EpCAM-expressing circulating tumor cells in colorectal cancer. Int. J. Biol. Markers 2017; 32: e415.

Patel, G. K., Khan, M. A., Zubair, H., et al. Comparative analysis of exosome isolation methods using culture supernatant for optimum yield, purity and downstream applications. Sci. Rep. 2019; 9: 5335.

Qi, H., Liu, C., Long, L., et al. Blood Exosomes Endowed with Magnetic and Targeting Properties for Cancer Therapy. ACS Nano 2016; 10: 3323.

Rappa, G., Green, T. M., Karbanová, J., et al. Tetraspanin CD9 determines invasiveness and tumorigenicity of human breast cancer cells. Oncotarget 2015; 6: 7970.

Reddy, L. H., Arias, J. L., Nicolas, J., et al. Magnetic Nanoparticles: Design and Characterization, Toxicity and Biocompatibility, Pharmaceutical and Biomedical Applications. Chem. Rev. 2012; 112: 5818.

Rembaum, A., Yen, R. C. K., Kempner, D. H., et al. Cell labeling and magnetic separation by means of immunoreagents based on polyacrolein microspheres. J. Immunol. Methods 1982; 52: 341.

Ross, B. A. A., Cooper, B. W., Lazarus, H. M., et al. Detection and viability of tumor cells in peripheral blood stem cell collections from breast cancer patients using immunocytochemical and clonogenic assay techniques. Blood 1993; 82: 2605.

Shiozawa, M., Guan, H.-B., Tanaka, K., et al. Prognostic significance of CD44 variant 2 upregulation in colorectal cancer. Br. J. Cancer 2014; 111: 365.

Soares Martins, T., Catita, J., Martins Rosa, I., et al. Exosome isolation from distinct biofluids using precipitation and column-based approaches. PLoS One 2018; 13: e0198820.

Sun, Y., Xia, Z., Shang, Z., et al. Facile preparation of salivary extracellular vesicles for cancer proteomics. Sci. Rep. 2016; 6: 24669.

Taylor, D. D., Gercel-Taylor, C. MicroRNA signatures of tumor-derived exosomes as diagnostic biomarkers of ovarian cancer. Gynecol. Oncol. 2008; 110: 13.

Théry, C., Amigorena, S., Raposo, G., et al. Isolation and Characterization of Exosomes from Cell Culture Supernatants and Biological Fluids. Curr. Protoc. Cell Biol. 2006; 30: 3.22.1.

Tominaga, N., Hagiwara, K., Kosaka, N., et al. RPN2-mediated glycosylation of tetraspanin CD63 regulates breast cancer cell malignancy. Mol. Cancer 2014; 13: 134.

Trams, E. G., Lauter, C. J., Norman Salem, J., et al.. Exfoliation of membrane ecto-enzymes in the form of micro-vesicles. Biochim. Biophys. Acta - Biomembr. 1981; 645: 63.

Vang, K. B., Jenkins, S. V., Zharov, V. P., et al. Triple-negative breast cancer targeting and killing by EpCAM-directed, plasmonically active nanodrug systems. npj Precis. Oncol. 2017; 1: 27.

Wang, J., Hu, J., Liu, S. et al. Expression of Intercellular Adhesion Molecule 1 by Hepatocellular Carcinoma Stem Cells and Circulating Tumor Cells. Gastroenterology 2013; 144: 1031.

Wang, L., Balasubramanian, P., Chen, A. P., et al. Promise and limits of the CellSearch platform for evaluating pharmacodynamics in circulating tumor cells. Semin. Oncol. 2016; 43: 464.

Wang, X., Ding, X., Nan, L., et al. Investigation of the roles of exosomes in colorectal cancer liver metastasis. Oncol. Rep. 2015; 33: 2445.

Wang, Y.-C., Wang, J.-L., Kong, X., et al. CD24 mediates gastric carcinogenesis and promotes gastric cancer progression via STAT3 activation. Apoptosis 2014; 19: 643.

Weissleder, R., Pittet, M. J. Imaging in the era of molecular oncology. Nature 2008; 452: 580.

Xu, J., Mahajan, K., Xue, W., et al. Simultaneous, single particle, magnetization and size measurements of micron sized, magnetic particles. J. Magn. Magn. Mater. 2012; 324: 4189.

Yashiro, M., Sunami, T., Hirakawa, K. CD54 expression is predictive for lymphatic spread in human gastric carcinoma. Dig. Dis. Sci. 2015; 50: 2224.

Yoo, T.-H., Ryu, B.-K., Lee, M.-G., et al. CD81 is a candidate tumor suppressor gene in human gastric cancer. Cell. Oncol. 2013; 36: 141.

Yoshioka, Y., Kosaka, N., Konishi, Y., et al. Ultra-sensitive liquid biopsy of circulating extracellular vesicles using ExoScreen. Nat. Commun. 2014; 5: 3591.

Zhang, H.-G., Grizzle, W.E. Exosomes. Am. J. Pathol. 2014; 184: 28.

Zhang, N., Zuo, L., Zheng, H., et al. Increased Expression of CD81 in Breast Cancer Tissue is Associated with Reduced Patient Prognosis and Increased Cell Migration and Proliferation in MDA-MB-231 and MDA-MB-435S Human Breast Cancer Cell Lines In Vitro. Med. Sci. Monit. 2018; 24: 5739.

Zhang, Y., Li, B., Zhang, X., et al. CD24 is a genetic modifier for risk and progression of prostate cancer. Mol. Carcinog. 2017; 56: 641.

Zhao, Z., Yang, Y., Zeng, Y., et al. A microfluidic ExoSearch chip for multiplexed exosome detection towards blood-based ovarian cancer diagnosis. Lab Chip 2016; 16, 489.

Zheng, R., Yano, S., Zhang, H., et al. CD9 overexpression suppressed the liver metastasis and malignant ascites via inhibition of proliferation and motility of small-cell lung cancer cells in NK cell-depleted SCID mice. Oncol. Res. 2005; 15, 365.

Zvereff, V., Wang, J.-C., Shun, K., Lacoste, J., Chevrette, M., Colocalisation of CD9 and mortalin CD9-induced mitotic catastrophe in human prostate cancer cells. Br J Cancer. 2007; 97: 941.

CHAPTER 4

Multiplex detection and characterization of breast cancer exosomes by magneto-actuated immunoassay

Silio Lima Moura, Carme García Martín, Mercè Martì and María Isabel Pividori

Talanta **2020**, 211; 120657

DOI: 10.1016/j.talanta.2019.120657

4.1. Abstract

The exosomes are emerging as biomarkers for the detection of cancer in early stages, as well as for the follow-up of the patients under treatment. This paper describes the characterization of exosomes derived from three different breast cancer cell lines (MCF7, MDA-MB-231 and SKBR3), and the quantification based on a magneto-actuated immunoassay. The exosomes are separated and preconcentrated on magnetic particles by immunomagnetic separation and labelled with a second antibody conjugated with an enzyme for the optical readout performed with a standard microplate reader. Several molecular biomarkers, including the general tetraspanins CD9, CD63 and CD81, and the receptors related with cancer (CD24, CD44, CD54, CD326 and CD340) were studied either for the immunomagnetic separation or the labelling, in different formats. After a rational selection of the biomarkers, this immunoassay is able to detect 10^5 exosomes μL^{-1} directly in human serum without any treatment, such as ultracentrifugation. The interference from free receptors in the samples could easily be prevented by performing the immunomagnetic separation with antiCD81 modified magnetic particles and the labeling based on either CD24 or CD340. Furthermore, the differentiation of healthy donors and breast cancer individuals was also demonstrated. This approach is a highly suitable alternative method for flow cytometry, providing a sensitive method for the multiplex detection but using instrumentation widely available in resource-constrained laboratories and requiring low-maintenance, as is the case of a microplate reader operated by filters.

4.2. Introduction

Besides the progress in emerging technologies for diagnosis, the identification of novel biomarkers represents a worldwide challenge not only for the improvement of early diagnosis, but also for the following-up of patient under treatment. Exosomes (Johnstone et al., 1987) are nano-sized and cup-shaped vesicles (Théry et al., 2002), which are currently under intensive study as potential diagnostic biomarkers for many health disorders, including cancer (An et al., 2015). They are produced by the cell as part of a complex endosomal secretory pathway and then released into the extracellular environment. The endosomal biogenesis becomes these nanovesicles as carriers of mRNA, microRNA, rRNA, tRNA, DNA, lipids and proteins (Samanta et al., 2018). Exosomes can be found in different biofluids including blood, saliva, serum, plasma, semen, urine, among others (Samanta et al., 2018).

Conventional procedures for exosome detection usually require relatively large sample volumes and involve a preliminary purification and preconcentration step by ultracentrifugation to prevent interferences from free receptors in the sample. Nanoparticle

tracking analysis (NTA), followed by the specific detection, including LC-MS/MS, Western Blot, RT-PCR, or flow cytometry are usually performed. The whole procedure is thus time consuming, requiring skilled personnel as well as laboratory facilities and benchtop instrumentation. Therefore, there is a growing need for novel methods to accurately characterize and specifically determine the concentration of exosomes in complex biological fluids.

Novel developments that are needed for the detection and characterization of exosomes in complex samples involve solid-phase preconcentration procedures which can be easily integrated in emerging technologies. Exosomes can be thus preconcentrated while the interfering matrix is removed at the same time, increasing the sensitivity and the specificity of the detection. Since the early reports on magnetic separation technology (Rembaum et al., 1982), magnetic particles (MPs) have been used as a powerful and versatile preconcentration tool in a variety of analytical and biotechnology applications (Reddy et al., 2012) and in emerging technologies including microfluidic devices and biosensors (Brandão et al., 2015; Carinelli et al., 2015; Zacco et al., 2006).

Since the introduction of the Enzyme-linked immunosorbent assays (ELISA) in 1971 (Engvall and Perlmann, 1971), this methodology is routinely used in clinical diagnosis in small centres due to its high sensitivity, specificity and accuracy, and is widely implemented for the detection of breast cancer related biomarkers using commercial ELISA kits, for instance: CA15-3 ELISA kit (Abnova), Apolipoprotein C–I (APOC1) ELISA kit (Abnova), IGFBP-3 Quantikine ELISA (R&D), CCL5/RANTES Quantikine ELISA (R&D), Osteopontin (OPN) Quantikine ELISA (R&D), Human SLPI Quantikine ELISA (R&D), PAI-1 ELISA Kit (Invitrogen), Hsp90α ELISA Kit (Stressgen), Pappalysin-1 (PAPPA) ELISA kit (DRG), among others).

In this work, an ELISA incorporating immunomagnetic separation (IMS) (magneto-actuated ELISA) for the characterization and quantification of exosomes derived from breast cancer cell lines is presented and studied in different formats, and compared in term of analytical performance with flow cytometry. The integration of the magnetic particles allowed the preconcentration of exosomes by immunomagnetic separation.

Firstly, the exosomes derived from three different breast cancer cell lines (MCF7, MDA-MB-231 and SKBR3) were isolated by ultracentrifugation and characterized by nanoparticle tracking analysis and cryogenic transmission electron microscopy. The expression of different biomarkers, including CD9, CD63 and CD81 as general biomarkers for exosomes, and the specific cancer-related molecules (CD24, CD44, CD54, CD326 and CD340) were studied by flow cytometry and correlated with the expression of the breast cancer cell lines. Different formats for the magneto-actuated immunoassay (magneto-ELISA) were assessed in terms of sensitivity and matrix effect, including the

immunomagnetic separation and the labeling using either general receptors (CD9, CD63 and CD81) and the biomarkers of cancer (CD24, CD44, CD54, CD326 and CD340). Among them, the IMS using specific antibodies for capturing the exosomes, followed by the direct labeling based on CD63 showed higher sensitivity, while the use of CD81 for immunomagnetic separation, followed by the indirect labeling based on specific biomarkers, avoided the interference of free receptors in serum, allowing the detection of exosomes directly in serum. Finally, the results obtained by the magneto-actuated immunoassay suggested that serum samples from breast cancer patients contained higher number of exosomes compared with samples form healthy serum donors. Besides, exosome this approach allows the analysis of a large number of specimens in low-resource settings with a comparable performance of flow cytometry, as well as for applicability in real samples, differentiating healthy individuals and breast cancer patients based on specific epithelial biomarkers. The results suggest that the magneto-actuated immunoassay can be proposed as a tool for screening serum samples to detect and quantify exosomes in biological liquid samples.

4.3. Experimental

4.3.1. Instrumentation

Nanoparticle tracking analysis (NTA) was performed using the NanoSight LM10-HS system with a tuned 405 nm laser (NanoSight Ltd, UK). The cryogenic transmission electron microscopy (TEM) images were collected by a Jeol JEM 2011 (JEOL USA Inc, USA) transmission electron microscope at an accelerating voltage of 200 kV. Flow cytometry was performed using BD FACSCANTO II (BD Biosciences, USA) equipment. The Media Fluorescence Intensity (MFI) and beads count data were obtained by FlowJo analysis software of every sample reading file. Optical measurements were performed on a TECAN Sunrise (TECAN AG, Switzerland) microplate reader with Magellan v4.0 software. Polystyrene microtiter plates were purchased from Nunc (Maxisorp, Roskilde, DK). The data were in all cases fitted with using a nonlinear regression (Four Parameter logistic Equation–GraphPad Prism Software).

4.3.2. Chemicals and biochemicals

Magnetic particles (Dynabeads® M450 Tosylactivated, nº 14013, 4.5 µm diameter) were purchased from Thermo Fisher. The mouse monoclonal antibodies (antiCDX) were purchased from i) Abcam: CD24 (Ref. ab76514), CD54 (Ref. ab2213), CD326 (Ref. ab7504), CD340 (Ref. ab30); ii) Thermo Fisher: CD9 (Ref. 10626D), CD63 (Ref. 10628D), CD81 (Ref. 10630D); and iii) eBioscience: CD44 (Ref. BMS113). The rabbit polyclonal antibody antiCD81 (Ref. HPA007234) was provided by Sigma-Aldrich. For direct labeling, mouse monoclonal CD63 antibody labelled with HRP (antiCD63-HRP) (Ref. NBP2–

42225H-100) was obtained from BioNova. For the indirect labeling, the secondary antibodies were provided by Abcam: a rabbit anti-mouse IgG conjugated with HRP (antimouse-HRP) (Ref. ab6728) for immunoassays; and a goat antimouse IgG (Cy5®) (antimouse-Cy5) (Ref. ab97037) for flow cytometry.

All other reagents were in analytical reagent grade used throughout the experiments and are listed in details in the Supp. Data.

4.3.3. Cell culture and exosome isolation and purification

Breast cancer cell lines MCF7 (ATCC® HTB-22™), MDA-MB-231 (ATCC® CRM-HTB-26™) and SKBr3 (ATCC® HTB-30™) were grown as described in the Supp. Data. Exosomes were purified from culture supernatant by differential ultracentrifugation (Théry et al., 2006). Exosomes are resuspended in 10 mmol L^{-1} PBS buffer solution (0.22 µm filtrated and sterile) and storage at −80 °C. All exosomes purification steps are detailed provided in the Supp. Data.

4.3.4. Characterization of exosomes by nanoparticle tracking analysis and transmission electron microscopy

The size distribution and concentration of exosomes were measured by nanoparticle tracking analysis (NTA). The purified exosomes were diluted in sterile-filtered PBS pH 7.5 buffer (50- to 100-fold). Nanosight NTA Software analysed raw data videos (see Video S1, Supp. Data) by triplicate during 60 s with 50 frames/s and the temperature of the laser unit set at 24.8 °C. For the cryogenic transmission electron microscopy (TEM), the exosomes (2.0×10^9) were directly laid on Formvar-Carbon EM grids and frozen in ethanol. Exosomes were maintained at −182 °C during the whole process.

4.3.5. Flow cytometry study

The analysis of the molecular biomarkers CD9, CD24, CD44, CD54, CD63, CD81, CD326 and CD340 expressed in three different cancer cell lines (MCF7, MDA-MB-231 and SKBr3) was firstly performed by flow cytometry. The indirect labeling of 2×10^5 cells was performed by incubation of 100 µL (5 µg mL^{-1}) of the antibodies antiCDX (mouse), (being CDX either CD9, CD24, CD44, CD54, CD63, CD81, CD326 and CD340 biomarkers), for 30 min with gentle shaking at 25 °C. After that, three washing steps with PBS pH 7.5 containing 0.5% BSA were performed. Afterwards, 100 µL (2 µg mL^{-1}) of antimouse-Cy5 antibody (a far-red fluorescent dye, excitation 647 nm, emission 665 nm) was incubated for 30 min at 25 °C. The labelled cells were resuspended in PBS pH 7.5 containing 0.5% BSA.

For labelling cell-derived exosomes, they were firstly immobilized on the surface of MPs by two different approaches, as described in the Supp data (Fig. S4.1 therein). In Fig.

S4.1 panel A is depicted the covalent immobilization of the 3.5 x 10^{10} exosomes on 1.6 x 10^{7} MPs (exosomes-MPs). The exosomes-MPs were analysed by indirect labelling with antiCDX (mouse) followed by antimouse-Cy5 as previously described by cell staining. In Fig. S4.1 panel B, 1 × 10^{6} MPs modified with rabbit antiCD81 (antiCD81-MPs) were incubated with 4 x 10^{9} exosomes (1:4000 MP/exosomes ratio). Exosomes immunocaptured by antiCD81-MPs were detected by the indirect labeling, as described below (Fig. 4.1).

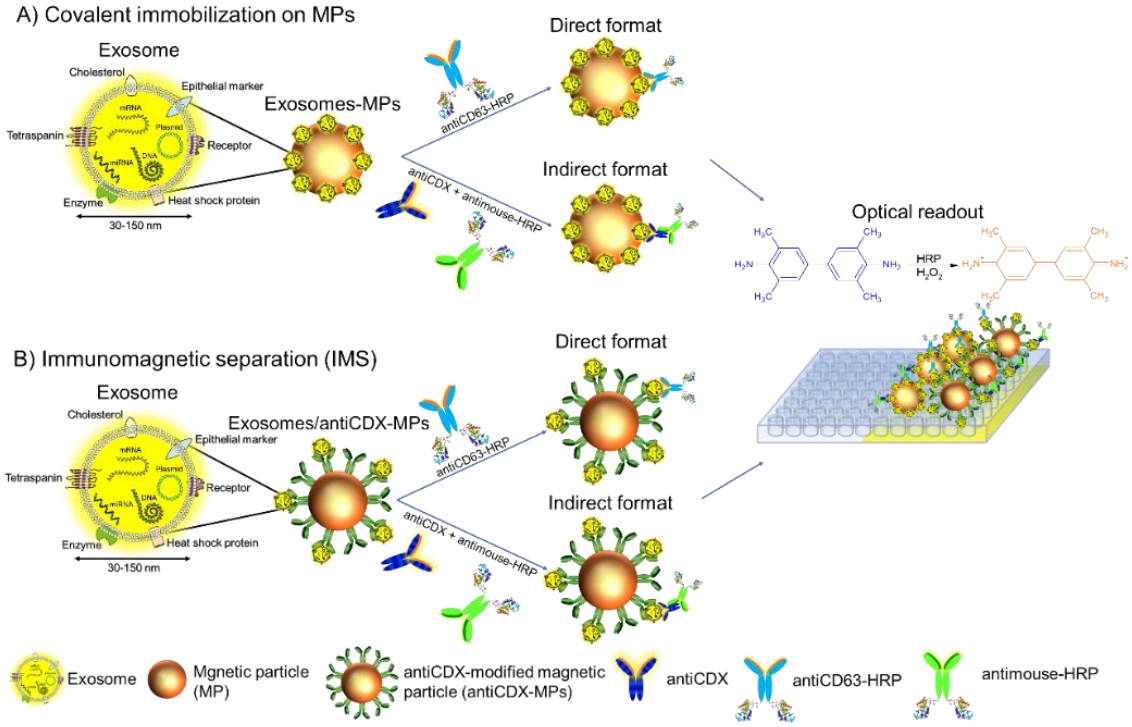

Fig. 4.1. Strategies for the detection of exosomes by magneto-actuated immunoassay in different formats. Further experimental details are provided in Fig. S4.3, Supp. Data.

4.3.6. Magneto-actuated immunoassay

Magneto-actuated immunoassay for the detection of exosomes covalently immobilized on magnetic particles. The immobilization of exosomes on magnetic particles (exosomes-MPs) is described in detail in the Supp. Data (Fig. S4.1, panel A). Two different approaches were evaluated for a magneto-actuated immunoassay: the direct and indirect format (Fig. 4.1, panel A), in all cases performed in 96-well microtiter plates. The direct immunoassay format involved the following steps: (i) incubation of the exosomes-MP with the antiCD63-HRP antibody; and (ii) optical readout. The indirect immunoassay format involved the following steps: (i) incubation of the exosomes-MP with antiCDX mouse monoclonal antibodies (being CDX either CD9, CD24, CD44, CD54,
CD63, CD81, CD326 or CD340 biomarkers); (ii) indirect labeling with antimouse-HRP antibody; and (iii) optical readout.

The indirect immunoassay format involved the following steps: (i) incubation of the exosomes-MP with antiCDX mouse monoclonal antibodies (being CDX either CD9, CD24,

CD44, CD54, CD63, CD81, CD326 or CD340 biomarkers); (ii) Indirect labeling with antimouse-HRP antibody; and (iii) optical readout.

In all instances, the modified MPs were separated by using a 96-well magnet plate separator (see Video S2, Supp Data), a pellet on the bottom corner is formed, followed by supernatant separation. The protocols for the magneto-actuated immunoassay are described in detail in Supp. Data.

Immunomagnetic separation of exosomes and magneto-actuated immunoassay. Two different approaches were evaluated, including the direct and indirect immunoassay format (Fig. 4.1, panel B), and in all cases performed in 96-well microtiter plates. The direct immunoassay format involved the following steps: i) IMS of the exosomes with antiCDX-MPs; ii) the direct labeling with the antiCD63-HRP antibody; and (iii) optical readout. It is important to highlight that in this approach a specific antibody against the different receptors (antiCDXMPs) was used for the IMS, followed by the direct labeling using a general biomarker (in this instance, antiCD63-HRP antibody). The indirect immunoassay format involved the following steps: i) IMS of the exosomes with antiCD81-MPs (rabbit); ii) incubation with the specific mouse monoclonal antibody antiCDX for each experiment (antiCDX, being CDX either CD9, CD24, CD44, CD54, CD63, CD81, CD326 or CD340 biomarkers); (iii) indirect labeling with antimouse-HRP antibody; and (iv) optical readout. Further experimental details can be found in the Supp. Data.

The concentration of the primary and secondary antibodies, the incubation steps, and the number of magnetic particles per assay were optimized as described in the Supp. Data (and Figs. S4.4, S4.5 and S4.6 therein).

4.3.7. Magneto-actuated immunoassay in human serum

The matrix effect produced by the free receptors in the human serum was evaluated by spiking the exosomes (4 x 10^9 exosomes) derived from MCF7 breast cancer cell line, in 100 µL of exosome-depleted human serum, following by IMS and magneto-actuated immunoassay. The detailed protocols, as well as the preparation of the exosome-depleted human serum used in this study are provided in Supp. Data and in Fig. S4.7 therein.

4.3.8. Magneto-actuated immunoassay for the detection of serum-derived from breast cancer patients

Blood samples from anonymized healthy female donors (n = 10, mean age 35/SD 5 years) and breast cancer female donors (n = 10, stage IV, mean age 50/SD 6 years) were obtained from the Hospital del Mar, Barcelona, Spain. The work was carried out in accordance with the principles of voluntariness and confidentiality. The samples n = 10 each were polled in two batches (healthy donors and breast cancer patients) and purified

as detailed described in Supp data. The two batches were then evaluated by NTA and the protein content (as described in Supp Data), and compared by magneto-actuated immunoassay on the basis of the same content of exosomal protein (0.235 μg of protein per assay) by two approaches: i) IMS with antiCD81-MPs in order to achieve a massive capture of the exosomes for further labeling with ephitelial-cell related biomarkers (CD24, CD44, CD326 and CD340), ii) IMS with antiCDX-MPs (being CDX: CD24 and CD340) in order to achieve only cancer-related exosomes for further labeling with a high expressed general exosome biomarker (CD63).

4.3.9. Statistical analysis

The statistical analyses were performed using GraphPad Prism 6 (San Diego, USA). The data were statistically compared using a paired-sample Student's t-test. The value $p > 0.05$ was considered significant.

4.3.10. Safety considerations

All works were performed in a Biosafety cabinet, and all material decontaminated by autoclaving or disinfected before discarding in accordance with U.S. Department of Health and Human Services guidelines for level 2 laboratory Biosafety (Chosewood and Wilson, 2009).

4.4. Results and discussion

4.4.1. Characterization of exosomes by nanoparticle tracking analysis and transmission electron microscopy

Purified exosomes from MCF7 cell line were firstly characterized by NTA. Fig. 4.2 shows the size diameter distribution of purified exosomes from MCF7 cell line ranges from approximately 50 nm to up to 360 nm (considering 95.4% of a Gaussian distribution), showing three peaks at 110 (50% of total counting), 150 (40%) and 255 nm (10%). However, it is important to highlight that NTA analysis is not able to distinguish isolated particles from aggregates. Similar results were obtained by NTA for the exosomes derived from the other cell lines (MDA-MB-231 and SKBr3) (as depicted in Fig. S4.8, Supp. Data). Further information was obtained by TEM. The micrographs revealed well-shaped exosome vesicles with close circular lipid bilayers comprising packed membrane proteins (Fig. 4.2, inset i) with 110 nm diameter. As expected, the TEM micrographs also reveals the presence of some aggregates of exosomes (Fig. 4.2, inset ii), confirming that the NTA analysis cannot distinguish vesicles and vesicle aggregates (as shown in Fig. S4.9, Supp. Data).

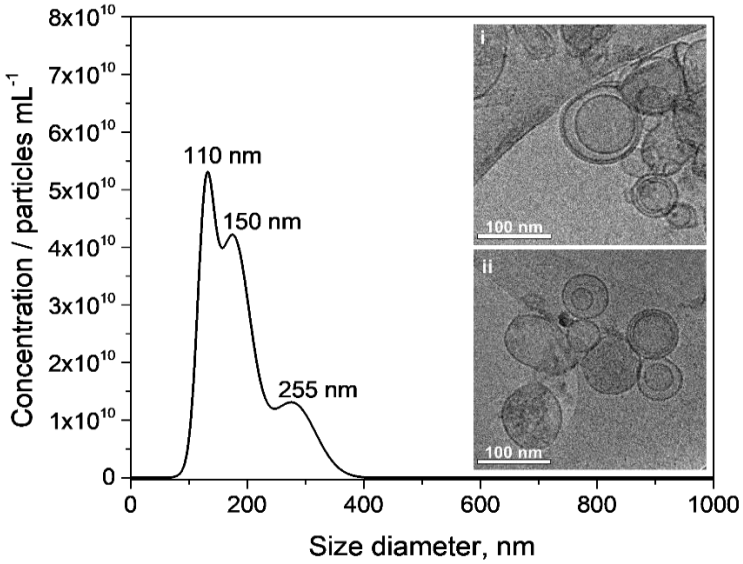

Fig. 4.2. Characterization by NTA of purified exosomes derived from MCF7 breast cancer cell line. Nanosight NTA Software analysed raw data videos by triplicate during 60 s with 50 frames per second and the temperature of the laser unit set at 24.8 °C. The corresponding TEM images at an acceleration voltage of 200 kV are also shown in the insets i and ii.

4.4.2. Comparison of key-molecular biomarkers expressed by breast cancer cell lines and their derived exosomes

The main goal of these set of experiments was firstly to assess the expression of different biomarkers (including general exosome biomarkers such as CD9, CD63 and CD81, and cancer-related biomarkers such as CD24, CD44, CD54, CD326 and CD340) on three different breast cancer cell lines (MCF7, MDA-MB-231 and SKBr3). Next, the expression of these receptors was evaluated in the exosomes derived from the different cell lines in order to perform the better design of the assay.

The percentage of labelled cells represent the total counting of positive cells for each biomarker, as shown in Fig. 4.3, panel A. As expected, the general tetraspanins (CD9, CD63 and CD81) were highly expressed (>95%) in all the breast cancer cell line (Fig. 4.3, Panel A, and the corresponding raw data shown in Fig. S4.10, Supp. Data). On the other hand, cancer-related biomarkers (CD24, CD44, CD54, CD326 and CD340) showed a different labelling pattern depending on the cell line. For instance, CD24 and CD326, although were highly expressed on MCF-7 and SKBr3 (both >95%), almost no expression on MDA-MB-231 cell line was detected (<20%). On the contrary, CD54 (>90%) and CD340 (>70%) were highly expressed by MDA-MB-231, but not by MCF-7 and SKBr3. It is also important to highlight that all the commercial antibodies showed good performance for the specific recognition in at least one experiment, confirming that they can be used for the identification of the selected biomarker.

The expression of the biomarkers on the exosomes derived from each cell line was also studied and compared to the parental cell line and among the exosomes produced by

each of them after the immobilization on MPs (exosomes-MPs). The percentage of labelled exosomes represent the total counting of positive exosomes-MPs for each biomarker, as shown in Fig. 4.3, panel A and B. In the first approach, the exosomes directly immobilized on MPs were assessed towards the expression of different biomarkers selected in this study followed by an incubation with antimouse-Cy5 secondary antibody. Then, the labelled exosomes-MPs were acquired by the flow cytometer and further analysed. As shown in Fig. 4.3, panel B and the corresponding raw data shown in Fig. S4.11, Supp Data, CD9, CD63 and CD81 were differentially expressed on exosomes produced by all the cell lines: highly, medium and low expressed in MCF7-, MDA-MB-231- and SKBr3-derived exosomes. In agreement with several studies, CD9, CD63 and CD81 as the most frequently identified proteins in exosomes and are considered classical biomarkers for exosomes (Chow et al., 2015; Hemler, 2013). Besides, cancer-related biomarkers showed in general poor labelling pattern (<5%).

In the second approach, the two biomarkers must be simultaneously expressed in the exosomes. One of the markers is involved in the IMS, while the other one, in the labelling. Accordingly, the general tetraspanin CD81 was used in this instance for the IMS by the antiCD81-MPs in order to achieve a massive capture of the exosomes, followed by further labelling by a second biomarker. As shown in Fig. 4.3, panel C and the corresponding raw data shown in Fig. S4.12, Supp. data, a better performance was in general achieved with this approach. Increased tetraspanin labelling on the exosomes from SKBr3 and MCF7 were respectively observed, although MDA-MB-231 also express low levels of these general biomarkers. Cancer-related exosome biomarkers (for instance CD44, CD340), that were negative when immobilized covalently on MPs, were detected by this approach. This experiment confirmed that CD81 tetraspanin can be successfully used for the magnetic immunoseparation of the exosomes. Comparing the expression of cells and their derived exosomes, and according to many studies (Rupp et al., 2011; Stoeck et al., 2006), cell-membrane biomarkers are not always present in the derived-exosomes. For example, is was previously reported the decrease of CD44 (Stoeck et al., 2006) and CD326 (Rupp et al., 2011), but not CD24 expression in exosomes from breast cancer cell lines, in accordance with our studies (and the corresponding raw data shown in Fig. S4.12, Supp. Data). Moreover, and as expected, Fig. 4.3 shows that there is a different pattern for the expression of exosomes from different cell cancer lines, being in general the SKBr3 cell line the one that shows a higher agreement in the expression of the receptors among cells and their corresponding exosomes. This data suggests that the exosome molecular profile needs of a multiplex immunoassay for the detection of more than one specific cell biomarker, in order to cover the differences in the expression among the exosomes-derived from different cellular sources.

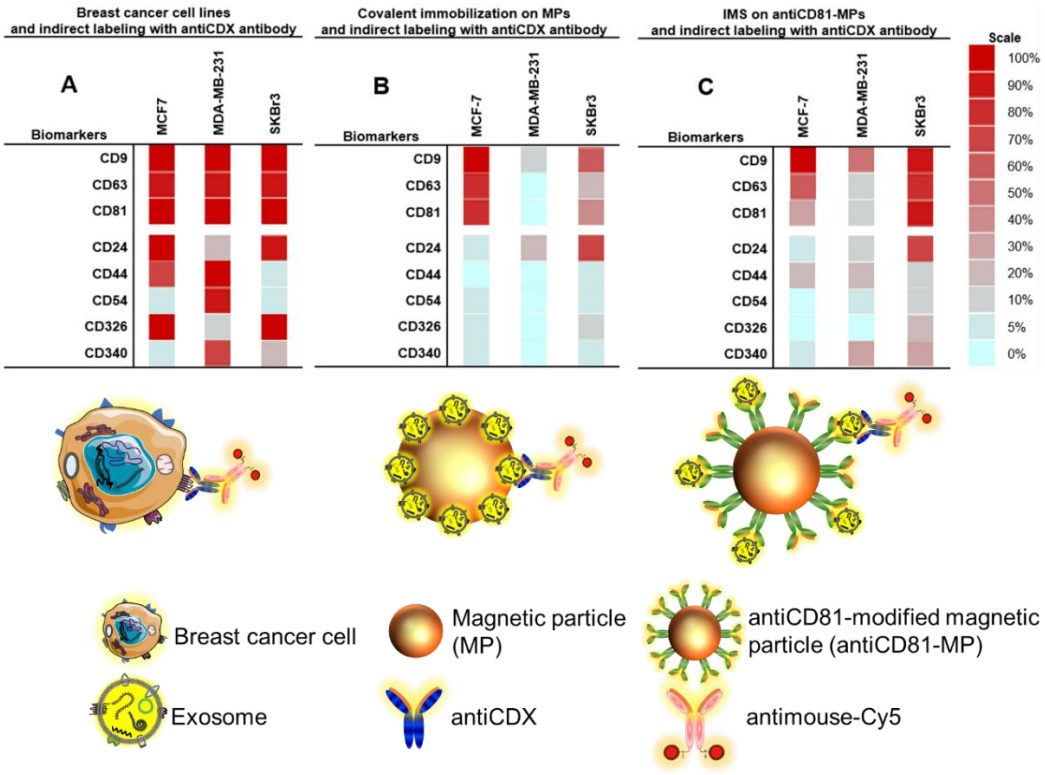

Fig. 4.3. Flow cytometry study for (A) MCF7, MDA-MB-231 and SKBr3 breast cancer cell lines and their corresponding exosomes attached on MPs, being (B) covalent immobilization of the exosomes on MPs (exosomes-MPs) and (C) IMS of the exosomes on antiCD81-MPs, followed by indirect labelling with mouse antiCDX (5 μg mL^{-1}), (being CDX either CD9, CD24, CD44, CD54, CD63, CD81, CD326 and CD340 biomarkers) and antimouse-Cy5 (2 μg mL^{-1}). The concentration of MPs and exosomes were set in 1 × 10^6 MPs and 4 x 10^9 exosomes per assay, respectively. Numbers indicate the percentage of positive cells or exosomes-coated MPs for each biomarker.

4.4.3. Magneto-actuated immunoassay

The characterization of the expression of exosomes derived from MCF7, MDA-MB-231 and SKBr3 cell lines was performed by magneto-ELISA (Fig. 4.4, panel A, B and C) using different approaches. The percentage of labelled exosomes was normalized by the highest absorbance value for a biomarker within each exosome immobilization approach, as shown in Fig. 4.4. The first approach (Fig. 4.4, panel A) involves the magneto-actuated immunoassay for the detection of exosomes covalently immobilized on magnetic particles and labelled by an indirect format using antiCDX antibodies (mouse) (being CDX either CD9, CD24, CD44, CD54, CD63, CD81, CD326 or CD340 biomarkers) and an antimouse-HRP antibody, while the second approach (Fig. 4.4, panel B), involves the IMS of exosomes with a general biomarker (antiCD81-MPs), followed by and indirect labelling. These two approaches are the same as those performed by flow cytometry (Fig. 4.3, panels B and C), just by changing the readout system (antimouse-HRP instead of antimouse-Cy5 for magneto-actuated immunoassay and flow cytometry, respectively). A similar expression pattern was obtained by flow cytometry (Fig. 4.3, panels B and C) and magneto-actuated immunoassay (Fig. 4.4, panels A and B), demonstrated a good analytical performance for

the immunoassay in order to detect exosomes. Furthermore, IMS followed by magneto-ELISA provided improved results than flow cytometry in the case of CD326 and CD340.

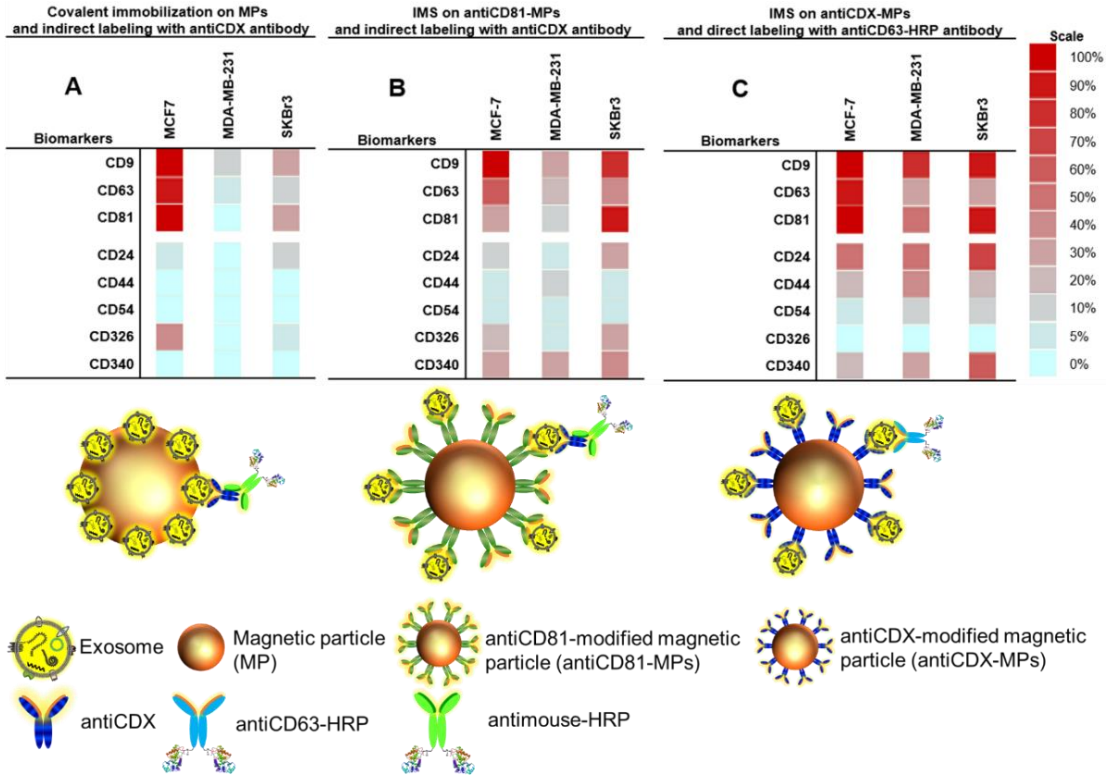

Fig. 4.4. Magneto-actuated immunoassay for exosomes derived from MCF7, MDA-MB-231 and SKBr3 breast cancer cell lines. The exosomes were attached on MPs by using three approaches, (A) covalent immobilization of exosomes on MPs (exosomes-MPs), (B) IMS of exosomes on antiCD81-MPs, followed by indirect labelling with antiCDX (mouse, 0.50 μg mL^{-1}), (being CDX either CD9, CD24, CD44, CD54, CD63, CD81, CD326 and CD340 biomarkers) and antimouse-HRP (0.08 ng mL^{-1}). (C) IMS of exosomes on antiCDX-MPs, followed by direct labelling with antiCD63-HRP antibody (1.24 μg mL^{-1}). The concentration of MPs and exosomes were set in 1 × 10^6 MPs and 4 x 10^9 exosomes per assay, respectively. Numbers indicate the percentage of positive cells or exosomes-coated MPs for each biomarker.

In the last approach (Fig. 4.4, panel C), instead of using for the IMS an antibody for a general exosome biomarker (antiCD81-MPs), followed by the indirect labelling using an specific biomarker (antiCDX antibody), the IMS was performed by using an specific biomarker antibody (antiCDX-MPs), followed by the optical readout using a general exosome biomarker (antiCD63-HRP antibody). By comparing the pattern of expression of Fig. 4.4, panels B and C, our data demonstrate that with the approach C (Fig. 4.4, panel C) in which exosome is captured with an ubiquitous biomarker followed by the detection of the specific biomarker, an increased level of detection was obtained. As shown in Fig. 4.3, panel C, a better performance was in general achieved with this approach, now revealing the presence of exosome biomarkers (for instance CD24, CD44, CD340) that were not detected by flow cytometry. It is important to highlight that in this procedure it was no possible to achieve the immobilization of antiCD326 antibody on MPs.

The format involving IMS, either in indirect or direct formats (Fig. 4.4, panels B and C, respectively), requires the coexistence of two biomarkers in the same exosomes to be

magneto-actuated and labelled. Interestingly, from the experiments shown in Fig. 4.4, a better approach can be obtained by using a general and over expressed biomarker for labelling, as is the case of CD63, and thus amplifying the signal and increasing the sensitivity, since it is expected than more receptors can be found in the exosome membrane. These results are in agreement with previous studies, reporting a higher biomarker expression to CD9, CD63 and CD81 tetraspanins as well as low biomarker expression to CD24, CD44, CD54, CD326 and CD340 cancer-related biomarkers on breast cancer exosomes (Dudani et al., 2015; Grasso et al., 2015).

The performance of the different approaches was further studied by calibration plots of exosomes (ranged from 150 to 2 x 10^7 exosomes μL^{-1}) derived from MCF7 cell line and spiked into PBS. Fig. S4.13, panel A, shows the results for the magneto-actuated immunoassay of exosomes covalently immobilized on magnetic particles and labelled by a direct (antiCD63-HRP) and indirect format (using antiCD63 and CD326 antibodies). The limit of detection (LOD) of 600 exosomes μL^{-1} (r^2 = 0.9997) and 326 exosomes μL^{-1} (r^2 = 0.9912) for indirect immunoassay format was reached using CD63 and CD326 biomarkers, respectively. A LOD of 230 exosomes μL^{-1} (r^2 = 0.9978) was reach for direct magneto-actuated immunoassay format using antiCD63-HRP.

The performance of the second approach involving the IMS with a specific biomarker (antiCDX-MPs, being CDX in this instance CD63 and CD24) followed by the optical readout using a general receptor (antiCD63-HRP antibody), is shown in Fig. S4.13, panel B. As previously discussed, this format requires the coexistence of two biomarkers in the same exosomes to be magneto-actuated and labelled. The optical responses were also fitted as above, obtained a LOD of 218 exosomes μL^{-1} (r^2 = 0.9950) when performing the IMS with the over expressed general receptor (antiCD63-MPs) and 2515 exosomes μL^{-1} (r^2 = 0.9915) when using antiCD24-MPs, as expected. The Table S4.1 shows a comparison of the magneto-ELISA with different platforms. The LOD achieved by magneto-ELISA of purified exosomes spiked in PBS was better than fluorescence (Zhao et al., 2016), electrochemical (Zhou et al., 2016), and SPR-based microfluidic (Sina et al., 2016) devices, and almost equivalent to other approaches, such as rolling cycle amplification (Huang et al., 2018) and microfluidic graphene oxide-based (Zhang et al., 2016) detection.

Magneto-actuated immunoassay in human serum

The exosomes were spiked on exosome-depleted human serum and submitted to IMS (with antiCDX-MPs), followed by direct labelling with antiCD63-HRP. In this instance, the IMS was directly performed in the undiluted human serum, thus evaluating the effect of free CDX receptors (or even other proteins) present in the sample matrix. The results are shown in Fig. S4.14 and discussed in Supp. Data. To summarize, and as expected, free

receptors were found in the serum which can interfere in the assay and which should be carefully evaluated. For instance, when using antiCD63-HRP for the direct labelling, the IMS cannot be performed with neither antiCD63 nor antiCD9-MPs, due to the high background of the human serum. Moreover, a severe decrease in the signal was observed in human serum for antiCDX-MPs (being CDX: CD24, CD44 and CD340), indicating a competition (and even blocking) of the binding site of the MPs attributed to free CD24, CD44 and CD340 (or even other protein) presents in human serum, which prevent the binding of the exosomes and the further labelling with antiCD63-HRP. However, a better performance was obtained by IMS with antiCD81-MPs, showing almost the same signal for the exosomes spiked in PBS buffer solution and exosome-depleted human serum, and a negligible background value.

The performance of the magneto-actuated immunoassay was further studied by calibration plots of exosomes (ranged from 3.9 x 10^4 to 2 x 10^7 exosomes μL^{-1}) derived from SKBr3 cell line and spiked on exosome-depleted human serum. Accordingly to the results obtained from the matrix effect study, and in order to avoid the interferences from free receptors in the serum, the IMS was performed on antiCD81-MPs, followed by the indirect labelling with the specific biomarkers, including CD24 and CD340 and the direct labelling with the general biomarker antiCD63-HRP. The results are shown in Fig. S4.15 and discussed in detail in Supp. Data. LODs in the order of 10^5 exosomes μL^{-1} were obtained for the exosomes detected in human serum, without any further pre-treatment (such as ultracentrifugation) (Table S4.1). The magneto-ELISA showed improved LODs than conventional ELISA, lateral flow colorimetric assay, electrochemical and microfluidic μNMR device. It is important to highlight that in some of the methods summarized in Table S4.1, the exosomes were previously separated from the matrix by ultracentrifugation. In other instances, the interferences of free receptors were not carefully evaluated.

Magneto-actuated immunoassay for the detection of serum-derived from breast cancer patients

Besides the direct detection of exosomes in undiluted human serum, the utility of this approach was also demonstrated for the detection of purified exosomes from healthy donors and breast cancer patients. It is important to highlight that the NTA counting as well as the protein content of exosomes in breast cancer individuals (n = 10) showed a 1.7-fold increase compared to healthy population (n = 10) (Fig. S4.16, Supp. Data). Accordingly, and in order to compare the expression of the receptors on exosomes from the two populations, the magneto-actuated immunoassay was performed with the same amount (0.235 μg) of exosome protein content per assay, for healthy donors and breast

cancer patients (n = 10 each). Fig. 4.5, shows comparatively the results for healthy donors and cancer patients using direct and indirect magneto-actuated immunoassay. The magneto-actuated immunoassay was able to statistically (paired-sample Student's t-test, $p < 0.05$) classified of healthy donors and breast cancer patients. Fig. 4.5, panel A, the assay was performed by IMS with antiCD81-MPs, followed by the indirect labelling with mouse antiCDX (CD24, CD44, CD326 and CD340 specific cancer-related biomarkers) and antimouse-HRP. The background signal (negative controls without exosomes) is also shown. Breast cancer patients remarkably overexpressed CD24, CD44, CD326 and CD340 biomarkers in CD81-positive exosomes (used for the IMS) compared to healthy donors ($p < 0.05$). This is in accordance with the highly expressed epithelial biomarkers CD326 and CD340 in breast cancer (Levva et al., 2017; Soysal et al., 2013). Moreover, and as expected, the exosomes-derived from healthy donors also contain at low expression level cancer-related biomarkers in CD81-positive exosomes, if compared with the negative control ($p < 0.05$). For instance, CD24 expression is involved in the regulation of cell binding capacity, proliferation, maturation in B-lymphocytes cells, but it is increased in cancer exosomes from different carcinomas (Tamkovich et al., 2018). This indirect format using antiCD81-MPs (antiCD81 from rabbit) allows flexibility in the detection of exosomes by different antibodies against cell-related biomarkers as CD24, CD44, CD326, and CD340. Moreover, this approach can prevent damage in the affinity of certain antibodies while being attached to the MPs, as was the case for CD326 antibody.

Fig. 4.5, panel B shows the results performed by IMS using antiCDX-MPs (CD24 and CD340 specific cancer-related exosomes biomarkers), followed by the direct labelling with the general antiCD63-HRP exosome biomarker. As above, the background signal performed without exosomes is also shown. Again, and by using a paired-sample Student's t-test, $p < 0.05$, healthy donors and breast cancer individuals were accordingly classified. The fact of using an overexpressed receptor for labelling (as is the case of CD63) provides a higher sensitivity, confirming the results also shown in Fig. 4.4, panel C. Nevertheless, although this approach is less time consuming, so performance is reduced in an incubation and their respective washing, it seems that works specially well for CD24 but not for CD340 that is similar to the data obtained by indirect detection. These results are in agreement with previous studies on cancer-related exosomes biomarkers in cancer and healthy donors (Grasso et al., 2015; Levva et al., 2017; Soysal et al., 2013; Tamkovich et al., 2018).

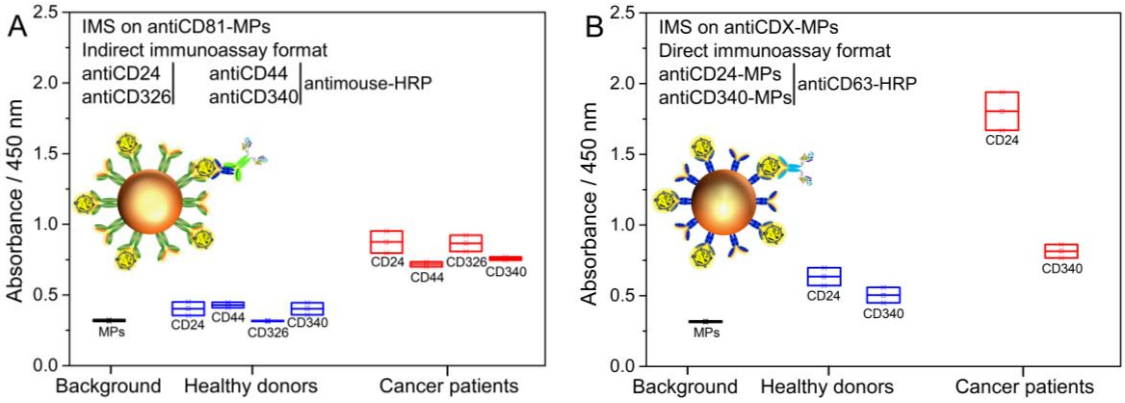

Fig. 4.5. Magneto-actuated immunoassay for detection of the purified exosomes derived from two population of polled samples of healthy donors (n = 10) and breast cancer (n = 10) patients. A) IMS of the exosomes on antiCD81-MPs, followed by indirect labelling with mouse antiCD24, antiCD44, antiCD326 and antiCD340, and antimouse-HRP. (B) IMS of the exosomes on antiCD24-MPs and antiCD340-MPs, followed by direct labelling with antiCD63-HRP antibody. In all cases, the concentration of MPs was fixed in 1×10^6 MPs, 0.50 μg mL^{-1} of primary antibody, 0.08 ng mL^{-1} of antimouse-HRP and 1.24 μg mL^{-1} of antiCD63-HRP antibody. In all cases, the number of exosomes containing 0.235 μg protein per assay was used. The error bars show the standard deviation for n = 3.

4.5. Conclusions

Breast cancer tumours are the most common malignancy in women. Although treatments have increased their survival, it is still considered a major cause of morbidity and mortality. Treatment efficacy is highly related to the early diagnose. The study of novel biomarkers including exosomes are currently under intense investigation. Among the different techniques for the detection and characterization of exosomes, only few cheaper alternatives to the nanoparticle tracking analysis and flow cytometer are available. The suitability of the magneto-actuated immunoassay reported here is based on the low limit detection achieved, 218 exosomes μL^{-1} in PBS and 10^5 exosomes μL^{-1} directly in human serum compared to conventional ELISA (10^6 exosomes μL^{-1}) (López-Cobo et al., 2018). The integration of magnetic particles provides improved analytical features regarding the sensitivity due to the preconcentration by magnetic actuation. Different format for the magnetic actuation were studied, including the direct covalent immobilization of exosomes on MPs (in which only one biomarker can be evaluated by further labelling) and the IMS followed by direct and indirect labelling, requiring in this instance the coexistence of two biomarkers in the same exosomes. Among the different formats studied in this work, the IMS using specific antibodies for capturing the exosomes, followed by the direct labelling based on CD63 showed higher sensitivity. On the other hand, the magneto-actuated immunoassay based on IMS on antiCD81-MPs is not affected by the presence of free biomarkers presents in serum and can be used for the quantification of exosomes based on the labelling with cancer biomarkers in serum, such as CD24 and CD340 with a LOD of 10^5 exosomes μL^{-1}. Besides the direct detection of exosomes in undiluted human serum, the utility of this approach was also demonstrated for the detection of purified exosomes

from healthy donors and breast cancer patients, being able to clearly differentiate healthy donors and breast cancer patients based on specific epithelial biomarkers.

Despite other reporter methods, the magneto-actuated immunoassay can solve the urgent need for improving exosomes detection method. The high-throughput and sensitive magneto-actuated immunoassay reported here represent a good alternative to the costly standard flow cytometry for the simultaneous and multiplex detection of several receptors in decentralized small-care centres by using common microplate reader operated by filters. This study is a prove of principle that to detect exosomes derived from different cellular sources, the test performed needs to include several detection biomarkers and therefore the magneto-ELISA is very suitable as allows the inclusion in the same test of a high number of samples as well as different biomarker analysis as it
is based in the same methodology. Since ELISA is currently the technique most widely used in clinical laboratories for the detection of cancer-related biomarkers by commercial immunoassay kits, personnel training or special equipment are not required, such as flow cytometers that are not available due to laboratory requirements, maintenance and cost of the assay. Moreover, this approach can be also used in low resource settings for exosome screening biomarkers, as well as for analysis of specific cancer-related exosomes in clinical applications.

4.6. Supplementary Data

4.6.1. Chemicals and biochemicals

Magnetic particles (Dynabeads® M450 Tosylactivated, nº 14013, 4,5 μm diameter) were purchased from Thermo Fisher. The mouse monoclonal antibodies (antiCDX) were purchased from i) Abcam: CD24 (Ref. ab76514); CD54 (Ref. ab2213); CD326 (Ref. ab7504); CD340 (Ref. ab30); ii) Thermo Fisher: CD9 (Ref. 10626D); CD63 (Ref. 10628D); CD81 (Ref. 10630D), and iii) eBioscience: CD44 (Ref. BMS113). The antiCD81 polyclonal antibody (produced in rabbit (antiCD81) (Ref. HPA007234) was provided by Sigma-Aldrich. For the indirect labeling in immunoassays, a rabbit anti-mouse IgG H&L (HRP) (antimouse-HRP) (Ref. ab6728) was used while a goat anti-mouse IgG H&L (Cy5®) (antimouse-Cy5) (Ref. ab97037) for flow cytometry, in both secondary antibodies were provided by Abcam. For direct labeling, the mouse monoclonal CD63 antibody (HRP) (antiCD63-HRP) (Ref. NBP2-42225H-100) was obtained from BioNova.

Pierce™ TMB Substrate Kit (Ref. 34021) and Pierce™ BCA Protein Assay Kit (Ref. 23227) were purchased from Thermo Fisher. The 10 mmol L^{-1} phosphate-buffered saline (PBS) buffer solution (pH 7.5) and boric acid buffer solution (pH 8.5) were prepared

with ultrapure water and all other reagents were in analytical reagent grade (supplied from Sigma Aldrich).

Ultrapure water (Millipore® System, resistivity 18.2 MΩ cm) was used throughout the experiments.

4.6.2. Cell culture

Breast cancer cell lines were the following: MCF7 (ATCC® HTB-22™), MDA-MB-231 (ATCC® CRM-HTB-26™) and SKBr3 (ATCC® HTB-30™). Expansion of cell population was carried out from 1,000,000 cell in T-175 flask containing 32 mL of Dulbecco's Modified Eagle Medium (DMEM) (Ref. 31966047, Thermo Fisher), supplemented with 10% exosome-depleted fetal bovine serum (FBS) (Ref. 12007C, Sigma-Aldrich), 100 U mL^{-1} penicillin-streptomycin (Ref. 15140122, Thermo Fisher). The temperature was maintained at 37 °C in humidified, concentrated CO_2 (5%) atmosphere. Once cells reached approximately 95% confluence on T-175 flask, the culture medium was removed and immediately centrifuged (300 *g* for 10 minutes, 2,000 *g* for 10 minutes and 10,000 *g* for 30 minutes), and stored at -80 ºC until to exosome isolation.

4.6.3. Exosome isolation and purification

The supernatant from MCF7, MDA-MB-231 and SKBr3 breast cancer cell lines or from human serum were subjected to differential centrifugation as follow: 300 *g* for 10 minutes (removal of residual cells), 2,000 *g* for 10 minutes and 10,000 *g* for 30 minutes (removal of cellular debris). Then, a Beckman Coulter Optima™ L-80XP Ultracentrifuge at 100,000 *g* for 60 minutes with a 70Ti rotor to pellet exosomes. After that, the supernatant was carefully removed, and crude exosome-containing pellets were resuspended in 1 mL of 10 mmol L^{-1} phosphate-buffered saline (PBS) solution and pooled. A second round of same ultracentrifugation setting was carried out, and the resulting exosome pellet resuspended in 500 µL (per 100 mL of supernatant) of 10 mmol L^{-1} PBS (0.22 µm filtrated and sterile) and storage at -80 °C. All centrifugation steps performed at a temperature of 4 °C.

4.6.4. Exosome protein quantification

The exosomal protein content was determined by using Pierce™ BCA Protein Assay Kit (Ref. 23227, Thermo Fisher), following the manufacture protocol. Prior to protein quantification, all exosomes resuspended in PBS were lysed by adding an equal volume of RIPA buffer (Sigma Aldrich) and cOmplete™, Mini, EDTA-free Protease Inhibitor CocktailTM (Roche), followed by incubation at RT for 5 min and sonicated for 15 seconds.

4.6.5. Human serum isolation

The human serum samples were separated from the blood cells using a sterile empty tube without any anticoagulant, leave the tube in a standing position for about 20-30 minutes for blood to be clotted. After that, centrifugation at 1,500 *g* (20 ºC) for 10 minutes was carried out for removal of residual cells and cellular debris. Following, the human serum (supernatant on top) was carefully removed, freeze at -80 ºC to preserve for further assays.

4.6.6. Exosome-depleted human serum

The whole human serum from healthy patients were subjected to differential centrifugation as follow: 300 *g* for 10 minutes (removal of residual cells), 2,000 *g* for 10 minutes and 10,000 *g* for 30 minutes (removal of cellular debris). Then, a Beckman Coulter Optima^{TM} L-80XP Ultracentrifuge at 100,000 *g* for 60 minutes with a 70Ti rotor to pellet exosomes. After that, the supernatant was carefully removed, and storage at - 80 °C. This exosome-depleted human serum was used in further immunoassay. All centrifugation steps performed at a temperature of 4 °C.

4.6.7. Immobilization of exosomes and antibodies on magnetic particles

Dynabeads® M450 tosylactivated superparamagnetic particles (MPs, 4.5 µm in diameter) has a core of iron oxide salt encapsulated by a polystyrene polymer, which has a polyurethane external layer with the p-toluenesulfonate group (Xu et al., 2012). It is a good leaving group, which allows an S_N2 reaction to occur in the presence of a nucleophile (Cahiez et al., 2012; Hoogenboom et al., 2010). A nucleophilic reaction by an antibody, protein, peptide, or glycoprotein removes and replaces the sulfonyl ester groups from the polyurethane layer.

Two different approaches were used, as depicted in Fig. S4.1. The first one involves the direct covalent immobilization of exosomes on magnetic particles (Fig. S4.1, panel A). The second approach is based on the covalent immobilization of the antibodies for a further immunomagnetic separation (IMS) of exosomes (Fig. S4.1, panel B).

Immobilization of exosomes on magnetic particles

The immobilization of exosomes on Dynabeads® M450 tosylactivated superparamagnetic particles (MPs) were performed as follows: 3.5 x 10^{10} exosomes were added to 40 µL (1.6 x 10^7 MPs) Dynabeads® M450 tosylactivated. The reaction kinetics are increased by adding 0.1 mol L^{-1} borate buffer pH 8.5, in order to ensure the

nucleophilic reaction by the amine group. The incubation step was performed overnight with gentle shaking at 4 ºC. After that, 0.5 mol L^{-1} glycine solution was added to ensure the blocking of the any remaining tosylactivated groups, by an incubation for 2 h at 25 ºC. After that, the exosomes-modified magnetic particles (exosomes-MP) were resuspended in 160 µL of 10 mmol L^{-1} phosphate-buffered saline (PBS) in order to achieve 1 x 10^6 MPs per 10 µL. The calibration plots were performed by using 1 x 10^6 MPs per well plate and the amount of exosomes ranging from 3.9 x 10^4 to 2 x 10^7 exosomes μL^{-1}.

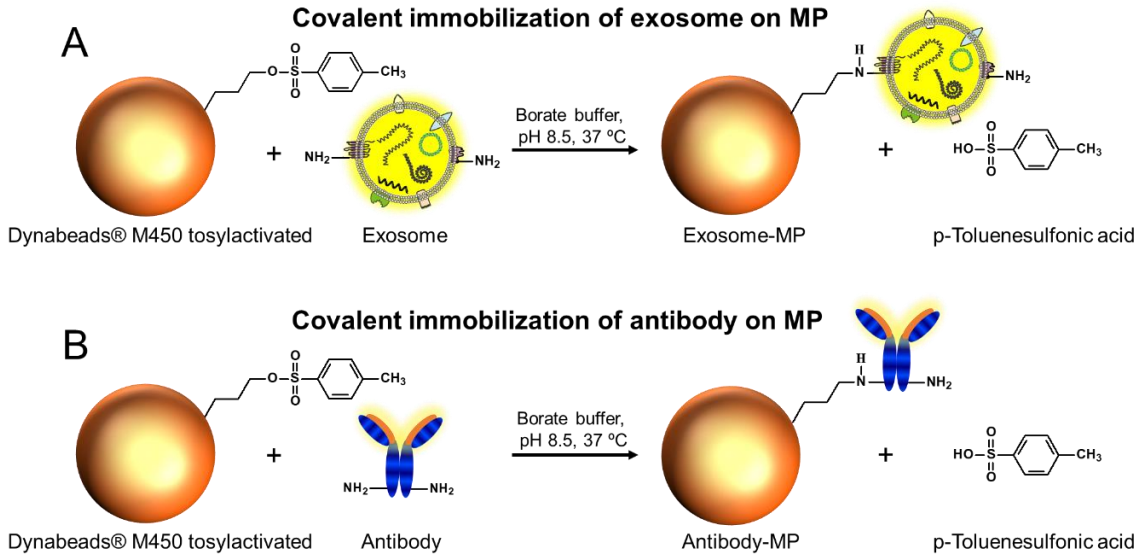

Fig. S4.1. Immobilization approaches of exosomes on Dynabeads® M450 tosylactivated (MPs). (A) Covalent immobilization on MPs, or (B) IMS on antibody-modified MPs.

Immobilization of antibodies on magnetic particles

The different specific antibody (15 µg mL^{-1}) (antiCD9, antiCD24, antiCD44, antiCD54, antiCD63, antiCD81, antiCD326 or antiCD340) was added to 55 µL (2.2 x 10^7 MPs) Dynabeads® M450 tosylactivated. The reaction kinetics are increased by adding 0.1 mol L^{-1} borate buffer pH 8.5. The incubation step was performed overnight with gentle shaking at 37 ºC. After that, a blocking step with 0.5 mol L^{-1} glycine solution was performed for 2 h to ensure the blocking of the any remaining tosylactivated groups. After that, the antibody-modified magnetic particles (herein, antiCDX-MP), where antiCDX = antiCD9, antiCD24, antiCD44, antiCD54, antiCD63, antiCD81, antiCD326 or antiCD340) were resuspended in 220 µL (10 µL per well to give 1 x 10^6 particles per well) 10 mmol L^{-1} phosphate-buffered saline (PBS). It was not possible to immobilize CD326 satisfactorily on magnetic particles (MP).

In order to quantify the amount of antibody immobilized on MPs, the supernatant

containing the remaining non-immobilized antibody, after the immobilization step, was separated and quantified. The immobilized antibody was thus calculated as a difference of the initial (C_i) and the final (C_f) concentration of antibody after immobilization (Eq. 1).

$$\text{Capture}_{(\%)} = \frac{C_i - C_f}{C_i} x100 \qquad \text{(Eq. 1)}$$

To achieve that, a calibration plot ranging from 0.0 to 1.0 μg mL^{-1} of antiCD9 antibody (as model) diluted in 10 mmol L^{-1} PBS was performed by a conventional immunoassay. Then, 50 μL of each antibody was added per well of the Maxisorp 96- Well plate (Ref. 442404, Thermo Fisher) for overnight immobilization at 4 °C. After that, three washing steps were performed with PBS containing 2% bovine serum albumin (BSA). Then, 100 μL of PBS containing 2% BSA as blocking solution was added to the plate for 30 min incubation at 25 ºC. A rabbit polyclonal secondary antibody to mouse IgG with horseradish peroxidase (HRP) conjugate (herein, antimouse-HRP) (100 μL, 0.08 ng mL^{-1}) was added to each well and incubated for 30 min at 25 ºC. Again, three washing steps were performed with PBS containing 2% BSA. Then, 100 μL of substrate solution (0.004% v/v H_2O_2 and 0.01% w/v TMB in citrate buffer) was incubated under dark conditions for 30 min at 25 ºC. The enzymatic reaction was stopped by adding 100 μL of H_2SO_4 (2.0 mol L^{-1}). Finally, the supernatant was transferred and measured in another micro plate reader at 450 nm. In the Fig. S4.2, panel A shows the optical responses which were fitted using a linear regression (Eq. 2), giving a coefficient of determination of r^2 = 0.9976, which demonstrates a good linearity of the calibration plot.

$$\text{Absorbance}_{(450\ nm)} = 0.2604 + 0.2307[\text{Antibody}_{(\mu g\ mL^{-1})}] \qquad \text{(Eq. 2)}$$

The antibody calibration plot was then used to know the amount of antibody to be used to fully cover 2.2 x 10^7 of MPs. Then, different concentration of antiCD9 antibody was subject to incubation with 2.2 x 10^7 MPs, as previously described. The incubation step was described in the previous paragraphs. After that, the supernatant was separated and the conventional Enzyme-Linked Immunosorbent Assay (ELISA) was used to quantify the concentration of antiCD9 antibody remaining on the supernatant. The optical responses of the supernatants were thus interpolated in the equation 2 (Fig. S4.2, panel B). It can be observed that at concentration of 12 μg mL^{-1} of the antiCD9 antibody used for immobilization, the antibody is fully immobilized on the MPs, and no remaining antibody can be detected in the supernatant. Accordingly, the optical signal is similar to the background. By using the equation 1, it is mean that 12 μg mL^{-1} of the antiCD9 antibody

is completely (~99.99%) immobilized on 2.2 x 10^7 of magnetic particles. At a concentration of 15 μg mL^{-1} the optical signal increased, thus suggesting an excess of antibody and ensuring the full coverage of the magnetic particles. Accordingly, 15 μg mL^{-1} as a concentration of antiCD9 antibody was used to ensure the complete covering 2.2 x 10^7 of magnetic particles. These results were considered for all other primary antibodies used in this work (antiCD24, antiCD44, antiCD54, antiCD63, antiCD81, antiCD326 and antiCD340).

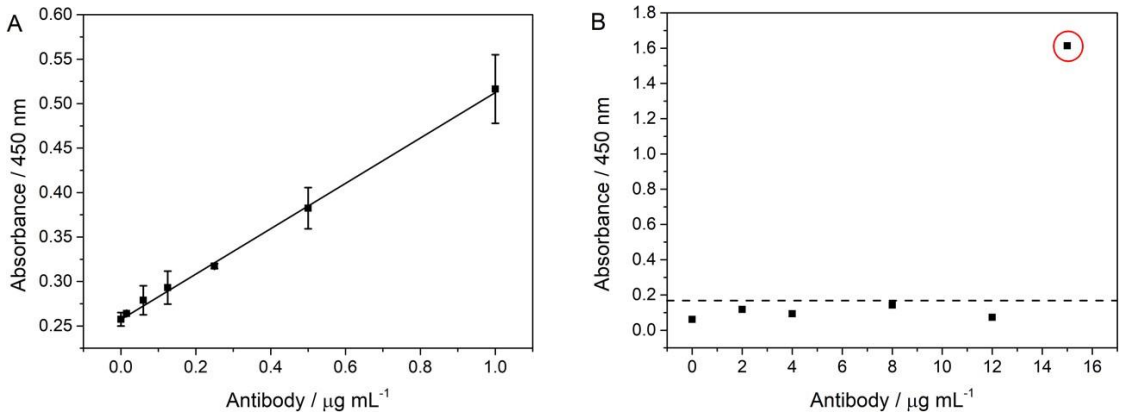

Fig. S4.2. (A) Calibration plot for antiCD9 antibody diluted in 10 mmol L^{-1} PBS, pH 7.5. (B) Optimization of the amount of antiCD9 antibody immobilized on 2.2 x 10^7 magnetic particles. The error bars show the standard deviation for n = 3.

4.6.8. Magneto-actuated immunoassay for the detection of exosomes covalently immobilized on magnetic particles

Direct format. The magneto-actuated immunoassay (Fig. S4.3, panel A) was performed in 96-well microtiter plates (Ref. 3364, Sigma-Aldrich) and involved the following steps: (i) Direct labeling. The exosomes-MPs (containing 1 x 10^6 MPs per well, with an amount of exosomes covalently immobilized from 0 to up to 2 x 10^9 exosomes per well) and a mouse monoclonal antibody to CD63 with horseradish peroxidase (HRP) (herein, antiCD63-HRP) (100 μL, 1.24 μg mL^{-1}), were simultaneously incubated for 30 min with shaking at 25 °C, followed by three washing steps with PBS containing 0.5% BSA. (ii) Optical readout.

Optical readout. Added 100 μL of substrate solution (0.004% v/v H_2O_2 and 0.01% w/v TMB in citrate buffer) for 30 min incubated under dark conditions. The enzymatic reaction was stopped by adding 100 μL of H_2SO_4 (2.0 mol L^{-1}). Then, exosomes-MPs were separated by using a magnet plate separator (see Video S2, Supp. Data), a exosomes-MPs pellet on the bottom tube is formed, followed by supernatant separation. The absorbance measurement of the supernatants was thus performed with the microplate reader at 450 nm. After each incubation or washing step, a 96-well magnet plate separator

was positioned under the microtiter plate until pellet formation on the bottom corner, followed by supernatant separation.

Indirect format. The magneto-actuated immunoassay (Fig. S4.3, panel A) was performed in 96-well microtiter plates and involved the following steps: (i) incubation of the exosomes-MPs with the antiCDX mouse monoclonal antibodies. The exosomes-MPs (containing 1 x 10^6 MPs per well, with an amount of exosomes covalently immobilized from 0 to up to 2 x 10^9 exosomes per well) and the antiCDX antibody (100 µL, 0.50 µg mL^{-1}) (being CDX any of CD9, CD24, CD44, CD54, CD63, CD81, CD326 or CD340 biomarkers), were simultaneously incubated for 30 min with shaking at 25 °C, followed by three washing steps with PBS containing 0.5% BSA. (ii) Indirect labeling. The exosomes-MPs were incubated with antimouse-HRP antibody (100 µL, 0.08 ng mL^{-1}) for 30 min with shaking at 25 °C, followed by three washing steps with PBS containing 0.5% BSA. (iii) Optical readout, as described above.

4.6.9. Immunomagnetic separation of exosomes and magneto-actuated immunoassay

Direct format. The magneto-actuated immunoassay (Fig. S4.3, panel B) was performed in 96-well microtiter plates and involved the following steps: i) IMS of the exosomes with antiCDX-MPs. The antiCDX-MPs (being CDX any of CD9, CD24, CD44, CD54, CD63, CD81, CD326 or CD340 biomarkers) (containing 1 × 10^6 antiCDX MPs per well) and the exosomes (100 µL, ranging from 0 to 2 x 10^9 exosomes per well), were simultaneously incubated for 30 min with shaking at 25 °C, followed by three washing steps with PBS containing 0.5% BSA. ii) Direct labeling. The exosomes-coated MPs were incubated with the antiCD63-HRP antibody (100 µL, 1.24 µg mL^{-1}) for 30 min with shaking at 25 °C, followed by three washing steps with PBS containing 0.5% BSA. (iii) Optical readout, as described above.

Indirect format. The magneto-actuated immunoassay (Fig. S4.3, panel B) was performed in 96-well microtiter plates and involved the following steps: i) IMS of the exosomes with antiCD81-MPs (rabbit) (containing 1 × 10^6 antiCD81-MPs per well) and the exosomes (100 µL, ranging from 0 to 2 x 10^9 exosomes per well), were simultaneously incubated for 30 min with shaking at 25 °C, followed by three washing steps with PBS containing 0.5% BSA. (ii) incubation with the antiCDX mouse monoclonal antibodies (100 µL, 0.50 µg mL^{-1}) (being CDX any of CD9, CD24, CD44, CD54, CD63, CD81, CD326 or CD340 biomarkers), were simultaneously incubated for 30 min with shaking at 25 °C, followed by three washing steps with PBS containing 0.5% BSA. (iii)

Indirect labeling. The exosomes-coated MPs were incubated with antimouse-HRP antibody (100 µL, 0.08 ng mL^{-1}) for 30 min with shaking at 25 °C, followed by three washing steps with PBS containing 0.5% BSA. (iv) Optical readout, as described above.

4.6.10. Optimization of primary and secondary antibodies on magnetic particles

Optimization of primary antibody. The magneto-actuated immunoassay (Fig. S4.4, panel A) was performed in 96-well microtiter plates and involved the following steps: (i) incubation of the blocked-MPs with the antiCD63 mouse monoclonal antibody. The blocked-MPs (containing 1 x 10^6 MPs per well) and the antiCD63 antibody (100 µL, ranging from 0.25 to 5.00 µg mL^{-1}) were simultaneously incubated for 30 min with shaking at 25 °C, followed by three washing steps with PBS containing 0.5% BSA. (ii) Indirect labeling. The blocked-MPs were incubated with antimouse-HRP antibody (100 µL, 0.08 ng mL^{-1}) for 30 min with shaking at 25 °C, followed by three washing steps with PBS containing 0.5% BSA. (iii) Optical readout, with 100 µL of substrate solution (0.004% v/v H_2O_2 and 0.01% w/v TMB in citrate buffer) for 30 min incubated under dark conditions.

The enzymatic reaction was stopped by adding 100 µL of H_2SO_4 (2.0 mol L^{-1}). The absorbance measurement of the supernatants was thus performed with the microplate reader at 450 nm. After each incubation or washing step, a 96-well magnet plate separator was positioned under the microtiter plate until pellet formation on the bottom corner, followed by supernatant separation.

Fig. S4.4, panel A, shows that by increasing the concentration of the primary antibody increases the signal background intensity. In indirect ELISA format, an absorbance signal near 0.50 was choice as optimum. Hence, a concentration of 0.50 µg mL^{-1} antiCD63 was selected as the most appropriate concentration and was used for all subsequent experiments. These results were considered for all other primary antibodies used in this work (antiCD9, antiCD24, antiCD44, antiCD54, antiCD81, antiCD326 and antiCD340).

Optimization of secondary antibody. The magneto-actuated immunoassay (Fig. S4.4, panel B) was performed in 96-well microtiter plates and involved the following steps: (i) incubation of the blocked-MPs with the antiCD63 mouse monoclonal antibody. The blocked-MPs (containing 1 x 10^6 MPs per well) and the antiCD63 antibody (100 µL, 0.50 µg mL^{-1}) were simultaneously incubated for 30 min with shaking at 25 °C, followed by three washing steps with PBS containing 0.5% BSA. (ii) Indirect labeling. The blocked-MPs were incubated with antimouse-HRP antibody (100 µL, ranging from 0.01 to 4.00 ng mL^{-1}) for 30 min with shaking at 25 °C, followed by three washing steps with PBS

containing 0.5% BSA. (iii) Optical readout, with 100 µL of substrate solution (0.004% v/v H_2O_2 and 0.01% w/v TMB in citrate buffer) for 30 min incubated under dark conditions. The enzymatic reaction was stopped by adding 100 µL of H_2SO_4 (2.0 mol L^{-1}). The absorbance measurement of the supernatants was thus performed with the microplate reader at 450 nm. After each incubation or washing step, a 96-well magnet plate separator was positioned under the microtiter plate until pellet formation on the bottom corner, followed by supernatant separation.

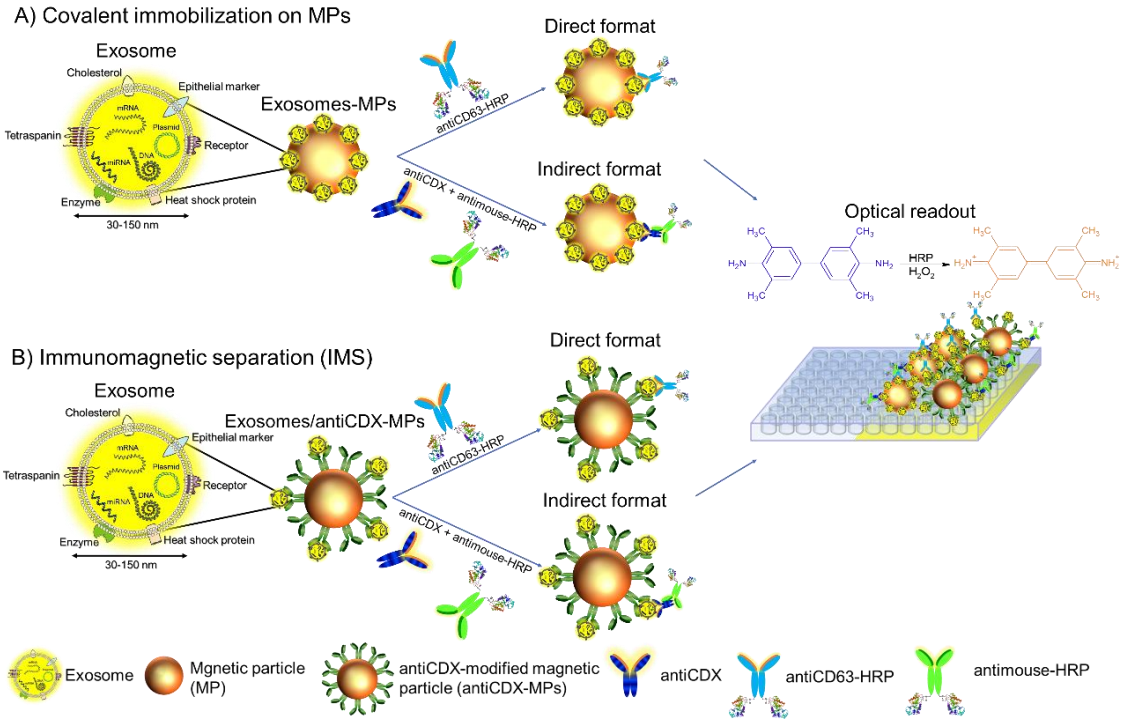

Fig. S4.3. Strategies for the detection of exosomes by magneto-actuated immunoassays in different formats. (A) Magneto-actuated immunoassays for the detection of exosomes covalently immobilized on magnetic particles (exosomes-MPs), performed by i) direct labeling (with antiCD63-HRP, 1.24 µg mL^{-1}) or, instead, ii) indirect labeling (with antiCDX antibody, 0.50 µg mL^{-1}) following by incubation with antimouse-HRP antibody (0.08 ng mL^{-1}) (B) IMS of exosomes and magneto-actuated immunoassay in direct and indirect format. For the i) direct format, the IMS is performed with antiCDX-MPs, followed bythe direct labeling with antiCD63-HRP (1.24 µg mL^{-1}); for the ii) indirect format, the IMS is performed with antiCD81-MPs, followed by the indirect labeling with antiCDX (mouse) antibody and an antimouse-HRP antibody. In all cases, antiCDX was an antibody towards CD9, CD24, CD44, CD54, CD63, CD81 or CD340 biomarkers. The concentration was fixed in 1 × 10^6 for the MPs.

Fig. S4.4, panel B, shows that the signal background intensity produced by 0.08 ng mL^{-1} is suitable (absorbance signal near 0.50) and was used for all subsequent experiments.

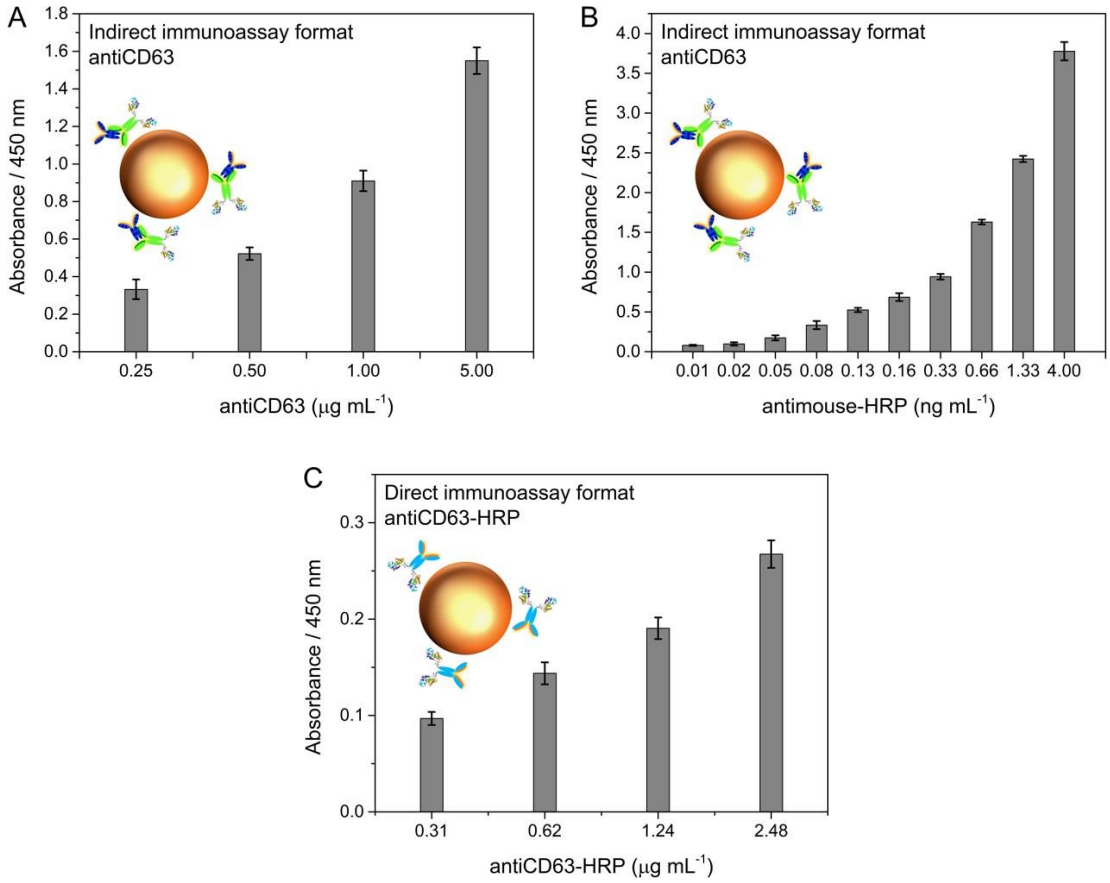

Fig. S4.4. Optimization of the (A) antiCD63 primary antibody, (B) antimouse-HRP and (C) antiCD63-HRP secondary antibodies on the signal on magnetic particles blocked (blocked-MPs). In all case, 1 × 10^6 blocked-MPs per assay was used. The error bars show the standard deviation for n = 3.

Optimization of antiCD63-HRP antibody. The magneto-actuated immunoassay (Fig. S4.4, panel B) was performed in 96-well microtiter plates and involved the following steps: (i) incubation of the blocked-MPs with the antiCD63-HRP antibody. The blocked-MPs (containing 1 x 10^6 MPs per well) and the antiCD63-HRP antibody (100 µL, ranging from 0.31 to 2.48 µg mL^{-1}) were simultaneously incubated for 30 min with shaking at 25 °C, followed by three washing steps with PBS containing 0.5% BSA. (ii) Optical readout, with 100 µL of substrate solution (0.004% v/v H_2O_2 and 0.01% w/v TMB in citrate buffer) for 30 min incubated under dark conditions. The enzymatic reaction was stopped by adding 100 µL of H_2SO_4 (2.0 mol L^{-1}). The absorbance measurement of the supernatants was thus performed with the microplate reader at 450 nm. After each incubation or washing step, a 96-well magnet plate separator was positioned under the microtiter plate until pellet formation on the bottom corner, followed by supernatant separation.

Fig. S4.4, panel C, shows the optimization for the antiCD63-HRP. In direct ELISA format, an absorbance signal near 0.20 was choice as optimum. Therefore, a concentration of 1.24 µg mL^{-1} was chosen and used for all subsequent experiments.

4.6.11. Optimization of incubation steps

For the time optimization of the magneto immunoassay, the direct and indirect ELISA format as well as order of the immunological steps were evaluated. The schematic procedure is detailed in Fig. S4.5. The magneto immunoassay was performed in 96-well microtiter plates, and all quantities of antibodies and magnetic particles per assay were previously optimized (Fig. S4.4 and Fig. S4.7). The quantity of exosomes and final reaction volume was maintained at 4 x 10^9 exosomes and 100 µL in all procedures. After each incubation or washing step, a 96-well magnet plate separator was positioned under the microtiter plate until pellet formation on the bottom corner, followed by supernatant separation, which is transferred and measured in a micro plate reader at 450 nm.

In direct ELISA format, two incubation steps were performed. The first step (Step 1) involved the IMS of 100 µL of exosomes (4 x 10^9 exosomes) with 1 × 10^6 antiCD81$_{Rabbit}$-MPs by incubation for 30 min with gentle shaking at 25 ºC. In the second step (Step 2), 1.24 µg mL^{-1} of antiCD63-HRP antibody was added and incubated for 30 min with gentle shaking at 25 ºC. After each incubation, three washing steps with PBS containing 0.5% BSA were performed. In this case, two-time steps are possible: the incubation of step 1 and step 2 together, or perform the incubation of step 1 and step 2 separately.

In indirect ELISA format, three incubation steps were performed. The first step (Step 1) involved the IMS of 100 µL of exosomes (4 x 10^9 exosomes) with 1 × 10^6 antiCD81$_{Rabbit}$-MPs by incubation for 30 min with gentle shaking at 25 ºC. In the second step (Step 2), 0.50 µg mL^{-1} of antiCD63 antibody was added and incubated for 30 min with gentle shaking at 25 ºC. The last incubation step (Step 3) involved the enzymatic labeling by adding 0.08 ng mL^{-1} of antimouse-HRP for 30 min with gentle shaking at 25 ºC. After each incubation, three washing steps with PBS containing 0.5% BSA were performed. In this case, three-time steps are possible: the incubation of step 1 and step 2 together or the three steps together, or perform the incubation of three steps separately.

In all cases, a 100 µL of substrate solution (0.004% v/v H_2O_2 and 0.01% w/v TMB in citrate buffer) was incubated under dark conditions. The enzymatic reaction was stopped by adding 100 µL of H_2SO_4 (2.0 mol L^{-1}). The exosomes-coated magnetic particles were separated by using a 96-well magnet plate separator, a pellet on the bottom corner is formed, followed by supernatant separation, which is transferred and measured in a micro plate reader at 450 nm.

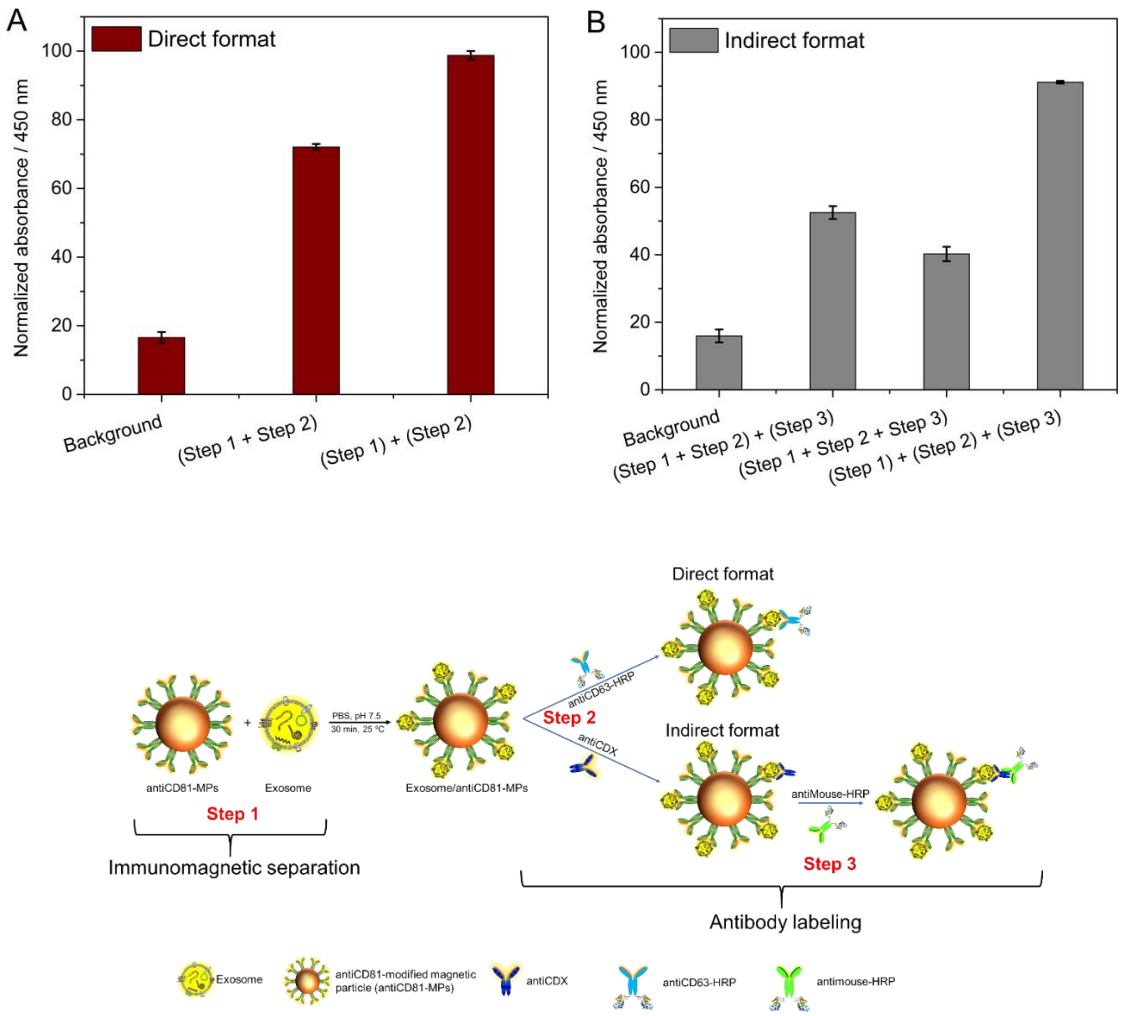

Fig. S4.5. Strategies comparison for the optimization of the incubation steps, performed with 4 x 10^9 exosomes. One step and step-by-step incubations, followed in all cases by the optical readout. The negative control (background) is also shown. In all cases, the concentration was fixed in 1 × 10^6 antiCD81$_{Rabbit}$-MPs per assay, 0.5 μg mL^{-1} antiCD63 antibody and 0.08 ng mL^{-1} antimouse-HRP or 1.24 μg mL^{-1} antiCD63-HRP. The error bars show the standard deviation for n = 3.

Although all the strategies are able to clearly detect exosomes, better results in terms of sensitivity were achieved when the immunocapture and labeling with the primary and secondary antibody were made in a separated step. It seems that the antimouse-HRP antibody difficult the union of the antiCD9 antibody with the membrane CD9 receptor. Another important factor is the steric hindrance produced by large size of the magnetic particles (4.5 μm in diameter) at the binding of the antimouse-HRP antibody. On the other hand, performing the IMS of the exosomes by antiCD63-MPs, following incubation with antiCD9 primary antibody and then with antimouse-HRP antibody, allows exosomes, as well as antibodies, to have the unique opportunity for binding to their receptors, decreasing the steric hindrance. Therefore, regardless of the ELISA format, for IMS of exosomes as well as the labeling steps with antibodies, were performed separately.

4.6.12. Optimization of the amount of magnetic particles per assay

The magneto-actuated ELISA was performed with different amount of magnetic particles per assay for evaluate the capture efficiency ratio of the exosomes by magnetic particles.

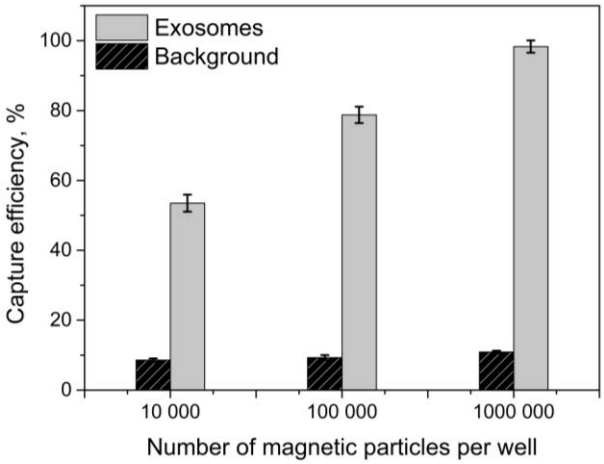

Fig. S4.6. Optimization of the amount of the magnetic particles per assay. In all cases, the amount the exosomes was fixed in 4 x 10^9 exosomes and 1.24 µg mL^{-1} antiCD63-HRP. The error bars show the standard deviation for n = 3.

Then, exosomes (4 x 10^9) were subjected to IMS by 1 *x* 10^4, 1 *x* 10^5 and 1 *x* 10^6 antiCD9-MPs per well. Following, the labeling was performed with 100 µL (1.24 µg mL^{-1}) of the antiCD63-HRP, as previously optimized (Fig. S4.4, panel C). After that, a 100 µL of substrate solution (0.004% v/v H_2O_2 and 0.01% w/v TMB in citrate buffer) incubated under dark conditions. The enzymatic reaction was stopped by adding 100 µL of H_2SO_4 (2.0 mol L^{-1}). The exosomes-coated magnetic particles were separated by using a 96-well magnet plate separator, a pellet on the bottom corner is formed, followed by supernatant separation, which is transferred and measured in a micro plate reader at 450 nm. The highest absorbance value obtained was used to normalize. These results were considered for all magnetic particles modified with other primary antibodies used in this work (antiCD24, antiCD44, antiCD54, antiCD63, antiCD81 and antiCD340).

Fig. S4.6 shows that at fixed exosomes amount (4 x 10^9 exosomes), the increasing the concentration of the magnetic particles per assay increases the signal intensity. Therefore, 1 x 10^6 magnetic particles per assaywas used in all further assays.

4.6.13. Magneto-actuated immunoassay in human serum

The matrix effect was firstly evaluated as schematically shown in Fig. S4.7. Purified exosomes from MCF7 breast cancer cell line were spiked on i) PBS and ii) exosome- depleted human serum.

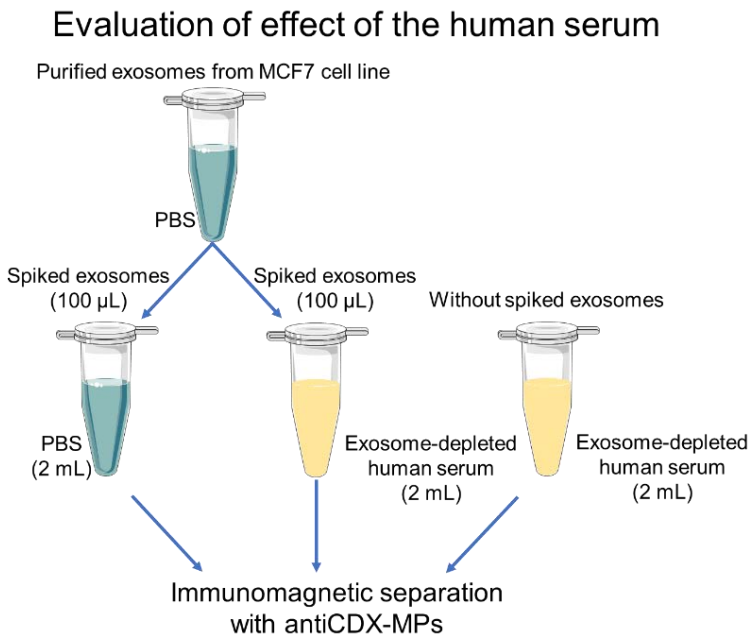

Fig. S4.7. Schematic procedure for the study of the human serum matrix in exosome- depleted human serum for exosomes derived from MCF7 cell line. IMS of exosomes spiked in PBS and exosome-depleted human serum. The IMS with 1 × 10^6 antiCDX-MPs (being CDX either CD9, CD24, CD44, CD54, CD63, CD81 and CD340), following by labelling with antiCD63-HRP (1.24 µg mL^{-1}).

Exosome-depleted human serum without spiking exosomes was used as control for exosome-depleted human serum spiked with exosomes. After that, a magneto-actuated immunoassay was performed (Fig. S4.3, panel B) in 96-well microtiter plates and involved the following steps: i) IMS of the exosomes with antiCD81-MPs (containing 1 × 10^6 antiCD81-MPs per well) and the exosomes (100 µL, 2 x 10^9 exosomes per well), were simultaneously incubated for 30 min with shaking at 25 °C, followed by three washing steps with PBS containing 0.5% BSA. ii) direct labeling. The exosomes-coated MPs were incubated with the antiCD63-HRP antibody (100 µL, 1.24 µg mL^{-1}) for 30 min with shaking at 25 °C, followed by three washing steps with PBS containing 0.5% BSA. (iii) optical readout.

4.6.14. Magneto-actuated immunoassay for the detection of serum-derived from breast cancer patients

Blood samples from healthy female donors ((n = 10, mean age 35/SD 5 years) and breast cancer female patients (n = 10, stage IV, mean age 50/SD 6 years) were obtained from the Hospital del Mar, Barcelona, Spain. The work was carried out in accordance with the principles of voluntariness and confidentiality. The preparation of the human serum from blood was detailed above. The samples n = 10 each were polled in two batches (healthy and breast cancer donors) by mixing 500 µL of each, and the exosomes were purified by ultracentrifugation, as previously described above.

The magneto-actuated immunoassay of circulating purified exosomes from healthy (n = 10, pooled) and breast cancer (n = 10, pooled) patients were examined. Serum-derived exosomes from healthy patients were used as controls. Two IMS approaches was performed: i) IMS with antiCD81-MPs in order to achieve a massive capture of the exosomes for further labeling with specific biomarkers (CD24, CD44, CD326 and CD340), ii) IMS with antiCDX-MPs (being CDX: CD24 and CD340) in order to achieve only cancer-related exosomes for further labeling with a high expressed general exosome biomarker (CD63). Optical readout, as described above. Both approaches may suggest molecular signatures for breast cancer diagnosis.

4.6.15. Nanoparticle tracking analysis

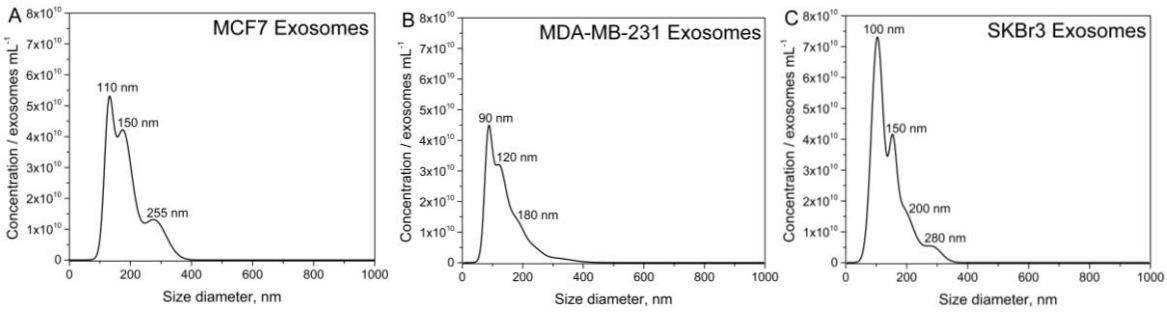

Fig. S4.8. Nanoparticle tracking analysis (NTA) on size distribution on purified exosomes- derived from (A) MCF7, (B) MDA-MB-231 and (C) SKBr3 breast cancer cell lines. The purified exosomes were diluted in sterile-filtered 10 mmol L^{-1} PBS buffer (pH 7.5). Nanosight NTA Software analyzed raw data videos by triplicate during 60 s with 50 frames per second and the temperature of the laser unit set at 24.8 ºC.

4.6.16. Characterization by cryogenic transmission electron microscopy

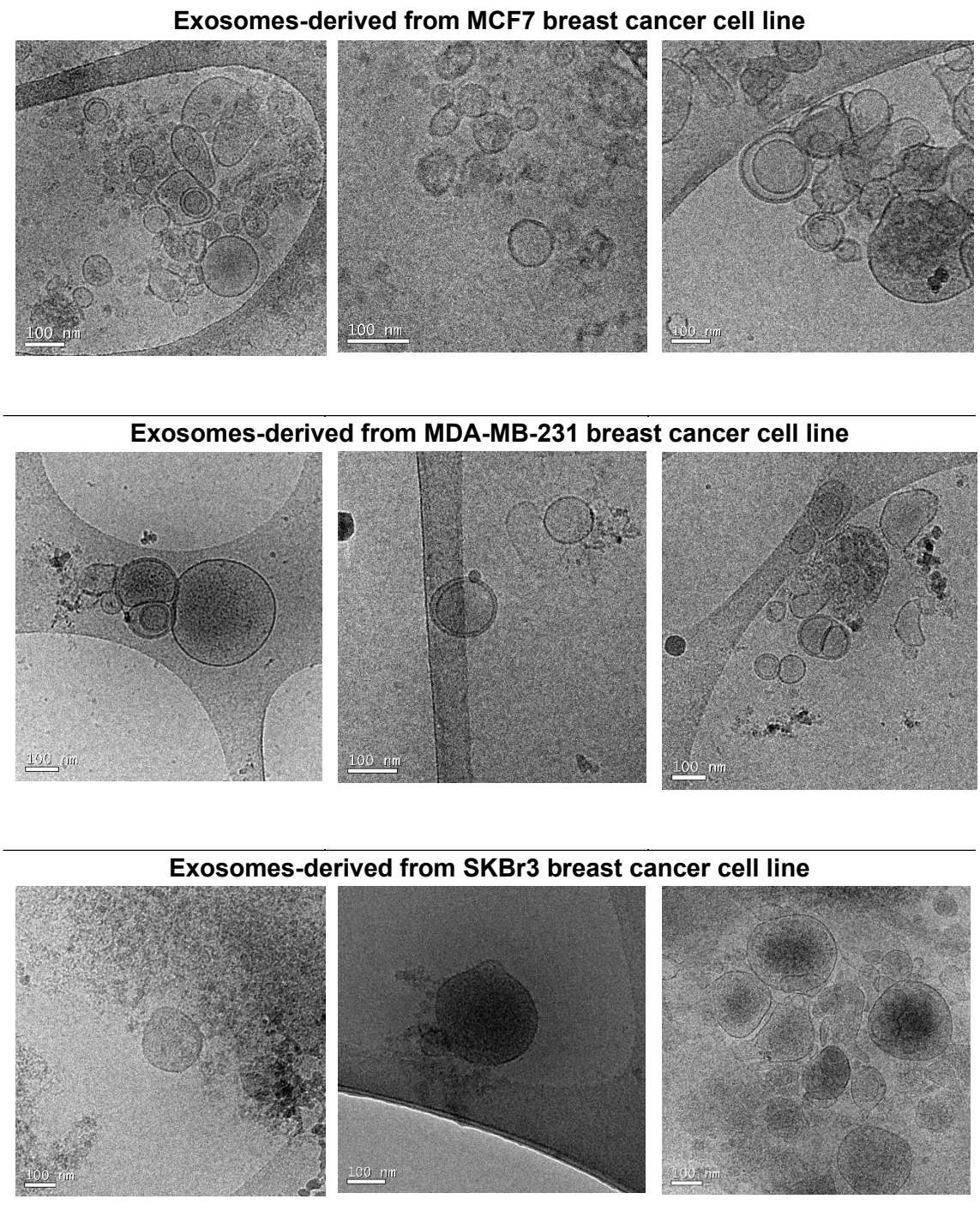

Fig. S4.9. Cryogenic Transmission Electron Microscopy (TEM). TEM images of exosomes derived from MCF7, MDA-MB-231 and SKBr3 breast cancer cell lines. Cup-shaped structures with 50-150 nm size were identified as being exosomes.

4.6.17. Flow cytometry analysis of breast cancer cell lines

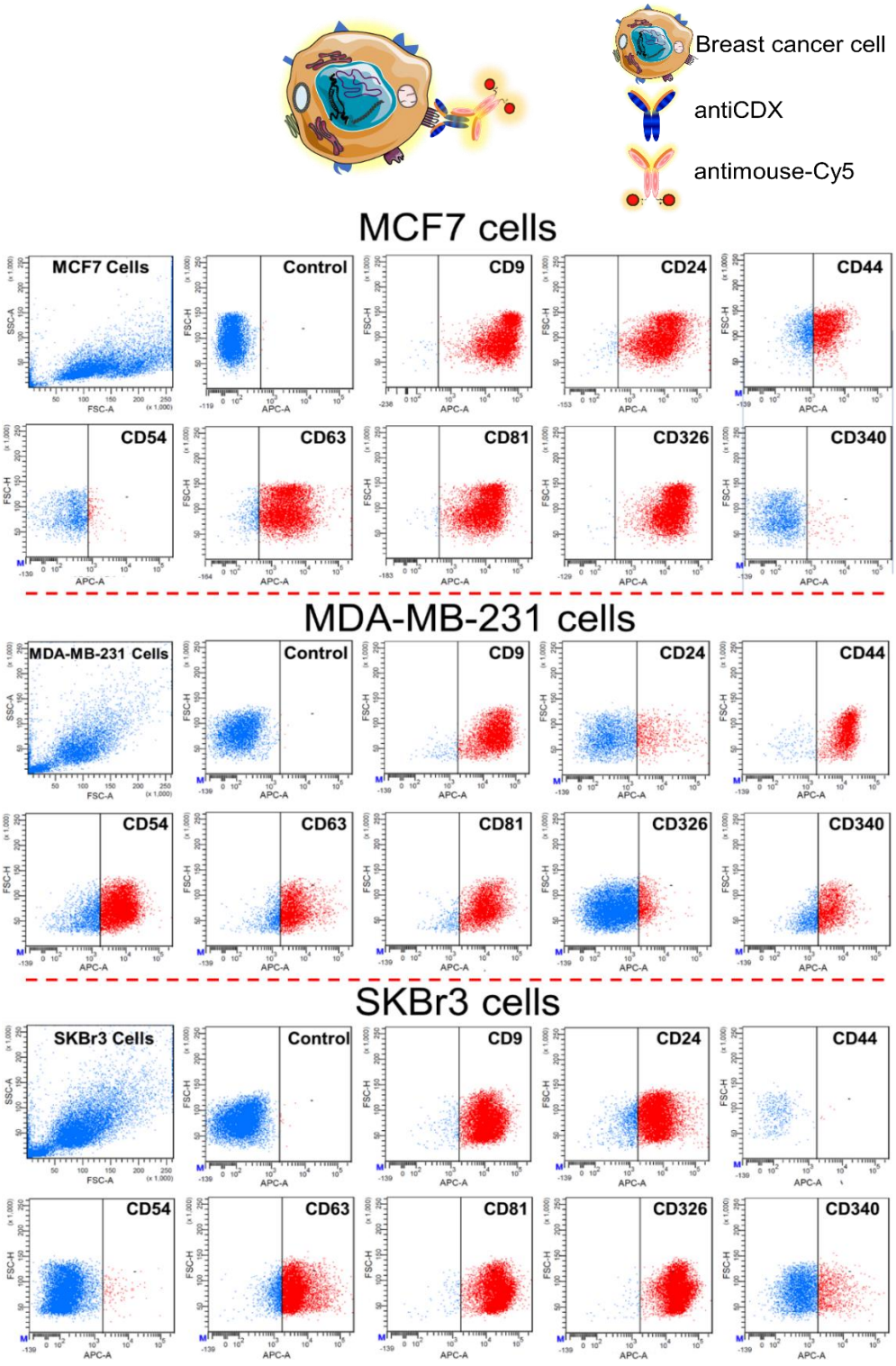

Fig. S4.10. Flow cytometry represented in dot-plot to evaluate the relative expression of CD9, CD24, CD44, CD54, CD63, CD81, CD326 and CD340 membrane protein markers in the MCF7, MDA-MB-231 and SKBr3 breast cancer cell lines. Population control onto the stained-blue regions on the left side and stained-red regions on the right side for a positive relative expression of membrane protein markers. In all cases, the amount the primary antibody was 5 μg mL^{-1} and 2 μg mL^{-1} of antimouse-Cy5 antibody

4.6.18. Flow cytometry analysis of membrane markers on breast cancer exosomes covalently immobilized on magnetic particles (exosomes-MPs)

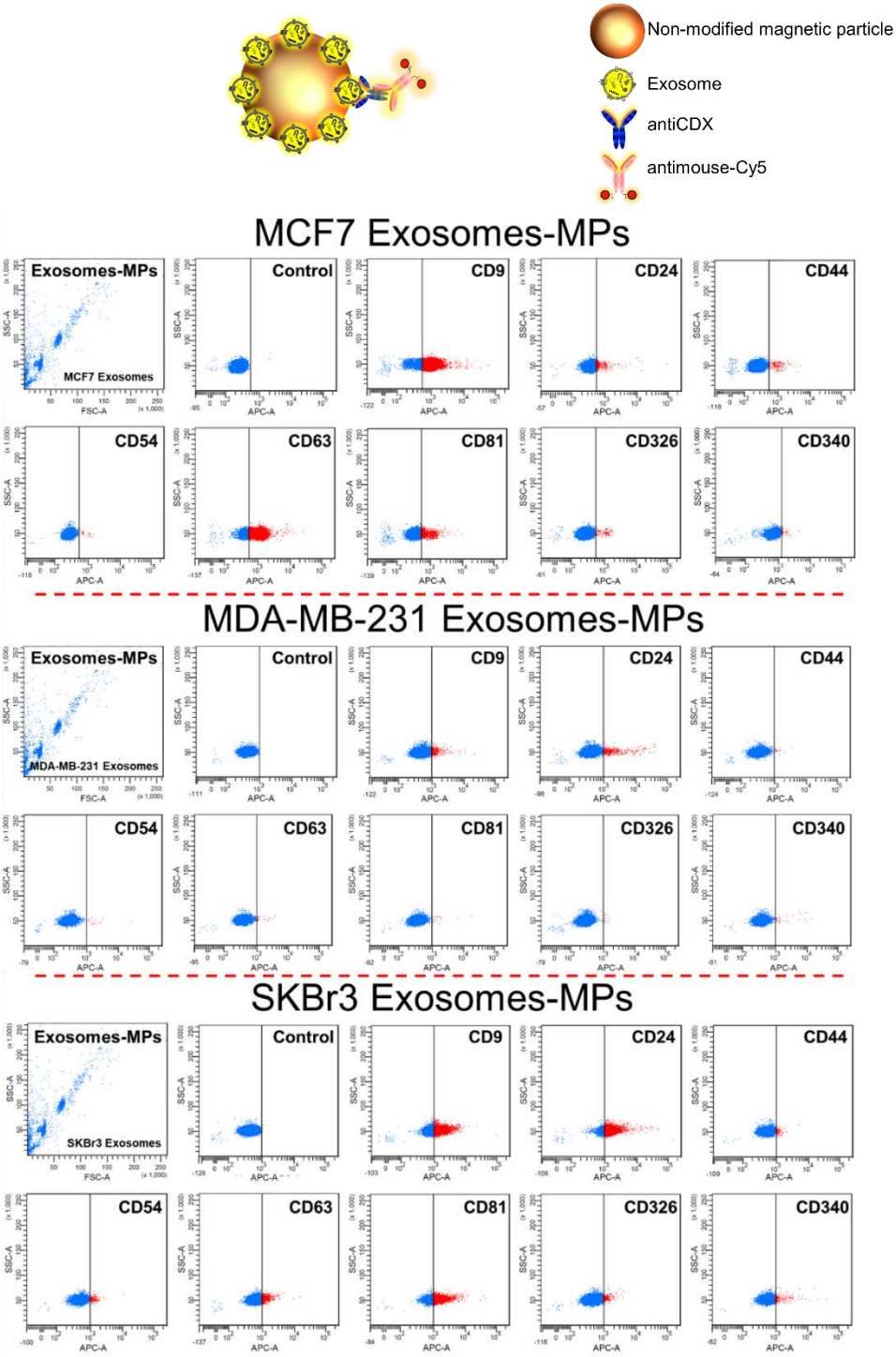

Fig. S4.11. Flow cytometry represented in dot-plot to evaluate the relative expression of CD9, CD24, CD44, CD54, CD63, CD81, CD326 and CD340 membrane protein markers in the exosomes-derived from MCF7, MDA-MB-231 and SKBr3 breast cancer cell lines. The exosomes were covalently immobilized on magnetic particles (Exosomes-MPs). Population control onto the stained-blue regions on the left side and stained-red regions on the right side for a positive relative expression of membrane protein markers. In all cases, the amount the primary antibody was 5 μg mL^{-1} and 2 μg mL^{-1} of antimouse-Cy5 antibody.

4.6.19. Flow cytometry analysis of membrane markers on breast cancer exosomes immunocaptured by antiCD81-modified magnetic particles (antiCD81-MPs)

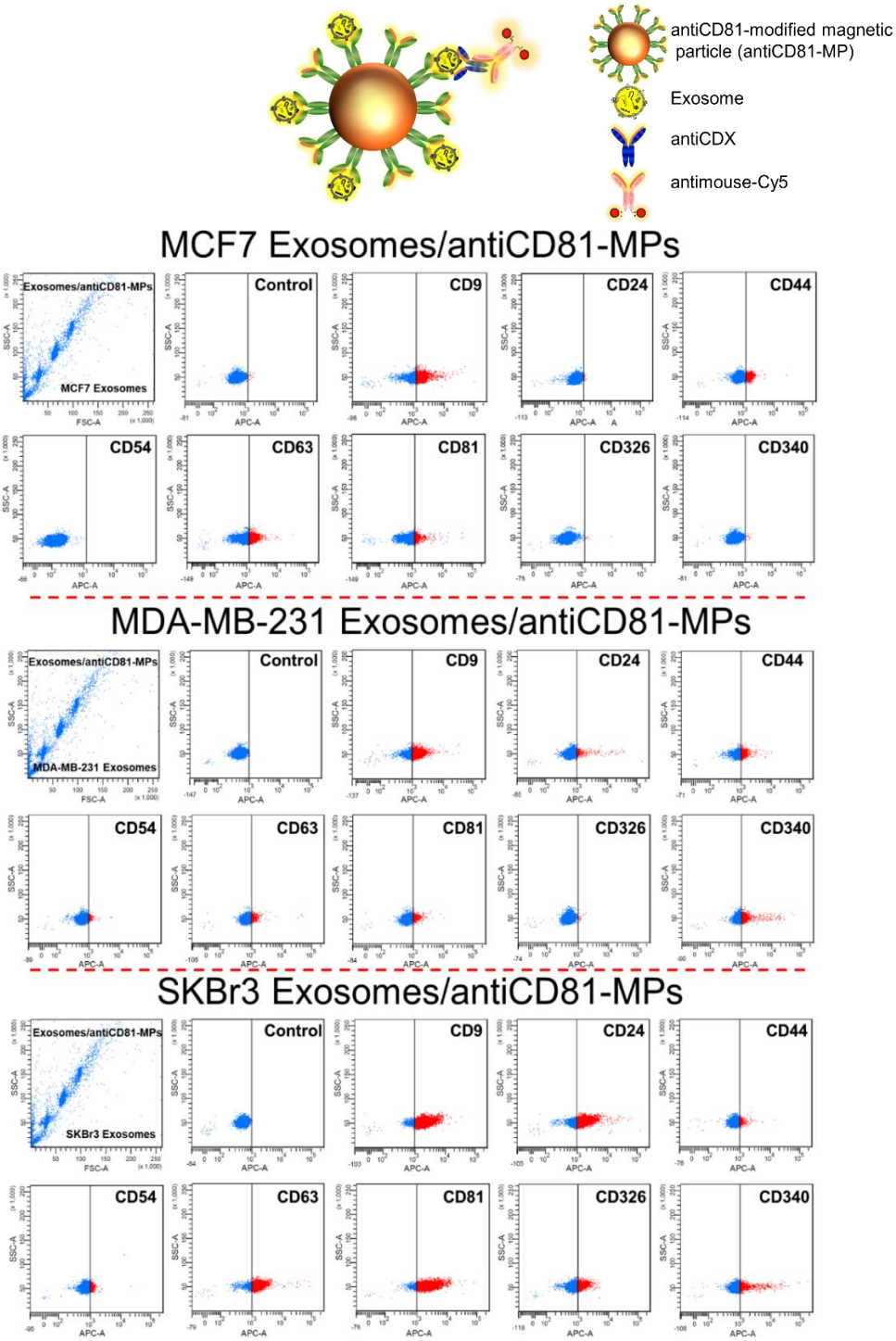

Fig. S4.12. Flow cytometry represented in dot-plot to evaluate the relative expression of CD9, CD24, CD44, CD54, CD63, CD81, CD326 and CD340 membrane protein markers in the exosomes-derived from MCF7, MDA-MB-231 and SKBr3 breast cancer cell lines. The exosomes were immunomagnetically captured on antiCD81$_{Rabbit}$-modified magnetic particles (Exosomes/antiCD81$_{Rabbit}$-MPs). Population control onto the stained-blue regions on the left side and stained-red regions on the right side for a positive relative expression of membrane protein markers. In all cases, the amount the primary antibody was 5 μg mL^{-1} and 2 μg mL^{-1} of antimouse-Cy5 antibody.

4.6.20. Magneto-actuated immunoassay in PBS

The performance of the different approaches was further studied by calibration plots of exosomes (ranged from 150 to 2 x 10^7 exosomes μL^{-1}) derived from MCF7 cell line and spiked into PBS buffer solution. Fig. S4.13, panel A, shows the results for the magneto-actuated immunoassay of exosomes covalently immobilized on magnetic particles and labeled by a direct (antiCD63-HRP) and indirect format (using antiCD63 and CD326 antibodies). The optical responses were fitted using a nonlinear regression (Four Parameter logistic Equation–GraphPad Prism Software). The limit of detection (LOD) of 600 exosomes μL^{-1} (r^2 = 0.9997) and 326 exosomes μL^{-1} (r^2 = 0.9912) for indirect immunoassay format was reached using CD63 and CD326 biomarkers, respectively. A LOD of 230 exosomes μL^{-1} (r^2 = 0.9978) was reach for direct magneto-actuated immunoassay format using antiCD63-HRP. In this approach, the presence of only one receptor was studied. This format based on the detection of a general biomarker, such as CD63, is thus suitable by the general quantification of exosomes in a sample, being also able to detect a specific epithelial biomarker as is the case of CD326.

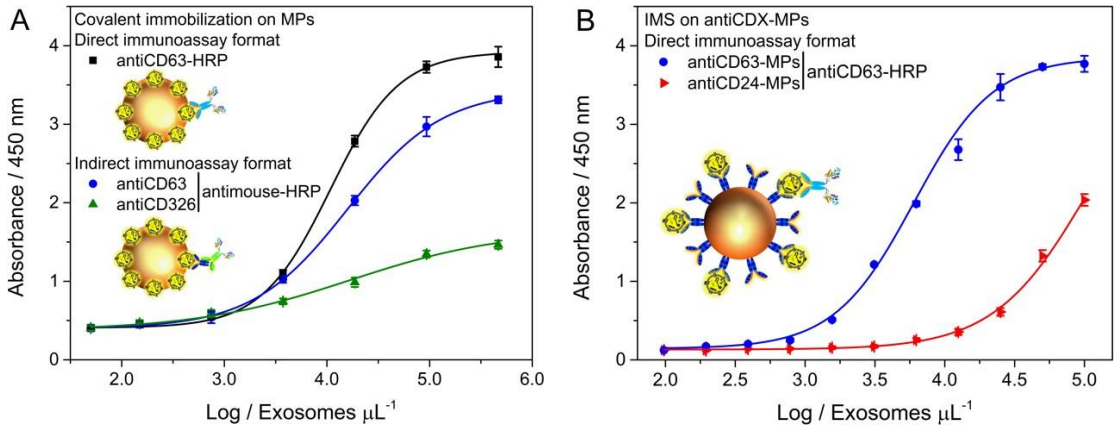

Fig. S4.13. Magneto-actuated immunoassay for detection of MCF7 exosomes ranging from 150 to 4.5 x 10^5 exosomes μL^{-1} spiked in 10 mmolL^{-1} PBS buffer solution. (A) covalently immobilization of the exosomes on MPs (exosomes-MPs), followed by indirect labeling with (●) antiCD63 and (▲) antiCD326, and by direct labeling with (■) antiCD63- HRP antibody. (B) IMS of the exosomes on (►) antiC24-MPs and (●) antiCD63-MPs, followed by direct labeling with antiCD63-HRP antibody. In all cases, the concentration of MPs was fixed in 1 × 10^6 MPs, 0.50 µg mL^{-1} of primary antibody, 0.08 ng mL^{-1} of antimouse-HRP and 1.24 µg mL^{-1} of antiCD63-HRP antibody. The error bars show the standard deviation for n = 3.

The performance of the second approach involving the IMS with a specific biomarker (antiCDX-MPs, being CDX in this instance CD63 and CD24) followed by the optical readout using a general receptor (antiCD63-HRP antibody), is shown in Fig. S4.13, panel B. As previously discussed, this format requires the coexistence of two biomarkers in the same exosomes to be magneto-actuated and labeled. The optical responses were also fitted as above, obtained a LOD of 218 exosomes μL^{-1} (r^2 = 0.9950) when

performing the IMS with the over expressed general receptor (antiCD63-MPs) and 2515 exosomes μL^{-1} (r^2 = 0.9915) when using antiCD24-MPs, as expected. From the results, there is a strong evidence that some biomarkers are not always present in all the exosomes population, as is the case of the specific receptors, being the general CD9, CD63 and CD81 receptors more likely to be found. In addition, these detection limits represent an improvement over the ones obtained by conventional immunoassays (López-Cobo et al., 2018).

4.6.21. Magneto-actuated immunoassay in human serum

The IMS performance towards isolation of exosomes directly in human serum was evaluated (Fig. S4.14). Exosome-depleted human serum was spiked with exosomes derived from MCF7 cell line, and submitted to magneto-actuated immunoassay, by IMS (with antiCDX-MP), followed by direct labeling with antiCD63-HRP.

The antiCDX-MPs (being CDX any of CD9, CD24, CD44, CD54, CD63, CD81, CD326 or CD340 biomarkers) (containing 1 × 10^6 antiCDX MPs per well) and the exosomes (100 µL, 4 x 10^9 exosomes), were simultaneously incubated for 30 min with shaking at 25 °C, followed by three washing steps with PBS containing 0.5% BSA. ii) Direct labeling. The modified-MPs were incubated with the antiCD63-HRP antibody (100 µL, 1.24 µg mL^{-1}) for 30 min with shaking at 25 °C, followed by three washing steps with PBS containing 0.5% BSA. (iii) Optical readout, as described above.

In this instance, the IMS was directly performed in the exosome-depleted undiluted human serum, thus evaluating the effect of free CDX receptors (or even other proteins) present in the sample matrix. The results shown in Fig S14 compare the exosomes spiked in PBS and a negative control performed with exosome-depleted human serum. From the results, as expected, a positive signal was obtained when processing the negative control by using antiCD63-MPs and antiCD63-HRP, suggesting the presence of free CD63 in serum. However, a high background (negative control) was surprisingly obtained when using antiCD9-MPs, indicating cross reactivity. As a consequence, and when using antiCD63-HRP for the direct labeling, the IMS cannot be performed with antiCD63 and antiCD9-MPs. On the other hand, a severe decrease in the signal was observed in human serum for antiCDX-MPs (being CDX: CD24, CD44 and CD340), indicating a competition (and even blocking) of the binding site of the MPs attributed to free CD24, CD44 and CD340 (or even other protein) presents in human serum, which prevent the binding of the exosomes and the further labeling with antiCD63-HRP. However, a better performance was obtained by IMS with antiCD81-MPs, showing almost the same signal for the exosomes spiked in PBS buffer solution

and depleted human serum, and a negligible background value.

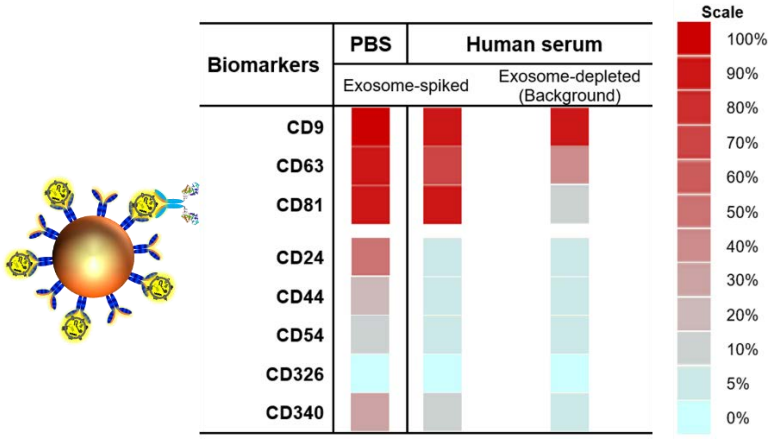

Fig. S4.14. Evaluation of matrix effect in exosome-depleted human serum for exosomes detection by IMS with antiCDX-MPs (being CDX either CD9, CD24, CD44, CD54, CD63, CD81, CD326 and CD340) and a direct labeling with antiCD63-HRP. The detection of exosomes in PBS buffer solution was performed and the background in depleted-human serum are also shown. In all cases, the concentration of MPs was fixed in 1 × 10^6 MPs, 4 x 10^9 exosomes and 1.24 μg mL^{-1} of antiCD63-HRP antibody per assay. Numbers indicate the percentage of positive exosomes for each biomarker.

In addition, the performance of the magneto-actuated immunoassay was further studied by calibration plots of exosomes (ranged from 3.9 x 10^4 to 2 x 10^7 exosomes μL^{-1}) derived from SKBr3 cell line and spiked on exosome-depleted human serum. Accordingly to the results obtained from the matrix effect study, and in order to avoid the interferences from free receptors in the serum, the IMS was performed on antiCD81-MPs, followed by the indirect labeling with the specific biomarkers, including CD24 and CD340 and the direct labeling with the general biomarker antiCD63-HRP. The results are shown in Fig. S4.15. The optical responses were fitted using a nonlinear regression (Four Parameter logistic Equation–GraphPad Prism Software). The LOD of 2.07 x 10^5 exosomes μL^{-1} (r^2 = 0.9936) and 4.76 x 10^5 exosomes μL^{-1} (r^2 = 0.9957) was reached using antiCD24 and antiCD340 biomarkers in non-diluted exosome-depleted human serum, respectively, while a LOD of 3.23 x 10^5 exosomes μL^{-1} (r^2 = 0.9960) was obtained with the general biomarker in direct immunoassay format (antiCD63-HRP).

Since the number of exosomes in biological fluids ranges from 1 × 10^1 to 3 × 10^7 exosomes μL^{-1} (Zhang et al., 2016), the LOD for magneto-ELISA approaches were feasible and reliable to detect and quantification of the cancer-related exosomes even in human serum (Fig. S4.15). The LOD of the magneto-ELISA developed in this work was compared with emerging methods (Table S4.1). The analytical performance of the magneto-ELISA was better than conventional ELISA, lateral flow colorimetric assay, electrochemical and microfluidic μNMR device, even in human serum. Although the other methods (Table S4.1) had higher sensitivity than magneto-ELISA, the approaches

involved complicated electrode pretreatment and labeling technology, as well as the high cost of the instrumentations and maintenance, such as cantilever arrays. Based on above facts, this reflects in the planning and implementing cancer control programs, which are not available in most low- and middle-income countries.

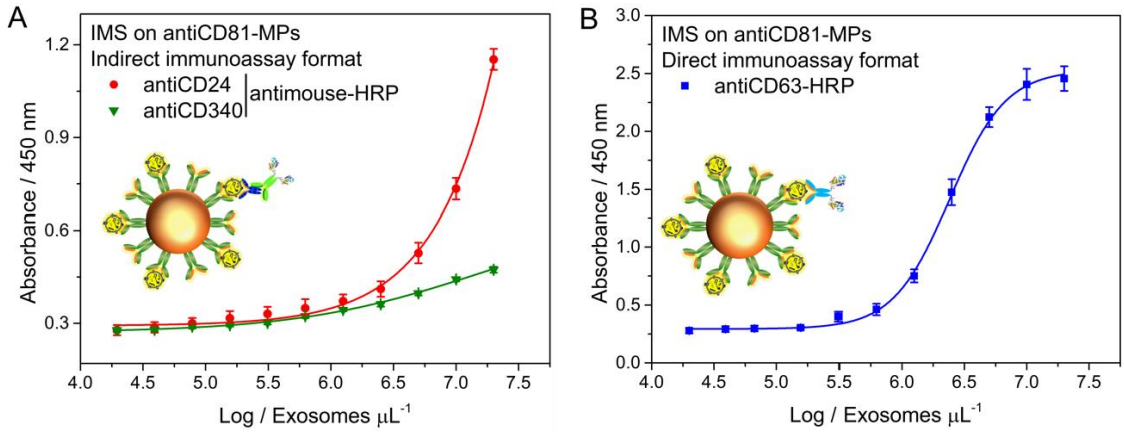

Fig. S4.15. Magneto-actuated immunoassay for detection of SKBr3 exosomes ranging from 3.9 x 10^4 to 2 x 10^7 exosomes μL^{-1} spiked in exosome-depleted human serum. IMS of the exosomes on antiCD81-MPs, followed by (A) indirect labeling with (●) antiCD24 and (▼) antiCD340, and by (B) direct labeling with (■) antiCD63-HRP antibody. In all cases, the concentration of MPs was fixed in 1 × 10^6 MPs, 0.50 μg mL^{-1} of primary antibody, 0.08 ng mL^{-1} of antimouse-HRP and 1.24 μg mL^{-1} of antiCD63-HRP antibody. The error bars show the standard deviation for n = 3.

Table S4.1. Comparison of different platforms for detection of exosomes.

Detection platform	Biomarker	Targeted disease	Real sample evaluated	LOD (Exosomes μL^{-1})	Reference
Electrochemical antiCD81-modified electrode	CD81	Breast cancer	NO	0.077	(Kilic et al., 2018)
Cantilever arrays	CD24, CD63, CD340 and GPC1	Breast cancer	50% human serum	0.2	(Etayash et al., 2016)
3D-nanopatterned microfluidic fluorescence-based device	CD24, CD326 and FRα	Ovarian cancer	10% human plasma	10	(Zhang et al., 2019)
Microfluidic graphene oxide-based interface	CD9, CD81 and EpCAM	Ovarian cancer	10% human plasma	50	(Zhang et al., 2016)
Rolling circle amplification with fluorescence detection	CD63 and nucleolin	Leukemia	50% fetal bovine serum	100	(Huang et al., 2018)
Magneto-ELISA	CD24, CD63, CD326 and CD340	Breast cancer	NO	218	This work
Microfluidic fluorescence-based detection	CD9, CA-125, CD24 and CD326	Ovarian cancer	NO	750	(Zhao et al., 2016)
Electrochemical antiCD63-modified electrode	CD63	Liver cancer	10% fetal bovine serum	1000	(Zhou et al., 2016)
Surface-enhanced Raman scattering	CD63 and CD340	Lung cancer	NO	1200	(Zong et al., 2016)
Microfluidic SPR-based assay	CD9, CD63 and CD340	Breast cancer	non-diluted human serum	2070	(Sina et al., 2016)
Microfluidic electrohydrodynamic assay	CD9 and CD340	Breast cancer	non-diluted human serum	2760	(Vaidyanathan et al., 2014)
Microfluidic SPR-based nanoholes arrays	CD24 and CD326	Ovarian cancer	Ascites fluid	~3000 exosomes	(Im et al., 2014)
Microfluidic fluorescence-based detection	CD81 and GluR2	Brain injury	non-diluted mouse serum	1.0×10^4	(Ko et al., 2016)
Microfluidic DLS-based detection	T7 phage	Viral infection	non-diluted mouse plasma	1.0×10^5	(Fraikin et al., 2011)
Magneto-ELISA	CD24, CD63 and CD340	Breast cancer	non-diluted human serum	2.0×10^5	This work
Electrochemical antiCD9-modified electrode Deferential Pulse Voltammetry	CD9 and CD340	Breast cancer	non-diluted human serum	4.7×10^5	(Yadav et al., 2017)
Colorimetric single-walled carbon nanotubes	CD63	Breast cancer	NO	5.2×10^5	(Xia et al., 2017)
Microfluidic μNMR-based detection	CD44, CD47, CD55 and CD235a	Blood quality	Packed red blood cells	2.0×10^6	(Rho et al., 2013)
Conventional ELISA	CD9, CD63 and MICA	Melanoma cancer	NO	1.0×10^7	(López-Cobo et al., 2018)
Nanoparticle tracking analysis (NTA)	-	-	NO	1.0×10^7	(Filipe et al., 2010)
Lateral flow colorimetric assay	CD9, CD63 and CD81	Melanoma cancer	NO	8.5×10^6	(Oliveira-Rodríguez et al., 2016)

4.6.22. Magneto-actuated immunoassay for the detection of serum-derived from breast cancer patients

Exosome protein content

Considering the same volume of human serum and exosome-pellet resuspended in PBS, the protein concentrations of the exosome from healthy and breast cancer patients were estimated to be 235 μg mL^{-1} and 335 μg mL^{-1}, respectively.

Nanoparticle tracking analysis

Purified exosomes from healthy and breast cancer patients were analyzed by NTA. Fig. S4.16, panel A, shows the size diameter distribution of purified exosomes from healthy ranges from approximately 40 nm to up to 400 nm (considering 95.4% of a Gaussian distribution), showing main peaks: 115, 147, 196, 240 and 295 nm. In addition, the concentration of the preconcentrated and purified solution under analysis was estimated to be 3.87 x 10^{10} (SD 9.72 x 10^{8}) particles mL^{-1}.

The size diameter distribution for purified exosomes from breast cancer patients ranges from approximately 40 nm to up to 400 nm, showing main peaks: 118, 150, 205, 300 and 460 nm. Moreover, the concentration of the preconcentrated and purified solution under analysis was estimated to be 6.49 x 10^{10} (SD 4.21 x 10^{8}) particles mL^{-1}.

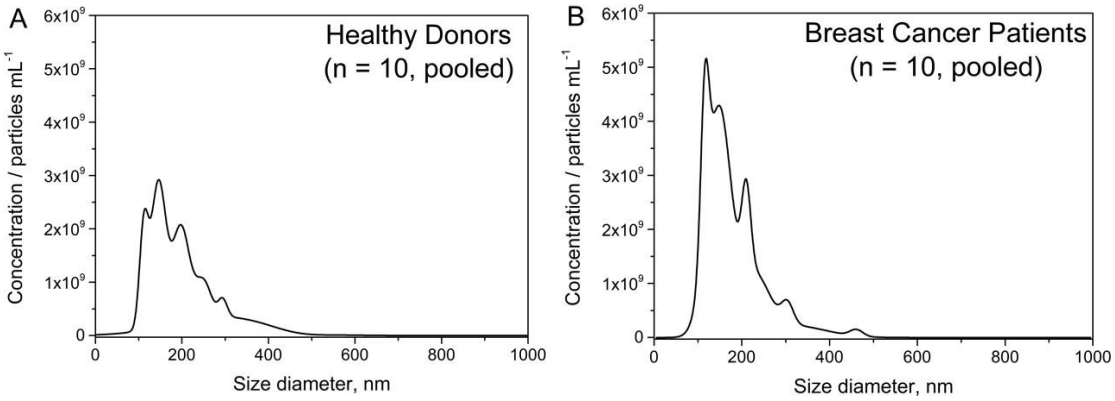

Fig. S4.16. Nanoparticle tracking analysis (NTA) on size distribution on purified exosomes- derived human serum from (A) healthy and (B) breast cancer patients. The purified exosomes were diluted in sterile filtered 10 mmol L^{-1} PBS buffer. Nanosight NTA Software analyzed raw data videos by triplicate during 60 s with 50 frames per second and the temperature of the laser unit set at 24.8 ºC.

4.7. References

An, T., Qin, S., Xu, Y., et al. Exosomes serve as tumour markers for personalized diagnostics owing to their important role in cancer metastasis. J. Extracell. Vesicles 2015; 4: 1.

Brandão, D., Liébana, S., Pividori, M. I. Multiplexed detection of foodborne pathogens based on magnetic particles. N. Biotechnol. 2015; 32: 511.

Cahiez, G., Lefèvre, N., Poizat, M., et al. A User-Friendly Procedure for the Preparation of Secondary Alkyl Chlorides. Synthesis (Stuttg). 2012; 45: 231.

Carinelli, S., Martí, M., Alegret, S., et al. Biomarker detection of global infectious diseases based on magnetic particles. N. Biotechnol. 2015; 32: 521.

Chosewood, L. C., Wilson, D. E. Biosafety in Microbiological and Biomedical Laboratories, 5th ed., in: U.S. Department of Health and Human Services. Centers for Disease Control and Prevention. 2009; 30.

Chow, A., Zhou, W., Liu, L., et al. Macrophage immunomodulation by breast cancer-derived exosomes requires Toll-like receptor 2-mediated activation of NF-κB. Sci. Rep. 2015; 4: 5750.

Dudani, J. S., Gossett, D. R., Tse, H. T. K., et al. Rapid inertial solution exchange for enrichment and flow cytometric detection of microvesicles. Biomicrofluidics 2015; 9: 014112.

Engvall, E., Perlmann, P. Enzyme-linked immunosorbent assay (ELISA) quantitative assay of immunoglobulin G. Immunochemistry 1971; 8: 871.

Etayash, H., McGee, A. R., Kaur, K., et al. Nanomechanical sandwich assay for multiple cancer biomarkers in breast cancer cell-derived exosomes. Nanoscale 2016; 8:15137.

Filipe, V., Hawe, A., Jiskoot, W. Critical Evaluation of Nanoparticle Tracking Analysis (NTA) by NanoSight for the Measurement of Nanoparticles and Protein Aggregates. Pharm. Res. 2010; 27: 796.

Fraikin, J.-L., Teesalu, T., McKenney, C. M., et al. A high-throughput label-free nanoparticle analyser. Nat. Nanotechnol. 2011; 6: 308.

Grasso, L., Wyss, R., Weidenauer, L., et al. Molecular screening of cancer-derived exosomes by surface plasmon resonance spectroscopy. Anal. Bioanal. Chem. 2015; 407: 5425.

Hemler, M. E. Tetraspanin proteins promote multiple cancer stages. Nat. Rev. Cancer 2013; 14: 49.

Hoogenboom, R., Fijten, M. W. M., Kickelbick, G., et al. Synthesis and crystal structures of multifunctional tosylates as basis for star-shaped poly(2-ethyl-2-oxazoline)s. Beilstein J. Org. Chem. 2010; 6: 773.

Huang, L., Wang, D.-B., Singh, N., et al. A dual-signal amplification platform for sensitive fluorescence biosensing of leukemia-derived exosomes. Nanoscale 2018; 10: 20289.

Im, H., Shao, H., Park, Y. Il, et al. Label-free detection and molecular profiling of exosomes with a nano-plasmonic sensor. Nat. Biotechnol. 2014; 32: 490.

Johnstone, R. M., Adam, M., Hammond, J. R., et al. Vesicle formation during reticulocyte maturation. Association of plasma membrane activities with released vesicles (exosomes). J. Biol. Chem. 1987; 262: 9412.

Kilic, T., Valinhas, A. T. D. S., Wall, I., et al. Label-free detection of hypoxia-induced extracellular vesicle secretion from MCF-7 cells. Sci. Rep. 2018; 8: 9402.

Ko, J., Hemphill, M. A., Gabrieli, D., et al. Smartphone-enabled optofluidic exosome diagnostic for concussion recovery. Sci. Rep. 2016; 6: 31215.

Levva, S., Kotoula, V., Kostopoulos, I., et al. Prognostic evaluation of epidermal growth factor receptor (EGFR) genotype and phenotype parameters in triple-negative breast cancers. Cancer Genomics and Proteomics 2017; 14: 181.

López-Cobo, S., Campos-Silva, C., Moyano, A., et al. Immunoassays for scarce tumour-antigens in exosomes: detection of the human NKG2D-Ligand, MICA, in tetraspanin-containing nanovesicles from melanoma. J. Nanobiotechnology 2018; 16: 47.

Oliveira-Rodríguez, M., López-Cobo, S., Reyburn, H.T., et al. Development of a rapid lateral flow immunoassay test for detection of exosomes previously enriched from cell culture medium and body fluids. J. Extracell. Vesicles 2016; 5: 31803.

Reddy, L. H., Arias, J. L., Nicolas, J., et al. Magnetic Nanoparticles: Design and Characterization, Toxicity and Biocompatibility, Pharmaceutical and Biomedical Applications. Chem. Rev. 2012; 112: 5818.

Rembaum, A., Yen, R. C. K., Kempner, D. H., et al. Cell labeling and magnetic separation by means of immunoreagents based on polyacrolein microspheres. J. Immunol. Methods 1982; 52: 341.

Rho, J., Chung, J., Im, H., et al. Magnetic Nanosensor for Detection and Profiling of Erythrocyte-Derived Microvesicles. ACS Nano 2013; 7: 11227.

Rupp, A.-K., Rupp, C., Keller, S., et al. Loss of EpCAM expression in breast cancer derived serum exosomes: Role of proteolytic cleavage. Gynecol. Oncol. 2011; 122: 437.

Samanta, S., Rajasingh, S., Drosos, N., et al. Exosomes: new molecular targets of diseases. Acta Pharmacol. Sin. 2018; 39: 501.

Sina, A. A. I., Vaidyanathan, R., Dey, S., et al. Real time and label free profiling of clinically relevant exosomes. Sci. Rep. 2016; 6: 30460.

Soysal, S. D., Muenst, S., Barbie, T., et al. EpCAM expression varies significantly and is differentially associated with prognosis in the luminal B HER2+, basal-like and HER2 intrinsic subtypes of breast cancer. Br. J. Cancer 2013; 108: 1480.

Stoeck, A., Keller, S., Riedle, S., et al. A role for exosomes in the constitutive and stimulus-induced ectodomain cleavage of L1 and CD44. Biochem. J. 2006; 393: 609.

Tamkovich, S. N., Yunusova, N. V., Somov, A. K., et al. Comparative Subpopulation Analysis of Plasma Exosomes from Cancer Patients. Biochem. (Moscow), Suppl. Ser. B Biomed. Chem. 2018; 12: 151.

Théry, C., Amigorena, S., Raposo, G., et al. Isolation and Characterization of Exosomes from Cell Culture Supernatants and Biological Fluids. Curr. Protoc. Cell Biol. 2006; 30: 3.22.1.

Théry, C., Zitvogel, L., Amigorena, S. Exosomes: composition, biogenesis and function. Nat. Rev. Immunol. 2002; 2: 569.

Vaidyanathan, R., Naghibosadat, M., Rauf, S., et al. Detecting Exosomes Specifically: A Multiplexed Device Based on Alternating Current Electrohydrodynamic Induced Nanoshearing. Anal. Chem. 2014; 86: 11125.

Xia, Y., Liu, M., Wang, L., et al. A visible and colorimetric aptasensor based on DNA-capped single-walled carbon nanotubes for detection of exosomes. Biosens. Bioelectron. 2017; 92: 8.

Xu, J., Mahajan, K., Xue, W., et al. Simultaneous, single particle, magnetization and size measurements of micron sized, magnetic particles. J. Magn. Magn. Mater. 2012; 324: 4189.

Yadav, S., Boriachek, K., Islam, M. N., et al. An Electrochemical Method for the Detection of Disease-Specific Exosomes. ChemElectroChem 2017; 4: 967.

Zacco, E., Pividori, M. I., Alegret, S., et al. Electrochemical Magnetoimmunosensing Strategy for the Detection of Pesticides Residues. Anal. Chem. 2006; 78: 1780.

Zhang, P., He, M., Zeng, Y. Ultrasensitive microfluidic analysis of circulating exosomes using a nanostructured graphene oxide/polydopamine coating. Lab Chip 2016; 16: 3033.

Zhang, P., Zhou, X., He, M., et al. Ultrasensitive detection of circulating exosomes with a 3D-nanopatterned microfluidic chip. Nat. Biomed. Eng. 2019; 3: 438.

Zhao, Z., Yang, Y., Zeng, Y., et al. A microfluidic ExoSearch chip for multiplexed exosome detection towards blood-based ovarian cancer diagnosis. Lab Chip 2016; 16: 489.

Zhou, Q., Rahimian, A., Son, K., et al. Development of an aptasensor for electrochemical detection of

CHAPTER 5

Electrochemical immunosensing of nanovesicles as biomarkers for breast cancer

Silio Lima Moura, Carme García Martín, Mercè Martì and María Isabel Pividori

Biosensors and Bioelectronics **2020**, 150; 111882

DOI: 10.1016/j.bios.2019.111882

5.1. Abstract

Exosomes are nano-sized vesicles, which are currently under intensive study as potential diagnostic biomarkers for many health disorders, including cancer. This paper addresses the study of an electrochemical immunosensor in different formats for the characterization and quantification of exosomes derived from three breast cancer cell lines (MCF7, MDA-MB-231 and SKBR3). To achieve that, the exosomes were preconcentrated from cell-culture supernatant (and eventually in human serum) on magnetic particles modified with antibodies against the general tetraspanins CD9, CD63 and CD81, as well as specific receptors of cancer (CD24, CD44, CD54, CD326 and CD340). The electrochemical immunosensor is able to reach a limit of detection of 10^5 exosomes μL^{-1} directly in human serum, when performing the immunomagnetic separation with antiCD81 modified magnetic particles and the labeling based on CD24 and CD340 as cancer-related biomarker, avoiding the interference from free receptors in the serum matrix. Furthermore, the electrochemical immunosensor shows reliable results for the differentiation of healthy donors and breast cancer individuals based on specific epithelial biomarkers. This approach is a highly suitable alternative method for the detection of exosomes in scarce resource settings.

5.2. Introduction

Nowadays, the study of novel biomarkers to prevent cancer in early stages and the risk of metastasis is a significant research topic. Exosomes are nanovesicles which are released in biological fluids (Samanta et al., 2018) during the fusion of the multivesicular endosomes (MVEs) with the plasmatic membrane. Therefore, the exosomes usually carry specific membrane biomarkers of cellular origin, including surface proteins such as those involved in the transport and fusion (e.g. flotillin, caveolin-1) and tetraspanins (e.g. CD9, CD63, CD81) among others (Samanta et al., 2018). Exosomes are thus currently under increasingly attention as biomarkers for cancer diagnosis and monitoring (Halvaei et al., 2018; Raposo and Stoorvogel, 2013). Unfortunately, realizing the potential of these vesicles as biomarker requires technical improvement, since the exosomes are exceptionally challenging to characterization with current technologies. Exosomes are between 30 and 200 nm in diameter, a size that makes them out of the sensitivity range to most cell-oriented sorting or analysis platforms, as is the case of the classical flow cytometers. The most common methods for targeting exosomes to date typically involve purification followed by the specific characterization of their cargo (Théry et al., 2006). The isolation of the exosomes is best performed with differential ultracentrifugation. Purification can also be done with precipitation, size-exclusion chromatography, or ultrafiltration (Patel et al., 2019),

although these methods can also affect the integrity of the exosomes (Witwer et al., 2013). Identification of membrane vesicles as exosomes also requires morphological analysis (Théry et al., 2006). Given their small size, exosomes can only be visualized with an electron microscope. Nanoparticle tracking analysis (NTA) is usually considered the gold standard to count the exosomes (Filipe et al., 2010; Li et al., 2017), followed by downstream processes for specific detection, including LC-MS/MS and Western Blot for proteins and qPCR for genetic material. The whole procedure is time consuming, requiring thus skilled personnel as well as laboratory facilities and benchtop instrumentation. To summarize, current methodologies have limitations in isolating, detecting and characterizing exosomes with high specificity, sensitivity and simplicity.

Significant improvements have been made in recent years, including optical (Di Noto et al., 2016; Grasso et al., 2015; Im et al., 2014; Su, 2015) and electrochemical biosensors (Jeong et al., 2016; Yadav et al., 2017; Q. Zhou et al., 2016; Y.-G. Zhou et al., 2016), and microfluidic devices (He et al., 2014; Shao et al., 2012; Zhang et al., 2016). Beside this, further technological improvement for exosome detection that are needed involved solid-phase preconcentration procedures that can be easily integrated in these emerging diagnosis technologies. Since the early reports on magnetic separation technology (Rembaum et al., 1982), magnetic particles (MPs) are widely used as a powerful and versatile preconcentration tool in a variety of analytical and biotechnology applications (Reddy et al., 2012). This technology is extensively incorporated for researchers worldwide in classical methods, in biomolecular tools and in emerging technologies, including biosensors and microfluidic devices. Therefore, the integration of MPs on emerging diagnostic platforms can simplify the analytical procedures, especially in resource-scarce settings.

In this paper, the development of an electrochemical immunosensor based on magnetic actuation for the detection of exosomes derived from three breast cancer cell lines is designed in different formats and assessed in terms of analytical performance. Furthermore, the application of the design procedure to the discrimination of breast cancer individuals from healthy donors based on specific cancer-related biomarkers is demonstrated as a probe of concept for the biosensor.

5.3. Experimental

5.3.1. Instrumentation

Nanoparticle tracking analysis (NTA) was performed using the NanoSight LM10-HS system with a tuned 405 nm laser (NanoSight Ltd, UK). The cryogenic transmission electron microscopy (TEM) images were collected by a Jeol JEM 2011 (JEOL USA Inc, USA) transmission electron microscope at an accelerating voltage of 200 kV. The

confocal images were collected on the microscope Leica, TCS SP5 (Leica Microsystems, Germany). All electrochemical experiments were performed using an AUTOLAB PGSTAT10 (Metrohm, Switzerland) potentiostat/galvanostat electrochemical analyzer. The data were in all cases fitted with using a nonlinear regression (Four Parameter logistic Equation–GraphPad Prism Software).

5.3.2. Chemicals and biochemicals

Magnetic particles (Dynabeads® M450 Tosylactivated, nº 14013, 4,5 µm diameter) were purchased from Thermo Fisher. The antibodies were purchased from Abcam, Thermo Fisher, eBioscience, and Sigma-Aldrich as detailed in Table S5.1, Supp Data. All other reagents were in analytical reagent grade as listed in details in the Supp. Data.

5.3.3. Cell culturing, exosome isolation and purification

Breast cancer cell lines MCF7 (ATCC® HTB-22™), MDA-MB-231 (ATCC® CRM-HTB-26™) and SKBr3 (ATCC® HTB-30™) were grown as described in the Supp. Data. Exosomes were purified from culture supernatant and human serum by differential ultracentrifugation according to Théry and co-workers (Théry et al., 2006) with slight modification (Supp. Data). Exosomes were resuspended in 10 mmol L^{-1} PBS pH 7.5 (0.22 µm filtrated and sterile) and storage at -80 ºC.

5.3.4. Characterization of exosomes by nanoparticle tracking analysis and transmission electron microscopy

NTA was used as a gold standard method to count the exosomes. This information was used for the calibration plots (Filipe et al., 2010; Li et al., 2017). NTA was also used to study the size distribution of exosomes purified from cell culture supernatant as well as from serum of healthy donors and breast cancer individuals. The purified exosomes diluted 50- to 100-fold in sterile-filtered PBS pH 7.5 buffer were studied. Nanosight NTA Software was used to analyze raw data videos by triplicate during 60 s with 50 frames/s at 24.8 ºC. For the TEM, the exosomes (2.0×10^9) were directly laid on Formvar-Carbon EM grids and frozen in ethanol. Exosomes were maintained at -182 ºC during the whole process.

5.3.5. Confocal microscopy study

Confocal microscopy was used for the assessment of the molecular biomarkers expressed in three different cancer cell lines (MCF7, MDAMB-231 and SKBr3). The presence of the following receptors was investigated: CD9, CD24, CD44, CD54, CD63,

CD81, CD326 and CD340. Firstly, the cell nucleus of 2 x 10^5 cells was stained with Hoechst dye (a blue-fluorescent dye, emission at 490 nm). Then, indirect labeling of cells was performed by incubation with 100 µL (5 µg mL^{-1}) of the antibodies antiCDX (mouse), (being CDX either CD9, CD24, CD44, CD54, CD63, CD81, CD326 and CD340 biomarkers), for 30 min with gentle shaking at 25 ºC. After that, three washing steps were performed. Afterwards, 100 µL (2 µg mL^{-1}) of antimouse-Cy5 antibody were incubated for 30 min at 25 ºC for further readout. The same labeling procedure was performed for the exosomes derived from the cells. In this approach, the exosomes were attached on the surface of MPs (Supp data, Fig S5.1, panel A). by covalent immobilization (exosomes-MPs). To achieve that, 3.5 x 10^{10} exosomes were covalently immobilized on 1.6 x 10^7 MPs, followed by the indirect labeling as described above, with antiCDX antibodies (mouse). In all instances, percentage of labelled entities was normalized by the highest fluorescence value for a labelled receptor.

5.3.6. Electrochemical immunosensing of breast cancer exosome

5.3.6.1. Electrochemical immunosensing of exosomes covalently immobilized on magnetic particles

The immobilization of exosomes on MP (exosomes-MPs) was performed as previously described (Supp. Data and Fig. S5.1, panel A therein). Two different approaches were evaluated, including the direct and indirect format (Fig. S5.2, panel A). The direct format involved the following steps: (i) incubation of the exosomes-MP with the antiCD63-HRP antibody; (ii) electrochemical readout.

The indirect format involved the following steps: (i) incubation of the exosomes-MP with antiCDX mouse monoclonal antibodies (being CDX either CD9, CD24, CD44, CD54, CD63, CD81, CD326 or CD340 biomarkers); (ii) indirect labeling with antimouse-HRP antibody; (iii) electrochemical readout.

For the electrochemical readout, the modified MPs were separated by using a magnetic tube separator, a MPs pellet on the bottom tube is formed, followed by supernatant removing. Afterwards, the MPs pellet was transferred to the surface of a working magnetic electrode (m-GEC, magneto-actuated graphite epoxy composite) and measured in an electrochemical cell by means of amperometry at -0.1 V vs. $Ag/AgCl/KCl_{(satd.)}$ and using hydroquinone as mediator (Supp. Data and Figs. S5.2–S5.4).

5.3.6.2. Immunomagnetic separation of exosomes and electrochemical immunosensing

Two different approaches were evaluated, including the direct and indirect format (Fig. S5.2, panel B). The direct format involved the following steps: i) Immunomagnetic separation (IMS) of the exosomes with antiCDX-MPs, followed by ii) the direct labeling with the antiCD63-HRP antibody; (iii) electrochemical readout, as described above. It is important to highlight that in this approach a specific antibody against the different receptors (antiCDX-MPs) is used for the IMS, followed by the direct labeling using a general biomarker (in this instance, antiCD63-HRP antibody).

The indirect format involved the following steps, as depicted in Fig. S5.2, panel B: i) IMS of the exosomes with antiCD81-MPs (rabbit), followed by ii) incubation with the specific mouse monoclonal antibodies (antiCDX, being CDX either CD9, CD24, CD44, CD54, CD63, CD81, CD326 or CD340 biomarkers); (iii) indirect labeling with antimouse-HRP antibody; (iv) electrochemical readout, as described above.

5.3.6.3. Electrochemical immunosensing of exosomes in human serum

The IMS with further electrochemical immunosensing was performed as above, but in human serum (previously depleted, as detailed in Supp data) and spiked with exosomes derived. The IMS was performed on antiCD81-MPs, followed by (A) indirect labeling with antiCD24 and antiCD340, and by direct labeling with antiCD63-HRP antibody. In all cases, the percentage of labelled exosomes was normalized by the highest current signal value for a labelled receptor within each exosome immobilization approach.

5.3.7. Electrochemical immunosensing of serum-derived exosomes from breast cancer individuals

Blood samples from anonymized healthy female donors (n = 10, mean age 35/SD 5 years) and breast cancer female donors (n = 10, stage IV, mean age 50/SD 6 years) were obtained from the Hospital del Mar, Barcelona, Spain. The samples were polled in two batches (healthy donors and breast cancer individuals) and purified as detailed described in Supp data. The two batches were then evaluated by NTA, TEM and the protein content, and compared by electrochemical immunosensing on the basis of the same content of exosomal protein (0.235 μg of protein per assay) by two approaches: i) IMS with antiCD81-MPs in order to achieve a massive capture of the exosomes for further labeling with specific biomarkers (CD24, CD44, CD326 and CD340), ii) IMS with antiCDX-MPs (being CDX: CD24 and CD340) in order to achieve only cancer-related exosomes for further labeling with a high expressed general exosome biomarker (CD63).

5.3.8. Statistical analysis

The statistical analyses were performed using GraphPad Prism 6 (San Diego, USA). The data were statistically compared using a paired-sample Student's t-test. The value $p > 0.05$ was considered significant.

5.3.9. Safety considerations

All the experiments were performed in a Biosafety cabinet, and all material decontaminated by autoclaving or disinfected before discarding in accordance with U.S. Department of Health and Human Services guidelines for level 2 laboratory Biosafety (Chosewood and Wilson, 2009).

5.4. Results and discussion

5.4.1. Characterization of exosomes by nanoparticle tracking analysis and transmission electron microscopy

An estimation of the size diameter distribution of purified exosomes derived from MCF-7 breast cancer cell line was performed by NTA, and the discussion can be found in Supp data (Fig. S5.5). Fig. S5.5 also show the results for exosomes purified from serum of healthy donors and breast cancer individuals as well as an estimation of the concentration of each instance. Fig. 5.1, panels A, B and C shows comparatively the TEM images of exosomes derived from MCF-7 breast cancer cell line, and serum exosomes of cancer and healthy donors.

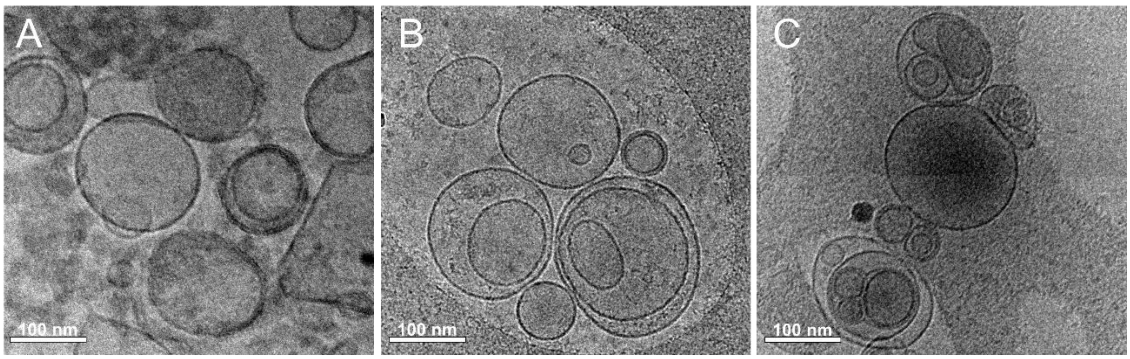

Fig. 5.1. Characterization by TEM of purified exosomes-derived from MCF7 breast cancer cell line (panel A), and for serum exosomes derived from healthy donors and breast cancer individuals (n = 10 each) (Panels B and C, respectively) (200 kV).

5.4.2. Confocal microscopy

Confocal microscopy was performed to comparatively study the expression patterns of different biomarkers on breast cancer cells (MCF-7, MDA-MB-231 and SKBr3) and their exosomes. CD9, CD63 and CD81 were, as expected, expressed in breast cancer cell lines at different levels (Fig. 5.2, panel A for MCF7 cells and Fig. S5.6, Supp. Data for MDA-MB-231 and SKBr3 cells). On the other hand, the cancer-related biomarkers CD24, CD44, CD54, CD326 and CD340 showed a different labeling pattern depending on the cell line. The quantitative results are also summarized in Fig. 5.2.

The expression of each cell line-derived exosomes was also studied after covalent immobilization on MPs (exosomes-MPs) (Fig. 5.2, panel B for exosomes derived from MCF7, MDA-MB-231 and SKBr3 cells lines). As expected, general tetraspanins (CD9, CD63 and CD81) (Chow et al., 2015; Hemler, 2013) were highly expressed in exosomes from MCF7 breast cancer cell line (Fig. 5.2, panel B). On the other hand, a poor labelling pattern was achieved for cancer-related biomarkers in MCF7, as well those derived from MDA-MB-231 and SKBr3 (Fig. 5.2, panel B). This issue can be attributed to steric hindrance of the receptor after immobilization of the exosomes on the MPs, as it will be further discussed.

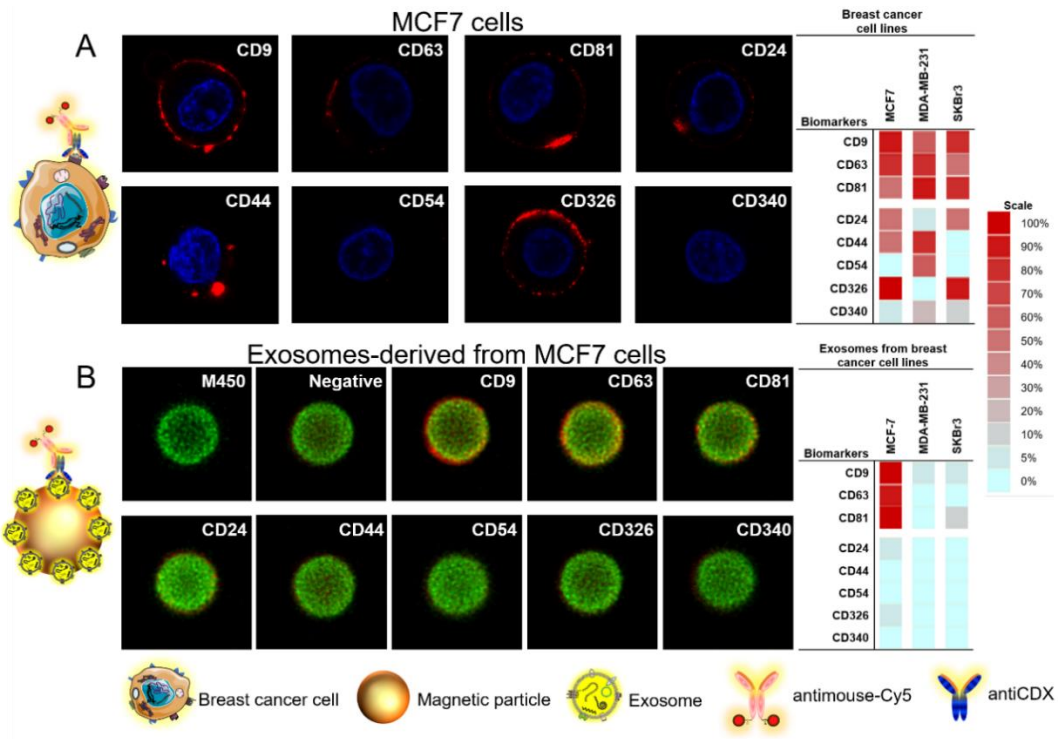

Fig. 5.2. Confocal microscopy study for (A) MCF7 breast cancer cell lines and their corresponding exosomes covalently immobilized on MPs (exosomes-MPs), followed by indirect labeling with mouse antiCDX (being CDX either CD9, CD24, CD44, CD54, CD63, CD81, CD326 and CD340 biomarkers) and antimouse-Cy5. The concentration of exosomes was set in 4 x 10^9 per assay. The scale indicates the percentage of positive entities (cells and exosomes-coated MPs in panels A and B, respectively. Further results are provided in Supp. data, Fig S5.6.

5.4.3. Electrochemical immunosensing of breast cancer exosomes

The electrochemical immunosensor was evaluated to measure the expression of general exosome biomarkers (CD9, CD63 and CD81), and cancer-related biomarkers (CD24, CD44, CD54, CD326 and CD340) firstly on exosomes derived from the three different breast cancer cell lines (MCF7, MDA-MB-231 and SKBr3). Since the biomarker expression on the exosomes showed differences among the breast cancer cell lines, the percentage of expression for each sample were represented as a graduated color scale.

For the approach involving exosomes covalently immobilized on MPs (exosomes-MPs), tetraspanins were detected on the exosomes derived from MCF7 cell line (Fig. 5.3, panel A). Surprisingly, the expression was weak or not detectable in exosomes from MDA-MB-231 and SKBr3, as in the case of confocal microscopy.

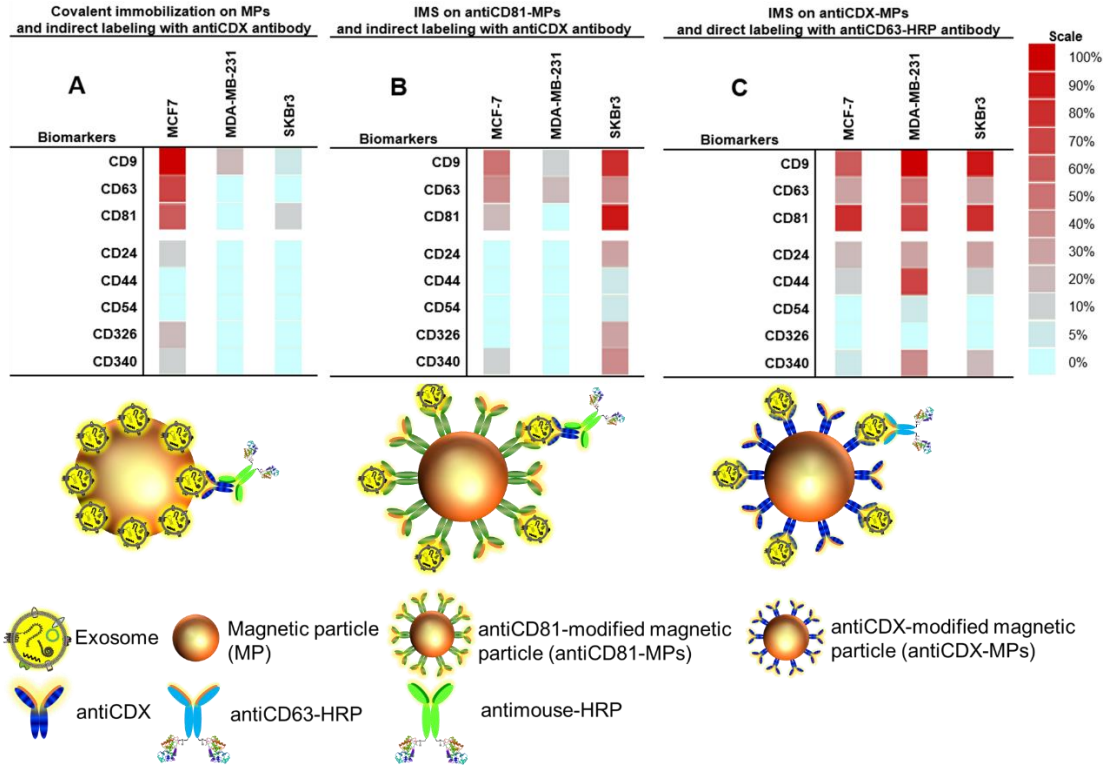

Fig. 5.3. Exosomal markers screening based on electrochemical immunosensing for exosomes derived from MCF7, MDA-MB-231 and SKBr3 breast cancer cell lines. The exosomes were attached on MPs by using three approaches, (A) covalent immobilization of exosomes on MPs (exosomes-MPs), (B) Immunomagnetic separation (IMS) of exosomes on antiCD81-MPs, followed by indirect labeling with antiCDX (mouse), (being CDX either CD9, CD24, CD44, CD54, CD63, CD81, CD326 and CD340 biomarkers) and antimouse-HRP. (C) IMS of exosomes on antiCDX-MPs, followed by direct labeling with antiCD63-HRP antibody. The concentration of exosomes was set in 4 x 10^9 exosomes per assay, respectively. Enzymatic electrochemical signal monitored at -0.1 V vs. $Ag/AgCl_{(sat.)}$.

In second approach involving the IMS, the recognition is thus achieved by two different antibodies, and the two biomarkers must be simultaneously expressed. As in the other approach (exosomes-MPs), the general tetraspanins (CD9, CD63 and CD81)

showed a higher expression, the IMS was performed with antiCD81-MPs to achieve a massive capture of the exosomes, for further electrochemical readout based on the specific biomarkers (CD24, CD44, CD54, CD326 and CD340). Fig. 5.3, panel B shows outstanding results for exosomes derived from SKBr3 cell line. Unexpectedly, results were poorer for exosomes derived from MCF7 and MDA-MB-231 breast cancer cell lines.

Finally, the third approach involved the IMS using a specific biomarker antibody (antiCDX-MPs), followed by the electrochemical readout using a general exosome biomarker widely expressed (as antiCD63-HRP antibody), in order to improve the sensitivity. The CD9, CD63 and CD81 marker expression was highly detected (>60%) in all the cell lines, as expected. Moreover, the immunosensing of exosomes from MDA-MB-231 and SKBr3 demonstrate that tetraspanins that were previously non-detected by other approaches, were clearly expressed using IMS with antiCD24-MPs, antiCD44-MPs, antiCD54-MPs and antiCD340-MPs and antiCD63-HRP, increasing the sensitivity of the electrochemical readout. The immobilization of antiCD326 antibody on MPs was not possible to achieve. The high sensitivity of this approach allowed the detection not only of overexpressed biomarker, but also those representing the epithelial origin of the exosomes.

To summarize, and by comparing the different procedures used such as TEM, confocal microscopy, and even for the different electrochemical immunosensing procedures, the IMS of the exosomes by antiCDX-MPs and the readout based on antiCD63-HRP antibody showed to be the more sensitive approach.

The calibration plots of exosomes previously purified by ultracentrifugation (ranged from 0 to 1 x 10^6 exosomes μL^{-1}, as determined by NTA) derived from MCF7 cell line and spiked in PBS buffer are shown in Fig. 5.4. Panel A shows comparatively the results for the electrochemical immunosensing of exosomes covalently immobilized on MPs and labelled by a direct (antiCD63-HRP) and indirect (antiCD63/antimouse-HRP) approach. The electrochemical responses for the exosomes-MPs, by the direct format in one-step incubation using antiCD63-HRP antibody showed an improved analytical performance, providing a limit of detection (LOD) of 65 exosomes μL^{-1} (r^2 = 0.9914), while in the case of the indirect format, a LOD of 70 exosomes μL^{-1} (r^2 = 0.9923) was achieved.

The performance of the immunomagnetic separation of exosomes based on the specific biomarker antibody (antiCDX-MPs, being CDX in this instance CD63 and CD24), followed by the electrochemical immunosensing using a general exosome biomarker (antiCD63-HRP antibody), is shown in Fig. 5.4, panel B. As previously discussed, this

format requires the coexistence of two biomarkers in the same exosomes. The signals were also fitted as above, obtained a LOD of 81 exosomes μL^{-1} (r^2 = 0.9967) when performing the IMS with the over expressed, general receptor (antiCD63-MPs) and 1550 exosomes μL^{-1} (r^2 = 0.9858) when using antiCD24-MPs, as expected. From the results, there is strong evidence that some biomarkers are not always present in all the exosomes population, as is the case of the specific receptors, being the general CD9, CD63 and CD81 receptors more likely to be found. These values represent an improvement over the LODs obtained by fluorescence (Zhao et al., 2016), electrochemical (Q. Zhou et al., 2016), and SPR-based microfluidic (Sina et al., 2016) devices, and almost equivalent to other approaches, such as rolling circle amplification (Huang et al., 2018) and microfluidic graphene oxide-based (Zhang et al., 2016) detection.

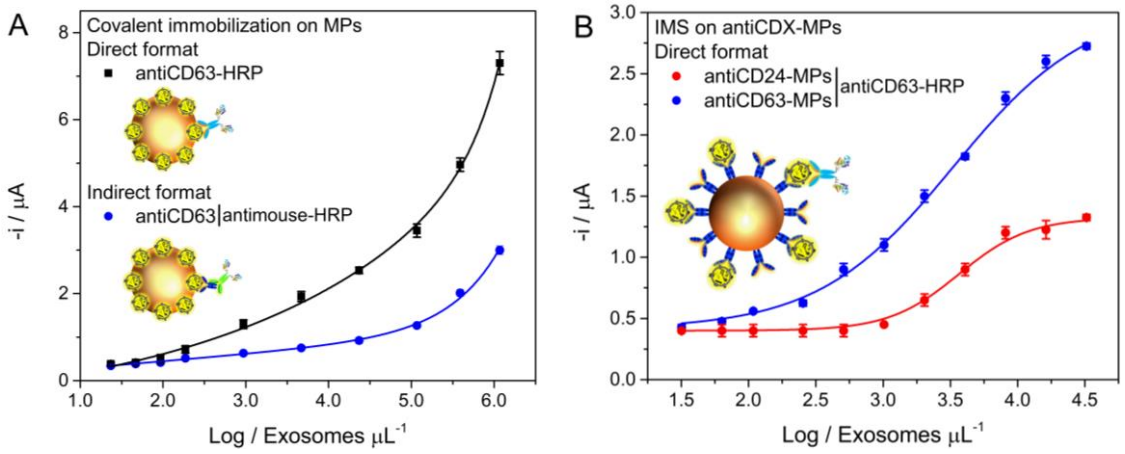

Fig. 5.4. Electrochemical immunosensor for detection of exosomes derived from MCF7 breast cancer cell line ranging from 0 to 1 x 10^6 exosomes μL^{-1} spiked in PBS buffer. (A) Covalent immobilization of the exosomes on MPs (exosomes-MPs), followed by indirect labeling with antiCD63 and by direct labeling with antiCD63-HRP antibody. (B) IMS of the exosomes on antiC24-MPs and antiCD63-MPs, followed by direct labeling with antiCD63-HRP antibody. The error bars show the SD for n = 3. The data were in all cases fitted with using a nonlinear regression (Four Parameter logistic Equation).

5.4.4. Electrochemical immunosensing of exosomes in human serum

The detection of exosomes in non-diluted human serum is critical for a routine clinical diagnosis, since it can suffer from interferences of free biomarkers. Fig. S5.7 shows the performance of the magneto-actuated electrochemical immunosensor evaluated by IMS of the exosomes on antiCD81-MPs and detection by cancer-related biomarkers (CD24 and CD340). The detection approach using antiCD24 and antiCD340 showed a detectable signal to exosomes spiked in non-diluted exosome-depleted human serum (Fig. S5.7, panel A). A LOD of 1.94 x 10^5 exosomes μL^{-1} (r^2 = 0.9879) and 1.02 x 10^6 exosomes μL^{-1} (r^2 = 0.9858) were obtained for CD24 and CD340 cancer-related

biomarkers, respectively. Nonetheless, the immunosensor for CD63 recognition, a LOD of 1.24 x 10^5 exosomes μL^{-1} (r^2 = 0.9901) was obtained with antiCD63-HRP (Fig. S5.7 panel B). These results demonstrate the good performance of the electrochemical immunosensor towards cancer-related exosomes and separated by IMS from non-diluted human serum samples, without any further pretreatment (such as ultracentrifugation).

5.4.5. Electrochemical immunosensing for the detection of serum-derived exosomes from breast cancer individuals

Finally, the biomarker expression of purified exosome from serum of healthy donors (n = 10, pooled) and breast cancer (n = 10, pooled) individuals were analyzed and compared, as shown in Fig. 5.5. It is important to highlight that the NTA counting as well as the protein content of exosomes in breast cancer population (n = 10) showed a 1.7-fold ($p < 0.05$) increase compared to healthy donors (n = 10) (Supp. Data). Accordingly, and in order to compare the expression of the receptors on exosomes from the two population, the electrochemical immunosensor was performed with the same amount (0.235 µg) of exosomal protein content per assay, for healthy donors and breast cancer individuals (n = 10, each). Fig. 5.5 panel A, shows the IMS of the exosomes on antiCD81-MPs, followed by indirect labeling with mouse antiCDX (CD24, CD44, CD326 and CD340 cancer-related biomarkers) and antimouse-HRP. A general overexpression of the cancer-related biomarkers in breast cancer individuals, when compared with healthy donors, is statistically demonstrated. The expression of CD24 biomarker on CD81-positive exosomes in healthy donors are higher (1.2-fold, $p < 0.05$) than the negative controls. In fact, the CD24 biomarker may also exist on the surface of the non-tumorigenic cells-derived exosomes, but at increased levels in cancer-related exosomes from various carcinomas, as previously reported (Tamkovich et al., 2018).

Fig. 5.5 panel B, shows the IMS of the exosomes on antiCDX-MPs (CD24 and CD340), followed by direct labeling with antiCD63-HRP antibody. As above, the background signal performed without exosomes is also shown. As expected, a discrimination (1.8-fold for CD24 and 1.6-fold for CD340, $p < 0.05$) between healthy donors and breast cancer individuals was achieved. This is related to a better approach using a general biomarker for IMS and over expressed biomarker for labeling, as discussed above in Fig. 5.3, panel C. These results are in agreement with previous literatures on cancer-related exosomes biomarkers in cancer and healthy donors (Grasso et al., 2015; Levva et al., 2017; Tamkovich et al., 2018). These findings provided

a good model for a further validation of the electrochemical immunosensor for the sensitive quantitative detection of specific cancer-related exosomes biomarkers in clinical samples.

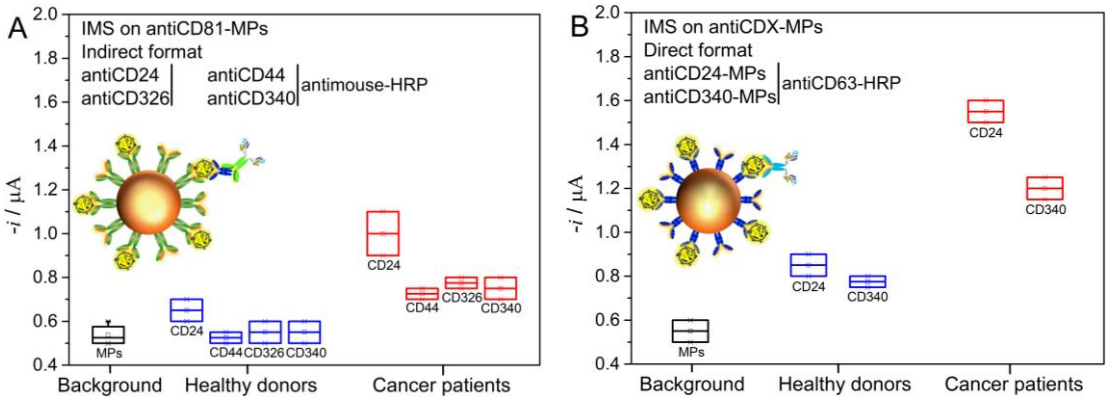

Fig. 5.5. Electrochemical immunosensing for detection of the purified exosomes derived from healthy donors (n = 10, pooled) and breast cancer (n = 10, pooled) individuals. (A) IMS of the exosomes (0.235 µg of protein per assay) on antiCD81-MPs, followed by indirect labeling with antiCD24, antiCD44, antiCD326 and antiCD340. (B) IMS of the exosomes (0.235 µg of protein per assay) on antiCD24-MPs and antiCD340-MPs, followed by direct labeling with antiCD63-HRP antibody. In all cases, the concentration of MPs was fixed in 1 x 10^6 MPs, 0.50 µg mL^{-1} of primary antibody, 0.08 ng mL^{-1} of antimouse-HRP and 1.24 µg mL^{-1} of antiCD63-HRP antibody. The error bars show the standard deviation for n = 3.

5.5. Conclusion

This work addresses the detection of exosomes by electrochemical immunosensing and the comprehensively study of the different formats in terms of the analytical performance. This study is mandatory in order to prevent the interference from free receptors in the matrix. To achieve that, in this work is proposed the use of IMS as a solid phase preconcentration method, in order to avoid the use of ultracentrifugation.

The electrochemical immunosensing of the exosomes in ultracentrifugated samples and based on general tetraspanin (for instance, CD63) can be used as an alternative method for the total count of purified exosomes, achieving LODs less than 100 exosomes μL^{-1}. Either the covalent immobilization or the IMS of the exosomes on the MPs provided comparable results in terms of LODs. Furthermore, the electrochemical immunosensor is able to reach a LOD of 10^5 exosomes μL^{-1} directly in human serum, when performing the IMS with antiCD81 modified magnetic particles. It seems that the separation based on antiCD81 antibody is less affected by the presence of free receptor on the samples, avoiding the need of ultracentrifugation to separate proteins from vesicles.

Finally, the approach based on IMS followed by electrochemical detection was study for the detection of purified exosomes from serum of breast cancer individuals. In

this approach, it is mandatory the coexistence of two receptors in the exosome, the first one for the IMS while the second one for the labelling. Two formats were assayed, combining general and cancer-related biomarkers. The combined used of IMS (based on a specific cancer receptor as CD24 and CD340) followed by the detection based on an overexpressed general receptor (as CD63) provided the improved results in terms of sensitivity, being able to clearly distinguish among healthy donors and breast cancer individuals.

In addition, it is important to conclude that exosomes are promising biomarkers for the detection of breast cancer if combined with emerging technologies such as electrochemical biosensors. However, the main drawback of exosomes as a biomarker, even if determined with the best current technologies, remains the need of single-vesicle level characterization with little or no sample preparation, in order to evaluate the rich information contained within exosome subpopulations. This is due to the high variability in the expression of the receptors. This fact is confirmed by our study, since differences in the expression were observed from the exosomes derived from the three breast cancer cell lines.

Despite this, the electrochemical immunosensor offers an exciting alternative, especially in resource-scarce settings, as rapid, cost-effective devices that can be handled for unskilled personnel at the community and primary care level. Future experiments will be focused on the study of a higher number of individually anonymized samples (instead of pooled) to validate these preliminary results.

5.6. Supplementary Data

5.6.1. Chemicals and biochemicals

Magnetic particles (Dynabeads® M450 Tosylactivated, nº 14013, 4,5 μm diameter) were purchased from Thermo Fisher. The antibodies are summarized in Table S5.1.

Pierce™ TMB Substrate Kit (Ref. 34021) was purchased from Thermo Fisher. The 10 mmol L^{-1} phosphate-buffered saline (PBS) buffer solution (pH 7.5) and boric acid buffer solution (pH 8.5) were prepared with ultrapure water and all other reagents were in analytical reagent grade (supplied from Sigma Aldrich).

Table S5.1. Summary of the antibodies used in this work.

Antibody	Target	Clonality	Conjugate	Host	Reference	Commercial source	Use/s
antiCD24	CD24	monoclonal	no	mouse	ab76514	Abcam	1, 2, 3
antiCD54	CD54	monoclonal	no	mouse	ab2213	Abcam	1, 2, 3
antiCD326	CD326	monoclonal	no	mouse	ab7504	Abcam	1, 2, 3
antiCD340	CD340	monoclonal	no	mouse	Ab30	Abcam	1, 2, 3
antiCD9	CD9	monoclonal	no	mouse	10626D	Thermo Fisher	1, 2, 3
antiCD63	CD63	monoclonal	no	mouse	10628D	Thermo Fisher	1, 2, 3
antiCD81	CD81	monoclonal	no	mouse	10630D	Thermo Fisher	1, 2, 3
antiCD44	CD81	monoclonal	no	mouse	BMS113	eBioscience	1, 2, 3
antiCD81	CD81	polyclonal	no	rabbit	HPA007234	Sigma-Aldrich	1, 2, 3
antimouse-HRP	mouse IgG H&L	polyclonal	HRP	rabbit	ab6728	Abcam	4
antimouse-Cy5	mouse IgG H&L	polyclonal	Cy5®	rabbit	ab97037	Abcam	5
antiCD63-HRP	CD63	monoclonal	HRP	mouse	NBP2-42225H-100	BioNova	6

Uses: (1) Immunomagnetic separation when attached to tosylactivated magnetic particles. (2) Indirect labeling in electrochemical immunosensing, as primary antibody. (3) Indirect labeling in confocal microscopy, as primary antibody. (4) Indirect labeling in electrochemical immunosensing, as secondary antibody. (5) Indirect labeling in confocal microscopy, as secondary antibody. (6) Direct labeling in electrochemical immunosensing, as secondary antibody.

5.6.2. Cell culture

Breast cancer cell lines were the following: MCF7 (ATCC® HTB-22™), MDA-MB-231 (ATCC® CRM-HTB-26™) and SKBr3 (ATCC® HTB-30™). Expansion of cell population was carried out from 1,000,000 cell in T-175 flask containing 32 mL of Dulbecco's Modified Eagle Medium (DMEM) (Ref. 31966047, Thermo Fisher), supplemented with 10% exosome-depleted fetal bovine serum (FBS) (Ref. 12007C, Sigma-Aldrich), 100 U mL^{-1} penicillin-streptomycin (Ref. 15140122, Thermo Fisher). The temperature was maintained at 37 °C in humidified, concentrated CO_2 (5%) atmosphere. Once cells reached approximately 95% confluence on T-175 flask, the culture medium was removed and immediately centrifuged (300 *g* for 10 minutes, 2,000 *g* for 10 minutes and 10,000 *g* for 30 minutes), and stored at -80 ºC until to exosome isolation.

5.6.3. Human serum treatment

The human serum samples were separated from the blood cells using a sterile empty tube without any anticoagulant, leave the tube in a standing position for about 20-30 minutes for blood to be clotted. After that, centrifugation at 1.500 g (20 ºC) for 10 minutes was carried out for removal of residual cells and cellular debris. Following, the human serum (supernatant on top) was carefully removed, stored at -80 ºC for further assays.

5.6.4. Exosome isolation and purification

Exosomes were purified according to Théry.[1] The supernatant from MCF7, MDA-MB-231, SKBr3 breast cancer cell lines and human serum were subjected to differential centrifugation as follow: 300 *g* for 10 minutes (removal of residual cells), 2,000 *g* for 10 minutes and 10,000 *g* for 30 minutes (removal of cellular debris). Then, a Beckman Coulter Optima™ L-80XP Ultracentrifuge at 100,000 *g* for 60 minutes with a 70Ti rotor to pellet exosomes. After that, the supernatant was carefully removed, and crude exosome-containing pellets were resuspended in 1 mL of 10 mmol L^{-1} phosphate-buffered saline (PBS) solution and pooled. A second round of same ultracentrifugation setting was carried out, and the resulting exosome pellet resuspended in 500 µL (per 100 mL of supernatant) of 10 mmol L^{-1} PBS buffer solution (0.22 µm filtrated and sterile) and storage at -80 °C. All centrifugation steps performed at a temperature of 4 °C.

5.6.5. Exosome-depleted human serum

The exosome-depleted human serum was used for several matrix effect studies. The depletion of exosomes in human serum was performed according to Théry (Théry et al., 2006). The whole human serum from healthy individuals were subjected to differential centrifugation as follow: 300 *g* for 10 minutes (removal of residual cells), 2,000 *g* for 10 minutes and 10,000 *g* for 30 minutes (removal of cellular debris). Then, a Beckman Coulter Optima™ L-80XP Ultracentrifuge at 100,000 *g* for 60 minutes with a 70Ti rotor to pellet exosomes. After that, the supernatant was carefully removed, and storage at -80 °C. This exosome- depleted human serum was used in further assays. All centrifugation steps performed at a temperature of 4 °C.

5.6.6. Exosome protein quantification

The exosomes protein content was determined by using Pierce™ BCA Protein Assay Kit (Ref. 23227, Thermo Fisher), following the protocol. Prior to protein quantification, all exosomes resuspended in PBS were lysed by adding an equal volume of RIPA buffer (Sigma Aldrich) and cOmplete™, Mini, EDTA-free Protease Inhibitor Cocktail™ (Roche), followed by incubation at room temperature for 5 min and sonicated for 15 seconds.

5.6.7. Covalent immobilization on magnetic particles

Dynabeads® M450 tosylactivated superparamagnetic particles (MPs, 4.5 μm in diameter) has a core of iron oxide salt encapsulated by a polystyrene polymer, which has a polyurethane external layer with the p-toluenesulfonate group (Xu et al., 2012). It is a good leaving group, which allows an S_N2 reaction to occur in the presence of a nucleophile (Cahiez et al., 2012; Hoogenboom et al., 2010). A nucleophilic reaction by an antibody, protein, peptide, or glycoprotein removes and replaces the sulfonyl ester groups from the polyurethane layer.

Immobilization of exosomes. The immobilization of exosomes on Dynabeads® M450 tosylactivated superparamagnetic particles (MPs) (Fig. S5.1, panel A) were performed as follows: 3.5 x 10^{10} exosomes were added to 40 μL (1.6 x 10^7 MPs) Dynabeads® M450 tosylactivated. The reaction kinetics were increased by adding 0.1 mol L^{-1} borate buffer pH 8.5, in order to ensure the nucleophilic reaction by the amine group. The incubation step was performed overnight with gentle shaking at 4 ºC. After that, 0.5 mol L^{-1} glycine solution was added to ensure the blocking of the any remaining tosylactivated groups, by incubation for 2 h at 25 ºC. After that, the exosome-modified magnetic particles (exosomes-MP) were resuspended in 160 μL of 10 mmol L^{-1} PBS buffer solution in order to achieve 1 x 10^6 MPs per 10 μL. The calibration plots were performed by using 1 x 10^6 MPs per well plate and the amount of exosomes ranging from 3.9 x 10^4 to 2 x 10^7 exosomes μL^{-1}.

Immobilization of antibodies. The different specific antibody (15 μg mL^{-1}, previously optimized (antiCD9, antiCD24, antiCD44, antiCD54, antiCD63, antiCD81, antiCD326 or antiCD340) was added to 55 μL (2.2 x 10^7 MPs) Dynabeads® M450 tosylactivated (Fig. S5.1, panel B). The reaction kinetics were increased by adding 0.1 mol L^{-1} borate buffer pH 8.5. The incubation step was performed overnight with gentle shaking at 37 ºC. After that, a blocking step with 0.5 mol L^{-1} glycine solution was performed for 2 h to ensure the blocking of the any remaining tosylactivated groups. After

that, the antibody-modified MPs (herein, antiCDX-MPs, where antiCDX = antiCD9, antiCD24, antiCD44, antiCD54, antiCD63, antiCD81, antiCD326 or antiCD340) were resuspended in 220 µL (10 µL per well to give 1 x 10^6 particles per well) 10 mmol L^{-1} PBS buffer. It was not possible to immobilize CD326 satisfactorily on MPs.

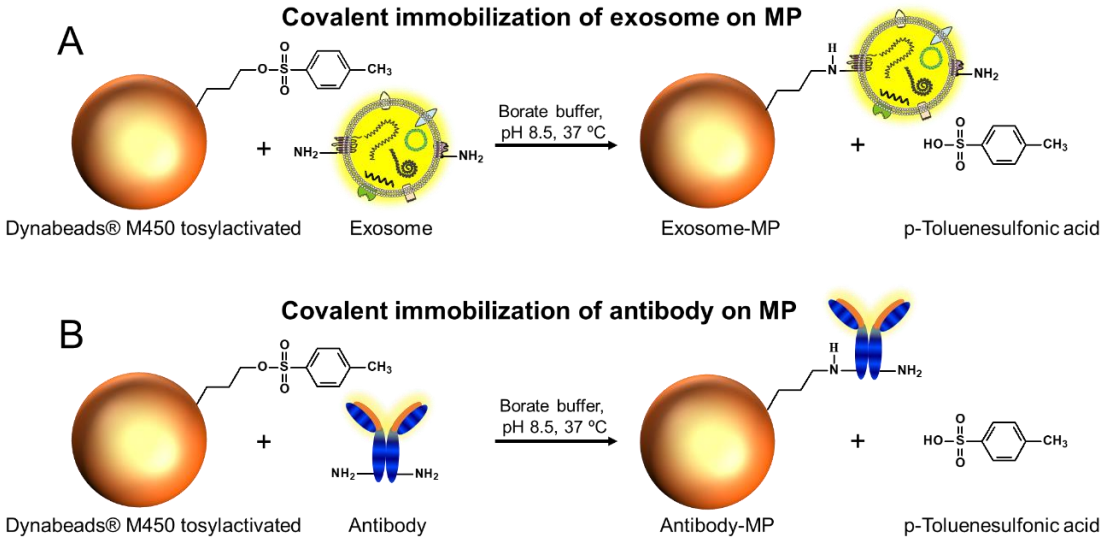

Fig. S5.1. Covalent immobilization of (A) exosome or (B) antibody on Dynabeads® M450 tosylactivated. Two different approaches were used, as depicted in Fig. S5.1. The first one involves the direct covalent immobilization of exosomes on magnetic particles (Fig. S5.1, panel A). The second approach is based on the covalent immobilization of the antibodies for a further immunomagnetic separation (IMS) of exosomes (Fig. S5.1, panel B).

5.6.8. Electrochemical immunosensing of exosomes covalently immobilized on magnetic particles

Direct format. The magneto-actuated electrochemical immunosensing (Fig. S5.2, panel A) was performed in tubes and involved the following steps: (i) Direct labeling. The exosomes-MPs (containing 1 x 10^6 MPs per well, with an amount of exosomes covalently immobilized from 0 to up to 2 x 10^9 exosomes per well) and a mouse monoclonal antibody to CD63 with horseradish peroxidase (HRP) (herein, antiCD63-HRP) (100 µL, 1.24 µg mL^{-1}), were simultaneously incubated for 30 min with shaking at 25 °C, followed by three washing steps with PBS containing 0.5% BSA. (ii) Electrochemical readout.

Electrochemical readout. The modified MPs were separated by using a magnet tube separator, a MPs pellet on the bottom tube is formed, followed by remove of the supernatant. Following, MPs pellet is resuspended in PBS buffer solution and a magneto-actuated graphite-epoxy composite electrode (m-GEC) is inserted into tube for remove the MPs pellet onto m-GEC surface, which is transferred into an electrochemical cell and measured by means of amperometry at -0.1 V *vs.* Ag/AgCl/$KCl_{(satd.)}$ by using

hydroquinone mediator. For that, a standard one compartment three-electrode electrochemical cell is filling with 19.8 mL of 100 mmol L^{-1} PBS containing 100 mmol L^{-1} KCl (pH 7.0), then, 100 µL of 400 mmol L^{-1} hydroquinone (HQ) mediator is added, with subsequent 100 µL of 400 mmol L^{-1} H_2O_2. A reproducible steady-current is obtained after 60 s (see Fig. S5.4, panel D, Supp. Data). The current generated by monitoring benzoquinone species (the reaction is described in Fig. S5.4) is associated with the amount of captured exosomes. The m-GEC surface cleaning procedure was carried out for every experiment by electrochemical treatment by applying a potential of +3 V for 5 s in 0.5 mol L^{-1} H_2SO_4 supporting electrolyte. More details are given in Fig. S5.4, Supp. Data.

The dilution optimizations of primary and secondary antibodies, the sequence of incubation steps, as well as the number of MPs per assay were previously optimized.

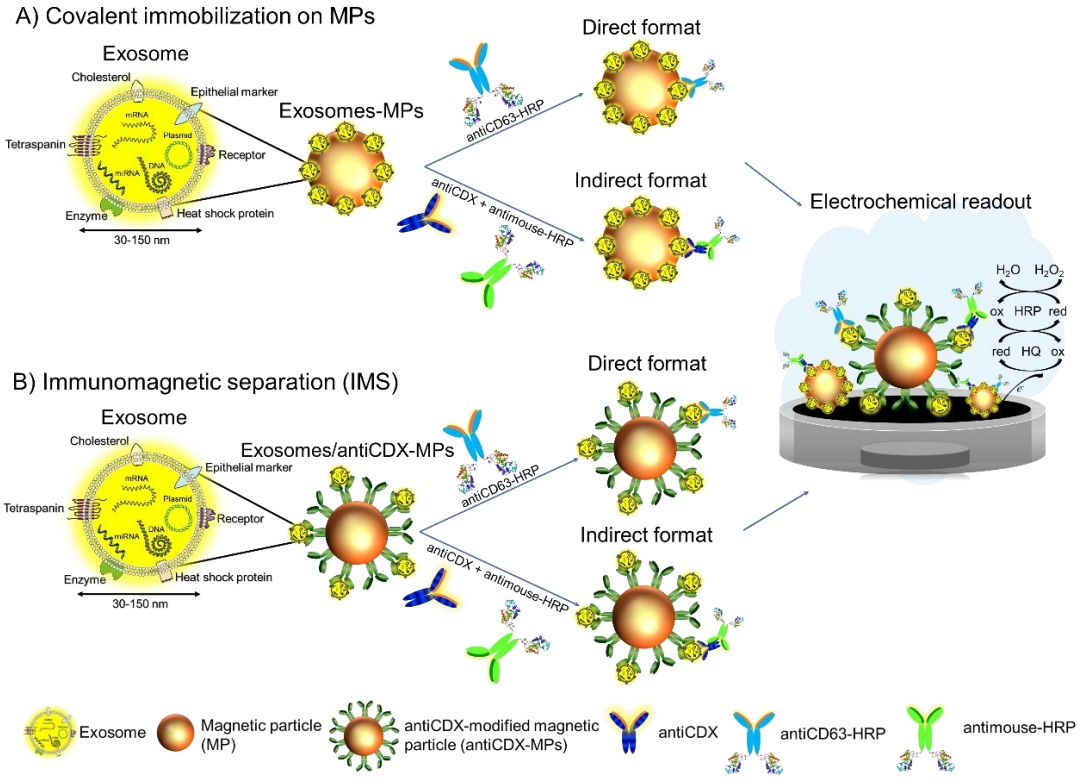

Fig. S5.2. Strategies for the detection of exosomes by electrochemical immunosensing in different formats. (A) Electrochemical immunosensing of exosomes covalently immobilized on magnetic particles (exosomes-MPs), performed by i) direct labeling (with antiCD63-HRP, 1.24 µg mL^{-1}) or, instead, ii) indirect labeling (with antiCDX antibody, 0.50 µg mL^{-1}) following by incubation with antimouse-HRP antibody (0.08 ng mL^{-1}) (B) Immunomagnetic separation of exosomes and electrochemical immunosensing in direct and indirect format. For the i) direct format, the IMS is performed with antiCDX-MPs, followed by the direct labeling with antiCD63-HRP (1.24 µg mL^{-1}); for the ii) indirect format, the IMS is performed with antiCD81-MPs, followed by the indirect labeling with antiCDX (mouse) antibody and an antimouse-HRP antibody. In all cases, antiCDX was an antibody towards CD9, CD24, CD44, CD54, CD63, CD81 or CD340 biomarkers. The concentration was fixed in 1×10^6 for the MPs.

Indirect format. The magneto-actuated electrochemical immunosensing (Fig. S5.2, panel A) was performed in tubes and involved the following steps: (i) incubation of the exosomes-MPs with the antiCDX mouse monoclonal antibodies. The exosomes-MPs (containing 1 x 10^6 MPs per well, with an amount of exosomes covalently immobilized from 0 to up to 2 x 10^9 exosomes per well) and the antiCDX antibody (100 µL, 0.50 µg mL^{-1}) (being CDX any of CD9, CD24, CD44, CD54, CD63, CD81, CD326 or CD340 biomarkers), were simultaneously incubated for 30 min with shaking at 25 °C, followed by three washing steps with PBS containing 0.5% BSA. (ii) Indirect labeling. The modified-MPs were incubated with antimouse-HRP antibody (100 µL, 0.08 ng mL^{-1}) for 30 min with shaking at 25 °C, followed by three washing steps with PBS containing 0.5% BSA. (iii) Electrochemical readout, as described above.

5.6.9. Immunomagnetic separation of exosomes and electrochemical immunosensing

Direct format. The magneto-actuated electrochemical immunosensing (Fig. S5.2, panel B) was performed in tubes and involved the following steps: i) IMS of the exosomes with antiCDX-MPs. The antiCDX-MPs (being CDX any of CD9, CD24, CD44, CD54, CD63, CD81, CD326 or CD340 biomarkers) (containing 1 × 10^6 antiCDX MPs per well) and the exosomes (100 µL, ranging from 0 to 2 x 10^9 exosomes per well), were simultaneously incubated for 30 min with shaking at 25 °C, followed by three washing steps with PBS containing 0.5% BSA. ii) Direct labeling. The modified-MPs were incubated with the antiCD63-HRP antibody (100 µL, 1.24 µg mL^{-1}) for 30 min with shaking at 25 °C, followed by three washing steps with PBS containing 0.5% BSA. (iii) Electrochemical readout, as described above.

Indirect format. The magneto-actuated electrochemical immunosensing (Fig. S5.2, panel B) was performed in tubes and involved the following steps: i) IMS of the exosomes with antiCD81-MPs (rabbit) (containing 1 × 10^6 antiCD81-MPs per well) and the exosomes (100 µL, ranging from 0 to 2 x 10^9 exosomes per well), were simultaneously incubated for 30 min with shaking at 25 °C, followed by three washing steps with PBS containing 0.5% BSA. (ii) incubation with the antiCDX mouse monoclonal antibodies (100 µL, 0.50 µg mL^{-1}) (being CDX any of CD9, CD24, CD44, CD54, CD63, CD81, CD326 or CD340 biomarkers), were simultaneously incubated for 30 min with shaking at 25 °C, followed by three washing steps with PBS containing 0.5% BSA. (iii) Indirect labeling. The modified-MPs were incubated with antimouse-HRP antibody (100 µL, 0.08 ng mL^{-1}) for 30 min with shaking at 25 °C, followed by three washing steps with PBS containing 0.5% BSA. (iv) Electrochemical readout, as described above.

5.6.10. Electrochemical immunosensor of serum-derived exosomes from breast cancer individuals

Blood samples from healthy female donors (n = 10, mean age 35/SD 5 years) and breast cancer female individuals (n = 10, stage IV, mean age 50/SD 6 years) were obtained from the Hospital del Mar, Barcelona, Spain. The work was carried out in accordance with the principles of voluntariness and confidentiality. The preparation of the human serum from blood was detailed above. The samples n = 10 each were pooled in two batches (healthy and breast cancer donors) by mixing 500 µL of each, and the exosomes were purified by ultracentrifugation, as previously described above.

5.6.11. Magneto-actuated graphite-epoxy composite (m-GEC) electrode

Construction

The construction of the electrode for the magnetic actuation is already well known and previously characterized.

The body of the electrodes consisted of a female electric connector with a metal league end of 2 mm diameter where a copper disk of 5.9 mm of diameter was welded at the end by using solder wire (tungsten), as schematically depicted in Fig. S5.3. Before welding the copper disk, it was cleaned by dipping in milli-Q water:HNO_3 (1:1) solution for a few seconds in order to remove the copper oxide formed that can increase the electric current resistance reducing thus the sensitivity of the transducer. This connector was set inside a cylindrical PVC tube of 6 mm i.d., 8 mm o.d. and 22 mm long using a hammer. A gap with a depth of 2 mm was thus obtained in the end of the electrode basis. The graphite-epoxy composite (GEC) paste (Pividori and Alegret, 2003) was prepared by hand mixing the epoxy resin and the hardener at a 20:3 (w/w) ratio, according to the manufacturer. When the resin and hardener were will mixed, the graphite powder was added in 1:4 (w/w) ratio. The resulting past was softly mixed thoroughly again until it became homogeneous (approximately 30 minutes). Once the paste was homogeneous, a thin layer of the resulting soft paste was placed in the gap of the PVC cylindrical basis (1st GEC layer), which has the electrical contact to a depth of 2 mm, to isolate the copper disc. A 3-mm diameter neodymium magnet was placed in the center and further filling and tight packaging of the gap with the soft GEC past was done (2nd GEC layer). After the construction, the magneto electrodes based on the graphite-epoxy composite (m-GEC) were cured at 80 °C for one week until the paste become completely rigid. After curing, the m-GEC was polished to uniform the surface.

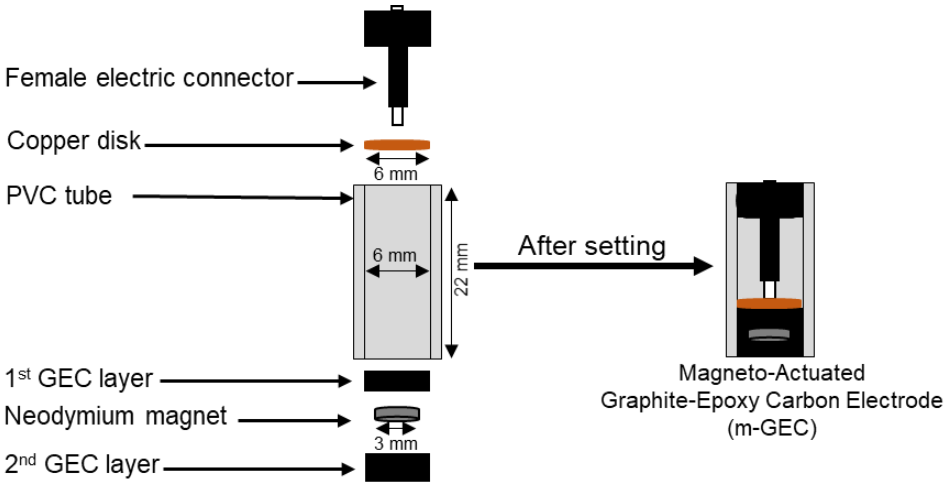

Fig. S5.3. Schematic representation of the construction of cylindrical magneto-actuated electrode based on rigid composites (m-GEC).

Characterization

Fig. S5.4, panel A shows the cyclic voltammetry in 2 mmol L^{-1} hydroquinone solution in 100 mmol L^{-1} PBS containing 100 mmol L^{-1} KCl (pH 7.0), obtained at 50 mV s^{-1} scan rate and -0.30 to 0.80 V potential window. In the forward anodic scan, no faradaic process is observed up to 0.0 V; above this potential, the oxidation of hydroquinone takes place, with maximum diffusion current reached at 0.18 V. In the reverse scan, cathodic current peak is evident at 0.0 V. From the second cycle on, the current peaks remain almost constant, which suggests a high stability of m-GEC electrode surface. After voltammetric cycling, hydroquinone/benzoquinone were strongly adhered on the m-GEC electrode surface by fouling, which needs to be renewed.

Carbon-based composite electrodes which have an intrinsic porous structure are susceptible the strong adsorption of organic molecules. To overcome this drawback, the electrode needs to be renewed after each experiment. The m-GEC electrode surface can be easily renewed by a simple electrochemical procedure. The electrode surface was submitted before each experiment to an electrochemical treatment, applying a potential of +3 V for 5 s, in 0.5 mol L^{-1} H_2SO_4 supporting electrolyte. Fig. S5.4, panel B shows the cyclic voltammograms of the cleaning treatment of the m-GEC electrode surface. As expected, the redox couple around 0.09 V attributed to hydroquinone oxidation is not observed. Negligible residual current is measured around 0.5 V, which is attributed to hydroquinone by-products. To evaluate the performance of the electrochemical cleaning procedure to renew the m-GEC electrode surface, cyclic voltammograms were performed in 2 mmol L^{-1} hydroquinone solution in 100 mmol L^{-1}

PBS containing 100 mmol L^{-1} KCl (pH 7.0). Fig. S5.4 panel C demonstrate that, without the electrochemical treatment, there was a decrease in the current and a shift of the redox potential. On the other hand, the current after the cleaning treatment was recovered to the initial current, as in Fig. S5.4, panel A. These results confirm the efficiency of the rapid electrochemical cleaning treatment. To confirm this, the active electrochemical surface area was calculated using the Randles-Sevcik equation (Eq. 1) for totally reversible charge transfer (Bard and Faulkner, 2001):

$$i_p = 2.68\ x\ 10^5 n^{3/2} A C_{bulk} D^{1/2} v^{1/2} \quad \text{(Eq. 1)}$$

where n is the number of electron equivalent exchanged involved in the charge-transfer step, A (cm^2) is the active area of the working electrode, D ($cm^2\ s^{-1}$) and C_{bulk} (mol cm^{-3}) are the diffusion coefficient and the bulk concentration of the electroactive species, respectively; v is the voltage scan rate ($V\ s^{-1}$).

The linear relationship of i_p vs. $v^{1/2}$ provide evidence for a chemically reversible redox process, where the known bulk concentration, electron transfer to be two and diffusion coefficient D_{HQ} = 3.42/SD 0.05 x 10^{-5} $cm^2\ s^{-1}$ (Salazar et al., 2015), it is possible to determine the active electrochemical surface area. The active electrochemical surface area for m-GEC before and after the cleaning by electrochemical polishing was found to be 0.63 (s = 0.01) cm^2 and 0.61 (s = 0.01) cm^2, respectively. The active electrochemical surface area showed a deviation of 3.17%, which demonstrate a good renewal of the m-GEC surface by electrochemical cleaning procedure. It is important to highlight that after the first electrochemical cleaning, the active area remains the same value of 0.61 (s = 0.01) cm^2.

5.6.12. Electrochemical readout based on enzymatic labeling

The performance of the electrode was also evaluated for electrochemical immunosensing based on an enzymatic labeling system. Horseradish peroxidase (HRP) is one of the most extensively label enzymes for the electrochemical biosensors. It contains heme as a prosthetic group, which is the protein active site, along with the heme iron Fe(III) (Ahammad, 2012). The direct electron transfer between HRP and an electrode is difficult because the active sites of HRP are deeply buried in a thick protein shell, and because the large distance between the active sites and the electrode surface will slow down the electron transfer (Ahammad, 2012). Therefore, hydrogen donors are used for facilitating the electron transfer between the redox centers of the enzyme and electrode surface.

Hydroquinone was used as mediator to the electron transfer of HRP used as enzymatic label on an immunosensor based on m-GEC electrode, which was monitored by chronoamperometric measurements. Fig. S5.4 panel D shows the chronoamperograms behavior in 100 mmol L^{-1} PBS containing 100 mmol L^{-1} KCl supporting electrolyte in the presence of 2 mmol L^{-1} hydrogen peroxide, 2 mmol L^{-1} hydroquinone and HRP enzyme label, applying a potential of -0.10 V vs. $Ag/AgCl_{(sat.)}$.

It is observed that in the presence of hydrogen peroxide, the reaction mechanism of the hydroquinone mediator based on the HRP enzyme label generates an increase in the cathodic current. Briefly, hydrogen peroxide in the solution is reduced by the HRP. Then the reduced HRP is regenerated with the aid of the mediator, while the mediator itself is oxidized in the enzymatic reaction.

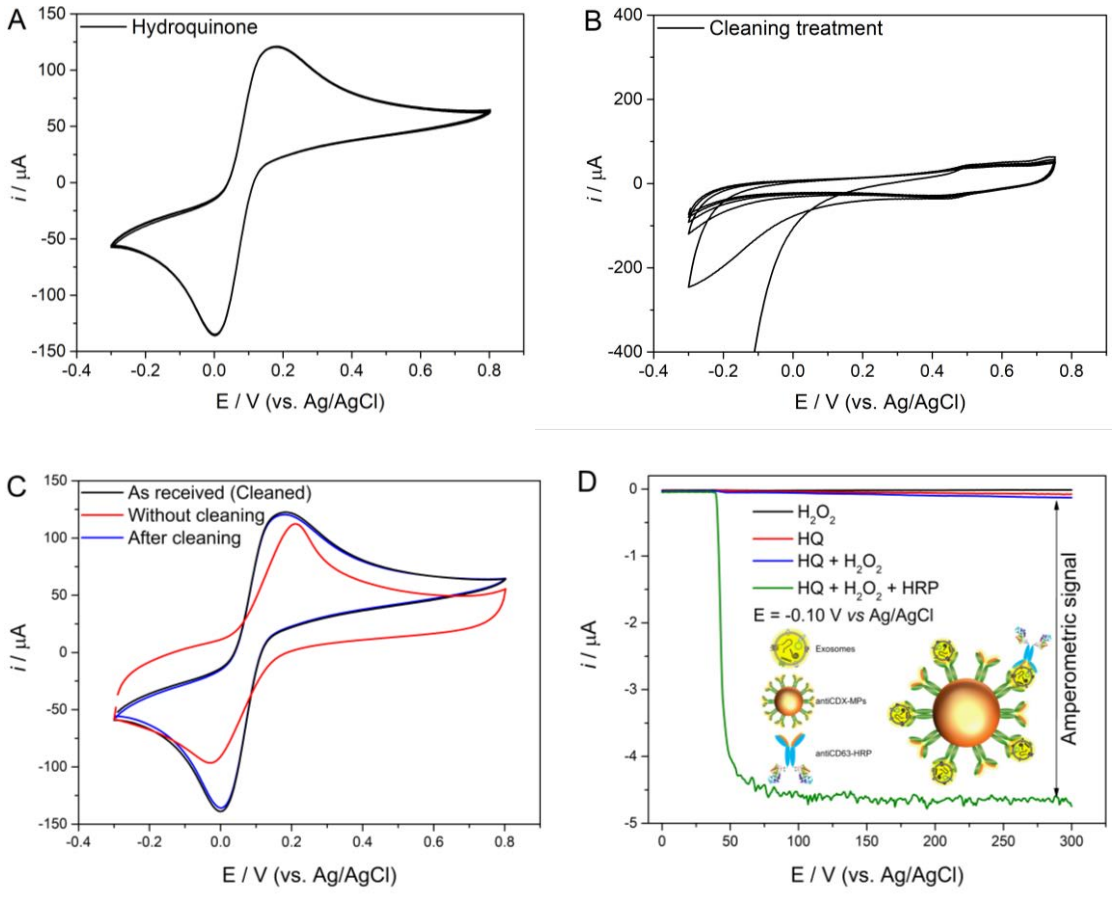

Fig. S5.4. (A) Voltammograms of 2 mmol L^{-1} hydroquinone solution (obtained at 50 mV s^{-1} scan rate) in 100 mmol L^{-1} PBS containing 100 mmol L^{-1} KCl supporting electrolyte (pH 7.0). (B) Voltammograms of electrochemical polishing treatment (obtained at 100 mV s^{-1} scan rate), after applying a potential of +3.0 V for 5 s, in 0.5 mol L^{-1} H_2SO_4 supporting electrolyte. (C) Voltammograms of 2 mmol L^{-1} hydroquinone solution (obtained at 50 mV s^{-1} scan rate) in 100 mmol L^{-1} PBS containing 100 mmol L^{-1} KCl supporting electrolyte (pH 7.0), using m-GEC electrode as received, without and after the electrochemical cleaning polishing. (D) Chronoamperograms behavior in 100 mmol L^{-1} PBS containing 100 mmol L^{-1} KCl supporting electrolyte in the presence of 2 mmol L^{-1} hydrogen peroxide, 2 mmol L^{-1} hydroquinone and HRP as enzymatic label for an immunosensor, applying a potential of -0.10 V vs. $Ag/AgCl_{(sat.)}$. A single m-GEC electrode was used in all experiments.

Finally, the oxidized mediator is electrochemically reduced on the electrode, leading to an increase in the reduction current, as schematically shown in Fig. S5.4 panel D. In the specific case of Fig. S5.4 panel D, antiCD9-MPs (1 x 10^6 MPs) were used for IMS of exosomes (4 x 10^9 exosomes), which were subsequently labeled with antiCD63-HRP (1.24 µg mL^{-1}). Thus, the electrochemical readout was performed as described above. Hydroquinone as a mediator, the current generated by monitoring benzoquinone is associated with the amount of immunocaptured exosomes. A reproducible steady-current is obtained after 60 s and used for exosomes calibration curve.

5.6.13. Characterization of exosomes by nanoparticle tracking analysis

An estimation of the size diameter distribution of purified exosomes derived from MCF-7 breast cancer cell line was performed by NTA (Fig. S5.5). A size from 50 to 300 nm (considering 95.4% of a Gaussian distribution), but with dominance around 105 and 153 nm (60 and 34% of counted particles, respectively) was obtained for the MCF-7 exosomes. Similar results were obtained for exosomes derived from other breast cancer cell lines (MDA-MB-231 and SKBr3).

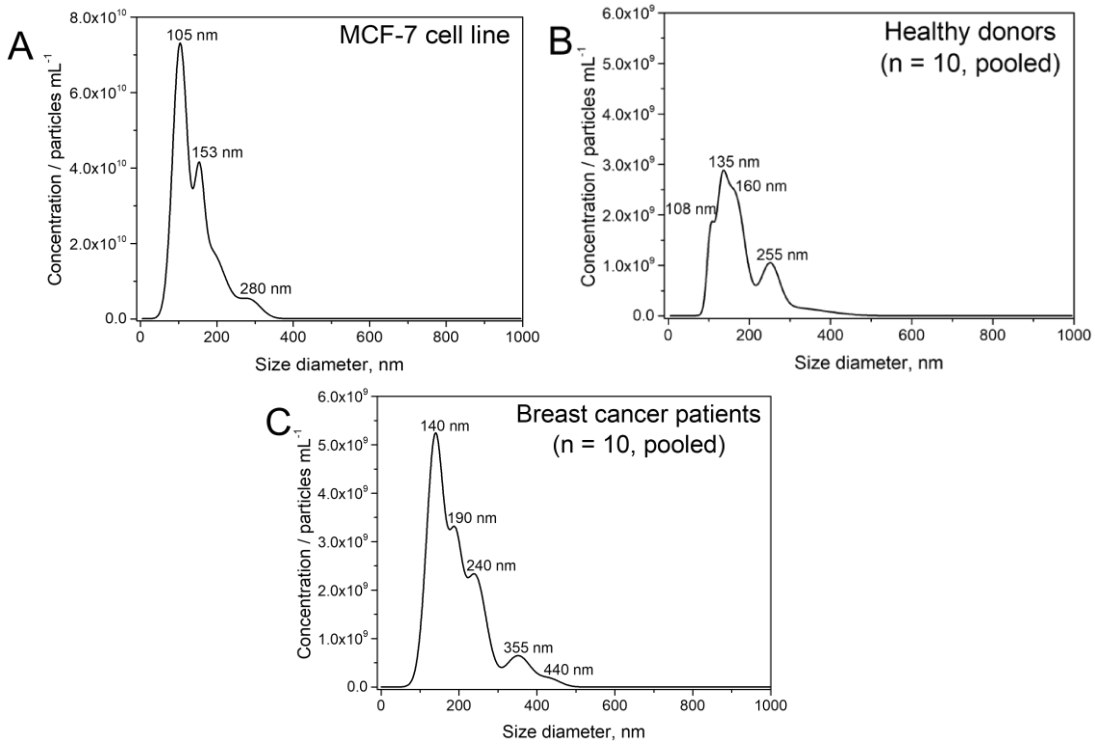

Fig. S5.5. Characterization by NTA of purified exosomes-derived from MCF7 breast cancer cell line (panel A). The NTAs for exosomes purified from serum of healthy donors and breast cancer individuals (n = 10, each) are also shown in Panels B and C, respectively). Nanosight NTA Software analyzed raw data videos by triplicate during 60 s with 50 frames per second and the temperature of the laser unit set at 24.8 ºC.

Fig. S5.5 also show the results for exosomes purified from serum of healthy donors and breast cancer individuals. In this instance, the exosomes obtained from healthy donors ranges from 40 nm to up to 400 nm (considering 95.4% of a Gaussian distribution), showing a more heterogeneous distribution pattern (with peaks in 115, 147, 196, 240 and 295 nm). The concentration was estimated to be 3.87 x 10^{10} (SD 9.72 x 108 mL^{-1}). For the serum exosomes from breast cancer individuals (n = 10), similar heterogeneous distribution was observed, with main peaks in 118, 150, 205, 300 and 460 nm. Moreover, the concentration was estimated to be 6.49 x 10^{10} (SD 4.21 x 10^{8} particles mL^{-1}). Fig. 5.1, panels A, B and C shows comparatively the TEM images of exosomes derived from MCF-7 breast cancer cell line, and serum exosomes of cancer and healthy donors.

5.6.14. Confocal microscopy of breast cancer cell lines

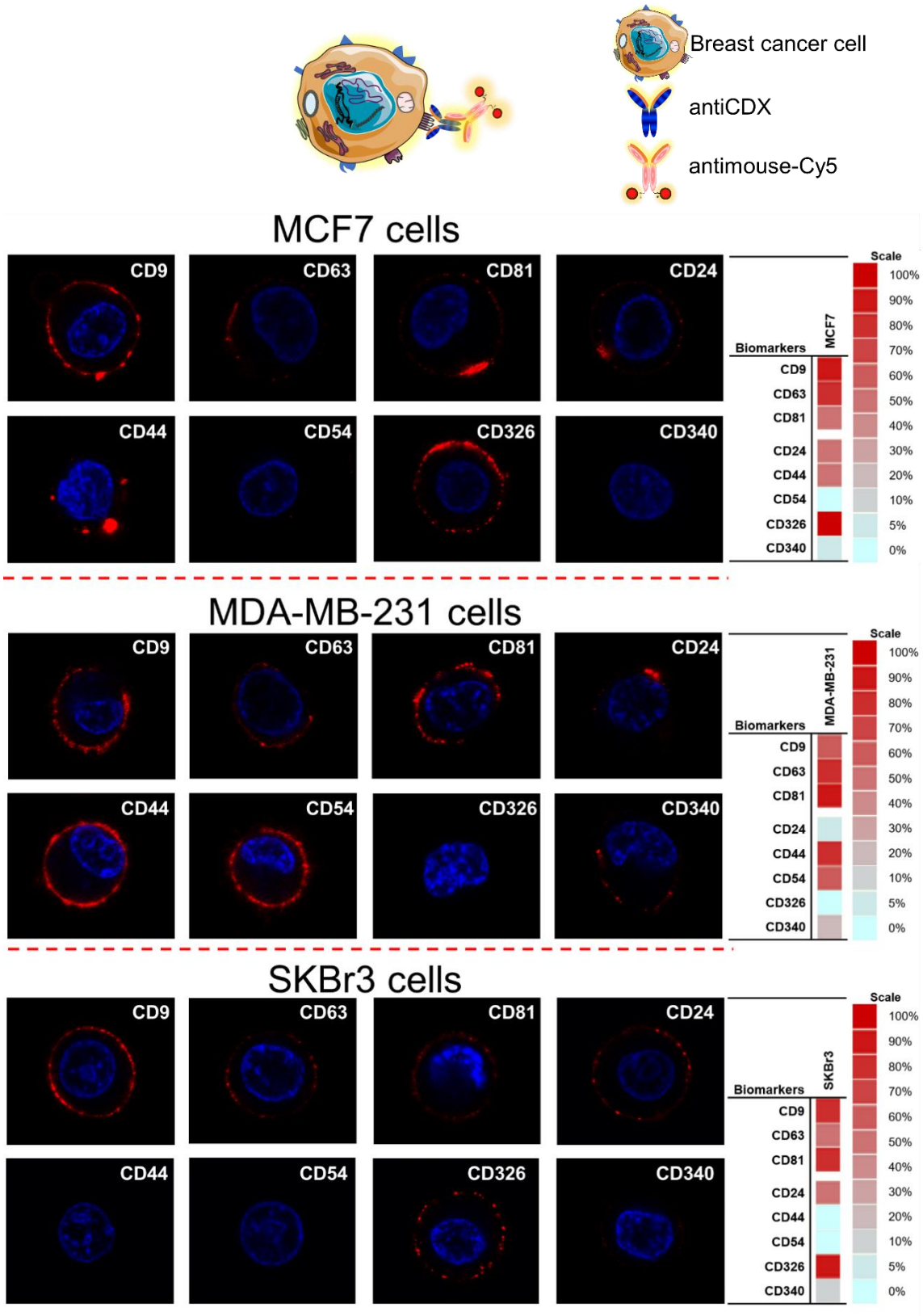

Fig. S5.6. Confocal microscopy to evaluate the expression of CD9, CD24, CD44, CD54, CD63, CD81, CD326 and CD340 membrane protein receptors on the MCF7, MDA-MB-231 and SKBr3 breast cancer cell lines. Cell nucleus appears stained in blue while the membrane protein receptors, in red, representing a positive expression on the membrane of the cells. In all cases, the primary antibody was 5 μg mL^{-1} and 2 μg mL^{-1} of antimouse-Cy5 antibody.

5.6.15. Electrochemical immunosensor in human serum

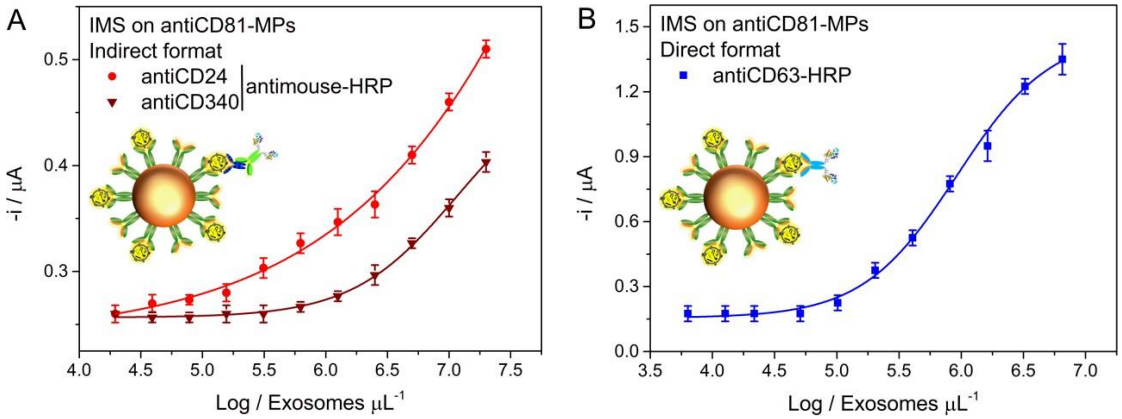

Fig. S5.7. Electrochemical immunosensor for the detection of exosomes derived from SKBr3 breast cancer cell line ranging from 3.9 x 10^4 to 2 x 10^7 exosomes μL^{-1} spiked in exosome-depleted human serum. IMS of the exosomes on antiCD81-MPs, followed by (A) indirect labelling with (●) antiCD24 and (▼) antiCD340, and by (B) direct labelling with (■) antiCD63-HRP antibody. In all cases, the concentration of MPs was fixed in 1 × 10^6 MPs, 0.50 μg mL^{-1} of primary antibody, 0.08 ng mL^{-1} of antimouse-HRP and 1.24 μg mL^{-1} of antiCD63-HRP antibody. Enzymatic electrochemical signal monitored at -0.1 V vs. $Ag/AgCl_{(sat.)}$. The error bars show the standard deviation for n = 3.

5.6.16. Electrochemical immunosensor for the detection of serum-derived from breast cancer individuals

Exosomal protein content

Considering the same volume of human serum and exosome-pellet resuspended in PBS, the protein concentrations of the exosome from healthy and breast cancer individuals were estimated to be 235 μg mL^{-1} and 335 μg mL^{-1}, respectively.

5.7. References

Ahammad, A. J. S. Hydrogen Peroxide Biosensors Based on Horseradish Peroxidase and Hemoglobin. J. Biosens. Bioelectron. 2012; s9.

Bard, A.J., Faulkner, L.R. Electrochemical Methods: Fundamentals and Applications, 2nd ed. John Wiley & Sons, Inc., New York, 2001.

Cahiez, G., Lefèvre, N., Poizat, M., et al. A User-Friendly Procedure for the Preparation of Secondary Alkyl Chlorides. Synthesis (Stuttg). 2012; 45: 231.

Chosewood, L. C., Wilson, D. E. Biosafety in Microbiological and Biomedical Laboratories, 5th ed., in: U.S. Department of Health and Human Services. Centers for Disease Control and Prevention. 2009; 30.

Chow, A., Zhou, W., Liu, L., et al. Macrophage immunomodulation by breast cancer-derived exosomes requires Toll-like receptor 2-mediated activation of NF-κB. Sci. Rep. 2015; 4: 5750.

Di Noto, G., Bugatti, A., Zendrini, A., et al. Merging colloidal nanoplasmonics and surface plasmon resonance spectroscopy for enhanced profiling of multiple myeloma-derived exosomes. Biosens. Bioelectron. 2016; 77: 518.

Filipe, V., Hawe, A., Jiskoot, W., Critical Evaluation of Nanoparticle Tracking Analysis (NTA) by NanoSight for the Measurement of Nanoparticles and Protein Aggregates. Pharm. Res. 2010; 27: 796.

Grasso, L., Wyss, R., Weidenauer, L., et al. Molecular screening of cancer-derived exosomes by surface plasmon resonance spectroscopy. Anal. Bioanal. Chem. 2015; 407: 5425.

Halvaei, S., Daryani, S., Eslami-S, Z., et al. Exosomes in Cancer Liquid Biopsy: A Focus on Breast Cancer. Mol. Ther. - Nucleic Acids 2018; 10: 131.

He, M., Crow, J., Roth, M., et al. Integrated immunoisolation and protein analysis of circulating exosomes using microfluidic technology. Lab Chip 2014; 14: 3773.

Hemler, M. E. Tetraspanin proteins promote multiple cancer stages. Nat. Rev. Cancer 2013; 14: 49.

Hoogenboom, R., Fijten, M. W. M., Kickelbick, G., et al. Synthesis and crystal structures of multifunctional tosylates as basis for star-shaped poly(2-ethyl-2-oxazoline)s. Beilstein J. Org. Chem. 2010; 6: 773.

Huang, L., Wang, D.-B., Singh, N., et al. A dual-signal amplification platform for sensitive fluorescence biosensing of leukemia-derived exosomes. Nanoscale 2018; 10: 20289.

Im, H., Shao, H., Park, Y. Il, et al. Label-free detection and molecular profiling of exosomes with a nano-plasmonic sensor. Nat. Biotechnol. 2014; 32: 490.

Jeong, S., Park, J., Pathania, D., et al. Integrated Magneto–Electrochemical Sensor for Exosome Analysis. ACS Nano 2016; 10: 1802.

Levva, S., Kotoula, V., Kostopoulos, I., et al. Prognostic evaluation of epidermal growth factor receptor (EGFR) genotype and phenotype parameters in triple-negative breast cancers. Cancer Genomics and Proteomics 2017; 14: 181.

Li, Q., Tofaris, G. K., Davis, J. J. Concentration-Normalized Electroanalytical Assaying of Exosomal Markers. Anal. Chem. 2017; 89: 3184.

Patel, G. K., Khan, M. A., Zubair, H., et al. Comparative analysis of exosome isolation methods using culture supernatant for optimum yield, purity and downstream applications. Sci. Rep. 2019; 9: 5335.

Pividori, M. I., Alegret, S. Graphite-Epoxy Platforms for Electrochemical Genosensing. Anal. Lett. 2003; 36: 1669.

Raposo, G., Stoorvogel, W. Extracellular vesicles: Exosomes, microvesicles, and friends. J. Cell Biol. 2013; 200: 373.

Reddy, L. H., Arias, J. L., Nicolas, J., et al. Magnetic Nanoparticles: Design and Characterization, Toxicity and Biocompatibility, Pharmaceutical and Biomedical Applications. Chem. Rev. 2012; 112: 5818.

Rembaum, A., Yen, R. C. K., Kempner, D. H., et al. Cell labeling and magnetic separation by means of immunoreagents based on polyacrolein microspheres. J. Immunol. Methods 1982; 52: 341.

Salazar, R., Vidal, J., Martínez-Cifuentes, M., et al. Electrochemical characterization of hydroquinone derivatives with different substituents in acetonitrile. New J. Chem. 2015; 39: 1237.

Samanta, S., Rajasingh, S., Drosos, N., et al. Exosomes: new molecular targets of diseases. Acta Pharmacol. Sin. 32018; 9: 501.

Shao, H., Chung, J., Balaj, L., et al. Protein typing of circulating microvesicles allows real-time monitoring of glioblastoma therapy. Nat. Med. 2012; 18: 1835.

Sina, A. A. I., Vaidyanathan, R., Dey, S., et al. Real time and label free profiling of clinically relevant exosomes. Sci. Rep. 2016; 6: 30460.

Su, J. Label-Free Single Exosome Detection Using Frequency-Locked Microtoroid Optical Resonators. ACS Photonics 2015; 2: 1241.

Tamkovich, S. N., Yunusova, N. V., Somov, A. K., et al. Comparative Subpopulation Analysis of Plasma Exosomes from Cancer Patients. Biochem. (Moscow), Suppl. Ser. B Biomed. Chem. 2018; 12: 151.

Théry, C., Amigorena, S., Raposo, G., et al. Isolation and Characterization of Exosomes from Cell Culture Supernatants and Biological Fluids. Curr. Protoc. Cell Biol. 2006; 30: 3.22.1.

Witwer, K. W., Buzás, E. I., Bemis, L. T., et al. Standardization of sample collection, isolation and analysis methods in extracellular vesicle research. J. Extracell. Vesicles 2013; 2: 20360.

Xu, J., Mahajan, K., Xue, W., et al. Simultaneous, single particle, magnetization and size measurements of micron sized, magnetic particles. J. Magn. Magn. Mater. 2012; 324: 4189.

Yadav, S., Boriachek, K., Islam, M. N., et al. An Electrochemical Method for the Detection of Disease-Specific Exosomes. ChemElectroChem 2017; 4: 967.

Zhang, P., He, M., Zeng, Y. Ultrasensitive microfluidic analysis of circulating exosomes using a nanostructured graphene oxide/polydopamine coating. Lab Chip 2016; 16: 3033.

Zhao, Z., Yang, Y., Zeng, Y., et al. A microfluidic ExoSearch chip for multiplexed exosome detection towards blood-based ovarian cancer diagnosis. Lab Chip 2016; 16: 489.

Zhou, Q., Rahimian, A., Son, K., et al. Development of an aptasensor for electrochemical detection of exosomes. Methods 2016; 97: 88.

Zhou, Y.-G., Mohamadi, R. M., Poudineh, M., Kermanshah, L., et al. Interrogating Circulating Microsomes and Exosomes Using Metal Nanoparticles. Small 2016; 12: 727.

CHAPTER 6

Electrochemical biosensing of the alkaline phosphatase activity in exosomes isolated by specific epithelial biomarker from serum of breast cancer patient

Silio Lima Moura, Luciano Sappia, Mercè Martì and María Isabel Pividori

6.1. Abstract

The identification of novel biomarkers of cancer represents a worldwide challenge not only for the improvement of early diagnostics, but also for patient monitoring and for the evaluation of the efficiency of a therapeutic strategy. Exosomes are nano-sized and cup-shaped vesicles, which are currently under intensive study as a promising biomarker. Therefore, there is a growing need for sensitive methods able to accurately and specifically determining exosomes. This work addresses a rational study of the intrinsic activity of phosphatase alkaline (ALP) in exosomes as a potential biomarker. First of all, nanovesicles purified from human fetal osteoblasts (hFOB) culture supernatants were used as a model. The characterization of exosomes was made by nanoparticle tracking analysis and transmission electron cryomicroscopy. The expression of CD9, CD63 and CD81 biomarkers was comparatively evaluated by flow cytometry and confocal microscopy. A biosensor, combining immunomagnetic separation and the electrochemical readout, based the ALP activity in exosomes is proposed. The readout based on ALP was detected and quantified by monitoring the rate of hydrolyzes of p-nitrophenyl phosphate substrate (pNPP) into p-nitrophenol (pNP) on boron-doped microcrystalline diamond (BDD) electrodes. It is demonstrated that the electrochemical biosensor is more sensitive than the gold standard colorimetric assay for the detection of ALP in the human fetal osteoblasts derived-exosomes used as a model, providing ALP activity with a detection limit of 4.39 mU L^{-1} (or 13.47 mU mg^{-1}), equivalent to 10^5 exosomes μL^{-1}, respectively. Finally, the electrochemical immunosensor showed reliable results for the differentiation of healthy donors and breast cancer individuals based on the immunomagnetic separation using specific epithelial biomarkers CD326 (EpCAM) and the intrinsic ALP activity readout.

6.2. Introduction

Alkaline phosphatase (ALP, EC 3.1.3.1.) is a ubiquitous enzyme present in all tissues. This membrane-bound, zinc-containing metalloenzyme is a hydrolase that catalyze the hydrolysis of a mono-ester acid in an alkaline medium, by releasing phosphate (Sharma et al., 2014). ALP is a key enzyme involved in the mineralization process, by increasing the local concentration of phosphate (Anderson, 2003) and consuming pyrophosphate ions from the medium, which inhibit the formation of hydroxyapatite crystals (Anderson et al., 2004).

Besides bone remodeling, overexpression of ALP is correlated with metastatic cancer, such as osteosarcoma (Kim et al., 2017), prostate (Rao et al., 2017), breast (Tsai et al., 2000) and colorectal carcinomas (Saif et al., 2005).

The standard method for ALP activity determination in clinical fluids is based in a spectrophotometric assay, in which the sample is mixed with an alkaline buffer and a substrate (p-nitrophenyl phosphate), and measuring the yellow product at 405 nm (Keiding et al., 1974). P-nitrophenyl phosphate is also one of the most widely used substrates for ALP in electrochemical biosensors since the enzymatically produced p-nitrophenol can be easily detected (Preechaworapun et al., 2008). Recently, our group reported an electrochemical biosensor for the determination of ALP in clinical samples (Sappia et al., 2019). We also demonstrated ALP activity on osteoblast-derived exosomes from culture supernatants (Sanchez et al., 2020) for the first time. The exosomes are nanovesicles involved in cells communication (Johnstone et al., 1987). They have their biogenesis arise from intraluminal vesicles (ILVs) formed in the endosomal membrane during maturation of multivesicular endosomes (MVEs) (Pan et al., 1985). Therefore, the exosomes usually carry specific and are somewhat unique in their cargo as proteins (e.g. tetraspanins CD9, CD63, CD81), RNA, DNA as well as enzymes of cellular origin (Samanta et al., 2018). Exosomes are currently under increasingly attention as biomarkers for cancer diagnosis and monitoring (Halvaei et al., 2018; Raposo and Stoorvogel, 2013).

In this work we propose a simple, quantitative and rapid electrochemical biosensing approach for cancer-derived exosome detection based on a double recognition: immunoseparation for the specific isolation and enzymatic activity for the readout. The method was firstly optimized using as a model the exosomes derived from human fetal osteoblastic (hFOB) cell line, and compared with the gold standard colorimetric ALP assay in terms of the analytical performance. The approach combines the immunomagnetic separation of the exosomes based on the general tetraspanin (CD9, CD63 or CD81) biomarkers, followed by the electrochemical readout relying on the ALP activity by reaction with pNPP substrate and further electrochemical sensing on boron-doped microcrystalline diamond electrode. Finally, the discrimination of breast cancer individuals from healthy donors is demonstrated as a probe of concept for the biosensor. In this instance, the exosomes were isolated by magnetic actuation using the specific CD326 (EpCAM) cancer-related biomarker, followed by the electrochemical biosensing, which differentiates healthy donors and breast cancer patients based on specific epithelial biomarkers.

6.3. Experimental

6.3.1. Instrumentation

Nanoparticle tracking analysis (NTA) was performed using the NanoSight LM10-HS system with a tuned 405 nm laser (NanoSight Ltd, UK). The cryogenic transmission

electron microscopy (TEM) images were collected by a Jeol JEM 2011 (JEOL USA Inc, USA) transmission electron microscope at an accelerating voltage of 200 kV. Flow cytometry was performed using BD FACSCANTO II (BD Biosciences, USA) equipment. The Media Fluorescence Intensity (MFI) and beads count data were obtained by FlowJo analysis software of every sample-reading file. The confocal images were collected on the microscope Leica, TCS SP5 (Leica Microsystems, Germany). Optical measurements were performed on a TECAN Sunrise (TECAN AG, Switzerland) microplate reader with Magellan v4.0 software. All electrochemical experiments were performed using an AUTOLAB PGSTAT10 potentiostat/galvanostat electrochemical analyzer. A boron-doped microcrystalline diamond (BDD) electrode (boron/carbon ratio of 20.000 ppm) as working electrode (geometric area = 0.5 cm^2) was kindly supplied by Prof. Dr. Neidenei Ferreira from Group of Electrochemistry and Carbon Materials, National Institute of Space Research (INPE), São José dos Campos, São Paulo, Brazil. The construction and characterization of the BDD electrode is described in the Supp. Data. $Ag/AgCl/KCl_{(satd.)}$ reference electrode, a disc platinum counter electrode (geometric area = 3.0 cm^2) and a standard 500-µL one compartment three-electrode cell was used in all experiments.

6.3.2. Chemicals and biochemicals

The magnetic particles (MPs) Dynabeads® M450 Tosylactivated (No. 14013) and the MPs modified with EpCAM antibody (Dynabeads™ Epithelial Enrich, Ref. 16102) were purchased from Thermo Fisher. The mouse monoclonal antibodies (antiCDX) were purchased from Thermo Fisher: CD9 (Ref. 10626D), CD63 (Ref. 10628D) and CD81 (Ref. 10630D). A goat anti-mouse IgG H&L (Cy5®) (antimouse-Cy5) (Ref. ab97037) was purchased from Abcam. Calf intestine alkaline phosphatase (ALP, nº 10713023001), Dulbecco's Modified Eagle's/Ham's F-12 Nutrient (DMEM/F12, nº D9785) medium, fetal bovine serum (FBS, nº 12007C) were purchased from Sigma-Aldrich. All other reagents were in analytical reagent grade.

6.3.3. Cell culturing, exosome isolation and purification

Human fetal osteoblastic (hFOB) cell line (hFOB 1.19 (ATCC® CRL-11372™) was grown as described in the Supp. Data. Exosomes were purified from culture supernatant by differential ultracentrifugation as previously reported by our research group (Moura et al., 2020a). Exosomes are resuspended in 10 mmol L^{-1} TRIS buffer solution (pH 7.5) (0.22 µm filtrated and sterile) and stored at -80 °C. All exosomes purification steps are provided in the Supp. Data.

6.3.4. Characterization of exosomes by nanoparticle tracking analysis and transmission electron microscopy

The size distribution and concentration of exosomes were measured by nanoparticle tracking analysis (NTA). The purified exosomes were diluted in sterile-filtered TRIS buffer solution (50- to 100-fold). Nanosight NTA Software analyzed raw data videos by triplicate during 60 s with 50 frames/s and the temperature of the laser unit set at 24.8 ºC. For the cryogenic transmission electron microscopy (TEM), the exosomes (2.0×10^9) were directly laid on Formvar-Carbon EM grids and frozen in ethanol. Exosomes were maintained at -182 °C during the whole process.

6.3.5. Confocal microscopy and flow cytometry study

The analysis of the molecular biomarkers expressed in hFOB cell line was carried out by flow cytometry. The presence of the following receptors was investigated: CD9, CD63 and CD81. The indirect labeling of 2×10^5 cells was performed by incubation of 100 µL (5 µg mL^{-1}) of the antibodies antiCDX (mouse), (being CDX either CD9, CD63 and CD81 biomarkers), for 30 min with gentle shaking at 25 ºC. After that, three washing steps with TRIS buffer solution containing 0.5% BSA solution were performed. Afterward, 100 µL (2 µg mL^{-1}) of the antimouse-Cy5 antibody (a far-red-fluorescent dye, excitation 647 nm, emission 665 nm) was incubated for 30 min in the darkness with gentle shaking at 25 ºC. The labeled cells were resuspended in 200 µL of TRIS buffer solution containing 0.5% BSA solution.

The same procedure of labeling was performed in the case of the osteoblastic-derived exosomes, but in this approach, and due to their size and resolution of the technique, the exosomes were firstly immobilized on the surface of MPs, as described in Fig. S6.1, Supp Data. To achieve that, 3.5×10^{10} exosomes were covalently immobilized on 1.6×10^7 MPs, as detailed described in the Supp data (Fig. S6.1, panel A), followed by the indirect labeling as described above, with antiCDX (mouse), (being CDX either CD9, CD63 or CD81 biomarkers).

The same samples of cells and exosomes analyzed by flow cytometry were subjected to confocal microscopy imaging for the study of the binding pattern of antibodies. In the case of cells, the cellular DNA was stained previous (before labeling with antibodies) with Hoechst dye (a blue-fluorescent dye, emission wavelength 490 nm).

6.3.6. ALP activity study in exosomes

6.3.6.1. Spectrophotometric determination of the ALP activity in exosomes

The gold standard colorimetric determination of the ALP activity was performed in 96-well microtiter plates (Fig. 6.1, panel B). The colorimetric assay for ALP activity in

osteoblastic-derived exosomes was detected and quantified by monitoring the activity (rate of micromoles hydrolyzes per minute, μmol min^{-1}) of pNPP substrate in DEA buffer into p-nitrophenol (pNP). A colorimetric calibration curve for pNP was carried out to express the rate of hydrolyzing in enzyme activity (U L^{-1}). The assay involved the following steps: i) IMS of the exosomes with antiCDX-MPs (Fig. 6.1, panel A), followed by ii) reaction with pNPP substrate; iii) optical readout (Fig. 6.1, panel B). The protocol in detail for the spectrophotometric assay is described in Supp. Data.

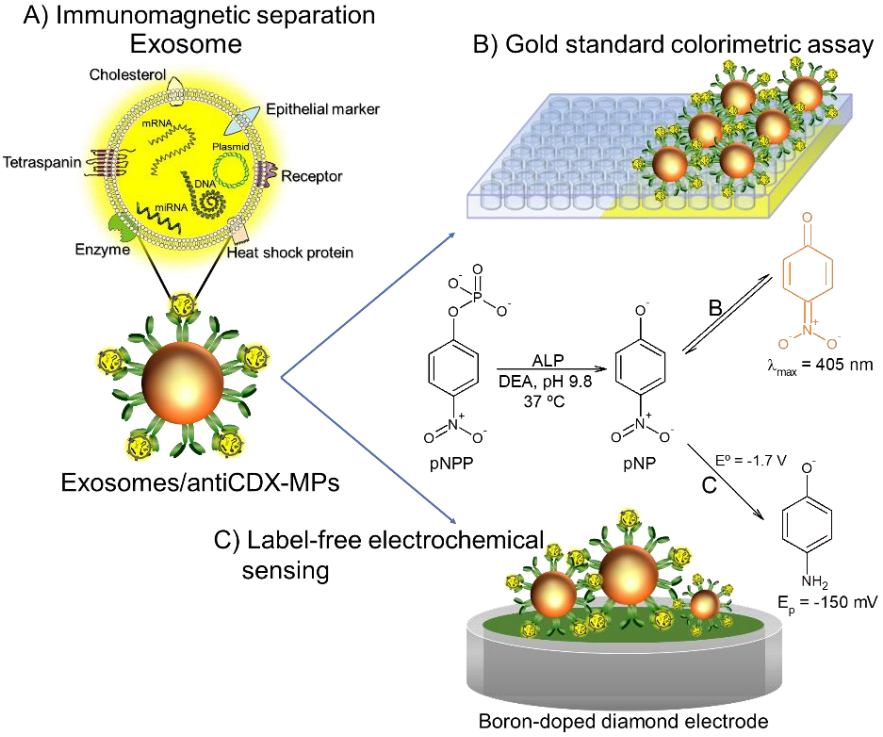

Fig. 6.1. Different approaches for the detection of alkaline phosphatase (ALP) activity in osteoblastic-derived exosomes by optical readout and electrochemical biosensor based on BDD electrode. Further experimental details are provided in Supp. Data.

6.3.6.2. Electrochemical biosensor for ALP activity in exosomes

The electrochemical biosensing for ALP activity in osteoblastic-derived exosomes involved the following steps: i) IMS of the exosomes with antiCDX-MPs (Fig. 6.1, panel A), followed by ii) reaction with pNPP substrate; (iii) electrochemical readout (Fig. 6.1, panel C). The detailed protocol for the electrochemical biosensor is provided in detail in Supp. Data. A standard 500-μL one compartment three-electrode cell was used. The readout was performed by monitoring the rate of micromoles hydrolyzes per minute (μmol min^{-1}) of pNPP substrate in DEA buffer into p-nitrophenol (pNP), followed by electrochemical conversion into p-aminophenol (pAP). A square wave voltammetry (SWV) calibration plot for pAP was carried out to express the rate of hydrolyzing in enzyme activity (U L^{-1}).

6.3.6.3. Electrochemical biosensing of the ALP activity in exosomes isolated by specific epithelial biomarker from breast cancer patients serum

Blood samples from anonymized healthy female donors (n = 10, mean age 35/SD 5 years) and breast cancer female donors (n = 10, stage IV, mean age 50/SD 6 years) were obtained from the Hospital del Mar, Barcelona, Spain. The work was carried out following the principles of voluntariness and confidentiality. The samples n = 10 each were polled in two batches (healthy and breast cancer donors) and purified as detailed described in Supp data. The two populations (healthy and breast cancer donors, n = 10, each) were then evaluated by NTA and the protein content (as described in Supp Data), and compared based on the same content of exosomal protein (3.35 μg of protein per assay). The electrochemical biosensing for ALP activity in exosomes from breast cancer patients serum involved the following steps: i) IMS of the exosomes with antiCD326-MPs (also known as EpCAM, a cancer-related biomarker) in order to isolate only cancer-related exosomes, followed by ii) reaction with pNPP substrate; (iii) electrochemical readout as described above.

6.3.7. Statistical analysis

The statistical analyses were performed using GraphPad Prism 6 (San Diego, USA). The data of the ALP activity were statistically compared between the gold standard colorimetric and the electrochemical endpoint assays using a paired-sample Student's t-test. The value $p > 0.05$ was considered significant.

6.3.8. Safety considerations

All works were performed in a Biosafety cabinet, and all material decontaminated by autoclaving or disinfected before discarding following U.S. Department of Health and Human Services guidelines for level 2 laboratory Biosafety (Chosewood and Wilson, 2009).

6.4. Results and discussion

6.4.1. Characterization of exosomes by nanoparticle tracking analysis and transmission electron microscopy

Fig. 6.2, panel A shows the size diameter distribution of osteoblastic-derived exosomes ranges from 50 up to 400 nm (considering 95.4% of a Gaussian distribution), which is represented by exosomes with 150 nm in diameter. Another peak was observed at 210 nm and broadband at 330 nm, and the concentration was estimated to be 8.70 x

10^{10}/ SD 3.2 x 10^{8} particles mL^{-1}. TEM micrographs on osteoblastic-derived exosomes show well-shape exosomal vesicles with closed circular lipid bilayers (Fig. 6.2, panel B) of around 150 nm in diameter. Similar results were obtained by NTA and TEM for the exosomes derived from the healthy and breast cancer donors (as depicted in Fig. S6.2 and Fig. S6.3 respectively).

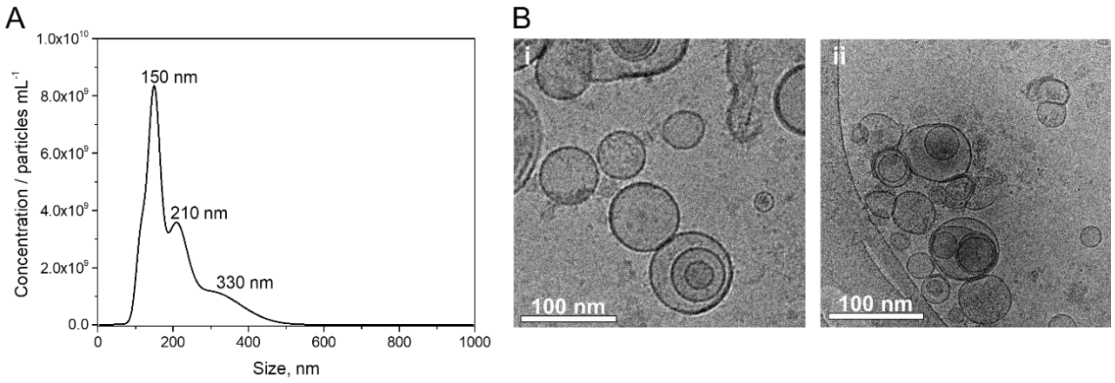

Fig. 6.2. Characterization by NTA and TEM of purified osteoblastic-derived exosomes. Panel A, shows the NTA characterization which was analyzed raw data videos by triplicate during 60 s with 50 frames per second and the temperature of the laser unit set at 24.8 ºC. Panel B, the corresponding TEM images at an acceleration voltage of 200 kV.

The micrographs revealed well-shaped osteoblastic exosome vesicles with close circular lipid bilayers (Fig. 6.2, panel B). As expected, the TEM micrographs also reveals the presence of some aggregates of exosomes, confirming the results obtained by NTA. it is important to highlight that NTA analysis provides information as counted entities, not only as isolated particles but also as aggregates. Accordingly, the NTA analysis cannot clearly distinguish vesicles and vesicle aggregates.

6.4.2. Confocal microscopy

The objective of these experiments was to assess the expression of general exosome biomarkers such as CD9, CD63 and CD81 on the hFOB cell line, as well as in their osteoblastic-derived exosomes for their further used in the immunomagnetic separation of the exosomes.

Expression patterns to CD9, CD63 and CD81 tetraspanins membrane receptors in hFOB cell line and their exosomes were evaluated qualitatively by confocal microscopy. In the case of hFOB cells, the cellular DNA was stained with Hoechst dye (blue color). CD9, CD63 and with highlight the CD81 tetraspanins membrane receptors are shown with strong labeling in the hFOB cell line (Fig. 6.3, panel A and C). The

percentage of labeled cells represent the total counting of positive cells for each biomarker, as shown in Fig. 6.3, panel C. The expression of osteoblastic-derived exosomes was done after covalent immobilization on MPs due to their size, and was then studied and compared to the parental cell line (Fig. 6.3, panel B). It is worth mentioning that the intense green color is due to autofluorescence on the MPs at 580 nm, approximately (Agrawal et al., 2007). The percentage of labeled exosomes represent the total counting of positive exosomes-MPs for each biomarker, as shown in Fig. 6.3, panel C. The quantitative analysis (Fig. 6.3, panel C) showed, as expected, a strong labeling pattern of osteoblastic-derived exosomes to all the general tetraspanins studied (CD9, CD63 and CD81).

The results for flow cytometry analysis is shown in Fig. 6.4. It is noteworthy that the flow cytometric analysis was performed with the same batch sample used in the confocal microscopy. The negative control, in which the signal appears onto the left side in blue, confirms that there a negligible (<0.1%) nonspecific adsorption of the secondary antibody (antimouse Cy®5 fluorophores) on the hFOB cells (Fig. 6.4, panel A, control). Flow cytometry also showed strong labeling to CD9, CD63 and CD81 biomarkers in hFOB cell line. The results of flow cytometry shown in Fig. 6.4, panel B and C, for the osteoblastic-derived exosomes covalently-immobilized on MPs also confirmed the high level of expression of CD9, CD63 and CD81 tetraspanins (Fig. 6.4, panel B and C). The percentage of labeled entities (either the cells or the exosomes-MPs) represent the total counting of positive entities for each biomarker, as shown in Fig. 6.4, panel C.

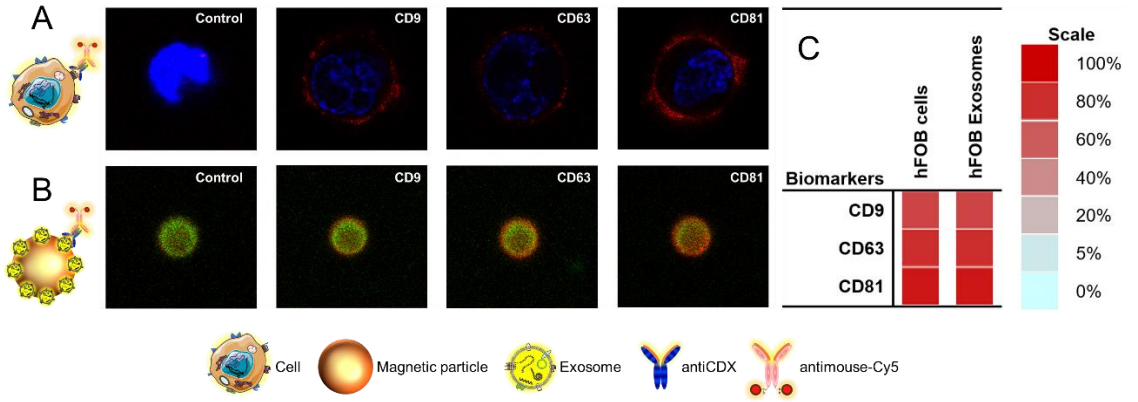

Fig. 6.3. Confocal microscopy images for (A) hFOB cell line and (B) their exosomes covalently immobilized on MPs (exosomes-MPs), followed by indirect labeling with mouse antiCDX (5 μg mL^{-1}), (being CDX either CD9, CD63, and CD81 biomarkers) and antimouse-Cy5 (2 μg mL^{-1}). The concentration of MPs and exosomes were set in 1 × 10^6 MPs and 4 x 10^9 exosomes per assay, respectively. DNA in blue color, magnetic particles in green color, exosomal protein membrane in red color.

As was for hFOB cells, the CD81 tetraspanin was most prominently displayed in their derived exosomes. In agreement with several studies, CD9, CD63 and CD81 as

the most frequently identified proteins in exosomes and are considered classical biomarkers for exosomes (Chow et al., 2015). Therefore, any of these tetraspanins can provide a good performance for the immunomagnetic separation of osteoblastic derived exosomes.

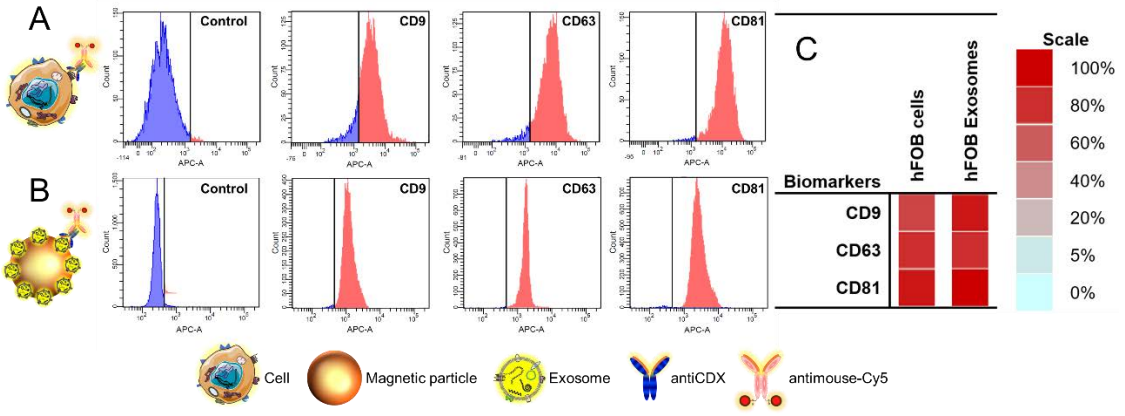

Fig. 6.4. Flow cytometry study represented in histograms for (A) hFOB cell line and (B) their exosomes covalently immobilized on MPs (exosomes-MPs), followed by indirect labeling with mouse antiCDX (5 μg mL^{-1}), (being CDX either CD9, CD63, and CD81 biomarkers) and antimouse-Cy5 (2 μg mL^{-1}). The concentration of MPs and exosomes were set in 1 × 10^6 MPs and 4 x 10^9 exosomes per assay, respectively. Population control onto the stained-blue regions on the left side and stained-red regions on the right side for a positive relative expression of membrane protein markers.

6.4.3. Optimization of the determination of ALP activity

Different parameters were optimized, including the composition of the buffer (Tris or DEA), pH, Mg^{2+} concentration, and the stop solution composition for ALP activity determination on osteoblastic-derived exosomes based on the colorimetric detection and the electrochemical biosensors to obtain the highest readout towards the determination of pNPP product. Furthermore, the kinetic parameters V_{max} and K_m were determined. All the experimental details are provided in the Supp. Data.

In this regard, some parameters were optimized to obtain the highest signal towards the determination of the pNP product. The optimized parameters for determination of the ALP activity in osteoblastic-derived exosomes immunocaptured by antiCDX-MPs were found using 10 mmol L^{-1} pNPP in 1 mol L^{-1} DEA buffer pH 9.8 containing 6.0 mmol L^{-1} MgCl2 and 100 mmol L^{-1} KCl. In all cases, the enzymatic reaction was performed during 60 min at 37 ºC and stopped by adding 25% (v/v) of 5.0 mol L^{-1} NaOH.

Furthermore, a comparative study of the kinetic parameter of free ALP and ALP in osteoblastic-derived exosomes were performed (Supp. Data). Similar kinetic

parameters were obtained, which indicates that a minimum effect in the kinetic was observed in the ALP when it is carried on exosomes (V_{max} 3.196/SD 0.018 μmol L^{-1} min^{-1} and K_m 763/SD 0.012 mmol L^{-1}), compared with if it is free in solution (2.170/SD 0.037 μmol L^{-1} s^{-1} and K_m 0.708/SD 0.015 mmol L^{-1}). These kinetic parameters were close to those reported for calf intestinal ALP *in vivo* (Chaudhuri et al., 2013; Li et al., 2017).

Beside this, the characterization of the electrochemical readout of pNP on BDD electrode by SEM, Raman, and SWV-parameters are also detailed optimized in the Supp. Data. The optimal experimental SWV-parameters for quantification of pAP in 1 mol L^{-1} DEA buffer (pH 9.8) containing 6.0 mmol L^{-1} $MgCl_2$ and 100 mmol L^{-1} KCl using microcrystalline BDD electrode were found to be E_{sw} = 200 mV pulse amplitude, f = 200 Hz frequency, E_{sp} = 8 mV pulse potential, E_{ap} = -1.70 V and t = 10 s for accumulation potential and time, respectively.

6.4.4. Comparative study of the electrochemical biosensor and the spectrophotometric determination for ALP activity in exosomes isolated on antiCDX-MPs

The ALP activity from osteoblastic-derived exosomes was detected and quantified by the gold standard spectrophotometric assay by monitoring the absorbance at 405 nm, and the analytical performance compared with the electrochemical biosensing monitoring the current peak at -150 mV. Fig. 6.5, panel A (spectrophotometric determination) and panel B (electrochemical biosensing) show the ALP activity of osteoblastic-derived exosomes isolated by immunomagnetic separation base on antiCDX-MPs (being CDX: CD9, CD63 and CD81). These results demonstrated an improved separation performance of the IMS based on antiCD81-MPs and in the detection of ALP activity in the exosome membrane, which can be attributed either to high expression of the receptor or higher affinity constant (K_a) of the antibody.

Both set of data were fitted using nonlinear regression (Four Parameter Logistic Equation, GraphPad Prism Software). The osteoblastic-derived exosomes separated by using antiCD81-MPs provided an improved analytical performance, giving a limit of detection (LOD) of 825 exosomes μL^{-1} (r^2 = 0.9907) and 105 exosomes μL^{-1} (r^2 = 0.9949) for spectrophotometric assay and electrochemical biosensor, respectively. The LOD for the electrochemical biosensor corresponds to the 4.39 mU L^{-1} or 13.47 mU mg^{-1} for ALP level, normalized by the total volume assay and the protein content, respectively. These LOD represent an improvement over the detection limits obtained by other methods for

total exosomes counting (López-Cobo et al., 2018; Oliveira-Rodríguez et al., 2016). These results demonstrate a more sensitive electrochemical platform than the gold standard spectrophotometric assay ($p<0.05$). Besides, the variation coefficient for the BDD electrode for determining the pAP was 2.9% ($p<0.05$) for ten replicative measurements, indicating good reproducibility (Fig. S6.14, Supp. Data). Nonetheless, the pNPP substrate solution on the BDD electrode surface has an excellent hydrolytic stability with no formation of pNP/pAP, remaining colorless in absence of ALP enzyme (Fig. S6.15, Supp. Data).

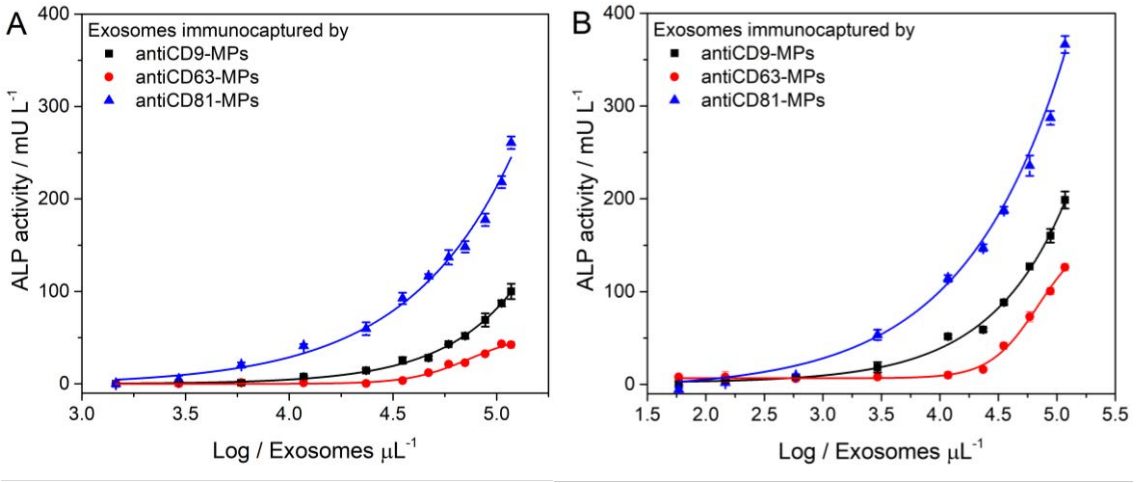

Fig. 6.5. Comparative study of (A) spectrophotometric gold standard determination and (B) electrochemical biosensor for the detection of ALP activity in osteoblastic-derived exosomes ranging 0 from 2.35 x 10^7 exosomes μL^{-1} spiked in 10 mmol L^{-1} TRIS buffer. Exosomes were immunocaptured by antiCDX-MPs (being CDX any of CD9, CD63, or CD81), followed by reaction with 10 mmol L^{-1} pNPP in 1 mol L^{-1} DEA buffer, containing 6.0 mmol L^{-1} $MgCl_2$ and 100 mmol L^{-1} KCl. In all cases, the enzymatic reaction was during 60 min at 37 ºC, the concentration of antiCDX-MPs was fixed in 1 × 10^6 MPs. An enzymatic colorimetric assay was monitored at 405 nm and the electrochemical signal monitored the current peak at -150 mV vs. $Ag/AgCl/KCl_{(satd.)}$. BDD electrode was used as a working electrode. SWV conditions: E_{sw} = 200 mV, E_{ap} = -1.70 V, E_{sp} = 8 mV, f = 200 Hz, t = 10 s. The error bars show the standard deviation for n = 3.

Concerning electrochemical biosensor, the ALP activity in human serum using a glassy carbon electrode monitoring determined the rate of hydrolysis of ascorbic acid 2-phosphate (AAP) (Sun and Jiao, 2005). ALP enzymatic hydrolysis product of AAP produced ascorbic acid (AA), which was monitored at 0.38 V (vs $Ag/AgCl/KCl_{(satd.)}$) by using differential pulse voltammetric (DPV) and ALP assay exhibited a LOD of 0.3 U L^{-1}. Although Sun et al cover a broad operating range (0.4 to 2000 U L^{-1}), as mentioned by the authors, the use of carbon electrode needs of a mechanical polishing and the spontaneous oxidation of the enzymatic product ascorbic acid in presence of atmospheric air turn the assay into not appropriate for implementation as a portable system for ALP activity determination. Nonetheless, the ascorbic acid undergoes oxidation at 0.38 V (vs $Ag/AgCl/KCl_{(satd.)}$), which is a high potential, not desirable and

relatively complicated in the determination of an electroactive analyte due to possible interfering molecules. This probably happens in the same way as in the dimerization of aniline (Sapurina et al., 2015) and dapsone (Moura et al., 2015). Other researchers have addressed to the electrochemical determination of ALP activity using indium–tin oxide (ITO) electrode (Qin et al., 2017), graphite screen-printed electrode (Sappia et al., 2019), graphite-IrO2 composites (Wang et al., 2009), graphene oxide-modified gold electrode (Shen et al., 2016), copper sulfide-decorated graphene sheet (Peng et al., 2015). Although these cited works and others found in the literature have demonstrated advances in the strategy towards ALP-based assays, some drawbacks are crucial in the ALP determination as to the cost-effectiveness, non-reusable and electrode surface fouling, high potential detection to phenolic-type substrates, which current peaks overlap with the oxygen-evolution region (>1.0 V vs. Ag/AgCl/$KCl_{(satd.)}$).

6.4.5. Electrochemical biosensing of the intrinsic activity of ALP in exosomes isolated by specific epithelial biomarker from breast cancer patients serum

The analysis of purified exosomes from healthy donors and breast cancer patients is shown in Fig. 6.6. The approach is based on the immunomagnetic separation of the exosomes using the specific CD326 (also known as EpCAM) cancer-related biomarker, followed by the detection of exosomes-derived ALP enzyme by reaction with pNPP substrate.

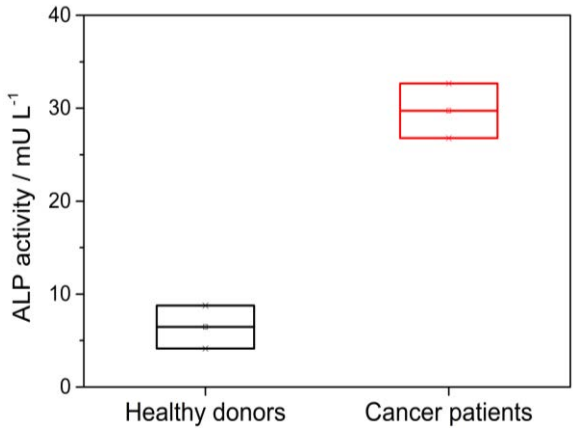

Fig. 6.6. Electrochemical biosensing for detection of the ALP activity from purified exosomes derived from healthy donors (n = 10, pooled) and breast cancer (n = 10, pooled) patients. The exosomes were immunomagnetically separated on antiCD326- MPs (1×10^6 MPs per assay), followed by reaction with 10 mmol L^{-1} pNPP in 1 mol L^{-1} DEA buffer, containing 6.0 mmol L^{-1} $MgCl_2$ and 100 mmol L^{-1} KCl. The electrochemical signal monitored the current peak at -150 mV *vs.* Ag/AgCl/$KCl_{(satd.)}$. BDD electrode was used as a working electrode. SWV conditions: E_{sw} = 200 mV, E_{ap} = -1.70 V, E_{sp} = 8 mV, f = 200 Hz, t = 10 s. In all cases, the enzymatic reaction was during 120 min at 37 ºC.

Accordingly, and in order to compare the expression of the receptors on exosomes from the two populations, the electrochemical biosensing was performed with the same amount (3.35 ug) of exosome protein content per assay, for healthy donors and breast cancer patients (n = 10 each). Fig. 6.6, shows that breast cancer patients overexpressed ALP enzyme in CD326-positive exosomes and can be well discriminated from exosomes-derived healthy donors (mean 4.5-fold, $p<0.05$).

6.5. Conclusion

To the best of the author's knowledge, this is the first electrochemical biosensor approach integrated the magnetic particles specific isolation to the detection of ALP activity, both in osteoblastic-derived and breast cancer exosomes. Furthermore, for the first time, the presence of ALP in osteoblastic-derived exosomes was detected and quantified. The ALP-based electrochemical biosensor for exosomes with a limit of detection of 10^5 exosomes μL^{-1} (4.39 mU L^{-1} or 13.47 mU mg^{-1}) represents an improvement in LODs regarding other exosome quantification (Xia et al., 2017; Yadav et al., 2017), and is more sensitive than the gold standard spectrophotometric assay. The low monitored potential of -150 mV vs. $Ag/AgCl/KCl_{(satd.)}$ avoids possible interfering molecules. These advantages are attributed to the conductivity, stability, very low absorptivity and excellent catalytic properties of the boron-doped diamond (BDD) electrode for ALP determination. Furthermore, the use of a boron-doped microcrystalline diamond (BDD) electrode enables the portability of the assay with sample volume minimization, avoiding the fouling of nitro-phenolic derivatives, an effect usually observed in conventional-based electrodes (Sappia et al., 2019). This approach demonstrated to be useful for the discrimination of healthy and breast cancer patient, confirming the simultaneous expression of cancer biomarkers in exosomes, as is the case of epithelial CD326 (EpCAM), used for the specific isolation, and the ALP intrinsic activity, used for the sensitivity electrochemical readout. The difference between healthy donors and breast cancer patients is in accordance with the highly expressed epithelial biomarker CD326 (Moura et al., 2020a, 2020b) and ALP in serum (Chen et al., 2017) enzyme in breast cancer patients.

6.6. Supplementary Data

6.6.1. Instrumentation

Construction of the boron-doped diamond electrode

BDD diamond films were grown on silicon sheet using a Hot Filament Chemical Vapor Deposition (HFCVD) reactor for 8 h. A gas mixture of 198/2 sccm (standard centimeter cubic per minute) of H_2/CH_4 was used to grow BDD films at 750 °C and pressure inside the reactor was 4×10^3 Pa. The doping process was made by an additional hydrogen line that passes through a bubbler containing B_2O_3 dissolved in methanol, with a boron/carbon ratio of 20,000 ppm in solution. The production and characterization of BDD electrodes were previously reported (Santos et al., 2014). The characterization of the electrodes by SEM (Fig. S9), RAMAN (Fig. S10) and electrochemical (Fig. S11) is provided in the Results and Discussion section (Supp. Data). The BDD electrode cleaning procedures were carried out for every experiment by electrochemical treatment by applying a potential of -2.0 V for 30 s in 0.5 mol L^{-1} H_2SO_4 supporting electrolyte.

6.6.2. Cell culture

Human fetal osteoblastic (hFOB) cell line (hFOB 1.19 (ATCC® CRL-11372™). Expansion of cell population was carried out from 1,000,000 cells in T-175 flask containing 32 mL of Dulbecco's Modified Eagle's/Ham's F-12 Nutrient medium, supplemented with 10% exosome-depleted fetal bovine serum (FBS), 100 U mL^{-1} penicillin-streptomycin. The temperature was maintained at 37 °C in a humidified, concentrated CO_2 (5%) atmosphere. Once cells reached approximately 95% confluence on the T-175 flask, the culture medium was removed and stored at -80 ºC until to exosome isolation.

6.6.3. Human serum treatment

The human serum samples were separated from the blood cells using a sterile empty tube without any anticoagulant, leave the tube in a standing position for about 20-30 minutes for the blood to be clotted. After that, centrifugation at 1,500 g (20 ºC) for 10 minutes was carried out for removal of residual cells and cellular debris. Following, the human serum (supernatant on top) was carefully removed, freeze at -80 ºC to preserve for further assays.

6.6.4. Exosome isolation and purification

Exosomes were purified according as previously reported by our research group (Moura et al., 2020a). The supernatant from the hFOB cell line and human serum were

subjected to differential centrifugation as follows: 300 *g* for 10 minutes (removal of residual cells), 2,000 *g* for 10 minutes and 10,000 *g* for 30 minutes (removal of cellular debris). Then, a Beckman Coulter OptimaTM L-80XP Ultracentrifuge at 100,000 *g* for 60 minutes with a 70Ti rotor to pellet exosomes. After that, the supernatant was carefully removed, and crude exosome-containing pellets were resuspended in 1 mL of 10 mmol L^{-1} tris(hydroxymethyl)aminomethane (TRIS) buffer (pH 7.4, adjusted with HCl) and pooled. The second round of the same ultracentrifugation setting was carried out, and the resulting exosome pellet resuspended in 500 µL (per 100 mL of supernatant) of 10 mmol L^{-1} TRIS (0.22 µm filtrated and sterile) and storage at -80 °C. All centrifugation steps performed at a temperature of 4 °C.

6.6.5. Exosome protein quantification

The exosomal protein content was determined by using Pierce™ BCA Protein Assay Kit (Ref. 23227, Thermo Fisher), following the protocol. Before protein quantification, all exosomes resuspended in PBS were lysed by adding an equal volume of RIPA buffer (Sigma Aldrich) and cOmplete™, Mini, EDTA-free Protease Inhibitor CocktailTM (Roche), followed by incubation at RT for 5 min and sonicated for 15 seconds.

6.6.6. Immobilization of exosomes and antibodies on magnetic particles

Dynabeads® M450 tosyl activated superparamagnetic particles (MPs, 4.5 µm in diameter) has a core of iron oxide salt encapsulated by a polystyrene polymer, which has a polyurethane external layer with the p-toluenesulfonate group (Xu et al., 2012). It is a good leaving group, which allows an S_N2 reaction to occur in the presence of a nucleophile (Cahiez et al., 2012; Hoogenboom et al., 2010). A nucleophilic reaction by an antibody, protein, peptide, or glycoprotein removes and replaces the sulfonyl ester groups from the polyurethane layer.

Two different approaches were used, as depicted in Fig. S6.1. The first one involves the direct covalent immobilization of exosomes on magnetic particles (Fig. S6.1, panel A). The second approach is based on the covalent immobilization of the antibodies for a further immunomagnetic separation (IMS) of exosomes (Fig. S6.1, panel B).

Immobilization of exosomes on magnetic particles

The immobilization of exosomes on Dynabeads® M450 tosyl activated superparamagnetic particles (MPs) (Fig. S6.1, panel A) were performed as follows: 3.5 x 10^{10} exosomes were added to 40 µL (1.6 x 10^7 MPs) Dynabeads® M450 tosyl activated. The reaction kinetics are increased by adding 0.1 mol L^{-1} borate buffer pH 8.5,

in order to ensure the nucleophilic reaction by the amine group. The incubation step was performed overnight with gentle shaking at 4 ºC. After that, 0.5 mol L^{-1} glycine solution was added to ensure the blocking of any remaining tosyl activated groups, by incubation for 2 h at 25 ºC. After that, the exosomes-modified magnetic particles (exosomes-MP) were resuspended in 160 µL of 10 mmol L^{-1} TRIS buffer solution in order to achieve 1 x 10^6 MPs per 10 µL.

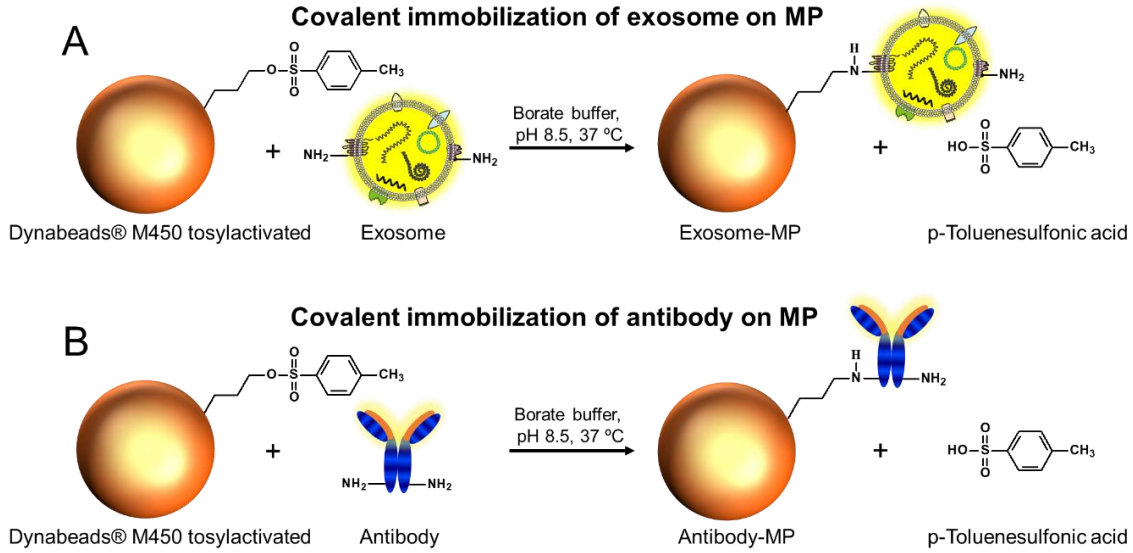

Fig. S6.1. Immobilization approaches of exosomes on Dynabeads® M450 tosylactivated (MPs). (A) Covalent immobilization on MPs, or (B) IMS on antibody-modified MPs.

Immobilization of antibodies on magnetic particles

The different specific antibody (15 µg mL^{-1}, previously optimized (Moura et al., 2020a) (antiCD9, antiCD63 or antiCD81) was added to 55 µL (2.2 x 10^7 MPs) Dynabeads® M450 tosyl activated (Fig. S6.1, panel B). The reaction kinetics are increased by adding 0.1 mol L^{-1} borate buffer pH 8.5. The incubation step was performed overnight with gentle shaking at 37 ºC. After that, a blocking step with a 0.5 mol L^{-1} glycine solution was performed for 2 h to ensure the blocking of any remaining tosyl activated groups. After that, the antibody-modified magnetic particles (herein, antiCDX-MPs, where antiCDX = antiCD9, antiCD63 or antiCD81) were resuspended in 220 µL (10 µL per well to give 1 x 10^6 particles per well) 10 mmol L^{-1} TRIS buffer solution.

6.6.7. Spectrophotometric determination of the ALP activity in exosomes

The gold standard spectrophotometric (Fig. 6.1, panel B) determination of the ALP activity from osteoblastic-derived exosomes was performed in 96-well microtiter plates and involved the following steps: i) IMS of the exosomes with antiCDX-MPs (Fig.

6.1, panel A). The immobilization of antibodies on magnetic particles (antiCDX-MPs) is described in detail in the Supp. Data (Fig. S6.1, panel B). The antiCDX-MPs (being CDX any of CD9, CD63 or CD81 biomarkers) (containing 1 × 10^6 antiCDX MPs per well) and the exosomes (100 µL per well, ranging from 1400 to 1.17 x 10^5 exosomes μL^{-1}), were simultaneously incubated for 30 min with shaking at 25 °C, followed by three washing steps with TRIS containing 0.5% BSA. ii) Reaction with pNPP substrate. The exosomes-coated MPs were incubated with 150 µL of 10 mmol L^{-1} pNPP in 1 mol L^{-1} DEA buffer pH 9.8 containing 6.0 mmol L^{-1} $MgCl_2$ and 100 mmol L^{-1} KCl. In all cases, the enzymatic reaction was allowed to proceed for 60 min at 37 ºC. The enzymatic reaction was stopped by adding 25% (v/v) of 5.0 mol L^{-1} NaOH. iii) Optical readout. The exosomes-coated MPs were separated by using a magnet plate separator, an exosomes-coated MPs pellet on the bottom tube is formed, followed by supernatant separation. The absorbance measurement of the supernatants was thus performed with the microplate reader at 405 nm. After the incubation or washing step, a 96-well magnet plate separator was positioned under the microtiter plate until pellet formation on the bottom corner, followed by supernatant separation. The gold standard colorimetric assay for ALP activity in osteoblastic-derived exosomes was detected and quantified by monitoring the rate of micromoles hydrolyzes per minute, µmol min^{-1}) of pNPP substrate into p-nitrophenol (pNP). Then, a colorimetric calibration curve for pNP was carried out to express the rate of hydrolyzing in enzyme activity (U L^{-1}) (Fig. S6.16, panel A).

6.6.8. Electrochemical biosensor for ALP activity in exosomes

The electrochemical biosensor (Fig. 6.1, panel C) for the determination of the ALP activity from osteoblastic-derived exosomes involved the following steps: i) IMS of the exosomes with antiCDX-MPs (Fig. 6.1, panel A). The immobilization of antibodies on magnetic particles (antiCDX-MPs) is described in detail in the Supp. Data (Fig. S6.1, panel B). The antiCDX-MPs (being CDX any of CD9, CD63 or CD81 biomarkers) (containing 1 × 10^6 antiCDX MPs per well) and the exosomes (100 µL per well, ranging from 60 to 1.17 x 10^5 exosomes μL^{-1}), were simultaneously incubated for 30 min with shaking at 25 °C, followed by three washing steps with TRIS containing 0.5% BSA. ii) Reaction with pNPP substrate. The exosomes-coated MPs were incubated with 150 µL of 10 mmol L^{-1} pNPP in 1 mol L^{-1} DEA buffer pH 9.8 containing 6.0 mmol L^{-1} $MgCl_2$ and 100 mmol L^{-1} KCl. In all cases, the enzymatic reaction was for 60 min at 37 ºC. The enzymatic reaction was stopped by adding 25% (v/v) of 5.0 mol L^{-1} NaOH. iii) Electrochemical readout. The electrochemical measurement of the supernatants was thus performed with the optimized square wave voltammetry (SWV) parameters: E_{sw} =

200 mV, E_{ap} = -1.70 V, E_{sp} = 8 mV, f = 200 Hz, t = 10 s, at potential window from -0.4 to 0.8 V (vs. Ag/AgCl/$KCl_{(sat.)}$). The electrochemical biosensing for ALP activity in osteoblastic-derived exosomes was detected and quantified by monitoring the rate of micromoles hydrolyzes per minute (μmol min^{-1}) of pNPP substrate into p-nitrophenol (pNP), followed by electrochemical conversion into p-aminophenol (pAP). Then, an electrochemical calibration curve for pAP was carried out to express the rate of hydrolyzing in enzyme activity (U L^{-1}).

6.6.9. Electrochemical biosensing of the ALP activity in exosomes isolated by specific epithelial biomarker from breast cancer patients serum

Blood samples from anonymized healthy female donors (n = 10, mean age 35/SD 5 years) and breast cancer female donors (n = 10, stage IV, mean age 50/SD 6 years) were obtained from the Hospital del Mar, Barcelona, Spain. The work was carried out following the principles of voluntariness and confidentiality. The preparation of the human serum from blood is detailed in § 6.7.3. The samples, n = 10 each, were polled in two batches (healthy and breast cancer donors) by mixing 500 μL of each and the exosomes were purified by ultracentrifugation, as previously described above.

The electrochemical biosensing of exosomes from healthy (n = 10, pooled) and breast cancer (n = 10, pooled) patients were examined. Serum-derived exosomes from healthy patients were used as controls. The electrochemical sensor involved the following steps: i) IMS of the exosomes with antiCD326-MPs (containing 1 × 10^6 MPs per well) and the exosomes (100 μL per well, 3.35 μg of protein per assay), were simultaneously incubated for 30 min with shaking at 25 °C, followed by three washing steps with TRIS containing 0.5% BSA. ii) Reaction with pNPP substrate. The exosomes-coated MPs were incubated with 150 μL of 10 mmol L^{-1} pNPP in 1 mol L^{-1} DEA buffer pH 9.8 containing 6.0 mmol L^{-1} $MgCl_2$ and 100 mmol L^{-1} KCl. In all cases, the enzymatic reaction was for 60 min at 37 ºC. The enzymatic reaction was stopped by adding 25% (v/v) of 5.0 mol L^{-1} NaOH. iii) Electrochemical readout, as described above.

6.6.10 Characterization of the exosomes by nanoparticle tracking analysis and transmission electron microscopy

Purified exosomes from hFOB cell line, healthy and breast cancer patients were analyzed by NTA (Fig. S6.2). A size from 50 to 400 nm (considering 95.4% of a Gaussian distribution), but with dominance around 150 and 210 nm was obtained for the hFOB exosomes (Fig. S6.2, panel A), and the concentration was estimated to be 8.70 x 10^{10}/ SD 3.2 x 10^8 particles mL^{-1}. The size diameter distribution of purified

exosomes from healthy ranges from approximately 50 nm to up to 400 nm (considering 95.4% of a Gaussian distribution), showing main peaks: 115, 150, 195, 250 and 295 nm (Fig. S6.2, panel B). Besides, the concentration was estimated to be 3.87 x 10^{10}/ SD 9.72 x 10^{8} particles mL^{-1}. The size diameter distribution for purified exosomes from breast cancer patients ranges from approximately 40 nm to up to 500 nm, showing main peaks: 120, 150, 210, 305 and 460 nm (Fig. S6.2, panel C). Moreover, the concentration was estimated to be 6.49 x 10^{10}/SD 4.21 x 10^{8} particles mL^{-1}. Fig. S6.2, panels A, B and C shows comparatively the TEM images of exosomes derived from hFOB cell line, and serum exosomes of cancer and healthy donors.

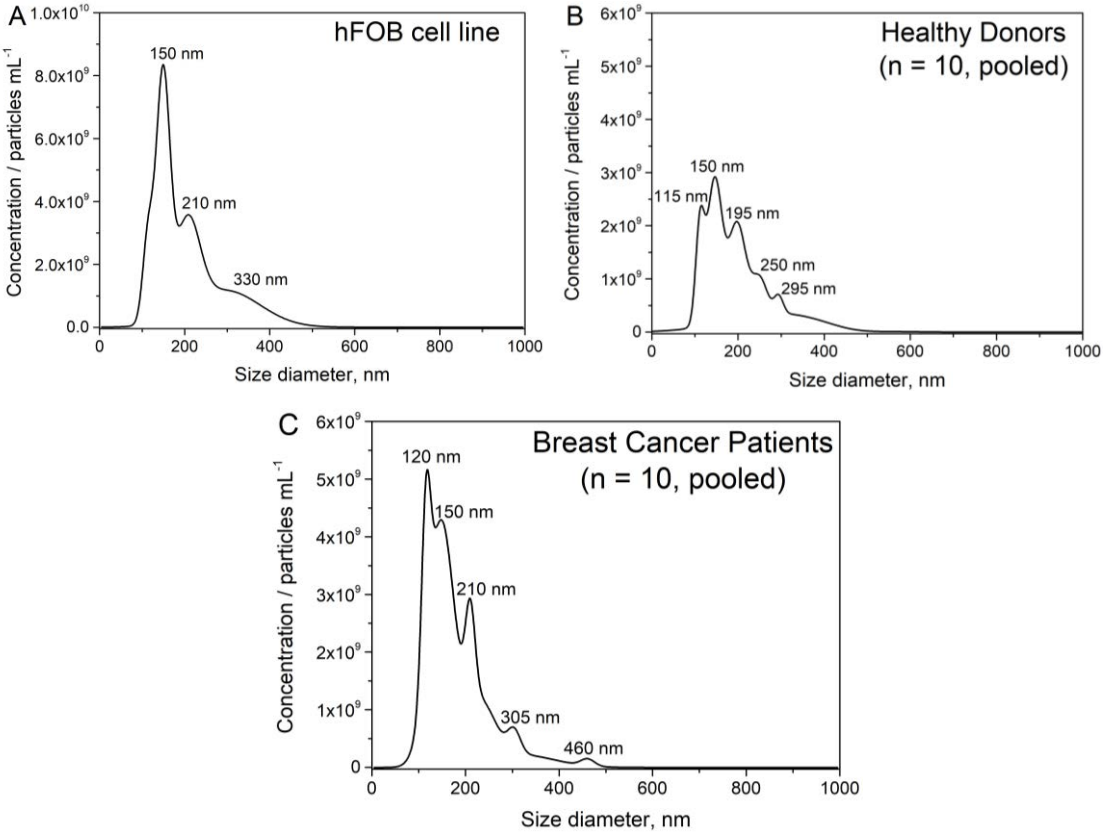

Fig. S6.2. Characterization by NTA of purified exosomes-derived from hFOB cell line (panel A). The NTAs for exosomes purified from serum of healthy donors and breast cancer individuals (n = 10, each) are also shown in Panels B and C, respectively). Nanosight NTA Software analyzed raw data videos by triplicate during 60 s with 50 frames per second and the temperature of the laser unit set at 24.8 ºC.

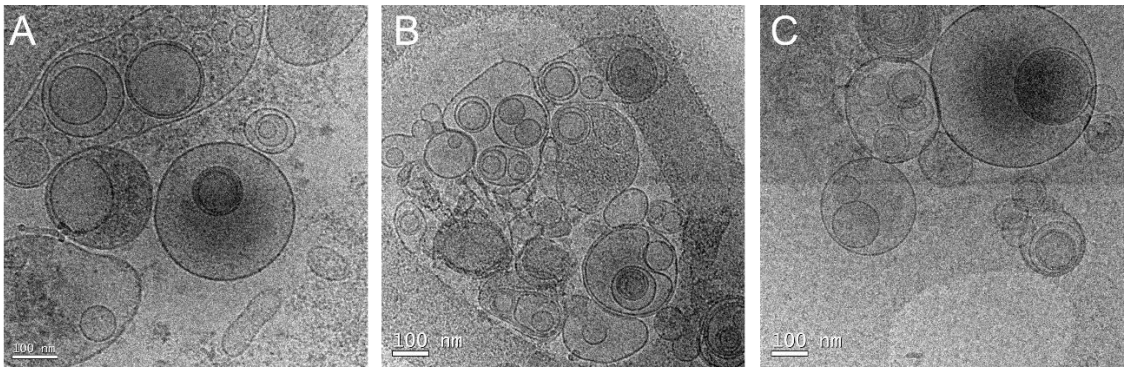

Fig. S6.3. Characterization by TEM of purified exosomes-derived from hFOB cell line (panel A), and for serum exosomes derived from healthy donors and breast cancer individuals (n = 10 each) (Panels B and C, respectively) (200 kV).

6.7.11 Optimization of the determination of ALP activity

Composition of the reaction buffer and pH effect

The activity of alkaline phosphatase enzymes is affected by various factors such as pH, temperature, buffer, substrate, cofactors, etc (Nelson et al., 2013). Among them, the buffer medium and pH in which the enzymatic reaction takes place is the most important parameter. The catalytic effect of the composition of the buffer tris(hydroxymethyl)aminomethane (TRIS) and diethanolamine (DEA) buffers on the rate of hydrolysis of pNPP substrate by ALP enzyme from osteoblast-derived exosomes was evaluated. Generally, the optimum ALP activity in vitro is observed in high pH alkaline medium (typical pH = 9.8).

The colorimetric assay for the study of the composition of the buffer was performed in 96-well microtiter plates and involved the following steps: (i) 20 µL of exosomes (1.76 x 10^9 exosomes per assay) incubated with 130 µL of 10 mmol L^{-1} pNPP in 1 mol L^{-1} DEA buffer pH 9.8 containing 6.0 mmol L^{-1} $MgCl_2$ and 100 mmol L^{-1} KCl. On the contrary; (ii) 20 µL of exosomes (1.76 x 10^9 exosomes) incubated with 130 µL of 10 mmol L^{-1} pNPP in 1 mol L^{-1} TRIS buffer pH 9.8 containing 6.0 mmol L^{-1} $MgCl_2$ and 100 mmol L^{-1} KCl. In all cases, the enzymatic reaction was performed during 5, 10, 15 and 20 min at 37 ºC. (iii) Optical readout. After each reaction time, the absorbance measurement of the supernatants was thus performed with the microplate reader at 405 nm.

Then, the results for the effect of the buffer composition on the rate of pNPP hydrolysis by ALP activity on osteoblast-derived exosomes are shown in Fig. S6.4, panel A (containing 6.0 mmol L^{-1} $MgCl_2$, pH 9.8).

The background absorbance for DEA and TRIS buffer remain unchanged in the whole reaction time, ensuring that both buffers do not influence the stability of substrate. As shown in Figure S6.4, panel A, the DEA buffer provides higher catalytic rates than

TRIS. The presence of amino and hydroxyl groups plays an activating effect on ALP activity, but the role in the mechanism on the ALP enzyme remains unclear. Recently, Sun et al (Sun et al., 2018) have demonstrated a role in the mechanism of the 4-aminophenyl phosphate substrate and DEA buffer as a novel DEA-participated ALP activity.

The colorimetric assay for the study of pH of the DEA buffer was performed in 96-well microtiter plates and involved the following steps: (i) 20 µL of exosomes (1.76 x 10^9 exosomes per assay), incubated with 130 µL of 10 mmol L^{-1} pNPP in 1 mol L^{-1} DEA buffer containing 6.0 mmol L^{-1} $MgCl_2$ and 100 mmol L^{-1} KCl with pH ranging from 9.0 to 11.5. In all cases, the enzymatic reaction was performed for 10 min at 37 ºC. (iii) Optical readout. After the reaction time, the absorbance measurement of the supernatants was thus performed with the microplate reader at 405 nm.

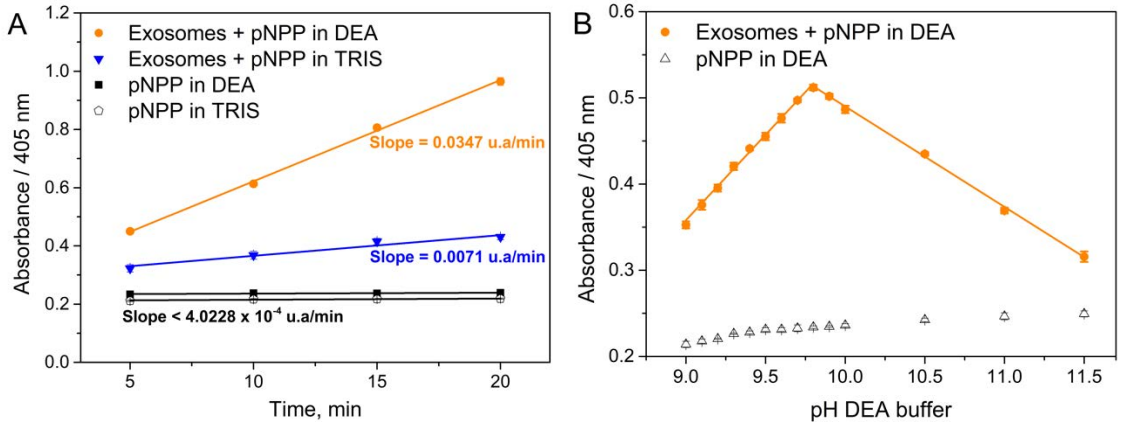

Fig. S6.4. Optimization of the determination of ALP activity in osteoblast-derived exosomes (1.76 x 10^9 exosomes per assay and 10 mmol L^{-1} pNPP/paranitrophenol) by using (A) 1 mol L^{-1} DEA or TRIS buffer, both in pH 9.8 containing 6.0 mmol L^{-1} $MgCl_2$ and 100 mmol L^{-1} KCl and (B) pH study for the 1 mol L^{-1} DEA buffer, ranging from 9.0 to 11.5. The enzymatic reaction was performed for 10 min at 37 ºC. In all cases, the absorbance was measured at 405 nm.

Fig. S6.4, panel B shows the effect of the pH on the rate of hydrolysis of pNPP substrate by ALP enzyme from osteoblast-derived exosomes in 1 mol L^{-1} DEA buffer containing 6.0 mmol L^{-1} $MgCl_2$ with pH ranging from 9.0 to 11.5, showing the optimum value at pH 9.8. Accordingly, 1 mol L^{-1} DEA buffer pH = 9.8 was selected in all further experiments.

Mg^{2+} concentration

The mechanism of the alkaline phosphatase reaction involves three metal-ion (Zn^{+}, Zn^{2+} and Mg^{2+}) which was demonstrated using X-Ray crystallography (Stec et al., 2000). A strong correlation between the third metal (Mg^{2+}) binding site occupancy and conformation of the serine 102 nucleophile, implying that the magnesium ion in the third metal site is required for catalysis (Stec et al., 2000). Therefore, it is necessary to study

the effect of magnesium cation on the catalytic activity of the ALP enzyme present in the osteoblastic-derived exosomes.

The colorimetric assay for the study of Mg^{2+} concentration was performed in 96-well microtiter plates and involved the following steps: (i) 20 µL of exosomes (3.52 x 10^9 exosomes per assay) incubated with 130 µL of 10 mmol L^{-1} pNPP in 1 mol L^{-1} DEA buffer pH 9.8 containing 100 mmol L^{-1} KCl and $MgCl_2$ ranging from 0 up to 50 mmol L^{-1}. In all cases, the enzymatic reaction was performed for 10 min at 37 ºC. (iii) Optical readout. After the reaction time, the absorbance measurement of the supernatants was thus performed with the microplate reader at 405 nm, as always.

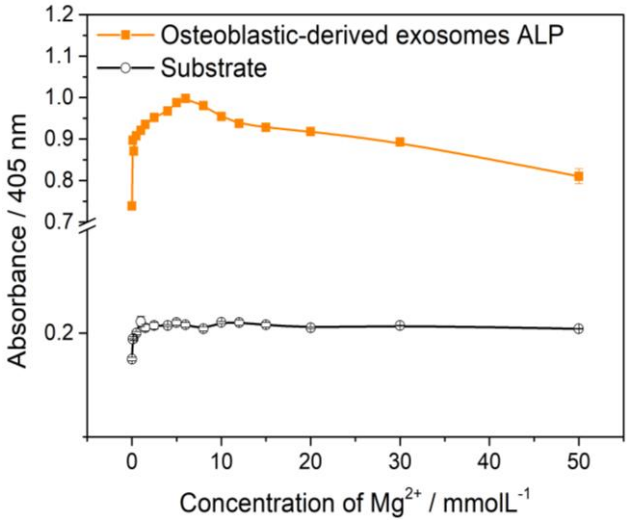

Fig. S6.5. Effect of the Mg^{2+} ion on ALP enzyme from osteoblast-derived exosomes (3.52 x 10^9 exosomes per assay) by using 10 mmol L^{-1} pNPP in 1 mol L^{-1} DEA buffer pH 9.8 containing 100 mmol L^{-1} KCl and $MgCl_2$ ranging from 0 up to 50 mmol L^{-1} as nominal concentration. In all cases, the enzymatic reaction was during 10 min at 37 ºC, followed by absorbance measurement at 405 nm.

Fig. S6.5 shows that the ALP enzyme from osteoblastic-derived exosomes presents a good pNPP hydrolysis even without additional Mg^{2+} ion. The cell culture medium (DMEM/F12, nº D9785) contains $MgCl_2$ (0.6 mmol L^{-1}) and $MgSO_4$ (0.4 mmol L^{-1}), i.e., it would be expected that osteoblastic-derived exosomes to carry some bound Mg^{2+} on the intrinsic ALP enzyme. However, as shown on Fig. S6.5, the reaction rate is enhanced in the presence of additional Mg^{2+} ion up to 6.0 mmol L^{-1}. Besides, an inhibitory effect in the ALP enzyme over 6.0 mmol L^{-1} Mg^{2+} ion is observed. These results on the Mg^{2+}-activator/inhibitor is in agreement with previous works (Butterworth, 1968; Nayudu and Miles, 1969). Regarding the optimal concentration of the Mg^{2+} ion, in-depth crystallographic investigations suggests that an octahedral Mg^{2+} is coordinated by side-chain oxygen atoms of aspartate acid 51, threonine 155 and glutamic acid 322, and three water molecules, which one of the water molecules is nearby (3.1 Å) of the side-chain of the hydroxyl group of serine 102, activating it for nucleophilic attack on the phosphate

monoester (Stec et al., 2000). On the other hand, at a high concentration of the Mg^{2+} ion, it was demonstrated by Hanes-Woolf and Hill plots that the Mg^{2+} ion is in the form of the complex ion with the phosphate monoester, and consequently, the concentration of free Mg^{2+} is dramatically reduced (Butterworth, 1968).

According to the results, 1 mol L^{-1} DEA buffer pH = 9.8 containing 6.0 mmol L^{-1} $MgCl_2$ and 100 mmol L^{-1} KCl was selected in all further experiments.

Study of the stop solution composition

The ALP reaction can be easily stopped, as any other enzyme, by adding an agent that denaturalizes the conformation (Nelson et al., 2013). Two different stop solutions were studied, in order to increase the readout sensitivity of enzymatic product using end-point assays: (i) alkalization of the enzyme reaction with NaOH or (ii) acidification with H_3PO_4.

The colorimetric assay for the study of Mg^{2+} concentration was performed in 96-well microtiter plates and involved the following steps: (i) 20 µL of exosomes (1.76 x 10^9 exosomes per assay), incubated with of 130 µL of 10 mmol L^{-1} pNPP in 1 mol L^{-1} DEA buffer pH 9.8 containing 6.0 mmol L^{-1} $MgCl_2$ and 100 mmol L^{-1} KCl. In all cases, the enzymatic reaction was performed for 10 min at 37 ºC. (iii) After the reaction time, the stop solution (either 5 mol L^{-1} NaOH or 2 mol L^{-1} H_3PO_4) was added at 10 or 25 % (v/v). (iv) Optical readout. After the reaction time, the absorbance measurement of the supernatants was thus performed with the microplate reader at 405 nm.

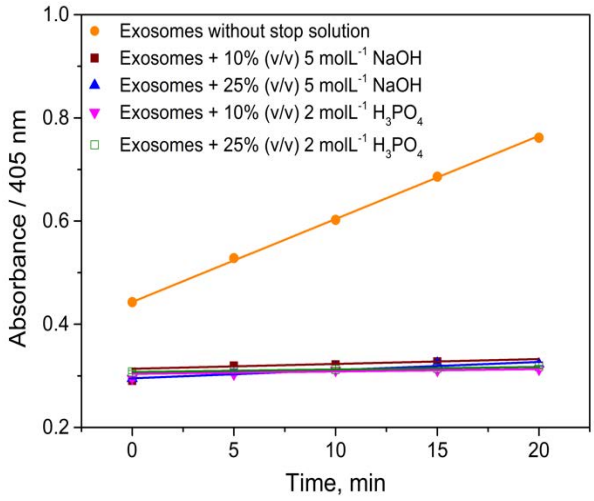

Fig. S6.6. Study of the stop solution composition on ALP enzyme activity in osteoblast-derived exosomes (1.76 x 10^9 exosomes per assay) by using 10 mmol L^{-1} pNPP in 1 mol L^{-1} DEA buffer pH 9.8 containing 6.0 mmol L^{-1} $MgCl_2$ and 100 mmol L^{-1} KCl. The graph shows the absorbance without stop solution (●) and after adding 10% (v/v) (■) and 25% (v/v) (▲) of 5 mol L^{-1} NaOH (pH 13.0) and 10% (v/v) (▼) and 25% (v/v) (□) of 2 mol L^{-1} H_3PO_4 (pH 5.5). In all cases, the enzymatic reaction was performed during 0, 5, 10 and 20 min at 37 ºC, followed by absorbance measurement at 405 nm.

Fig. S6.6 shows that the addition of either 5 mol L^{-1} NaOH or 2 mol L^{-1} H_3PO_4 at 10 and 25% (v/v) can effectively stop of the ALP enzymatic reaction. However, 5 mol L^{-1} NaOH at 25% (v/v), showed a lower background signal.

Beside the effectiveness of all stop solution in preventing the enzymatic activity of ALP, another important parameter that must be evaluated is the effect of such drastic change of pH in the product of the enzymatic reaction, para-nitrophenol. Accordingly, a change in the pH can dramatically affect the readout (optical and electrochemical).

The effect of the stop solution on the optical and electrochemical readout involved the following steps: (i) 130 µL of 250 µmol L^{-1} pNP in 1 mol L^{-1} DEA buffer pH 9.8 containing 6.0 mmol L^{-1} $MgCl_2$ and 100 mmol L^{-1} KCl, followed by the addition of ii) 25% (v/v) of 5 mol L^{-1} NaOH or 2 mol L^{-1} H3PO4. (iii) Optical and electrochemical readout. The absorbance measurement of the supernatants in microplates was thus performed with the microplate reader at 405 nm. The electrochemical readout was performed by square wave voltammogram (SWV) in a standard 500-µL one compartment three-electrode cell. The SWV measurement of the supernatants was thus performed by using a BDD electrode as a working electrode in potential windows ranging from -0.4 to 0.8 V (Ag/AgCl/$KCl_{(satd.)}$). SWV conditions: E_{sw} = 200 mV, E_{ap} = -1.70 V, f = 200 Hz, E_{sp} = 8 mV.

Fig. S6.7, panel A, shows the effect of the stop solution on the optical spectrum of the para-nitrophenol (pNP). With the addition of 20 % (v/v) of 5 mol L^{-1} NaOH, the pH of the pNP in 1 mol L^{-1} DEA solution changes from 9.8 to 13.0 but no shift occurs on maximum absorbance peak (λ_{max} 405 nm). As pNP in 1 mol L^{-1} DEA solution becomes more acid with the addition of H_3PO_4, the solution loses a bright yellow color corresponding to a bathochromic shift in the absorbance spectrum from λ_{max} of 405 nm (pH 9.8) to λ_{max} of 318 nm (pH 5.5). With a pKa of 7.2, pNP is almost exclusively neutral at low pH, but in basic conditions, pNP will be in its anionic form, p-nitrophenoxide (pNP^-) (Woods and Walker, 2013).

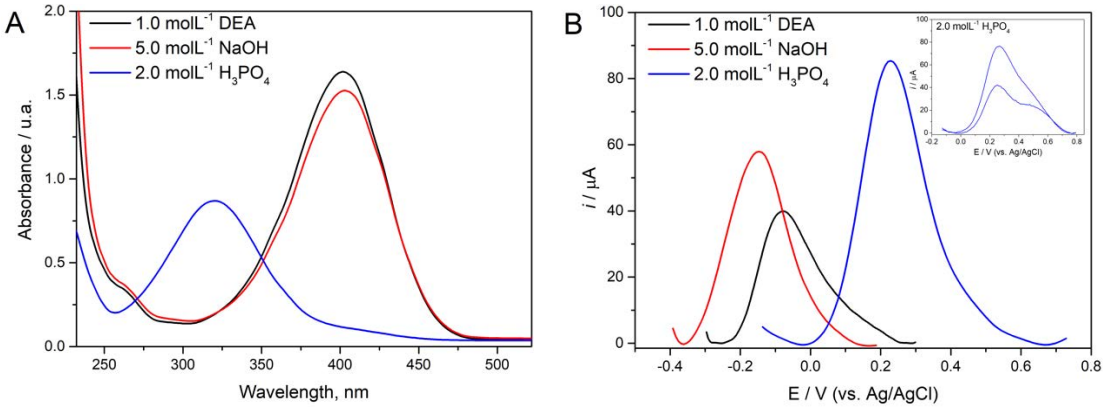

Fig. S6.7. (A) UV-vis spectra and (B) SVW of 250 µmol L^{-1} pNP in (-) 1 mol L^{-1} DEA solution pH 9.8; after adding 25% (v/v) of (–) 5 mol L^{-1} NaOH (pH 13.0) and (–) 2 mol L^{-1} H3PO4 (pH 5.5). BDD electrode was used as working electrode. SWV conditions: E_{sw} = 200 mV, E_{ap} = -1.70 V, E_{sp} = 8 mV, f = 200 Hz, t = 10 s.

Fig. S6.7, panel B, shows the effect of the stop solution on SWV of the pNP. As expected, the potential and current peaks at -77 mV observed in 1 mol L^{-1} DEA solution were affected by the addition of NaOH and H_3PO_4. An increase in the current peak of 18 µA is accompanied by a shift from -77 mV to -150 mV with the addition of NaOH. On the other hand, with the addition of H_3PO_4, an increase in the current peak of 45 µA and a potential shift from -77 mV to 228 mV is observed. However, some details should be pointed out: first, the great increase in the current peak is accompanied by the strong fouling of the electrode surface, probably due to dimers/oligomers. Second, a split of two peaks is observed when the concentration of pNP is decreasing (Fig. S6.7, panel B, inset). As pNP in 1 mol L^{-1} DEA buffer pH 9.8 becomes with pH 5.5 with the addition of H_3PO_4, and after the electron transfer, the formation of dimer/oligomers via amino-amino coupling is facilitated. This probably happens in the same way as in the dimerization of aniline (Sapurina et al., 2015) and dapsone (Moura et al., 2015). Then, the electrochemical determination of pNP in H3PO4 as a stop solution is not desirable and relatively complicated. Therefore, NaOH is used in further determination as stop solution since it proved to be more suitable for both electrochemical and optical measurements.

6.7.12. Comparative study of the kinetic parameters of ALP and ALP in exosomes

Michaelis-Menten constants (K_m) and maximal rates (V_{max}) for the hydrolysis of p-nitrophenyl phosphate (pNPP) by ALP enzyme from osteoblastic-derived exosomes and calf intestinal ALP were comparatively determined by the spectrophotometric method.

The colorimetric assay for determining the kinetic parameters of the ALP enzyme from osteoblastic-derived exosomes was performed in 96-well microtiter plates and involved the following steps: (i) 20 µL of exosomes (5.8 x 10^6 exosomes μL^{-1} per assay), incubated with 130 µL of pNPP in a concentration ranging from 0.01 to 23 mmol L^{-1} in 1 mol L^{-1} DEA buffer pH 9.8 containing 6.0 mmol L^{-1} $MgCl_2$ and 100 mmol L^{-1} KCl. In all cases, the enzymatic reaction was performed for 10 min at 37 ºC. The enzymatic reaction was stopped by adding 25% (v/v) of 5.0 mol L^{-1} NaOH. (iii) Optical readout. The absorbance measurement of the supernatants was thus performed with the microplate reader at 405 nm.

Fig. S6.8, panel A shows that the ALP activity from osteoblast-derived exosomes obeys the Michaelis-Menten relationship (r^2 = 0.8333) (Ariyawansha et al., 2018). To characterize the ALP-catalyzed reaction from osteoblastic-derived exosomes, the catalytic parameters V_{max} and K_M were determined using the Lineweaver-Burk plot (Lineweaver and Burk, 1934). A suitable linear plot of the reciprocal of the rate of

hydrolysis of pNPP versus reciprocal of different pNPP substrate concentrations was obtained. For osteoblast-derived exosomes, the linear fitting yields a straight line (r^2 = 0.9886) (Fig. S6.8, panel B), and the V_{max} and K_m were estimated to be 3.196/SD 0.018 μmol L^{-1} min^{-1} and 0.763/SD 0.012 mmol L^{-1}, respectively. The V_{max} and K_m values were close to those reported for ALP (Chaudhuri et al., 2013; Li et al., 2017). As is well-known, the substrate concentration must be higher (normally 10-fold) than its Km value in order to ensure saturation of the enzyme. Thus, 10 mmol L^{-1} was selected as the optimum pNPP concentration for further ALP determination.

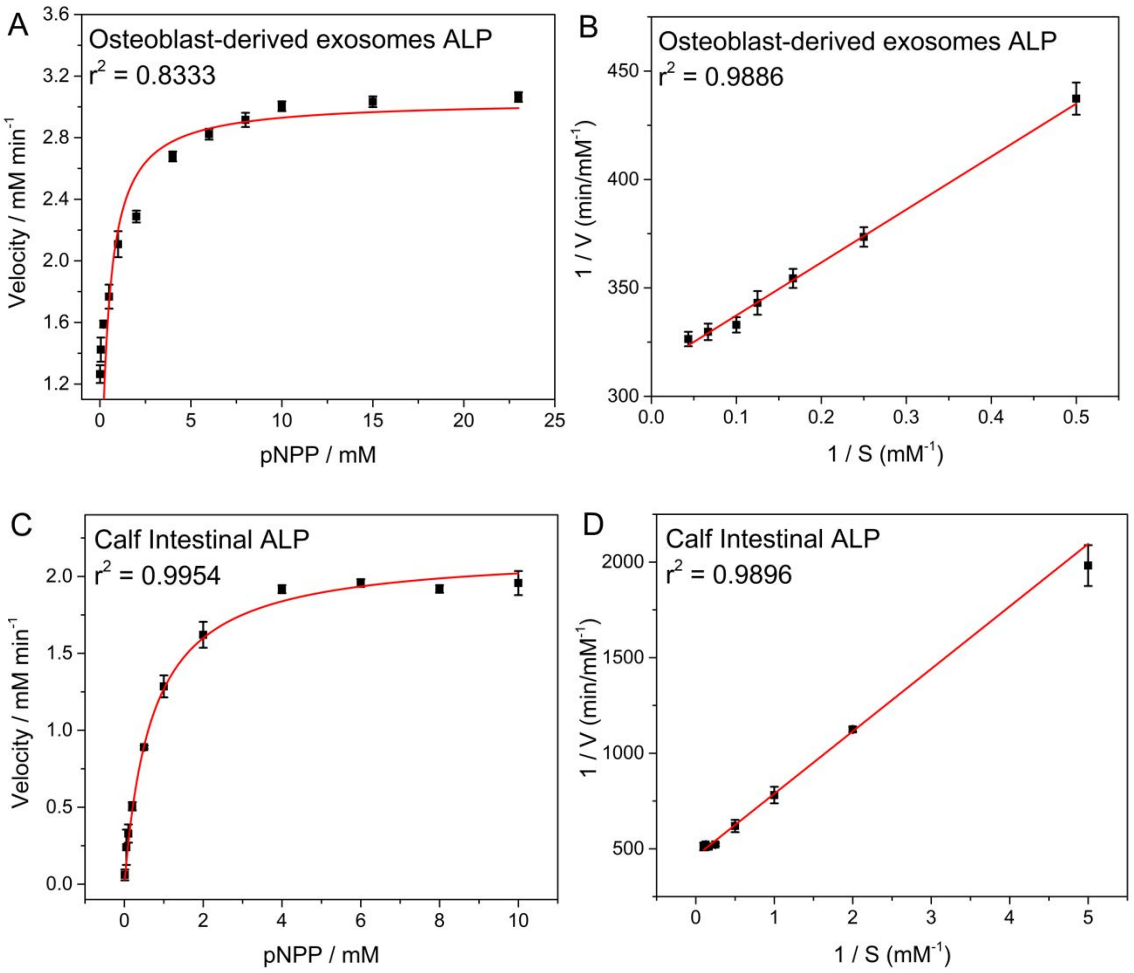

Fig. S6.8. Michaelis-Menten relationship and Lineweaver-Burk plot for the hydrolysis of pNPP by ALP enzyme from (A-B) osteoblastic-derived exosomes (5.8 x 10^6 exosomes μL^{-1}) and (C-D) calf intestinal ALP (0.67 U L^{-1}) in 1 mol L^{-1} DEA buffer (pH 9.8) containing 6.0 mmol L^{-1} $MgCl_2$ and 100 mmol L^{-1} KCl, during 10 min at 37 ºC. The concentration of pNPP was varied from 0.01 to 23 mmol L^{-1}. The absorbance intensity was monitored at 405 nm.

For comparison, the determination of the kinetics parameters of the calf intestinal ALP was determined at same conditions (buffer, temperature and pH), but with 0.67 U L^{-1} calf intestinal ALP per assay and pNPP concentrations ranging from 0.01 to 10 mmol L^{-1} containing 2.5 mmol L^{-1} $MgCl_2$ ($MgCl_2$ concentration was optimized as shown in the Fig. S6.5, panel B), during 30 min (Fig. S6.8, panel C-D). Here, for calf intestinal ALP,

the V_{max} and K_m were estimated to be 2.170/SD 0.037 μmol L^{-1} s^{-1} and 0.708/SD 0.015 mmol L^{-1}, respectively. In this case, similar kinetic parameters were obtained to those from osteoblast-derived exosomes, which indicates that a minimum effect in the kinetic was observed in the ALP when it is carried on exosomes, compared with if it is free in solution.

6.6.13. Characterization of the Boron-doped diamond electrode by SEM and Raman spectroscopy

Fig. S6.9 shows the SEM images of the boron-doped microcrystalline diamond (BDD) electrode with a boron/carbon ratio of the 20,000 ppm. A homogeneous and rough diamond film on Si substrate with the formation of microcrystalline grains randomly oriented is observed. The small diamond grains are observed, which increases the area over the substrate and allows a better response in the electroanalytical applications (Cobb et al., 2018).

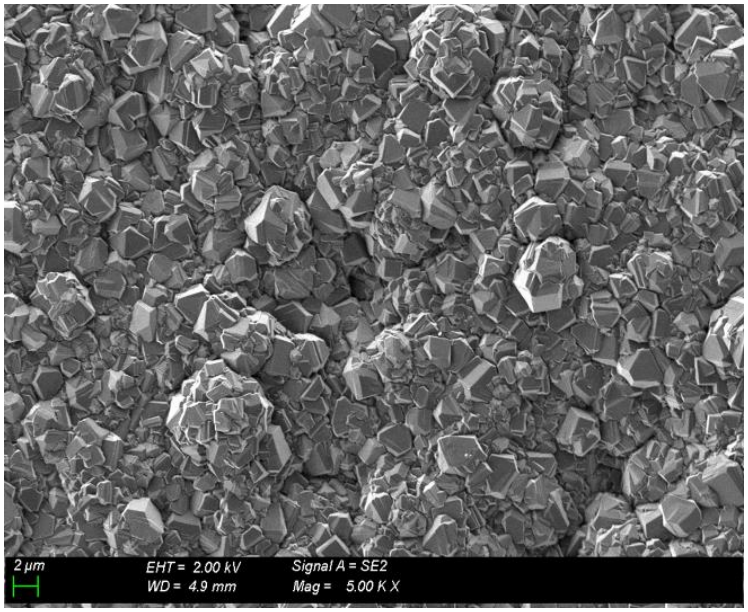

Fig. S6.9. SEM photographs of the BDD/Si electrodes with boron/carbon ratio of the 20,000 ppm. The image was obtained in the Service of Microscopy, Universitat Autònoma de Barcelona.

Fig. S6.10 shows the Raman spectrum of the boron-doped microcrystalline diamond (BDD) electrode with a boron/carbon ratio of the 20,000 ppm. A characteristic diamond peak at 1332 cm^{-1} and 1200 cm^{-1} can be attributed to the disorder-induced in the diamond lattice due to the incorporation of boron (Wei et al., 2012). A band around 500 cm^{-1} can be attributed to the vibration modes of pairs of boron, distorting the diamond network (May et al., 2008). The absence of peaks around 1500 cm^{-1} can be

noticed related to the graphitic bonds, indicating the quality of the electrode (Trava-Airoldi et al., 1995).

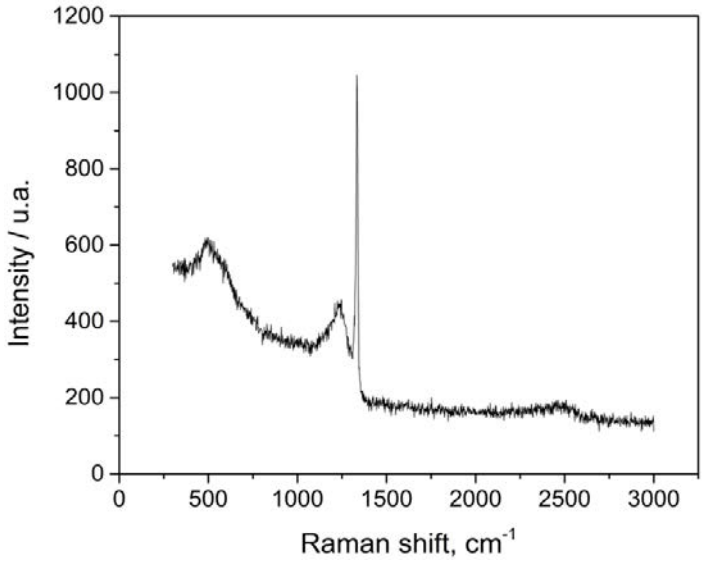

Fig. S6.10. RAMAN spectrum of the BDD/Si electrodes with boron/carbon ratio of the 20,000 ppm.

6.6.14. Characterization of the electrochemical readout on BDD electrode

The cyclic voltammetric studies were carried out to examine the redox behavior of the boron-doped diamond (BDD) electrode in 0.5 mol L^{-1} H_2SO_4 in a wide potential window from -1.0 to 2.5 V at a scan rate of 50 mV s^{-1}. In Fig. S6.11, panel A, no faradaic processes were observed for the BDD electrode in the potential range of -0.70 to 2.20 V.

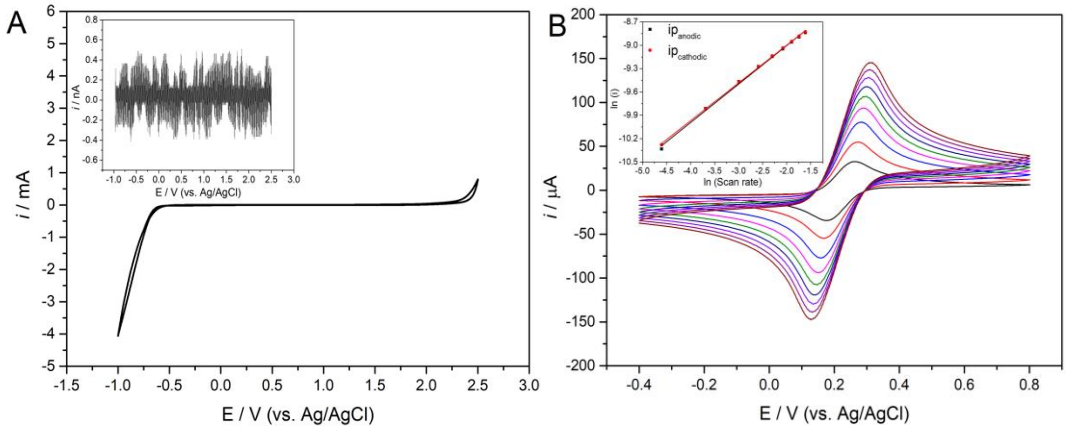

Fig. S6.11. (A) Cyclic voltammograms of the BDD electrode in 0.5 mol L^{-1} H_2SO_4 at a scan rate of 50 mV s^{-1}. Inset: background current measured after 30 min at open-circuit potential (OCP). (B) Cyclic voltammograms of the 5.0 mmol L^{-1} $Fe(CN)_6^{-4/-3}$ redox pair in 100 mmol L^{-1} KCl supporting electrolyte for the BDD electrode at different scan rates from 10 to 200 mV s^{-1}. Inset: natural logarithm of current peaks (i_{p_a} and i_{p_c}) versus scan rate.

The high overpotential for hydrogen and oxygen evolution were consistent with low adsorption of protons or hydronium ions on the fully hydrogenated diamond surface (Martin, 1996). This working wide potential window is comparable with experimentally for

the BDD film deposited on silicon, as well as with the values described in the literature (Martin, 1996). This wide potential window allows the detection of oxy-reduction reactions in certain potentials that would be outside the working potential range of conventional electrodes, such as platinum, glassy carbon and the graphite. Besides, the very low background currents (< 5 nA) (inset of the Fig. S6.11, panel A) observed is an indication that other electrochemically active species are not strongly adsorbed on diamond.

Further characterization was performed by cyclic voltammograms using the BDD electrode in 5.0 mmol L^{-1} $Fe(CN)_6^{-4/-3}$ at different scan rates from 10 to 200 mV s^{-1} in a potential window from -0.4 to 0.8 V. As observed in Fig. S6.11, panel B, all the scan rates shows one couple well-defined redox pair correspondent to the Fe(III)/Fe(II) ions. The anodic peak potential (E_{pa}) and cathodic peak potential (E_{pc}) are located at 26 and 17 mV (vs. Ag/AgCl/$KCl_{(sat.)}$, 10 mV s^{-1}), respectively. The formal potential (E_0) is 21 mV and peak-to-peak separation (ΔE_p) of 52 mV was observed, which is close to the value of 59 mV of the Nernst equation (Adams, 1969). Further, both anodic (i_{p_a}) and cathodic (i_{p_c}) peak currents are linearly proportional with the scan rate as shown in the inset of Fig. S6.11, panel B, which indicates that the electrode reaction corresponds to a surface-controlled reversible process.

The expression for current peak, ip, for a reversible charge transfer is given by the Randles-Sevcik equation (Bard and Faulkner, 2001):

$$i_p = 2.69\ x\ 10^5 n^{3/2} A C_{bulk} D^{1/2} v^{1/2} \qquad \text{(Eq.1)}$$

where n is the number of electron equivalent exchanged involved in the charge-transfer step, A (cm^2) is the active area of the working electrode, D (cm^2 s^{-1}) and C_{bulk} (mol cm^{-3}) are the diffusion coefficient and the bulk concentration of the electroactive species, respectively; v is the voltage scan rate (V s^{-1}). The diffusion coefficient for the $Fe(CN)_6^{-3}$ and $Fe(CN)_6^{-4}$ are 7.6 × 10^{-6} cm^2 s^{-1} and 6.3 × 10^{-6} cm^2 s^{-1} (Adams, 1969), respectively.

In the limiting case, where the non-adsorbed electroactive species undergo charge transfer either reversibly or irreversibly, a slope for $ln\ ip\ vs\ ln\ v$ of 0.50 is predicted (Nicholson and Shain, 1964). The plot of lni_p versus lnv for i_{p_a} (r^2 ≥ 0.9978) and i_{p_c} (r^2 ≥ 0.9994) for 5.0 mmol L^{-1} $Fe(CN)_6^{-4/-3}$ using the BDD electrode in scan rates from 10 to 200 mV s^{-1} has slope 0.494 and 0.485 (inset of the Fig. S6.11, panel B), respectively. The electro-active area of the BDD electrode was estimated from Eq. 1.

The real electro-active area, A_{real}, which provides information on active surface area and may also be taken by some as to be the “roughness factor”, was estimated from the following: $A_{real} = A_{active}/A_{Geo}$, where A_{Geo} is the geometric area of the BDD electrode. The electro-active area (A_{active}) of the BDD electrode were estimated to be 3.83 cm^2. This increase in the electrochemical area of approximately eight times the geometric area occurs because the material is extremely rough as shown in the SEM images (Fig. S6.9). Therefore, a large electrochemical area also allows a better response in the electroanalytical applications, as in this case, the detection of p-aminophenol (pAP) by means the conversion of the p-nitrophenol (pNP) generated by hydrolysis of p-nitrophenyl phosphate (pNPP) substrate on reaction with alkaline phosphatase (ALP) enzyme.

The cyclic voltammograms (CV) of a 10 mmol L^{-1} paranitrophenol (pNP) were obtained in 1 mol L^{-1} DEA supporting electrolyte (pH 9.8) containing 6.0 mmol L^{-1} $MgCl_2$ and 100 mmol L^{-1} KCl, using a microcrystalline boron-doped diamond (BDD) electrode, in a potential window from -2.0 to 1.5 V, at a scan rate of 50.0 mV s^{-1}, at a temperature of 25 ºC. CV behavior is shown in Fig. S6.12 panel A.

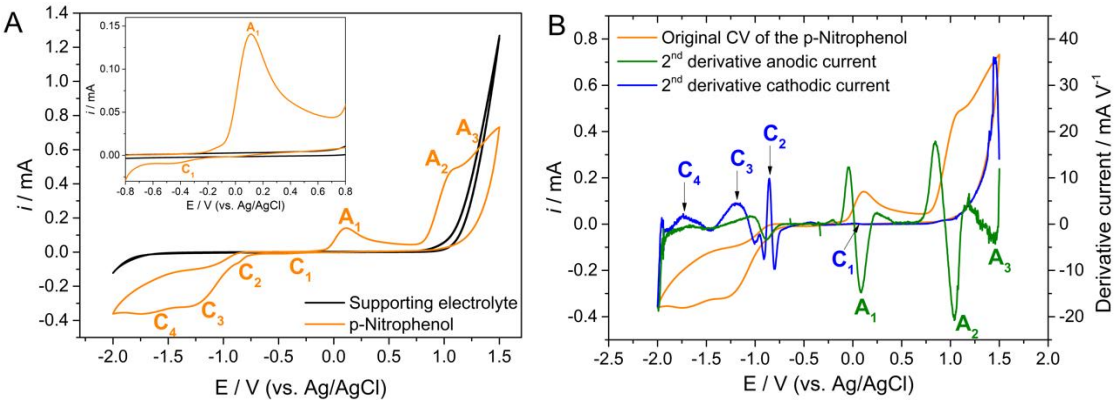

Fig. S6.12. (A) Cyclic voltammograms for BDD electrode in 10 mmol L^{-1} pNP in 1 mol L^{-1} DEA buffer (pH 9.8) containing 6.0 mmol L^{-1} $MgCl_2$ and 100 mmol L^{-1} KCl, at a scan rate of 50 mV s^{-1}. Inset: close view of the A1/C3 quasi-reversible process. The cyclic voltammogram of the supporting electrolyte, i.e., 1 mol L^{-1} DEA buffer (pH 9.8) containing 6.0 mmol L^{-1} $MgCl_2$ and 100 mmol L^{-1} KCl is also presented for comparison. (B) Original cyclic voltammogram (orange line) for BDD electrode in 10 mmol L^{-1} pNP in 1 mol L^{-1} DEA buffer (pH 9.8) containing 6.0 mmol L^{-1} $MgCl_2$ and 100 mmol L^{-1} KCl, at a scan rate of 50 mV s^{-1}, and its 2nd derivative current of electrode: 2nd derivative anodic current (green line) and 2nd derivative cathodic current (blue line).

In Fig. S6.12 panel A, no faradaic processes were observed for BDD electrode in 1 mol L^{-1} DEA supporting electrolyte (pH 9.8) containing 6.0 mmol L^{-1} $MgCl_2$ and 100 mmol L^{-1} KCl, in the potential range of -1.60 to 0.70 V. This wide potential window remains even in high alkaline medium (pH 9.8). The anodic current peaks at 1.05 V (A_2) correspond to the oxidation of a phenolate (dominant form in alkaline solution), to phenoxy radicals and subsequently to phenoxy cation at 1.42 V (A_3), which both current peaks overlap with the oxygen-evolution region (>1.0 V vs. Ag/AgCl, DEA solution pH

9.8). The products generated from this reaction undergoes adsorption process and the oxidation peak current gradually decreased with increasing the number of cyclic potential scans (data not shown). This result may be attributed to a progressive deposition of the oxidative product of pNP (dimer or polymer) on the electrode surface, impeding further electrooxidation of pNP. Due to the overlapping of the anodic faradaic processes with the oxygen-evolution region, and the small and broad current for the cathodic peaks, for an accurate assignment of the potential peaks derivative voltammetry was performed (Fig. S6.12, panel B). As can be seen on the second derivative curves, the small variations of the current in the original voltammogram are revealed. This is most evident for the C1, C_2, C_3 and C_4 cathodic peaks in the CV. The cathodic current peak at -0.86 V (C_2) may be attributed to the reduction of nitrophenol (-NO_2) to nitrophenol anion (-NO_2^-) by one-electron transfer (slow) and at -1.19 V (C_3) represents the reduction to hydroxyaminophenol (-NHOH) with three electrons and four protons transfer electrochemical process (fast), and subsequent reduction at -1.73 V (C_4) to p-aminophenol (-NH_2) by two-electron and two-proton process. Then, a well-defined anodic current is observed at 85 mV (A_1) corresponding to oxidation of the p-aminophenol (-NH_2), and a small cathodic current peak (C_1) is observed at 25 mV in the reverse scan. These electrochemical mechanisms for p-nitrophenols were widely reported using the BDD electrode in alkaline media (Cañizares et al., 2004, 2003; Jiang et al., 2010; Zhu et al., 2007).

As shown in Fig. S6.12 panel A, the p-nitrophenol undergoes oxidation at high potential, which overlaps to the oxygen-evolution region which is not desirable and relatively complicated in the determination of an electroactive analyte at the same redox potential of the oxygen-evolution region. Besides, according to the CVs results, it was observed that the oxidation of p-aminophenol was more sensitive and well-shaped than the oxidation of pNP as well as the reduction of pNP towards p-hydroxyaminophenol or p-aminophenol. Therefore, we applied the electron transfer mechanism in our study which involves the detection of the pNP (generated by hydrolysis of p-nitrophenyl phosphate (pNPP) substrate on reaction with alkaline phosphatase (ALP) enzyme) by means of the oxidation of p-aminophenol. This provides various advantages as the low potential applied to avoid oxidation of interferer substances, as well as potential so far from the oxygen-evolution region.

Square wave voltammetry (SWV) is a modified staircase voltammetry, in which the potential waveform provides an improvement in the current signal resulting in a minimal capacitive current. The combination of the SWV and BDD electrodes has proved to be an interesting and desirable alternative for the analytical determination of organic molecules (Pecková et al., 2009). It is well established that BDD electrodes have several

advantages compared with conventional electrodes, including a wide potential window in aqueous solutions, very low background current, weak adsorption for most types of organic molecules, high stability of response, and good electroactivity toward certain organic species all of which deactivate the surface of other (Cobb et al., 2018). Depending on the nature of the electrode and analyte, an optimization of the parameters (frequency, pulse amplitude, step potential) should be performed. Here, as the analyte to be determinate is p-aminophenol (pAP) by means the conversion of the p-nitrophenol (pNP) generated by hydrolysis of pNPP substrate on reaction with ALP enzyme, a systematic study of the best SWV-parameters in order to obtain a high, reliable and reproducible current signal was performed.

Frequency study. Fig. S6.13 panel A shows the set of CVs obtained for different frequency (f) values from 10 up to 250 Hz. For larger values of the effect on the peak current was negligible. In the inset 1 of Fig. S6.13, panel A, indicates a nonlinear function between peak current and frequency.

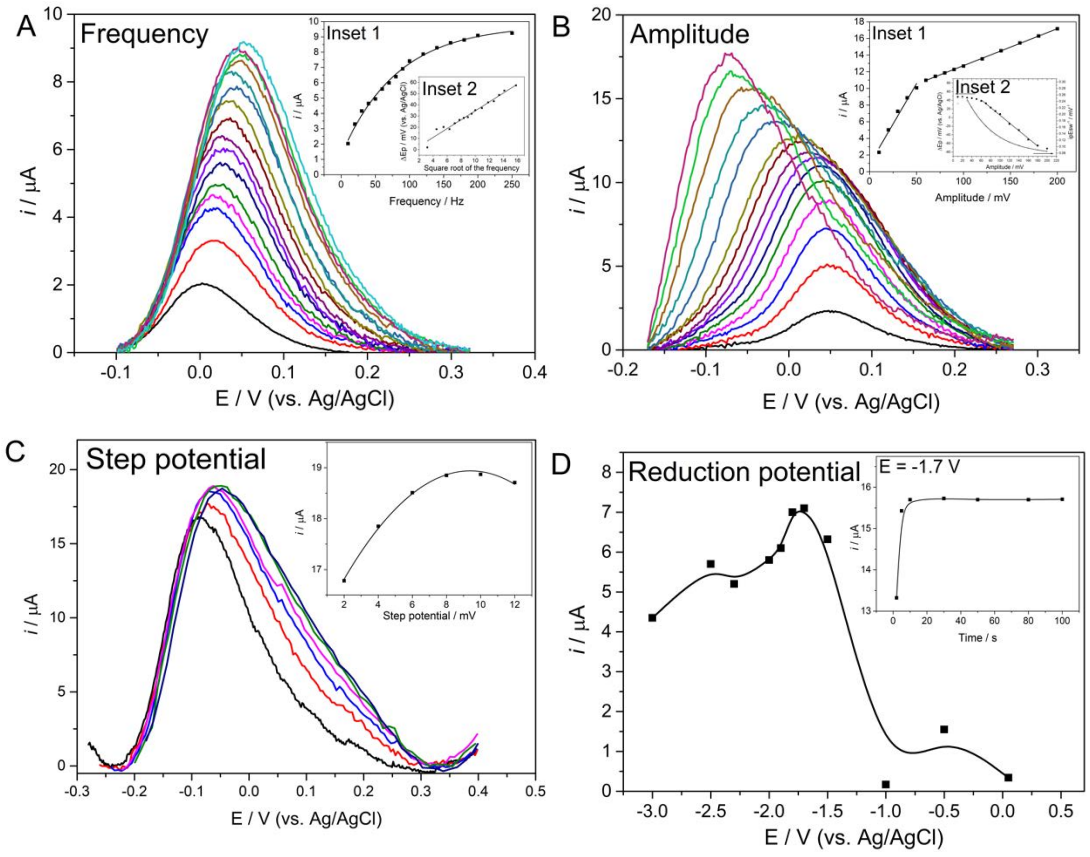

Fig. S6.13. Square wave voltammograms for BDD electrode in 100 µmol L^{-1} pNP in 1 mol L^{-1} DEA buffer (pH 9.8) containing 6.0 mmol L^{-1} $MgCl_2$ and 100 mmol L^{-1} KCl. (A) Influence of the frequency ranging from 10 to 250 Hz. Inset 1: dependence of the current peak with the square wave frequency. Inset 2: dependence of the potential peak with the square root wave frequency. (B) Influence of the pulse amplitude ranging from 10 to 200 mV. Inset 1 and 2: dependence of the current peak and potential peak with pulse amplitude, respectively. (C) Influence of the step potential ranging from 2 to 12 mV. Inset: parabolic dependence of the current peak with step potential. (D) Influence of the reduction potential ranging from -3.0 to 0.05 V. Inset 1: dependence of the current peak (applied -1.7 V) with time.

According to the accepted theories for SWV (Lovrić and Komorsky-Lovric, 1988), this behavior corresponds to a quasi-reversible process. Moreover, inset 2 revealed that the peak potential varies linearly with the logarithm of the frequency, which indicates that no product is adsorbed on the electrode surface (Lovrić and Komorsky-Lovric, 1988).

Amplitude. Fig. S6.13 panel B shows the set of CVs obtained for different pulse amplitudes (E_{sw}) values from 10 up to 200 mV. Fig. S6.13 panel B shows that the peak is sensitive to the change of the E_{sw}. Besides, the limiting current is shifted to negative potentials with the increasing of E_{sw}. The dependence of ip on E_{sw} exhibits changes on the slope at 50 mV. The Ep decreases linearly on E_{sw} from 50 up to 180 mV, meanwhile, the dependence of Ep and ipE_{sw}^{-1} on E_{sw} decreases exponential, which indicates a quasi-reversible process (Lovrić and Komorsky-Lovric, 1988; Vettorelo and Garay, 2016).

Step potential. In the staircase step potential (E_{sp}) measurement, the applied voltage is the difference between two consecutive steps in voltage, and the resulting current behavior should reflect a better symmetrical and Gaussian-shaped around of the Ep, depending on the kinetic rate of specie. Fig. S6.13 panel C shows the set of CVs obtained for different potential (Eps) values from 2 up to 12 mV. Fig. S6.13 panel C shows that there an increase from 2 to 8 mV, however, the increment value was almost negligible. This behavior could correspond to a reversible or quasi-reversible process, wherein this case the increment in the E_{sp} do not influence the fast kinetic.

Accumulation potential. The conversion of the 4-nitrophenol (pNP) into hydroxyaminophenol (-NHOH) involves a four-electron and proton transfer electrochemical process, and subsequent conversion to p-aminophenol (pAP). Then, pAP could be formed by applying a fixed-single potential (accumulation potential, E_{ap}). The anodic current peak at 85 mV corresponds to the oxidation of the pAP. In order to evaluate the yield of conversion of pNP into pAP, cyclic voltammograms were recorded at different reduction potentials applying by 10 seconds: -3.0, -2.5, -2.0, -1.5, -1.0, -0.5, 0.05 V. Fig S6.13, panel D shows that the yield of conversion of pNP into pAP is strongly dependent of the reduction potential. The ideal reduction potential is observed on -1.70 V, meanwhile at -1.0 V is the current-poorest potential. This cathodic potential is the exact potential for the reduction of the hydroxyaminophenol (-NHOH) towards pAP (-NH_2), as shown in Fig. S6.12. The quasi-reversible redox couple (A_1/C_1) increases at the expense of the cathodic irreversible peak (C_4), which indicated that the product of pNP by irreversible reduction remained on or near the BDD electrode surface and was oxidized on the anodic sweep. The influence of the deposition time applied to reduction potential did not increase with increasing deposition time (Fig. S6.13, panel D, inset). These results are in agreement with those observed for pNP and other nitro-substituted phenols (Barek et al., 1994; Ni et al., 2001).

The optimal experimental SWV-parameters for quantification of pAP in 1 mol L^{-1} DEA buffer (pH 9.8) containing 6.0 mmol L^{-1} $MgCl_2$ and 100 mmol L^{-1} KCl using microcrystalline BDD electrode were found to be E_{sw} = 200 mV pulse amplitude, f = 200 Hz frequency, E_{sp} = 8 mV pulse potential, E_{ap} = -1.70 V and t = 10 s for accumulation potential and time, respectively.

Reproducibility of the BDD electrode. The reproducibility of the BDD electrode toward p-nitrophenol was investigated for ten replicative measurements. To improve the reproducibility of the experiments, the BDD electrode was subjected to a cathodic polarization at -2.0 V for 30 s in 0.5 mol L^{-1} H_2SO_4 supporting electrolyte before the measurements. Fig. S6.14 shows the inter-assay variation current with the BDD electrode in 150 mmol L^{-1} pNP in 1 mol L^{-1} DEA buffer (pH 9.8) containing 6.0 mmol L^{-1} $MgCl_2$ and 100 mmol L^{-1} KCl. A statistical analysis demonstrates that there no significant difference ($p < 0.05$) between the first SWV cycle and followed cycles. The variation coefficient was 2.9% for ten replicative measurements, indicating good reproducibility.

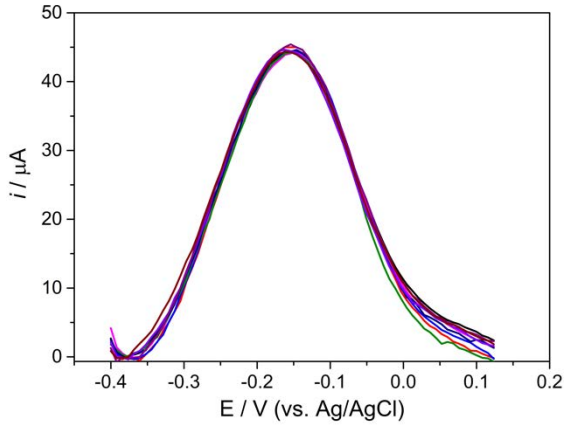

Fig. S6.14. Square wave voltammograms of 150 µmol L^{-1} pNP in 1 mol L^{-1} DEA buffer (pH 9.8) containing 6.0 mmol L^{-1} $MgCl_2$ and 100 mmol L^{-1} KCl. SWV conditions: E_{sw} = 200 mV, E_{ap} = -1.70 V, E_{sp} = 8 mV, f = 200 Hz, t = 10 s.

Stability of pNPP substrate on BDD electrode. The stability of 10 mmol L^{-1} pNPP in 1 mol L^{-1} DEA buffer (pH 9.8) containing 6.0 mmol L^{-1} $MgCl_2$ and 100 mmol L^{-1} KCl was evaluated by cyclic voltammetry (CV) and square wave voltammetry (SWV) at -1.70 V deposition potential (Fig. S6.15).

Fig. S6.15, panel A, shows the CV for 10 mmol L^{-1} pNPP in 1 mol L^{-1} DEA buffer (pH 9.8) containing 6.0 mmol L^{-1} $MgCl_2$ and 100 mmol L^{-1} KCl at -1.70 V deposition potential, in a potential window from -0.3 to 0.4 V, at 50 mV s^{-1} scan rate. This potential window was selected because it is the region that will be monitored for the conversion of p-nitrophenol (pNP) into p-aminophenol (pAP) (see Fig. S6.12). As expected, no faradaic process is observed in the potential window from -0.3 to 0.4 V, i.e., no measurable hydrolysis of pNPP substrate is observed.

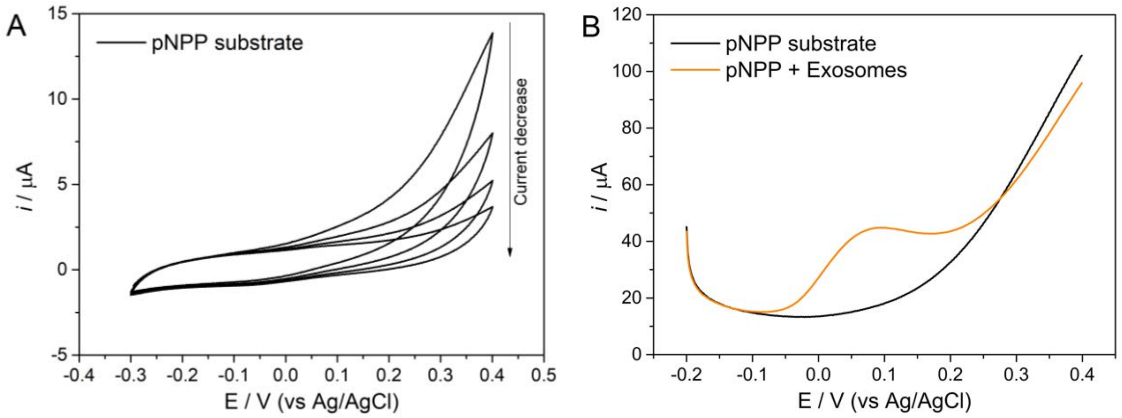

Fig. S6.15. (A) Cyclic voltammograms of 10 mmol L^{-1} pNPP in 1 mol L^{-1} DEA buffer (pH 9.8) containing 6.0 mmol L^{-1} MgCl2 and 100 mmol L^{-1} KCl, 50 mV s^{-1} scan rate and (B) square wave voltammograms of the same pNPP solution in (–) absence and (–) presence of ALP enzyme from osteoblastic-derived exosomes (3.17 x 109 exosomes per assay). SWV conditions: E_{sw} = 200 mV, E_{ap} = -1.70 V, E_{sp} = 8 mV, f = 200 Hz, t = 10 s.

Fig. S6.15 panel B shows the SWV for 10 mmol L^{-1} pNPP in the presence of ALP-derived from osteoblastic-derived exosomes in 1 mol L^{-1} DEA buffer (pH 9.8) containing 6.0 mmol L^{-1} $MgCl_2$ and 100 mmol L^{-1} KCl at -1.70 V deposition potential, in a potential window from -0.2 to 0.4 V, at 50 mV amplitude, 100 Hz frequency, 2 mV step potential. The SWV technique is considered more sensitive than CV, but even so, no measurable hydrolysis of pNPP is observed. On the other hand, with the presence of ALP-derived from osteoblastic-derived exosomes, a great current signal of pNPP product is observed at 55 mV. These results demonstrate that the pNPP substrate solution has excellent hydrolytic stability with no formation of pNP/pAP, remaining colorless in the absence of the ALP enzyme.

6.6.15. Calibration plots for optical and electrochemical readout

The ALP activity from osteoblastic-derived exosomes was determined by the end-point enzymatic assay, correlating the maximal values of absorbance and current peak (baseline corrected) for the pNP and pAP product, respectively, as a function of the number of exosomes per microliter. Once the best parameters for colorimetric and electrochemical detection are known for the pNP and pAP product, analytical curves were obtained (Fig. S6.16). The standard deviation of the mean absorbance or current (Sb) measured at enzyme reaction medium, together with the slope of the straight line of the analytical curves (s) were used in the determination of the limit of detection (LOD), according to guidelines recommended by IUPAC (Mocak et al., 1997).

Fig. S6.16 shows the colorimetric (panel A) and electrochemical (panel B) calibration curves for pNP at a concentration ranging from 1.95 to 125 µmol L^{-1} in 1 mol L^{-1} DEA buffer (pH 9.8) containing 6.0 mmol L^{-1} $MgCl_2$ and 100 mmol L^{-1} KCl, and 25%

(v/v) of 5 mol L^{-1} NaOH. The linear response yielded a straight line, which was applied a linear regression in the colorimetric (r^2 = 0.9999) and electrochemical (r^2 = 0.9983) readouts. The linearity for the electrochemical read-out demonstrates good stability to the non-fouling effect, good electron transferability, and low absorptivity to pNP and/or pNP products using the BBD electrode. The limit of detection (LOD) was found to be 0.10 µmol L^{-1} and 3.35 µmol L^{-1} for electrochemical and colorimetric readouts, respectively. These results demonstrated that the developed approaches have potential as sensitive platforms for the detection of the pNPP substrate.

The colorimetric and electrochemical assay consisted of the measurement of the absorbance at 405 nm and the current peak at -150 mV in the end-point enzymatic assay (fixed time), respectively. The absorbance and/or current peak increment is related to the hydrolysis rate of the p-nitrophenyl phosphate substrate (pNPP) to p-nitrophenol (pNP). Then, the values are interpolated in the calibration curves and normalized by the time reaction to give the enzymatic activity in U L^{-1}.

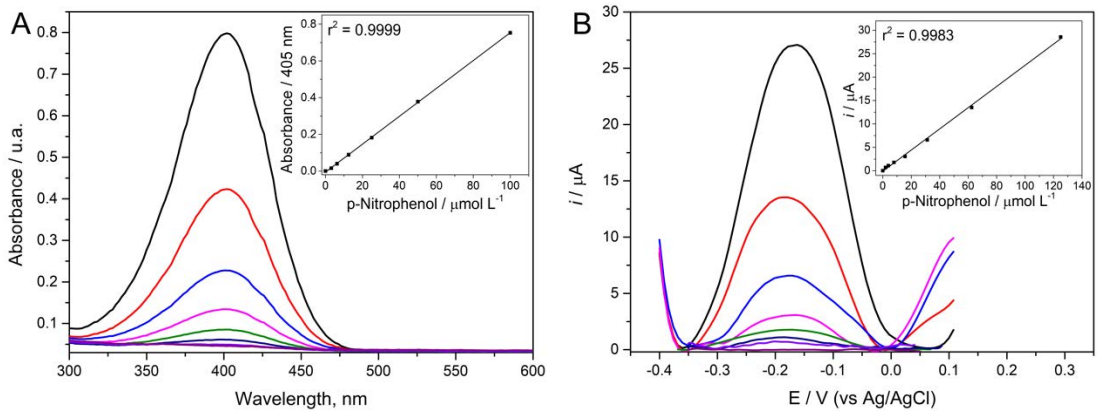

Fig. S6.16. Calibration curve by using (A) UV-vis spectra and (B) square wave voltammograms (SWV) of p-nitrophenol (pNP) at concentration ranging from 1.95 to 250 µmol L^{-1} in 1 mol L^{-1} DEA buffer (pH 9.8) containing 100 mmol L^{-1} KCl, 6.0 mmol L^{-1} $MgCl_2$ and 25% (v/v) of 5 mol L^{-1} NaOH. SWV conditions: E_{sw} = 200 mV, E_{ap} = -1.70 V, E_{sp} = 8 mV, f = 200 Hz, t = 10 s.

6.7. References

Adams, R. N. Electrochemistry at Solid Electrodes. Marcel-Dekker, New York, 1969.

Agrawal, A., Sathe, T., Nie, S., Single-bead immunoassays using magnetic microparticles and spectral-shifting quantum dots. J Agric Food Chem 2007; 55: 3778.

Anderson, H. C., Matrix vesicles and calcification. Curr. Rheumatol. Rep. 2003; 5: 222.

Anderson, H. C., Sipe, J. B., Hessle, L., et al. Impaired Calcification Around Matrix Vesicles of Growth Plate and Bone in Alkaline Phosphatase-Deficient Mice. Am. J. Pathol. 2004; 164: 841.

Ariyawansha, R. T. K., Basnayake, B. F. A., Karunarathna, A. K., et al. Extensions to Michaelis-Menten Kinetics for Single Parameters. Sci. Rep. 2018; 8: 16586.

Bard, A. J., Faulkner, L. R. Electrochemical Methods: Fundamentals and Applications, 2nd ed. John Wiley & Sons, Inc., New York, 2001.

Barek, J., Ebertová, H., Mejstřík, V., et al. Determination of 2-Nitrophenol, 4-Nitrophenol, 2-Methoxy-5-nitrophenol, and 2,4-Dinitrophenol by Differential Pulse Voltammetry and Adsorptive Stripping Voltammetry. Collect. Czechoslov. Chem. Commun. 1994; 59: 1761.

Butterworth, P. J. The pyrophosphatase activity of pig kidney alkaline phosphatase and its inhibition by magnesium ions and excess of pyrophosphate. Biochem. J. 1968; 110: 671.

Cahiez, G., Lefèvre, N., Poizat, M., et al. A User-Friendly Procedure for the Preparation of Secondary Alkyl Chlorides. Synthesis (Stuttg). 2012; 45: 231.

Cañizares, P., García-Gómez, J., Sáez, C., et al. Electrochemical oxidation of several chlorophenols on diamond electrodes Part I. Reaction mechanism. J. Appl. Electrochem. 2003; 33: 917.

Cañizares, P., Sáez, C., Lobato, J., et al. Electrochemical Treatment of 4-Nitrophenol-Containing Aqueous Wastes Using Boron-Doped Diamond Anodes. Ind. Eng. Chem. Res. 2004; 43: 1944.

Chaudhuri, G., Chatterjee, S., Venu-Babu, P., et al. Kinetic behaviour of calf intestinal alkaline phosphatase with pNPP. Indian J. Biochem. Biophys. 2013; 50: 64.

Chen, W.-Z., Shen, J.-F., Zhou, Y., et al. Clinical characteristics and risk factors for developing bone metastases in patients with breast cancer. Sci. Rep. 2017; 7: 11325.

Chosewood, L. C., Wilson, D. E. Biosafety in Microbiological and Biomedical Laboratories, 5th ed., in: U.S. Department of Health and Human Services. Centers for Disease Control and Prevention. 2009; 30.

Chow, A., Zhou, W., Liu, L., et al. Macrophage immunomodulation by breast cancer-derived exosomes requires Toll-like receptor 2-mediated activation of NF-κB. Sci. Rep. 2015; 4: 5750.

Cobb, S. J., Ayres, Z. J., Macpherson, J. V. Boron Doped Diamond: A Designer Electrode Material for the Twenty-First Century. Annu. Rev. Anal. Chem. 2018; 11: 463.

Halvaei, S., Daryani, S., Eslami-S, Z., et al. Exosomes in Cancer Liquid Biopsy: A Focus on Breast Cancer. Mol. Ther. - Nucleic Acids 2018; 10: 131.

Hoogenboom, R., Fijten, M. W. M., Kickelbick, G., et al. Synthesis and crystal structures of multifunctional tosylates as basis for star-shaped poly(2-ethyl-2-oxazoline)s. Beilstein J. Org. Chem. 2010; 6: 773.

Jiang, Y., Zhu, X., Li, H., et al. Effect of nitro substituent on electrochemical oxidation of phenols at boron-doped diamond anodes. Chemosphere 2010; 78: 1093.

Johnstone, R. M., Adam, M., Hammond, J.R., et al. Vesicle formation during reticulocyte maturation. Association of plasma membrane activities with released vesicles (exosomes). J. Biol. Chem. 1987; 262: 9412.

Keiding, R., Hörder, M., Denmark, W.G., et al. Recommended Methods for the Determination of Four Enzymes in Blood. Scand. J. Clin. Lab. Investig.1974; 33: 291–306.

Kim, S. H., Shin, K.-H., Moon, S.-H., et al. Reassessment of alkaline phosphatase as serum tumor marker with high specificity in osteosarcoma. Cancer Med. 2017, 6: 1311.

Li, S.-J., Li, C.-Y., Li, Y.-F., et al. Facile and Sensitive Near-Infrared Fluorescence Probe for the Detection of Endogenous Alkaline Phosphatase Activity In Vivo. Anal. Chem. 2017; 89: 6854.

Lineweaver, H., Burk, D. The Determination of Enzyme Dissociation Constants. J. Am. Chem. Soc. 1934; 56: 658.

López-Cobo, S., Campos-Silva, C., Moyano, A., et al. Immunoassays for scarce tumour-antigens in exosomes: detection of the human NKG2D-Ligand, MICA, in tetraspanin-containing nanovesicles from melanoma. J. Nanobiotechnology 2018; 16: 47.

Lovrić, M., Komorsky-Lovric, Š. Square-wave voltammetry of an adsorbed reactant. J. Electroanal. Chem. Interfacial Electrochem. 1988; 248; 239–253.

Martin, H. B. Hydrogen and Oxygen Evolution on Boron-Doped Diamond Electrodes. J. Electrochem. Soc. 1996; 143: L133.

May, P. W., Ludlow, W. J., Hannaway, M., et al. Raman and conductivity studies of boron-doped microcrystalline diamond, facetted nanocrystalline diamond and cauliflower diamond films. Diam. Relat. Mater. 2008; 17: 105.

Mocak, J., Bond, A. M., Mitchell, S., Scollary, G. A statistical overview of standard (IUPAC and ACS) and new procedures for determining the limits of detection and quantification: Application to voltammetric and stripping techniques (Technical Report). Pure Appl. Chem. 1997; 69: 297.

Moura, S. L., Martín, C. G., Martí, M., et al. Multiplex detection and characterization of breast cancer exosomes by magneto-actuated immunoassay. Talanta 2020a; 211: 120657.

Moura, S. L., Martín, C. G., Martí, M., et al. Electrochemical immunosensing of nanovesicles as biomarkers for breast cancer. Biosens. Bioelectron. 150, 111882.

Moura, S. L., Santos Júnior, J. R. dos, Machado, F. B. C. Conductive organic polymers: an electrochemical route for the polymerization of dapsone. J. Electroanal. Chem. 2015; 757: 230.

Nayudu, P. R. V., Miles, P. L., Inhibition of pyrophosphatase activity of mouse duodenal alkaline phosphatase by magnesium ions. Biochem. J. 1969; 115: 29.

Nelson, D., Cox, M.M., Lehninger, A.L. Lehninger Principles of Biochemistry. W.H. Freeman, New York, NY, 2013.

Ni, Y., Wang, L., Kokot, S., Simultaneous determination of nitrobenzene and nitro-substituted phenols by differential pulse voltammetry and chemometrics. Anal. Chim. Acta 2001; 431: 101.

Nicholson, R. S., Shain, I. Theory of Stationary Electrode Polarography. Single Scan and Cyclic Methods Applied to Reversible, Irreversible, and Kinetic Systems. Anal. Chem. 1964; 36: 706.

Oliveira-Rodríguez, M., López-Cobo, S., Reyburn, H.T., et al. Development of a rapid lateral flow immunoassay test for detection of exosomes previously enriched from cell culture medium and body fluids. J. Extracell. Vesicles 2016; 5: 31803.

Pan, B. T., Teng, K., Wu, C., et al. Electron microscopic evidence for externalization of the transferrin receptor in vesicular form in sheep reticulocytes. J. Cell Biol. 1985; 101, 942.

Pecková, K., Musilová, J., Barek, J., Boron-Doped Diamond Film Electrodes—New Tool for Voltammetric Determination of Organic Substances. Crit. Rev. Anal. Chem. 2009; 39: 148.

Peng, J., Han, X.-X., Zhang, Q.-C., et al. Copper sulfide nanoparticle-decorated graphene as a catalytic amplification platform for electrochemical detection of alkaline phosphatase activity. Anal. Chim. Acta 2015; 878: 87.

Preechaworapun, A., Ivandini, T. A., Suzuki, A., et al. Development of Amperometric Immunosensor Using Boron-Doped Diamond with Poly(o -aminobenzoic acid). Anal. Chem. 2008; 80: 2077.

Qin, S., Wang, K., Ma, X., et al. Electrochemical Determination of Alkaline Phosphatase as a Potential Marker of Reperfusion Injury. Int. J. Electrochem. Sci. 2017; 12: 8908.

Rao, S. R., Snaith, A. E., Marino, D., et al.Tumour-derived alkaline phosphatase regulates tumour growth, epithelial plasticity and disease-free survival in metastatic prostate cancer. Br. J. Cancer 2017; 116: 227.

Raposo, G., Stoorvogel, W., Extracellular vesicles: Exosomes, microvesicles, and friends. J. Cell Biol. 2013; 200: 373–383.

Saif, M.W., Alexander, D., Wicox, C.M., Serum Alkaline Phosphatase Level as a Prognostic Tool in Colorectal Cancer: A Study of 105 patients. J. Appl. Res. 2005; 5: 88.

Samanta, S., Rajasingh, S., Drosos, N., et al. Exosomes: new molecular targets of diseases. Acta Pharmacol. Sin. 2018; 39: 501–513.

Sanchez, M. A., Felice, B., Sappia, L.D., et al. Osteoblastic exosomes. A non-destructive quantitative approach of alkaline phosphatase to assess osteoconductive nanomaterials. Mater. Sci. Eng. C 2020; 110931.

Santos, N. M., Ferreira, N. G., Baldan, M. R. Production and Characterization of BDD/Si Electrodes for Environmental Analysis. J. Phys. Conf. Ser. 2014; 480: 012039.

Sappia, L., Felice, B., Sanchez, M.A., et al. Electrochemical sensor for alkaline phosphatase as biomarker for clinical and in vitro applications. Sensors Actuators B Chem. 2019-281, 221–228.

Sapurina, I., Tenkovtsev, A. V, Stejskal, J. Conjugated polyaniline as a result of the benzidine rearrangement. Polym. Int. 2015; 64: 453–465.

Sharma, U., Pal, D., Prasad, R. Alkaline Phosphatase: An Overview. Indian J. Clin. Biochem. 2014; 29: 269.

Shen, C., Li, X., Rasooly, A., et al. A single electrochemical biosensor for detecting the activity and inhibition of both protein kinase and alkaline phosphatase based on phosphate ions induced deposition of redox precipitates. Biosens. Bioelectron. 2016; 85: 220.

Stec, B., Holtz, K. M., Kantrowitz, E. R. A revised mechanism for the alkaline phosphatase reaction involving three metal ions. J. Mol. Biol. 2000; 299: 1303–1311.

Sun, J., Zhao, J., Bao, X., et al. Alkaline Phosphatase Assay Based on the Chromogenic Interaction of Diethanolamine with 4-Aminophenol. Anal. Chem. 2018; 90: 6339–6345.

Sun, W., Jiao, K. Application of ascorbic acid 2-phosphate as a new voltammetric substrate for alkaline phosphatase determination in human serum. Bull. Chem. Soc. Ethiop. 2005; 19: 163.

Trava-Airoldi, V. J., Corat, E. J., Peña, A. F. V. Application of ascorbic acid 2-phosphate as a new voltammetric substrate for alkaline phosphatase determination in human serum Columnar CVD diamond growth structure on irregular surface substrates. Diam. Relat. Mater. 1995; 4: 1255.

Tsai, L.-C., Hung, M.-W., Chen, Y.-H., et al. Expression and regulation of alkaline phosphatases in human breast cancer MCF-7 cells. Eur. J. Biochem. 2000; 267: 1330.

Vettorelo, S. N., Garay, F. Adsorptive square-wave voltammetry of quasi-reversible electrode processes with a coupled catalytic chemical reaction. J. Solid State Electrochem. 2016; 20: 3271.

Wang, J. H., Wang, K., Bartling, B., et al. The detection of alkaline phosphatase using an electrochemical biosensor in a single-step approach. Sensors (Basel). 2009; 9: 8709.

Wei, J. J., Li, C. M., Gao, X. H., et al. The influence of boron doping level on quality and stability of diamond film on Ti substrate. Appl. Surf. Sci. 2012; 258: 6909.

Woods, B. L., Walker, R. A. pH Effects on Molecular Adsorption and Solvation of p -Nitrophenol at Silica/Aqueous Interfaces. J. Phys. Chem. A 2013; 117: 6224.

Xia, Y., Liu, M., Wang, L., et al. A visible and colorimetric aptasensor based on DNA-capped single-walled carbon nanotubes for detection of exosomes. Biosens. Bioelectron. 2017; 92: 8–15.

Xu, J., Mahajan, K., Xue, W., et al. Simultaneous, single particle, magnetization and size measurements of micron sized, magnetic particles. J. Magn. Magn. Mater. 2012; 324: 4189.

Yadav, S., Boriachek, K., Islam, M. N., et al. An Electrochemical Method for the Detection of Disease-Specific Exosomes. ChemElectroChem 2017; 4: 967.

Zhu, X., Shi, S., Wei, J., et al. Electrochemical Oxidation Characteristics of p-Substituted Phenols Using a Boron-Doped Diamond Electrode. Environ. Sci. Technol. 2007; 41: 6541.

CHAPTER 7

Final remarks and future perspectives

There is a growing demand for biomarkers that can help detect diseases at an early stage, as well as for follow-up of patients and therapeutic strategies. Exosomes could be the next big step to reach this goal. They carry a cargo of active molecules to proximal and distal cells of the body as a mechanism of physiological communication, to maintain natural homeostasis as well as pathological responses. All types of cells use exosomes for this purpose. Importantly, one of the most remarkable features is that they are present in all the biological fluids, such as blood, saliva, urine, among others. Their easy accessibility is one of the most compelling reasons for developing exosomes as clinical biomarkers. Another striking characteristic is their molecular cargo, which can be useful for diagnosis and prognosis of several conditions and diseases. During the biogenesis, components of the cell remain in the exosomes, including tetraspanins (CD9, CD63, CD81), membrane proteins, lipids and different RNA species (mRNA and microRNA) and DNA3. This cargo provides a specific signature about their cellular origin and contains critical information about processes happening at different areas of the body.

The exosomes are thus promising biomarkers for a more sensitive, non-invasive, early detection of non-communicable diseases, for instance cancer. Furthermore, the exosomes could be useful as a biomarker beyond cancer, into areas such as cardiology, regenerative medicine, neurodegenerative diseases, among many other conditions.

In addition to their potential role as biomarker, the exosomes are designed to bring molecular cargo from one cell to another. The exosomes could thus be loaded with a therapeutic cargo, enabling highly targeted delivery of drugs to specific types of cells, and sparing all the other kinds of cells from damage.

Unfortunately, realizing the potential of these vesicles as biomarker will require technical improvement, since the exosomes are exceptionally challenging to characterization with current technologies. Exosomes have a size that makes them out of the sensitivity range to most cell-oriented sorting or analysis platforms, as is the case of the classical flow cytometers.

The most common methods for targeting exosomes to date typically involve purification followed by the specific characterization of their cargo. The whole procedure is time consuming, requiring thus skilled personnel as well as laboratory facilities and benchtop instrumentation. Current methodologies have limitations in isolating, detecting and characterizing exosomes with high specificity, sensitivity and simplicity. These three major challenges are be addressed in this dissertation, considering that a systematically study of exosomes will improve liquid biopsies and advance nanomedicine.

Due to their low concentration, conventional procedures for exosome characterization and detection usually require relatively large sample volumes and involve

a preliminary purification and preconcentration step. Moreover, the physical separation of the exosome fraction from the biological fluids is usually mandatory prior to their characterization, to prevent the interference of free receptors present in the sample. The isolation of the exosomes is best performed with differential ultracentrifugation. Among others, the major drawback is the lack of specificity, since it separates the whole population of exosomes, regardless their cell origin, without taking advantage of the rich information contained within exosome subpopulations. These subpopulations could reveal data about processes happening at different areas of the body, such as disease signatures, which would otherwise fade into the background of a global analysis. Therefore, there is a global demand for simple and robust exosome isolation methods from complex biological fluids amenable to point-of-care diagnosis. Novel developments that are needed involve solid-phase preconcentration procedures which can be easily integrated in emerging technologies. Ideally, exosomes should be specifically preconcentrated while the interfering matrix is removed at the same time, increasing also the sensitivity of the detection. Since the early reports on magnetic separation technology, magnetic particles (MPs) have been used as a powerful and versatile preconcentration tool in a variety of analytical and biotechnology applications and in emerging technologies including microfluidic devices and biosensors. During this dissertation, we developed our own methodologies and procedures for exosomes production, isolation, characterization by classical methodologies and also explored the immunomagnetic separation of exosomes for the isolation in biological fluids.

Beside the amazing properties of MPs, this advanced material shows low cost of production, stability and magnetic actuation, and can be easily integrated in electrochemical sensors, magneto-actuated immunoassays, among other platforms and readouts, for the detection of exosomes, as it is demonstrated in this dissertation.

Although they showed very promising features, all these approaches for the detection of exosomes should be further validated for the isolation and detection of exosomes in other biological fluids than serum.

This doctoral thesis shown the potential application of the exosomes as novel biomarkers in cancer diagnosis, and how the integration of magnetic particles can improve the simplification of its isolation, purification and sensing, especially in electrochemical biosensing. Some future works could explore the isolation of exosomes from less invasive samples than human serum, such as urine and saliva.

Although in this PhD thesis a rational study of the membrane proteins for the specific isolation by IMS of the exosomes in different biological fluids was made, further studies should be done based on novel membrane proteins. Moreover, different approaches for a further increment of the sensitivity in the detection of exosomes directly in complex biological samples should be study. It is important to highlight that the use of exosomes in

this proposal, is based on the expected improvement in the sensitivity compared to conventional biomarkers, considering that one altered cell can produce (and eventually release) a huge number of exosomes. This high number of exosomes released by a single cell reveals the potential application of exosomes as biomarkers in liquids biopsies instead of CTCs for the sensitive detection at early stages of a disease.

Moreover, the genetic cargo of the exosomes could be assessed for a further increase of the sensitivity in the detection of the exosomes. Therefore, a rational study of the overexpressed mRNA in cancer-derived exosomes should be done. The first candidate that can be explored is the overexpression of Glyceraldehyde 3-phosphate dehydrogenase (GAPDH). It was demonstrated that the cancer cells exhibit increased aerobic glycolysis, generating ATP and metabolic intermediates for cancer cell proliferation. GAPDH is thus considered a key glycolytic enzyme and responsible for the dysregulation of glycolysis in cancer and it is found overexpressed not only in breast cancer, but also in lung, prostate, renal, pancreatic and colorectal carcinomas, when compared to normal tissues. The overexpression of GAPDH transcript cargo is thus a promising biomarker in many types of cancers that can be potentially used to increase the sensitivity. Besides GAPDH, others genetic material can be considered included microRNAs.

CHAPTER 8

Science communications

8.1. List published works (2015-2020)

1. Moura, S. L., Sappia, L. D., Martí, M., Pividori, M. I. Electrochemical biosensing of the alkaline phosphatase activity in exosomes isolated by specific epithelial biomarker from serum of breast cancer patient. **2020**. *In preparation.*

2. Moura, S. L., Martí, M., Pividori, M. I. *Matrix effect in the isolation of breast cancer-derived nanovesicles by immunomagnetic separation and electrochemical immunosensing — A comparative study*. Sensors. **2020**, 20(4), 965.

3. Moura, S. L., Martín, C. G., Martí, M., Pividori, M. I. *Multiplex detection and characterization of breast cancer exosomes by magneto-actuated immunoassay*. Talanta. **2020**, 211, 120657.

4. Moura, S. L., Martín, C. G., Martí, M., Pividori, M. I. *Electrochemical immunosensing of nanovesicles as biomarkers for breast cancer*. Biosens. Bioelectron. **2020**, 150, 111882.

5. Sanchez, M. A., Felice, B., Sappia, L. D., Moura, S. L., Martí, M., Pividori, I. P. *Osteoblastic exosomes. A non-destructive quantitative approach of alkaline phosphatase to assess osteoconductive nanomaterials*. Mat. Sci. Eng. C-Mater. **2020**, 110931.

7. Hassan, A. H. A., Sappia, L., Moura, S. L., Ali, F. H.M., Moselhy, W. A., Sotomayor, M. P. T., Pividori, M. I. *Biomimetic magnetic sensor for electrochemical determination of scombrotoxin in fish*. Talanta. **2019**, 194, 997.

8. Hassan, A. H. A., Moura, S. L., Ali, F. H.M., Moselhy, W. A., Sotomayor, M. P. T., Pividori, M. I. *Electrochemical sensing of methyl parathion on magnetic molecularly imprinted polymer*. **2018**, 118, 181.

9. Moura, S. L., Fajardo, L. M., Cunha, L. A., Sotomayor, M. P. T., Machado, F. B. C., Ferrão, L. F. A., Pividori, M. I. *Theoretical and experimental study for the biomimetic recognition of levothyroxine hormone on magnetic molecularly imprinted polymer*. Biosens Bioelectron. **2018**, 107, 203.

Other related published works

1. Moura, S. L., Fernandes, G. F. S., Machado, F. B. C., Ferrão, L. F. A. *Theoretical and experimental electronic spectra of neutral, monoprotonated and diprotonated dapsone*. Theor. Chem. Acc. **2020**, 139(3), 1.

2. Moura, S. L., Santos Júnior, J. R., Machado, F. B. C., Kawachi, E. Y., Ferrão, L. F. A. *Conductive organic polymers: An electrochemical route for the polymerization of dapsone*. J. Electroanal. Chem. **2015**, 757, 230.

8.2. List of national and international congresses (2015-2020)

1. Authors: S. L. Moura, S. Carinelli, M. Martì, M. I. Pividori
Title: “Quantification of exosomes from breast cancer cells by magneto-actuated immunoassay”
Type of participation: Poster presentation
Congress: XXI Transfrontier Meeting of Sensors and Biosensors
Place: Barcelona, Spain
Date: 29 to 30 September, 2016

2. Authors: A. H. A. Hassan, L. M. Fajardo, S. L. Moura, L. Sappia, F. H. M. Ali, A. W. A. Moselhy, M. I. Pividori
Title: “Magnetic molecularly imprinted polymer for the detection of methyl parathion in fish”
Type of participation: Poster presentation
Congress: NanoBio&Med2016
Place: Barcelona, Spain
Date: 22 to 24 November, 2016

3. Authors: S. L. Moura, M. Martì, M. I. Pividori
Title: “Magneto-actuated platform for the detection of exosomes from breast cancer cells”
Type of participation: Poster presentation
Congress: 5th International Conference on Bio-Sensing Technology
Place: Riva del Garda, Italy
Date: 07 to 10 May, 2017

4. Authors: S. L. Moura, L. M. Farjado, L. A. Cunha, M. D. P. T. Sotomayor, L. F. A. Ferrao, M. I. Pividori
Title: “Theoretical and experimental approach on thyroid hormone levothyroxine for its biomimetric recognition on magneto-molecularly imprinted polymer”
Type of participation: Poster presentation
Congress: 5th International Conference on Bio-Sensing Technology
Place: Riva del Garda, Italy
Date: 07 to 10 May, 2017

5. Authors: S. L. Moura, M. Martì, M. I. Pividori
Title: “Magneto immunoassay for the detection of exosomes in breast cancer”
Type of participation: Poster presentation
Congress: IX Jornada del Departament de Biologia Cel·lular, Fisiologia i Immunologia
Place: Barcelona, Spain
Date: 09 June, 2017

6. Authors: S. L. Moura, M. Martì, M. I. Pividori
Title: “Electrochemical magneto-actuated platform for the detection of nanovesicles from breast cancer cells”
Type of participation: Oral presentation
Congress: XXXVI Biennial Meeting – Spanish Royal Society of Chemistry (RSEQ)
Place: Sitges, Spain
Date: 25 to 29 June, 2017

7. Authors: M. M. Gómez, A. P. Rusiñol, S. L. Moura, A. Ben Aissa, M. Martì, M. I. Pividori
Title: “Detection of circulating tumor cells by electrochemical magneto immunosensing and genosensing”
Type of participation: Poster presentation
Congress: XXXVI Biennial Meeting – Spanish Royal Society of Chemistry (RSEQ)
Place: Sitges, Spain
Date: 25 to 29 June, 2017

8. Authors: A. H. A. Hassan, L. M. Fajardo, S. L. Moura, F. H. M. Ali, A. W. A. Moselhy, M. D. P. T. Sotomayor, M. I. Pividori
Title: “Magnetic molecularly imprinted polymers. Synthesis and Applications”
Type of participation: Poster presentation
Congress: XXXVI Biennial Meeting – Spanish Royal Society of Chemistry (RSEQ)
Place: Sitges, Spain
Date: 25 to 29 June, 2017

9. Authors: S. L. Moura, M. Martì, M. I. Pividori
Title: “Electrochemical and optical magneto-actuated platform for the detection of nanovesicles from breast cancer cells”
Type of participation: Oral presentation
Congress: XXII Transfrontier Meeting of Sensors and Biosensors
Place: Montpellier, France
Date: 21 to 22 September, 2017

10. Authors: A. P. Rusiñol, M. M. Gómez, S. L. Moura, A. Ben Aissa, M. Martì, M. I. Pividori
Title: “Comparing electrochemical magneto immunosensing and genosensing for the detection of circulating tumor cells”
Type of participation: Oral presentation
Congress: XXII Transfrontier Meeting of Sensors and Biosensors
Place: Montpellier, France
Date: 21 to 22 September, 2017

11. Authors: A. H. A. Hassan, L. M. Fajardo, S. L. Moura, M. D. P. T. Sotomayor, F. H. M. Ali, A. W. A. Moselhy, M. I. Pividori
Title: “Magnetic molecularly imprinted polymers. Synthesis and Applications”
Type of participation: Poster presentation
Congress: XXII Transfrontier Meeting of Sensors and Biosensors
Place: Montpellier, France
Date: 21 to 22 September, 2017

12. Authors: S. L. Moura, M. Martì, M. I. Pividori
Title: “Electrochemical biosensing of cancer exosomes in human serum based on magnetic separation”
Type of participation: Oral presentation
Congress: 12th International Conference on the Scientific and Clinical Applications of Magnetic Carries
Place: Copenhagen, Denmark
Date: 22 to 26 May, 2018

13. Authors: A. P. Rusiñol, M. M. Gómez, S. L. Moura, M. Martì, M. I. Pividori
Title: “Magneto-actuated rapid test for the detection of circulating tumor cells”
Type of participation: Oral presentation
Congress: 12th International Conference on the Scientific and Clinical Applications of Magnetic Carries
Place: Copenhagen, Denmark
Date: 22 to 26 May, 2018

14. Authors: A. H. A. Hassan, L. M. Fajardo, S. L. Moura, M. D. P. T. Sotomayor, M. I. Pividori
Título: “Magnetic molecularly imprinted polymers. Synthesis and Applications”
Type of participation: Oral presentation
Congress: 12th International Conference on the Scientific and Clinical Applications of Magnetic Carries
Place: Copenhagen, Denmark
Date: 22 to 26 May, 2018

15. Authors: S. L. Moura, M. Martì, M. I. Pividori
Title: “Rapid methods for the detection of exosomes as a novel biomarker for cancer diagnosis”
Type of participation: Oral presentation
Congress: Jornades Doctorals 2018
Place: Barcelona, Spain
Date: 30 May to 01 June, 2018

16. Authors: A. P. Rusiñol, M. M. Gómez, S. L. Moura, M. Martì, M. I. Pividori
Title: “Comparing rapid diagnostic test for the detection of circulating tumor cells”
Type of participation: Poster presentation
Congress: XXIII Congreso de la Sociedad Iberoamericana de Electroquímica
Place: Cusco, Peru
Date: 03 to 08 June, 2018

17. Authors: S. L. Moura, M. Martì, M. I. Pividori
Title: “Electrochemical biosensing of cancer exosomes in human serum”
Type of participation: Poster presentation
Congress: 28th Anniversary World Congress on Biosensors
Place: Miami, USA
Date: 12 to 15 June, 2018

18. Authors: A. H. A. Hassan, L. M. Fajardo, S. L. Moura, F. H. M. Ali, A. W. A. Moselhy, M. D. P. T. Sotomayor, M. I. Pividori
Title: “Direct electrochemical magneto-actuated sensing of electroactive analytes preconcentrated on Magnetic Molecularly Imprinted Polymers”
Type of participation: Poster presentation
Congress: 28th Anniversary World Congress on Biosensors
Place: Miami, USA
Date: 12 to 15 June, 2018

19. Authors: A. P. Rusiñol, M. M. Gómez, S. L. Moura, M. Martì, M. I. Pividori
Title: “Comparing rapid diagnostic test for the detection of circulating tumor cells”
Type of participation: Poster presentation
Congress: 28th Anniversary World Congress on Biosensors
Place: Miami, USA
Date: 12 to 15 June, 2018

20. Authors: S. L. Moura, M. Martì, M. I. Pividori
Title: “Electrochemical biosensing of cancer exosomes in human serum based on magnetic separation”
Type of participation: Poster presentation
Congress: 5th Europen Congress of Immunology
Place: Amsterdam, Netherlands
Date: 02 to 05 September, 2018
21. Authors: A. P. Rusiñol, S. L. Moura, M. M. Gómez, M. Martì, M. I. Pividori
Title: “Magneto-actuated rapid test for the detection of circulating tumor cells”
Type of participation: Poster presentation
Congress: 5th Europen Congress of Immunology
Place: Amsterdam, Netherlands
Date: 02 to 05 September, 2018

22. Authors: S. L. Moura, A. P. Rusiñol, M. Martì, M. I. Pividori
Title: “Electrochemical immunosensing and genosensing for the detection of exosomes in human serum”
Type of participation: Oral presentation
Congress: XI Ibero-American Congress of Sensors
Place: Barcelona, Spain
Date: 17 to 20 September, 2018

23. Authors: A. P. Rusiñol, M. M. Gómez, S. L. Moura, M. Martì, M. I. Pividori
Title: “Comparing rapid diagnostic test for detection of circulating tumor cells”
Type of participation: Oral presentation
Congress: XI Ibero-American Congress of Sensors
Place: Barcelona, Spain
Date: 17 to 20 September, 2018

24. Authors: J. Cassasayas Cos, S. L. Moura, L. Sappia, M. Martì, M. I. Pividori
Title: “Magneto-actuated platforms for the detection of alkaline phosphatase in exosomes from human osteoblasts”
Type of participation: Poster presentation
Congress: XXIII Transfrontier Meeting of Sensors and Biosensors
Place: Barcelona, Spain
Date: 20 to 21 September, 2018

8.3. Other merits

1. Best Poster Award, 12th International Conference on the Scientific and Clinical Applications of Magnetic Carries. **2018**, July 12th-16th, Copenhagen, Denmark.

2. Best Poster Award, XXXVI Biennial Meeting Spanish Royal Society of Chemistry. **2017**, June 25th-29th, Sitges, Spain.

3. Best Poster Award, XXII Transfrontier Meeting of Sensors and Biosensors. **2017**, 21st-22nd, Montpellier, France.